DOCTOR OF PHILOSOPHY

Computation of risk to life from a finite element pedestrian model in pedestrian accident cases

Wen, Lianjie

Award date:
2019

Awarding institution:
Coventry University

Computation of Risk to Life from a Finite Element Pedestrian Model in Pedestrian Accident Cases

by

Lianjie Wen

A thesis submitted in partial fulfilment of the University's requirements for the Degree of Doctor of Philosophy

Coventry University

Table of Contents

Table of Figures

List of Tables

List of Equations

Nomenclature

a	Translational acceleration
α	Rotational acceleration
t	Time
ω	Angular velocity
D	Displacement
σ	Stress
ε	Strain
E	Young's modulus
ρ	Density
l	Length
UKPF	UK Police Force
PM	Post Mortem
PVP	Peak Virtual Power
$\dot{\varepsilon}$	Strain rate
FE	Finite Element
AEB	Autonomous Emergency Braking
EuroNCAP	European New Car Assessment Programme
UNECE	United Nations Economic Commission for Europe
UTS	Ultimate Tensile Strain
CFC	Channel Frequency Class
ATD	Anthropometric Test Device
FEA	Finite Element Analysis
THOR	Test Device for Human Occupant Restraint
SID	Side Impact Dummy
MADYMO	Mathematical Dynamic Model

THUMS	Total Human Model for Safety
GHBMC	Global Human Body Models Consortium
HIC	Head Injury Criterion
HPC	Head Protection Criterion
GAMBIT	Generalised Acceleration Model for Brain Injury Threshold
RIC	Rotational Injury Criterion
BRIC	Kinematic Rotational Brain Injury Criterion
HIP	Head Impact Power
VC	Viscous Criterion
MPS	Maximum Principal Strain
AIS	Abbreviation Injury Scale
MAIS	Maximum AIS
ISS	Injury Severity Score
DAI	Diffuse Axonal Injury
m	Million
k	Thousand
HGV	Heavy Goods Vehicle
TfL	Transport for London
PCaTS	Pedestrian Countdown at Traffic Signals
YTA	Youth Travel Ambassador
HIII	Hybrid III Crash Test Dummy

Acknowledgement

First of all, greatest thanks are delivered to my direct of study, Dr Christophe Bastien. He is a professional, wise, dedicated and enthusiastic supervisor who always guided me throughout the journey of my research. His brilliant professional knowledge and life wisdom will always light up my way in my life.

After that, huge appreciation must be spread to Prof Clive Neal-Sturgess. He is a great and dedicated professor who is full of knowledge and wisdom. He is so committed to his work and research. He is always ready to inspire and enlighten young researchers.

Also, many thanks are delivered to people who have supported this research, including my colleague Rohit Kshirsagar, Dr Jesper Christensen and Dr Michal Orlowski (part of the supervision team), as well as Lisa Millard and Sam Morgan from the research and registration team.

Finally, I would like to give special thanks to the UK Police Force and the UK Coroner for providing the accident data used in this thesis and for their devotion to improve pedestrian safety and making the world a better place.

Abstract

Traumatic injuries are evaluated using the Abbreviated Injury Scale (AIS), which is a risk to life measurement. Human computer models currently use stresses and strains to evaluate the critical points of injuries. This is problematic if these assessment values are below the cut-off stain thresholds as these current indicators bear no direct relation to AIS. This critical limitation prevents vehicle design and pedestrian safety protocols to use human computer models as the AIS levels cannot be predicted. This research proposes to use for the first time a power method, named Peak Virtual Power (PVP), on the Total Human Model for Safety (THUMS) to extract all the AIS levels of pedestrian trauma at organ and tissue level. This coding was created by calibrating the critical AIS for brain tissue and critical organs against a critical principal strain injury cut-off value. This was achieved by impacting a human model in critical impact directions observed in pedestrian accidents with speeds varying from 2.0m/s to 17.0m/s, covering the EuroNCAP test speed as well as the maximum impact speed provided in real-life pedestrian accident scenarios by the UK Police Force (UKPF). The AIS response was then scaled and bound using corridors using the relationship between AIS and probability of death, which was known to be a cubic. These unique trauma injury corridors were tested against four real-life pedestrian accidents which were reconstructed, and for which the Post Mortem information was available. The study concludes that the PVP method can predict pedestrian head trauma, and in some cases slightly under-estimate it by 1 AIS level, because of post-impact haemorrhage which cannot be captured using a Lagrangian solver. However, for other body organs there are significant differences between the estimates of trauma from PVP and the PM reports. This may be due to a) the head calibration using cylindrical impactors to mimic the impact contact between vehicle and pedestrian head, whereas the body contact against the bonnet may be more diffuse, and b) problems with the THUMS model for which the heart may be oversimplified

For the first time, this work provides a foundation for the development of a numerical tool to predict AIS in vehicle design.

1.0 Introduction

Over decades, much work has been done to improve vehicle safety. Regulations have been established to specify the testing procedure and determine the vehicle safety performance. By using test instruments, engineers can only obtain physical outcomes from crash test dummies and rigid body parts such as acceleration and force. Linking to a risk curve, the probability of threat to life, the Abbreviated Injury Scale (AIS) can be assessed from the output of test instruments. However, the lack of biofidelity makes crash test instruments unsuitable to further investigate injury severity.

With the development of computing technology and the application of the finite element method, detailed human models have been created to overcome the dilemma in furthering injury investigation. Finite Element (FE) human models provide a high-level of biofidelity by using the data from real human body Computerised Tomography (CT) scans. Also, biomechanical material and structures are used to present an actual human body model including outer geometry, bones, muscles, ligaments, tendons, and internal organs. With such details, various engineering outputs such as stresses and strains are accessible. Compared to crash test instruments, FE human models are the most advanced tools for injury severity studies and provide new horizons to improve safety.

Across the world, the number of reported road accidents involving pedestrians is increasing every year (World Health Organization, 2018). Compared with occupants, pedestrians are more vulnerable in the event of multiple injuries (Crandall et al., 2002). Attempts were made to reduce pedestrian injuries have focused largely on precaution isolation techniques such as pedestrian bridges and foot lanes, however pedestrian mortality and death rate are still in a high amount. In such situations, pedestrian safety requires in-depth study and development.

The common drawback of current injury criterion could be the lack of definition of precise and detailed organ trauma. Injury indicators such as HIC can only provide injury probability by using risk curves. To evaluate injury severity directly from the engineering output, a new method is proposed. Using an energy-based Peak Virtual Power (PVP), human injury severity can be directly assessed using a systematic

corridor. Furthermore, by using PVP, the human injury severity of multiple injuries, the Injury Severity Score (ISS), can also be evaluated from the engineering measurements.

The aim of this research was, for the first time, to predict pedestrian trauma using an engineering measurement (PVP) at organ level and to extract the ISS. Tin order to achieve the aim of this work, the following objectives were fulfilled:

1 Coding the trauma threshold of pedestrian head and critical organs (Chapter 4 to 6).

2 Reconstructing real-world accidents using Computing Aided Engineering (CAE) technology (data provided by the UK Police Force (UKPF)) (Chapter 7).

3 Calculating trauma using FE results (Chapter 8).

4 Extracting trauma provided Post-Mortem (PM) report in real-life accident cases (Chapter 9)

5 Comparing the injuries severity and location from CAE and the PM report (Chapter 10).

Consequently, the overall thesis structure is demonstrated in Figure 1.

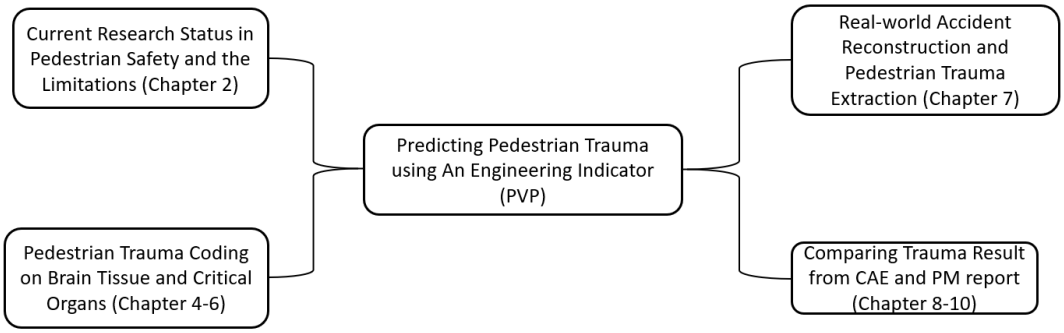

Figure 1 General thesis structure

The work shows that PVP has the potential to predict organ/tissue trauma. This work was based using original accident data from the UK coroner and the UK Police Force (UKPF).

2.0 Literature Review

2.1 Road Traffic Statistics

Across the world, the number of reported road accidents involving pedestrians is increasing every year. More than 1.35 million deaths in road traffic accidents occurred in 2018, making road traffic injuries globally the leading cause of death. Almost half (49%) of the all traffic deaths occur among pedestrians (22%), cyclist and motorcyclists (World Health Organization, 2018). Compared with the data published in 2015 (World Health Organisation, 2015), there is a 12.5% increment in total fatalities of road traffic accidents. In the European Union (EU), the total number of road fatalities in 2017 was 25300, 21% of all people killed on the road were pedestrians (European Union, 2018). During the decade 2006-2015, in the European Union, pedestrian fatalities were reduced by 36%, however the number of pedestrian fatalities in the EU has remained stable since 2013 (Figure 2).

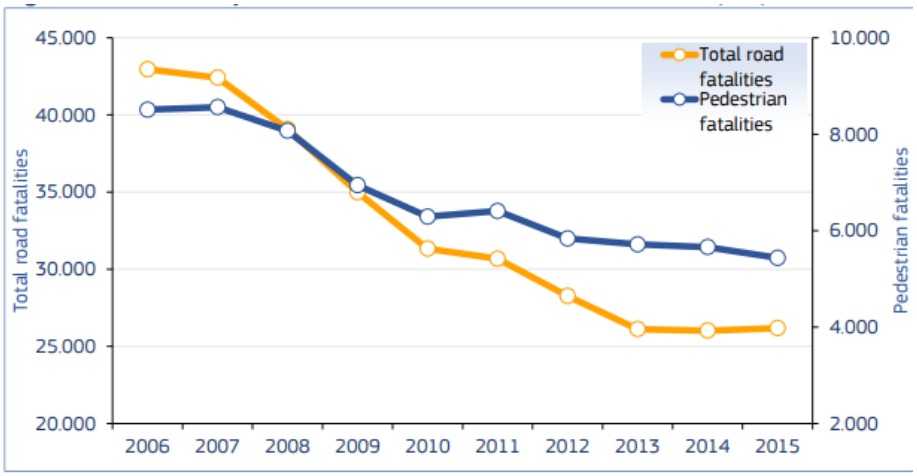

Figure 2 Number of pedestrian fatalities and all road fatalities, EU, 2006-2015 (European Union, 2018)

As illustrated in Figure 2, compared with decrease in total road fatalities, pedestrian fatalities show more of a flat and slow trend in reduction.

In United States (US), a total of 5,977 pedestrian deaths occurred in 2017. Pedestrian fatalities increased by 2 percent from 2016, which was their highest level since 1990. Although pedestrian deaths were 20 percent lower in 2017 than in 1975, they have increased 45 percent since reaching their lowest point in 2009 (Figure 3) (Insurance Institute for Highway Safety and Highway Loss Data Institute, 2018).

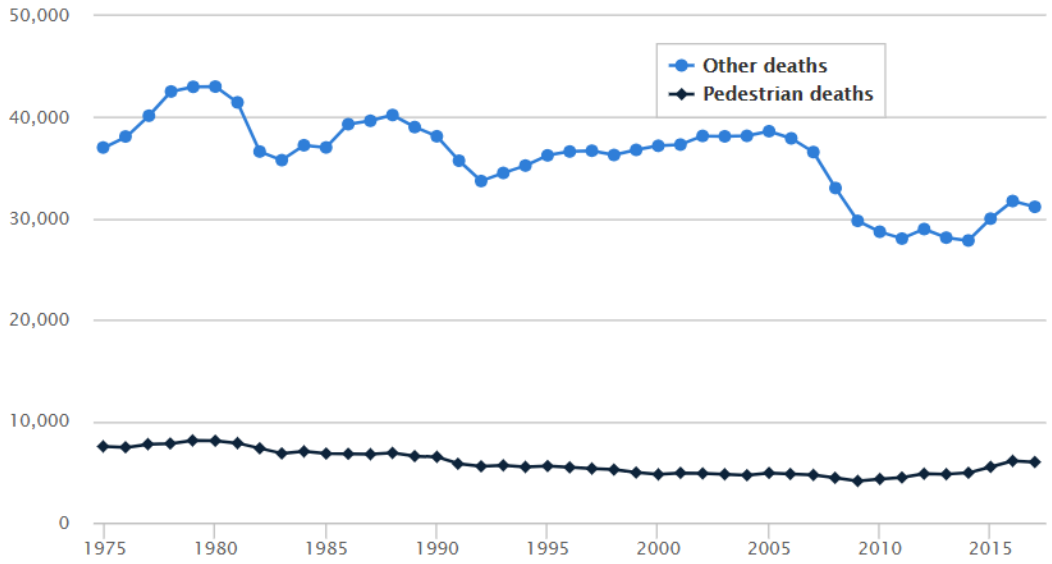

Figure 3 Pedestrian deaths and other motor vehicle deaths, 1975-2017 (Insurance Institute for Highway Safety and Highway Loss Data Institute, 2018)

As illustrated in Figure 3, the trend of pedestrian fatalities in US show a stable trend from 1975 to 2015. In recent years from 2010-2015, the fatality number of pedestrians even increases. Consequently, pedestrian safety is still a concern.

Compared to injured vehicle occupants, pedestrians sustain more multiple injuries, with concomitantly higher injury severity scores and mortality. Despite the size of the pedestrian injury problem, research to reduce traffic related injuries has concentrated almost exclusively on increasing the survival rates for vehicle occupants (Crandall et al., 2002). Since the 1990's, occupant safety established itself as a leading marketing tool for motor vehicles. Safety features such as energy absorbing front and side structures, airbags, seats with integrated seatbelts, and various crash avoidance devices are safety features offered as standard equipment for occupant protection (Du Bois et al., 2004). Most attempts made to reduce pedestrian injuries have focused largely on isolation techniques such as pedestrian bridges, public education, and traffic regulations and have not included changes to vehicle design and pedestrian protection (Crandall et al., 2002). As in such situations, pedestrian safety and protection requires deeper study and development.

The next section will explain the current evaluation method of injury severity and provide the fundamental understanding of injury severity classification method. Based

on this knowledge, an investigation of pedestrian injury pattern was performed to show the injury situation of pedestrians.

2.2 Pedestrian Injury Pattern

2.2.1 Evaluation Methods of Injury Severity- Abbreviated Injury Scale (AIS) and Injury Severity Score (ISS)

2.2.1.1 Abbreviated Injury Scale (AIS)

Single human injury severity is measured using the Abbreviated Injury Scale (AIS). The AIS is an anatomically based, consensus derived, global severity scoring system that classifies each injury by body region according to its relative importance (threat to life) on a 6-point ordinal scale (1=minor and 6=maximal). AIS is internationally accepted and is the primary tool to conclude injury severity (Association for the Advancement of Automotive, 2015). It provides a standardized terminology to describe injuries and ranks injuries by severity. The AIS is ordinal, i.e. it is only evaluated at integer values, and there are no fractional values of AIS; this is largely a resolution issue.

In AIS rating system, seven digital numbers were used to classify an injury which was separated using a period in AIS coding rule. These codes describe location, type and severity of an injury (Association for the Advancement of Automotive, 2015). The first digit is used to specify injured body region, the second one indicates the type of anatomical structure, the third and fourth digits are used to describe specific anatomical structure, and the fifth and sixth digits indicate the injury level. Specific injuries are assigned consecutive two-digit numbers beginning with 02. The last digit after the period indicates the injury severity.

Examples of injury severities with a typical explanation is are proposed below:

- 1-Minor (0% probability of death): superficial laceration
- 2-Moderate (0.1%-0.4% probability of death): fractured sternum
- 3-Serious (0.8%-2.1% probability of death): open fracture of humerus

- 4-Severe (7.9%-10.6% probability of death): perforated trachea
- 5-Critical (53.1%-58.4%probability of death): ruptured liver with tissue loss
- 6-Maximum (100% probability of death): total severance of aorta (Association for the Advancement of Automotive, 2015, Hayes et al., 2007)

2.2.1.2 The Injury Severity Score (ISS)

The Injury Severity Score (ISS) is an anatomical scoring system that provides an overall score for patients with multiple injuries (Trauma.Org, 2016). The ISS is based upon the AIS and is calculated based on six body regions (head and neck, face, chest, abdomen and pelvis, extremity and external) (Trauma.Org, 2016).

ISS uses the maximum AIS severity code (MAIS) in each of the three most severely injured ISS body regions, square each MAIS code and add the three squared numbers for an ISS ($ISS = A^2 + B^2 + C^2$ where A, B, C are the MAIS scores of the three most injured ISS body regions). The ISS scores range from 1 to 75 (i.e. AIS scores of 5 for each category). If any of the three scores is a 6, the score is automatically set at 75. Since a score of 6 ("maximum") indicates the futility of further medical care in preserving life, this may mean a cessation of further care in triage for a patient with a score of 6 in any category (Trauma.Org, 2016).

2.2.1.3 Pedestrian Injury Pattern in Road Traffic Accidents

Compared to injured vehicle occupants, pedestrians sustain more multiple injuries, with concomitantly higher injury severity scores and mortality (Crandall et al., 2002).

The injury percentages vary from the outcomes of the project APROSYS (Neal-Sturgess et al., 2007), where the total pedestrian injury situation was documented in Table 2 and Table 3.

Minor injuries (AIS 1,2)	Serious injuries (AIS 3+)	All injuries
316 (75%)	94 (22%)	423

Table 1 Total pedestrian injury summary (Neal-Sturgess et al., 2007)

As shown in Table 1, among all the 423 injuries recorded, 75% are classified as minor injuries (AIS 1-2), while serious injuries, classified as AIS 3+, represent 22% of all recorded injuries.

Regarding the pedestrian injury location, the summary of pedestrian injury distribution is presented in Table 2.

Body Region	AIS 2+ Injury Distribution Percent	Fatal Injury Distribution Percent
Head	37.16%	39.58%
Thorax	No data	7.81%
Upper Extremity	19.13%	10.42%
Spine	2.73%	5.20%
Abdomen	3.26%	2.08%
Lower extremity	33.33%	33.86%
Unspecified	1.60%	1.04%
Sample size	183	192

Table 2 Pedestrian AIS 2+ injury distribution (Neal-Sturgess et al., 2007)

As illustrated in Table 3, the pedestrian head is the most vulnerable location in the case of AIS 2+ and fatal injuries. Lower extremities, which are the second vulnerable location, have a similar percentage in AIS 2+ and fatal injury.

In Crandall's research (Crandall et al., 2002), the injury profile is also given as Figure 4

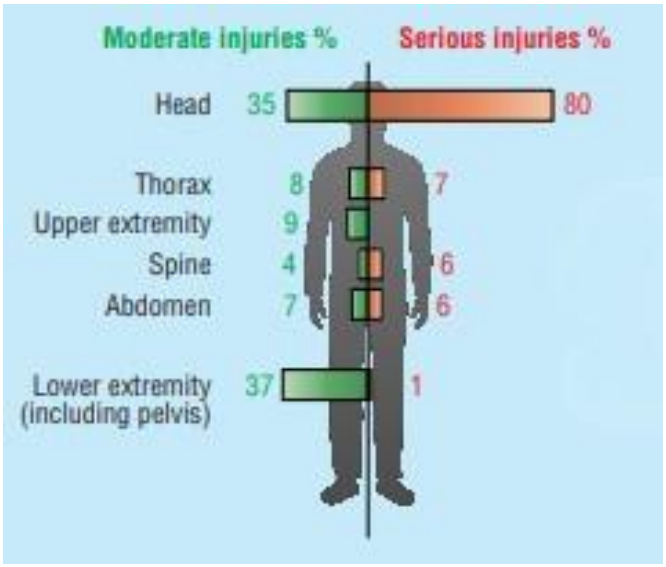

Figure 4 Pedestrian injury profile (Crandall et al., 2002)

As illustrated in Figure 4, 37% of the moderate injury (AIS 2) relate mostly to the lower extremities. Head injury is the second common injury, which represents 35% of all moderate injuries. All the injuries are located in the chest and the abdomen areas. In serious injuries (AIS 3), head injury represents 80% of all injuries sustained on pedestrians. The thorax, spine and abdomen represent nearly equally the rest of the serious injuries (6% to 7% each). Since pedestrians are so vulnerable in road traffic accidents, the next section will review the current pedestrian protection methods aimed at reducing the pedestrian injuries.

2.3 Current Pedestrian Protection Methods

When protecting pedestrians, two main approaches were investigated: isolating the pedestrian from the vehicle to prevent any impact and the second one being pedestrian protection and mitigation through vehicle design.

2.3.1 General Protection Methods

Most attempts made to reduce pedestrian injuries have focused largely on precaution isolation techniques such as pedestrian bridges and footpath (Crandall et al., 2002). Improvements in city infrastructure includes safer public transport, improved sidewalks and cycle lanes, regulations and their enforcement of seat-belt wearing and drink-driving penalties can reduce traffic death dramatically. Setting urban speed

limits appropriate to road function, layout and design is another means to create a framework for safer road use (World Health Organization, 2018).

London has already started to reassess the road space and priority given to cars to reduce vehicle speeds and improve road safety. Transport for London (TfL) recently commissioned research into 20mph (8.94m/s) zones in London and the published results show a significant improvement in pedestrian safety (Transport for London, 2004). In 2010, TfL introduced Pedestrian Countdown at Traffic Signals (PCaTS) at eight trial sites across London. PCaTS provide a visible countdown period on a far sided signal head that replaces the pedestrian 'blackout' period following the green man at crossings. This gives pedestrians better, more consistent information about the time they have available to cross (Transport for London, 2010). TfL has been improving and expanding educational and enforcement activities to improve pedestrian safety. Pedestrian safety messaging has been an integral part of the Youth Travel Ambassador (YTA) programme with young people raising awareness of road safety issues in their schools and local communities. YTAs have also played an important role in supporting the delivery of TfL's teen road safety campaigns. Successful Exchanging Places events that allow cyclists to experience the driver's eye view from a Heavy Goods Vehicle (HGV) cab. TfL has also been working with the Metropolitan Police Service to improve enforcement activity against dangerous and careless road user behaviour. An example of this is Operation Safeway which ran from November 2013 to January 2014 and saw police officers positioned at key junctions across London as part of a high profile engagement and enforcement operation aimed at all road users (Transport for London, 2010).

2.3.2 Pedestrian Protection Protocols

2.3.2.1 The European New Car Assessment Programme (EuroNCAP)

Since the establishment of the EuroNCAP programme in 1997, pedestrian safety and protection has also been brought into consideration. Under the EuroNCAP protocol, pedestrian tests assess the areas of the bumper, bonnet leading edge and bonnet which are most hazardous to both child and adult pedestrians. The tests involve firing dummy body parts at the car simulating accidents at 40km/h (25mph) - a simulated leg is impacted against the bumper, an upper leg against the front edge of the bonnet,

and dummy heads, both child and adult-sized, at points on the bonnet (EuroNCAP, November 2017) (Figure 5).

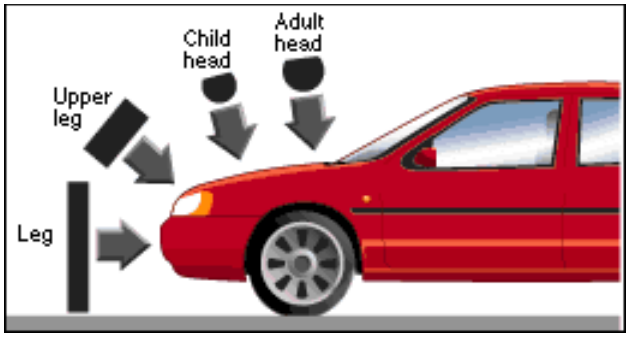

Figure 5 EuroNCAP pedestrian tests scenario (The Automobile Association, 2016)

The assessment of pedestrian protection is performed with the use of a headform, an upper legform, a lower legform impact and AEB test data. In the legform areas, the bumper and the front of the bonnet of the car are marked with a grid and are assessed using the two legform impactors (EuroNCAP, November 2017). EuroNCAP will test "worst case" grid points and manufacturers may nominate additional tests to be performed and the results are included in the assessment (Sievert, 2000).

In the headform impact area, a grid is marked on the outer surface of the vehicle. Marks are placed on the bumper/grille, bonnet top, windscreen, A-pillars and/or roof the wrap around distances of 775mm, 930mm, 1000mm, 1500mm, 1700mm and 2100mm. Points located from 1000mm to 1500mm Wrap Around Distance (WAD) inclusive will be assessed using the child/small adult headform. Points from 1700mm to 2100 mm WAD inclusive will be assessed with the adult headform (EuroNCAP, Nov 2017). The vehicle manufacturer is required to provide EuroNCAP with data detailing the protection offered by the vehicle at all grid locations before any test preparation begins. The predicted level of protection offered by the vehicle is verified by EuroNCAP by means of testing a sample of randomly selected grid-points and the overall prediction is adjusted accordingly. The protection provided by each grid location is illustrated by a coloured area, on an outline of the front of the car. The same five colour boundaries and HIC 650 – HIC 1700 (Head Injury Criteria) values will be applied here, as per Table 3.

Green	HIC15 < 650
Yellow	650 ≤ HIC15 < 1000
Orange	1000 ≤ HIC15 < 1350
Brown	1350 ≤ HIC15 < 1700
Red	1700 ≤ HIC15

Table 3 HIC tolerance boundary in EuroNCAP assessment (EuroNCAP, November 2017)

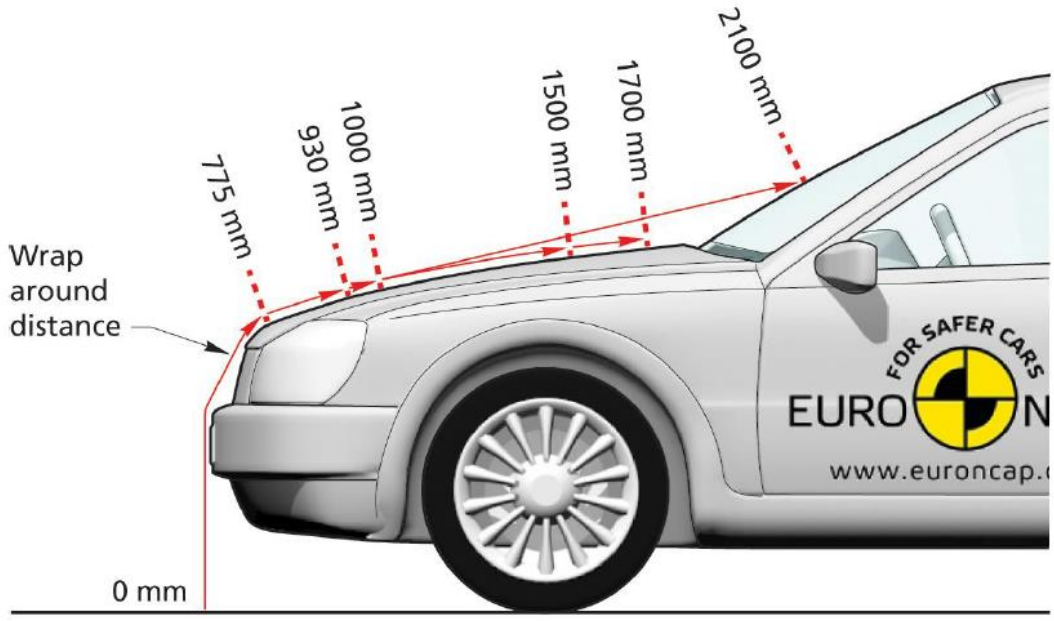

Figure 6 Marking wrap around lines (EuroNCAP, November 2017)

However, the pedestrian tests under EuroNCAP protocol still use stiff body part impactors to conduct safety assessment, which provides limited outputs, especially for organ injuries.

2.3.2.2 United Nations Economic Commission for Europe (UNECE) Regulation No. 127

Regarding pedestrian protection, the United Nation's agreement called "Agreement Concerning the Adoption of Uniform Conditions of Approval and Reciprocal Recognition of Approval for Motor Vehicle Equipment and Parts" which was decided in Geneva in 1958; it is now UNECE 127. In order to investigate the pedestrian safety performance of a motor vehicle, a pedestrian lower leg form and an upper leg form

are used to impact against the bumper, whilst a headform is impacted against the bonnet. The impact velocity of the impactor when striking all parts of the vehicle is 11.1 ± 0.2 m/s. The injury criteria used are similar with the ones in EuroNCAP, however the 2/3 of the head impact zone must not exceed a HIC of 1700, with no HIC values to exceed 2000. This is illustrated in Figure 7 (United Nations, 2012).

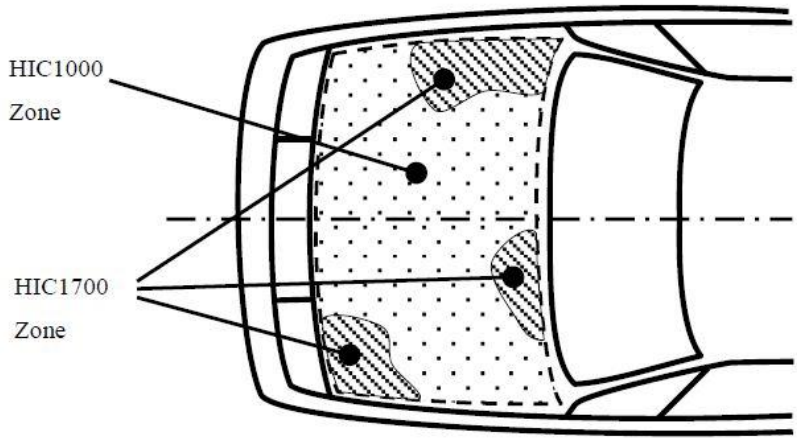

Figure 7 Example of marking of HIC1000 zone and HIC1700 zone(United Nations, 2012)

The limitation is that UNECE 127 is applied to motor vehicles of categories M1 and N1 (Vehicles in category N1 with a maximum mass not exceeding two tons (United Nations Economic Commission for Europe, 2016).

2.4 Crash Test Dummy as a Mean to Test for Pedestrians

In this section, a detailed discussion of the test instruments used in pedestrian protection protocols, as well as the ability of the testing tools to consider injuries are highlighted.

A crash test dummy is a full-scale anthropomorphic test device (ATD) that simulates the dimensions, weight proportions and articulation of the human body, and is instrumented to record data about the dynamic behavior of the ATD in simulated vehicle impacts. The 50th percentile Crash Test Dummy, or HIII, is widely used by researchers and automobile companies to predict the biomechanics, force, impact, and injury of a human being in an automobile crash. This data can include variables

such as velocity of impact, crushing force etc. during a collision for use in crash tests (Kurczewski, 2011).

Figure 8 Hybrid III 50th male pedestrian dummy (Humanetics Innovative Solutions, 2016)

In the field of pedestrian safety there are no dummies to use in full-scale tests. This is because the experiments process and dummies are not able to reproduce the pedestrian kinematics in real accidents fairly. Furthermore, the reproducibility of full-scale tests of pedestrian-car-crashes is not guaranteed (Kuehn et al., 2005, Stürtz, 1984). Despite this limitation, the HIII is not used for pedestrian assessment because of the lack of biofidelity in the lateral motion as well as an over-rigid pelvis. Consequently, testing with a HIII will provide an unrealistic and inconsistent kinematics, which is unsuitable to validate vehicle design. HIII crash test dummies are also not able to capture the detailed relevant response of the inner organs and other soft tissues during the impact. Therefore, in injury investigation research, crash test dummies are not a suitable tool.

2.5 Pedestrian Safety Testing Impactors

In order to overcome the limitation of unrepeatable crash test dummy in pedestrian safety test, rigid body part impactors are used. In this section, pedestrian test procedures and outputs using rigid body part impactors are discussed.

2.5.1 The Legform Impactor

The legform impactor was designed to represent pedestrian leg being impacted by vehicle bumper. The design philosophy of this impactor and test method was to reproduce the significant interactions between a pedestrian's leg and the car front whilst taking measurements that could be related to the risk of injury to the knee joint and the fracture of the leg bones (Lawrence and Hardy, 1998). The legform impactor consists of "femur" and "tibia" sections joined by a mechanical knee. The shapes of the sections have been simplified but have physical properties. The impactor has a 25 mm layer of heavy energy absorbing foam flesh covered with a 6 mm thick neoprene skin (Lawrence and Hardy, 1998). The test method requires the legform impactor to be propelled to strike the car front in free-flight at 40 km/h (EuroNCAP, November 2017) (Figure 9).

Figure 9 The lower leg impact in EuroNCAP pedestrian test (EuroNCAP, 2019)

The knee instrumentation reports knee bending angle and shear displacement whilst the accelerometer measures the tibia acceleration (Lawrence and Hardy, 1998, EuroNCAP, November 2017).

2.5.2 The Upper Legform Impactor

The design philosophy of this impactor and test method was to reproduce the significant interactions between a pedestrian's upper leg, or hip, and the bonnet

leading edge whilst taking measurements that can be related to the risk of femur and pelvic fractures (Lawrence and Hardy, 1998). The upper legform impactor is propelled into a stationary car so as to represent a pedestrian's accident at an initial car impact speed of 40 km/h (Lawrence and Hardy, 1998) (Figure 10).

Figure 10 The upper legform impact in EuroNCAP pedestrian test (EuroNCAP, 2019)

The front member is equipped with strain gauges to measure bending and is covered by a 50 mm thick layer of heavy energy absorbing foam to represent the flesh covering a pedestrian's upper leg.

2.5.3 The Headform Impactor

As explained in section 2.3, adult head impacts points were most frequently towards the rearward part of the top of the bonnet and wings, the windscreen frame and the windscreen. The head impacts of young children were more frequently to the frontal part of the top of the bonnet and wings (Lawrence and Hardy, 1998, Harris, 1993, EuroNCAP, November 2017). Therefore, two assessments have been included (Figure 11).

Figure 11 The headform impact in EuroNCAP pedestrian test (EuroNCAP, 2019)

One is based on an impactor representing a child headform to evaluate the forward section of the bonnet and wings and the second based on an adult headforrn to assess the rear of the bonnet, wings and the scuttle. The child headform is propelled to strike the car in free-flight at 40 km/h at an angle of 50” to the horizontal and the adult headform to strike the car in free-flight at 40 km/h at an angle of 65 o to the horizontal. Both of the headforms that have been developed for these tests are of spherical shape (to give more repeatable results), with a 7.5 mm thick silicone outer flesh. The headforms are equipped with tri-axial accelerometers. The acceptance criterion (Head Injury Criterion of 1000) is intended to prevent serious, life threatening, head injuries (Lawrence and Hardy, 1998, EuroNCAP, November 2017).

In dynamics, rigid body parts can duplicate the human behaviour in traffic accidents and repeatable in pedestrian safety test procedure. However, a lack of biofidelitic details of the human body and engineering outputs are still a great problem for injury investigation.

2.6 Human Computer Models

With the development of computing technology and application of the finite element method, detailed human models were created to overcome the deficiencies observed in pedestrian impactors, as the current test tool, cannot provide enough data for injury

investigation during an impact. Finite Element Method (FEM) or Finite Element Analysis (FEA) is a numerical method, which is used to obtain useful solution of extremely complicated structures. Initially, the finite element method was applied in aerospace only to solve linear structure problems. Nowadays, finite element method is used throughout the field of fluid mechanics, thermal mechanics and even medicine to solve complex non-linear structure to get deformation, stress and natural frequencies. The core of FE is discretisation. By dividing the real world complex structure into equivalent, smaller and easy-accessible units which are referred as elements, the question is becoming to solve the equations formulated of each unit and combine them (integration) to obtain the solution of the entire structure (Christensen, 2012). Advanced computing technology enables engineers to perform large and complicated calculations in shorter time. With these new technologies, new human computer models were created.

2.6.1 MAthematical DYnamic MOdel (MADYMO)

In 1975, Netherlands Organization for Applied Scientific Research (TNO) created a MAthematical DYnamic MOdel (MADYMO) (Schmitt et al., 2009). MADYMO is a combination of multi-body system technology and finite element technology. The MADYMO model was initially created based on the Hybrid III dummy model with biomechanical data of important body segments and areas. Modifications were made by adding elongation of the neck and the spine, and deformable leg. In MADYMO, each body segment is presented by an ellipsoid. Every ellipsoid is connected with kinematic joints (Tass International, 2016). The pedestrian models each consist of 52 rigid bodies, organised in seven configuration branches. MADYMO pedestrian model family is illustrated in Figure 12.

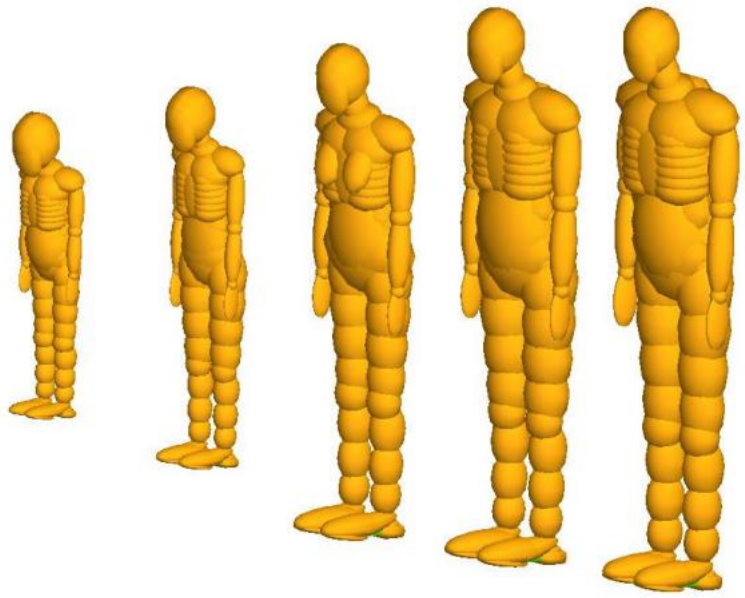

Figure 12 MADYMO pedestrian model family (Tass International, 2016)

The Madymo model is able to output forces and moments, however it does not contain organs. Consequently, no trauma can be established by computation.

2.6.2 Total Human Model for Safety (THUMS)

In 2000, the Toyota Motor Corporation and Toyota Central R&D Labs started to develop a finite element human model called the Total Human Model for Safety (THUMS) (Livermore Software Technology Corporation, 2011). The THUMS model provides a high-level of bio-fidelity using similar material property and structure to present actual human body including outer geometry, bones, muscles, ligaments, tendons, and internal organs. With such details, the THUMS 4.0 model enables engineers and scientists to obtain more detailed physical data such as stress and strain to allow the investigation of kinematics and injury mechanisms of human body in various impact scenarios (Dynamore, 2016, Livermore Software Technology Corporation, 2011, Tomoyuki and Junji 2011). The 50^{th} percentile male THUMS 4.0 human model is illustrated in Figure 13.

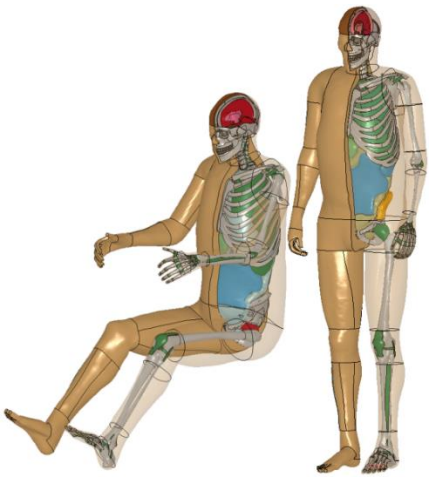

Figure 13 50th male occupant (left) and pedestrian (right) THUMS model (Dynamore, 2016)

The 50th percentile adult male (AM50) model represents an average adult with a height of 175cm and a weight of 77kg, thus leading to a BMI (body mass index) of about 25 (Toyota Motor Corporation, 2011). The model version 4.0 possesses a total number of 1.8 million elements and about 630,000 nodes. The model mainly consists of solid (hexahedrons and tetrahedrons) as well as shell elements. Discrete and beam elements are also used to model connections like tendons, ligaments and also (passive) muscles (Dynamore, 2016). The details of AM50 Version 4 pedestrian model is shown in Figure 14.

Figure 14 Details of AM50 Version 4 THUMS model (upper torso (upper left), head (upper right), knee (lower left), chest skeleton (lower right) (Dynamore, 2016)

Details of the THUMS 4.0's head, knee and chest bone structures represent the modelling details of the human soft tissue, joint and bones are presented in Figure 11. With such details, the THUMS human model enables users to compute stresses and strains observed in the human body when subjected to impacts.

2.6.3 Global Human Body Models Consortium (GHBMC)

In 2006, besides the THUMS model, the Global Human Body Models Consortium (GHBMC) was built with the purpose of creating family of virtual humans, from children to elderly. The virtual package is completed by several centres of expertise listed in Table 4.

Centres of Expertise	Body Region
Wayne State University	Head model
University of Waterloo	Neck model
University of Virginia	Thorax model
University of Virginia	Pelvis and Lower Extremities model
IFSTTAR	Abdomen model

Table 4 Centres of expertise of CHBMC model (John Combest, 2016)

In 2016, GHBMC released the 5th percentile female occupant detailed model and by 2017, all pedestrian detailed models including 5th female, 50th male and 95th male. The difference between the detailed model and simplified model is presented in Figure 15

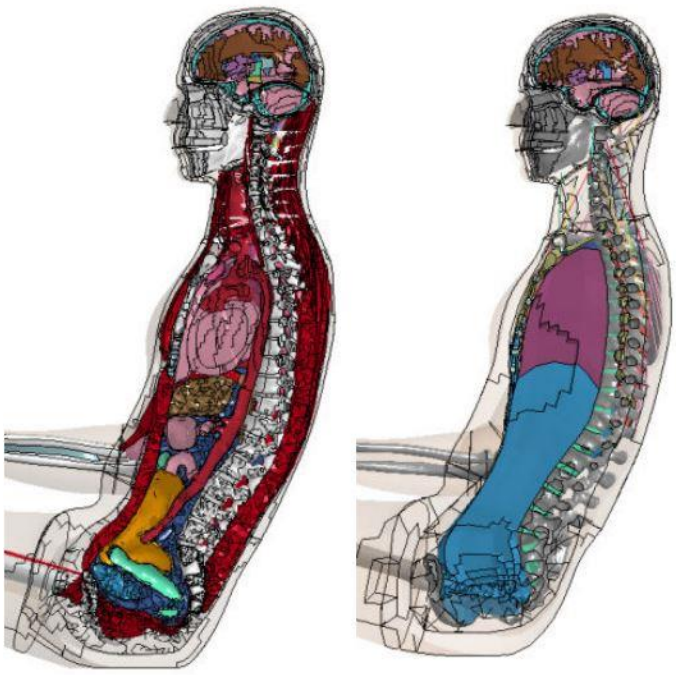

Figure 15 GHBMC detailed model (left) and GHBMC simplified model (right)(John Combest, 2016)

Considerable detail differences can be observed on the inner organs of the chest area in Figure 10. The simplified model (right) consists of 150,000 deformable elements, while the detailed model (left) consists of in-excess of 2.0m deformable elements. The GHBMC 50th percentile male (M50) occupant model also possesses more details of the inner organs compared to the simplified model, allowing more physical outputs in injury investigation. However, the simplified model is computationally more efficient, and can be preferred over the complex one for kinematics studies. As per the THUMS model, it meets a catalogue of impact force corridor responses and is able to calculate internal organ stresses and strains.

If crash test dummies have brought us a long way in occupant safety research (Bell, 2018), they cannot predict organ trauma which are observed in real-life accidents (Neal-Sturgess et al., 2007). The superior bio-fidelity of the FE human models such as THUMS and the GHBMC models provide sufficient engineering outputs for non-fatal injury investigation as well as fatal injury computation. Both THUMS and GHBMC models' force deflection responses have been validated, consequently either model can be used with confidence in safety studies (Gayzik et al., 2011, Toyota Motor Corporation, 2011). This thesis uses THUMS, for historical reasons, as Coventry

University's human computer model research's experience is in the THUMS model. This work could have been executed with the GHBMC: the methodology proposed in the thesis is transferable to any human models, which includes internal organs.

After the investigating the testing tools, the next chapter will discuss the injury evaluation indicators currently used from an engineering perspective, their respective advantages and their limitations.

2.7 Currently-used Injury Criterion

2.7.1 Acceleration-based Head Injury Criteria

Acceleration-based injury criteria are calculated based on the acceleration pulse recorded on specific parts/ areas of the body. These acceleration-based criteria are listed in Table 3, and are HIC, HPC, 3ms clip and the GAMBIT criteria.

Injury Metric	Equation	Notation
Head Injury Criterion (HIC)	$HIC = max\left\{(t_2 - t_1)\left[\frac{1}{t_2 - t_1}\int_{t_1}^{t_2}\lvert a(t)\rvert dt\right]^{2.5}\right\}$	Acceleration units are (g) and t_1, t_2 are selected from the time domain in (s) such that the value of HIC is maximized. Based on current standards, $t_2 - t_1 \leq 15$ ms
Head Protection Criterion (HPC)	Same as HIC_{36}	
3ms Criterion (A_{3ms})	Acceleration level obtained for an impact duration of 3ms.	
Generalized Acceleration Model for Brain Injury Threshold (GAMBIT)	$GAMBIT = max\left\{\left[\left(\frac{\lvert a(t)\rvert}{a_{cr}}\right)^n + \left(\frac{\lvert \alpha(t)\rvert}{\alpha_{cr}}\right)^m\right]^{\frac{1}{s}}\right\}\pi r^2$	

Table 5 Acceleration-based injury criteria

2.7.2 Head Injury Criterion (HIC)

The actual version of HIC was proposed by U.S National Highway Traffic Safety Administration (NHTSA) 1972 (Mchenry, 2004) and is included in FMVSS No.208 (Schmitt et al., 2013). As explained in Table 5, $t_2 - t_1$ is a time interval during the acceleration pulse. The result is called HIC_{15}, if Δtmax is no more than 15 ms, while HIC_{36} refers to a window of Δt max not exceeding 36 ms. FMVSS No. 208 requires the HIC time interval to be 36ms (thus called HIC_{36}). In 1998, NHTSA also introduced HIC_{15}

(Schmitt et al., 2013) usually used for high speed impacts exceeding 6.5m/s. A maximum HIC_{36} not exceeding 1000 is suggested for 50^{th} percentile male and HIC_{15} of 700 for a 50^{th} percentile male. However, research indicates that only HIC intervals of 15 ms or less are relevant to cerebral concussion (Hodgson and Thomas, 1972, Mertz et al., 1996)

As for the limitation of HIC, HIC is an effective criterion for head injuries correlated with linear acceleration, such as skull fractures, however not considering for rotational acceleration. As such, it is often criticised. A further drawback is the lack of functional relationship between the human head injury and the acceleration response measured with an anthropomorphic test device (Schmitt et al., 2013). Also as an injury indicator, HIC correlates to the risk of AIS ≥ 2 skull fracture (Mertz et al., 1997).

2.7.3 Head Protection Criterion (HPC)

The Head Protection Criterion (HPC) is the equivalent to HIC used in the European market. It is required in regulation ECE R94 and R95. Consequently, HPC is used to quantify head impact in both frontal and lateral impact (Schmitt et al., 2013). The definition and calculation method of HPC is identical to HIC_{36}. The corresponding HPC threshold is 1000 in frontal and lateral impacts (Schmitt et al., 2013).

2.7.4 3ms Criterion (A_{3ms})

The 3ms Criterion is defined as the acceleration level obtained for an impact duration of 3ms (Schmitt et al., 2013). A_{3ms} should not exceed 80g for a 3ms duration (Got et al., 1978). This threshold is also incorporated in ECE R21 and R25, which are regulations dealing with impact of occupant to interior structure of a vehicle and the impact to the head restraints (Schmitt et al., 2013).

2.7.5 Generalized Acceleration Model for Brain Injury Threshold (GAMBIT)

Generalized Acceleration Model for Brain Injury Threshold (GAMBIT) was proposed in 1985. It combines rotational acceleration and translational acceleration assuming that a combined load case of rotational and translational acceleration can cause head injury (Schmitt et al., 2013). To date, GAMBIT still lacks validation and is therefore hardly ever used, nor is it included to date in any regulations (Schmitt et al., 2013).

2.8 Kinematic Rotational Brain Injury Criterion

Head rotation as a mechanism for brain injury was proposed back in the 1940s. Since then a multitude of studies by various institutions were conducted to confirm/reject this hypothesis (Takhounts et al., 2011). BRIC (BRain Injury Criterion) and RIC (Rotational Injury Criterion) have been proposed as Mild Traumatic Brain Injury (MTBI) predictors. Both predictors had been only verified with football players' head impact data (Kimpara and Iwamoto, 2012, Takhounts et al., 2013). The calculation method of BRIC and RIC are listed in Table 6.

Injury Metric	Equation	Notation
Rotational Injury Criterion (RIC)	$RIC = max\left\{(t_2 - t_1)\left[\frac{1}{t_2 - t_1}\int_{t_1}^{t_2}\lvert\alpha(t)\rvert dt\right]^{2.5}\right\}$	A constraint of t_2-$t_1 \leq 36$ ms was proposed for RIC
Kinematic Rotational Brain Injury Criterion (BRIC)	$BRIC = \frac{\omega_{max}}{\omega_{cr}}$ (Takhounts et al., 2013)	ω_{max} is the maximum resultant angular velocity of centre of gravity of the Anthropometric Test Dummy (ATD). ω_{cr} is the critical values of maximum angular velocity.

Table 6 Calculation method for BRIC and RIC (Takhounts et al., 2011, Kimpara and Iwamoto, 2012)

2.8.1 Head Impact Power (HIP)

The Head Impact Power (HIP) injury criteria was proposed in 2000 (Newman and Shewchenko, 2000), assuming the head to be a one mass structure. HIP is computed using both linear and angular accelerations measured at the centre of gravity of a Hybrid III dummy head as:

$$HIP = \underbrace{C_1 a_x \int a_x dt + C_2 a_y \int a_y dt + C_3 a_z \int a_z dt} + \underbrace{C_4 a_x \int a_x dt + C_5 a_y \int a_y dt + C_6 a_z \int a_z dt}$$

The C_i coefficients are set as the mass and appropriate moments of inertia for the human head: $C_1 = C_2 = C_3 = 4.5$ kg, $C_4 = 0.016$ N.m.s², $C_5 = 0.024$ N.m.s², $C_6 = 0.022$ N.m.s². The values a_x, a_y and a_z (m.s^{-2}) are the linear acceleration components along the three axes of the inertial reference space attached to the dummy head. The terms α_x, α_y and α_z (rad.s^{-2}) are the angular acceleration components around the three axes of the inertial reference space attached to the dummy head (Newman and Shewchenko, 2000).

Since the HIP is a time-dependant function, the value taken as an injury predictor candidate is the maximum value reached by this function. The algorithm has been implemented and only validated using the results provided on the same footballer cases as the ones used in the present study (Newman and Shewchenko, 2000). The HIP criteria was designed only for brain injury and not for subdural haematoma (SDH) or skull fracture (Marjoux et al., 2008).

2.9 Injury Metrics on Human Internal Organs

2.9.1 The Acceleration Criterion

The Acceleration Criterion is best known for its application in whole-body response studies and in the assessment of chest injury potential in frontal impacts. The theoretical basis of using acceleration as an injury criterion is Newton's second law, which states that the force on a rigid mass is proportional to its acceleration (Lau and Viano, 1986). The human torso is far more complex than a rigid mass, and body deformation plays a very important. Such deformation cannot be accounted for by the Acceleration Criterion, and injury can be induced well before the peak is reaching in the acceleration response. Since acceleration cannot be measured on soft tissues as a practical matter, the usefulness of the Acceleration Criterion is restricted to predicting the severity of skeletal injury. In practice, the acceleration of the spine indicates the initiation of back movement of the torso (Lau and Viano, 1986).

2.9.2 The Force Criterion

The reactive force tends to be an aggregate response of the inertial, the elastic and the viscous components of the torso (Lobdell et al., 1973). The Force Criterion does not delineate the mechanism of injury fully because of the variable contributions of the inertial, elastic and viscous components that contribute to the force measurement (Lobdell et al., 1973).

2.9.3 The Compression Criterion

As evidenced from accumulated cadaver experiments, it became apparent that spinal acceleration or impact force did not adequately predict the risk of internal injuries which tended to pose greater threats toward occupant survival (Lau and Viano, 1986). Based on blunt thoracic impact experiments using cadavers, it was found that maximum chest compression was a superior indicator of chest injury severity (Kroell et al., 1971, Kroell et al., 1974). Sternal impact was shown to compress the chest until rib fractures began. The reactive force induced by the impact, which was transmitted across the rib cage to the spine, subsequently induced spinal acceleration and movement (Lau and Viano, 1986). Spinal acceleration did not predict injury severity adequately (Kroell et al., 1971, Kroell et al., 1974), however, the first integral of the spinal acceleration, which is a reflection of the relative chest velocity of deformation, correlated almost as well as normalized compression with injury severity (Nahum et al., 1975). A maximum allowable compression of 32% was recommended (Viano, 1978). Latest analysis indicates that 40% of maximum chest compression corresponds to a 50-50 chance of the occupant sustaining severe cage stability (Lau and Viano, 1986). Nowadays, it has been evidenced that injuries at even moderate impact velocity can occur well before maximum compression, which is an issue not addressed by the Compression Criterion (Lau and Viano, 1986).

2.9.4 The Viscous Criterion (VC)

Since vital organs, such as the heart, the lung, the liver and the central nervous system are soft tissues, understanding their mechanism is critical to the improvement of occupant protection systems. Over the years of research, it has become clear that soft tissue injury is induced by excessive deformation that is rate sensitive (Lau and Viano, 1986). Therefore, acceleration of a bony structure does not address the mechanism of

soft tissue injury and cannot be a good injury criterion for it. Since soft tissue can be injured by excessive deformation, the Compression Criterion does address one of the mechanisms of injury (Lau and Viano, 1986). The VC, on the other hand, representing any generic biomechanical index of injury potential for soft tissue, is defined by the rate sensitive torso compression. Viscous response is a time function formed by the product of the velocity of deformation, v(t), and the instantaneous compression C(t) (Lau and Viano, 1986). The deformation is the instantaneous deformation along the direction of the applied impact to the torso. C(t) is the ratio between deformation and the Initial torso thickness (Figure 16). As C(t) is a dimensionless number, therefore VC has the same unit as v(t).

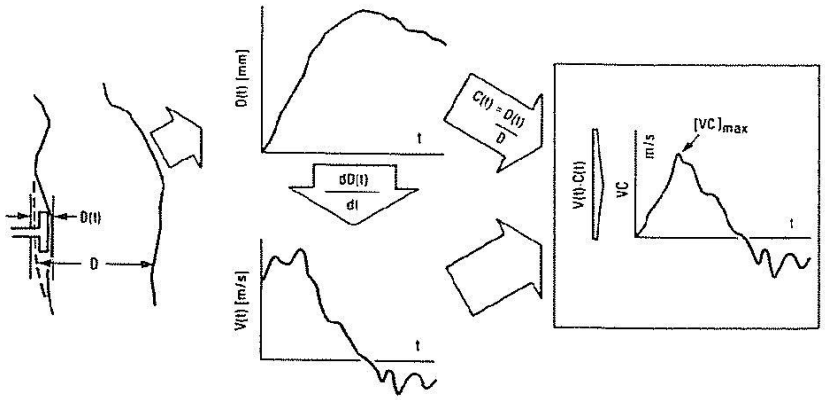

Figure 16 Viscous Criterion defined by the instantaneous deformation(Lau and Viano, 1986)

The Acceleration Criterion, Compression Criterion and Viscous Criterion have different but complementary roles to play as injury predictors. Although the Acceleration Criterion has only a minimal basis on skeletal forces and injuries, it is least dependent on the impact location and is a reasonable indicator for the whole body response and the general severity of the crash. The Compression Criterion becomes inadequate when the velocity of deformation exceeds 3 m/s (Lau and Viano, 1986). Scenarios where the VC may be the most sensitive index of soft tissue injury in an automobile crash environment include an unrestrained occupant in a frontal crash, a restrained or an unrestrained occupant in a lateral impact, and impact by inflatable restraint deployment against an occupant directly above it (Lau and Viano, 1986). From an energy perspective, VC can be expressed as production of deformation and the rate

of deformation which shares the same concept as Peak Virtual Power (PVP) (Neal-Sturgess, 2001) which will be discussed later on in the thesis.

2.9.5 Strains at Organ Level

At organ and tissue level, strain was proposed as a metric for injury based on cadaver tests (Yamada and Evans, 1970, Melvin et al., 1973), as shown in Table 7. Human Computer models, like THUMS 4.0, lists its internal organ trauma tolerance to meet also the same requirements as Table 7.

Body Part	Criteria	Threshold	Reference
Brain contusion	Maximum principal strain	>30%	(Ward et al., 1980)
Diffuse Axonal Injury (DAI)	Maximum principal strain	>21%	(Bain and Meaney, 2000)
Heart	Maximum principal strain	30%	(Yamada and Evans, 1970)
Liver	Maximum principal strain	30%	(Melvin et al., 1973)
Spleen	Maximum principal strain	30%	(Melvin et al., 1973)
Kidney	Maximum principal strain	30%	(Melvin et al., 1973)

Table 7 Strain threshold at organ level

Strain based indicators aim to describe the deformation of the body during the impact. Plastic strain is used as the criterion in bone fracture, but principal strain is often used in soft organ injury studies. This assumption is nevertheless not correct. In the human body injury, elastic strain decreases when the load is decreasing, however plastic strain remains, i.e., injury remains although the impact pulse is removed. Consequently, in concept, elastic strain based indicators are different to human body

injury. Also, time effects, or strain rates, are not considered when using strain as an injury indicator. Considering the Eiband injury graphs (Shanahan, 2004), injuries are linked with impulse duration, hence a time dependency factor is necessary when computing trauma.

2.10 Energy Dissipation Process during an Accident and Peak Virtual Power (PVP)

In order to overcome the dilemma of linking injury severity (AIS) and engineering outcome, an energy-based concept was proposed in 2001 (Neal-Sturgess, 2001). This method is based on the Clausius-Duhem Inequality, from the rate dependent form of the 2nd law of thermodynamics, which considers that irreversible work in a human body is equivalent to injury. As previously described, current injury metrics would increase during the impact and then reduce when impact stops. Power, as a metric of work, is also going up and down during the time history; however peak power is taken as the unique value throughout the time history. PVP relates to the cumulative power sustained by an organ and is computed as being the cumulative or memory product between stress and strain rate for each finite element of each organ (Neal-Sturgess, 2001). At organ (micro) level, the equation of calculating PVP is:

$$PVP = maximum\ (\sigma \cdot \dot{\varepsilon})$$

Equation 1 PVP calculation

Based on the Hooke's Law, there are several candidates which can be used to calculate PVP including plastic strain, principal strain and Von Mises stresses and strains. The Plastic stress/strain indicates the stress/strain tensor, which occurs in the plastic stage of the material when its yield stress is exceeded. In the plastic range, the initial state is not restored after the load is removed. Internal organs generally have a low Bulk Modulus (Neal-Sturgess, 2001), as they are either water or collagen based. This is the reason why these internal organs are modelled as nearly incompressible visco-elastic materials. This means that inner organs exhibit both viscous and elastic characteristics when undergoing deformation. Under high strain-rate deformation, visco-elastic materials behave essentially as elastic, as there is no time for recovery to take place.

In such instance, considering only plastic stress to calculate PVP at organ level is incorrect.

Principal stress, on the other hand, is the stress acting on main or principal plane where shear stress is zero. Maximum principal stress is the maximum value amongst all principal stresses, however biomechanical injuries result in the separation (fracture, shearing, tearing or rupture) of biological tissues. Ignoring shear stress in injury investigation is also incorrect (Neal-Sturgess, 2001). The Von Mises stress is a vector resultant and a mathematical-derived equivalent stress, which follows the general expression in Equation 2, where σ_1, σ_2 and σ_3 are the 1st, 2nd and 3rd principal stresses and σ_{12}, σ_{23}, σ_{31} the shear stresses:

$$\sigma_v = \sqrt{\frac{1}{2}[(\sigma_{11} - \sigma_{22})^2 + (\sigma_{22} - \sigma_{33})^2 + (\sigma_{33} - \sigma_{11})^2 + 6({\sigma_{12}}^2 + {\sigma_{23}}^2 + {\sigma_{31}}^2)]}$$

Equation 2 General form of Von Mises stress

It can be observed that the Von Mises stress tensor contains shear stress terms expressed as the differences between the principal stresses, therefore it can be used to represent the tearing of soft tissues. As Von Mises stress is usually used as a yield criterion for plastic deformations, it is the most appropriate candidate to derive PVP in complex loading situations, as it can capture all the loading scenarios.

The second part of Equation 1will use the strain rate computed from the strain value generated by the Von-Mises stress (same equations as table 5, but with the strain components instead of stress) differentiated against time. The ultimate value from the function multiplying these 2 entities is the PVP, which is linked with AIS (Neal-Sturgess et al., 2001).

Since PVP takes the peak value of virtual power, which is the monotonically increasing throughout the time history, PVP shares the same concept with injury on the human body. Theoretically, PVP is capable of injury prediction, which this thesis will aim to investigate. The previous work linked PVP to the cubic of the velocity for belted drivers (coupled system) and the square of the velocity for an unbelted driver (uncoupled system) (Neal-Sturgess et al., 2001). However, the relationship between PVP and

impact speed has not been fully validated for pedestrians yet and will be also answered later in the thesis

2.11 Research Gap and Direction

In the current pedestrian safety regulation, the rigid test instruments can only provide limited engineering outputs, which have limited meaning in real-life. These devices are unable to provide sufficient information for detailed injury investigation at organ and tissue level to state whether trauma has occurred and to what level was reached. Human models, which consist of enough biofidelitic details of human body, are only included in the pedestrian test to assess the deployment timing on pedestrian active bonnets (EuroNCAP, November 2017), but not to calculate pedestrian trauma, as not numerical methos is to date able to do.

Under the current pedestrian assessment procedure, HIC, chest acceleration and chest velocity are the most widely used injury criterion on the human body, when using a crash test device. Strain is the mostly acceptable injury indicator on organ injury, as recommended by human body model manufacturers. However, the most critical point of the literature review is that there is no direct link between risk of life and injury criterion (mechanical or strain based). Therefore, the proposed research direction, which is unique, can be summarised as correlating an engineering indicator (PVP) against injury severity (AIS), and therefore ISS, by using the finite element technique. To fill this gap, the aim of this study can be expressed as “to define and use a physical indicator (PVP) to predict human injury severity by deriving a relationship between PVP, injury severity (AIS) and ISS”.

Worldwide, statistical data shows that pedestrian casualties still represent a large portion of road traffic mortality. Compared to occupants, pedestrians sustain more multiple injuries, with concomitantly higher injury severity scores and mortality. This study will therefore focus on pedestrian accidents and will investigate whether improved trauma predictions could be found in order to complement current pedestrian safety testing protocols.

3.0 Methodology

The methodology used in this research is split in two phases. The first phase will define an organ and tissue traumatology model (OTM). The second phase will validate this OTM model based on the real-world accident reconstruction information provided by the UKPF. The OTM procedure of phase I is illustrated in Figure 17.

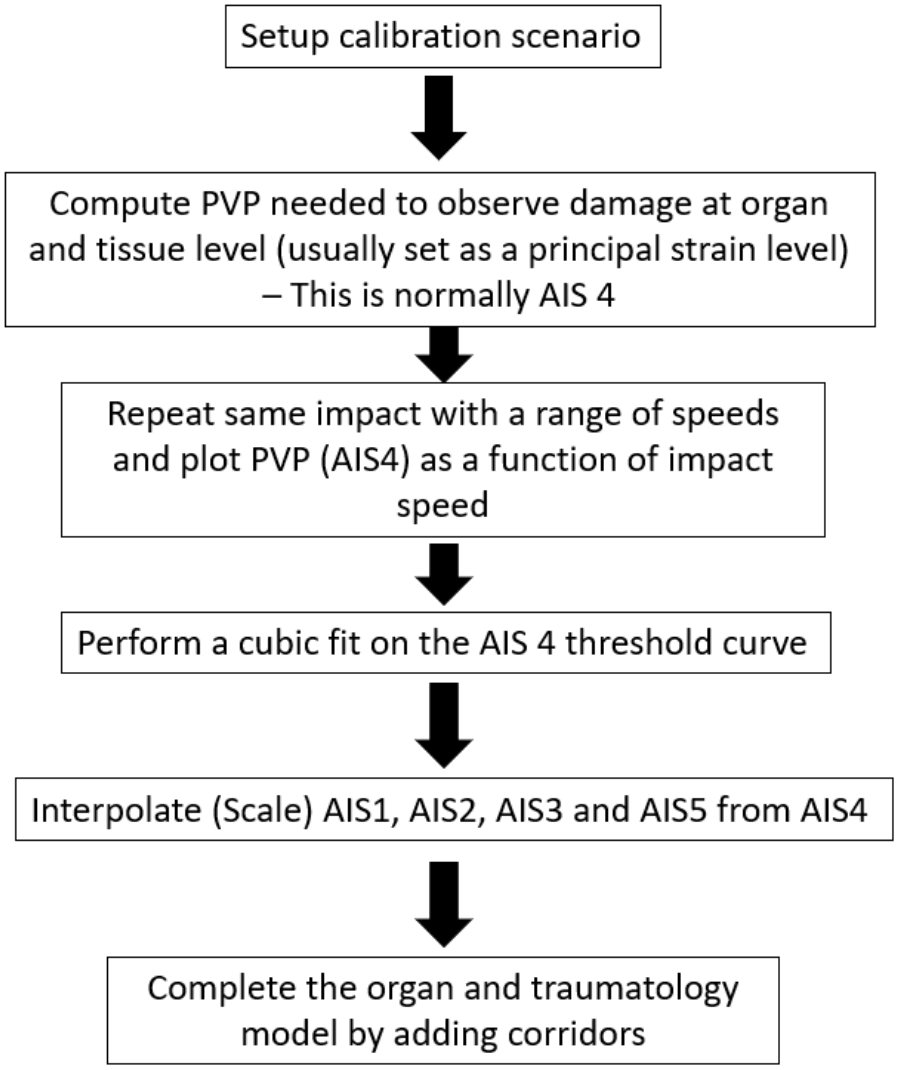

Figure 17 PHASE I: Organ Traumatology Model (OTM)

The research will investigate the traumatology of the brain tissue and critical organs in pedestrian impact scenarios and focus more particularly on the white matter, grey matter, heart, liver, spleen and the kidneys. The base calibration method will be applied on the THUMS head model, which will be impacted in three strategic locations (frontal, lateral and occipital/rear), as documented by previous research (Bastien et

al., 2018). Once the calibration settings method is complete, it will be extended to all the other critical organs. The organ calibration will be conducted using a similar configuration as Kroell (Kroell et al., 1971) which is using a linear impactor. The organ calibrations will also include frontal, lateral and rear impacts. The velocity increments ranging from 2m/s to 20m/s will cover the impact velocity documented in the United Kingdom Police Force (UKPF) accident reports

For each impact velocity in a defined scenario (frontal, lateral and rear), the PVP of the first element in an organ or tissue reaching the critical level listed in Table 7, known as the critical “trauma point” using maximum principal strain, has its PVP value extracted at the time and plotted as a function of impact speed. Normally, this recorded element represents an AIS 4 injury of this organ or tissue. The next stage will then to capture the intermediate and ultimate AIS levels (AIS 1, AIS 2, AIS 3 and AIS 5), as well as their level of uncertainty.

Due to the limit number of accidents, it is not possible to perform a statistical study to obtain the full spectrum of AIS corridors, therefore a mathematical method will be used to extract these corridors of uncertainty. Various studies, collected from previous clinical research (Neal-Sturgess, 2010), have recorded the relationship between AIS and the risk to life. This data is plotted in Figure 18, and contains data from Baker, CCIS, NASS and Walder (Ulman and Stalnaker, 1986).

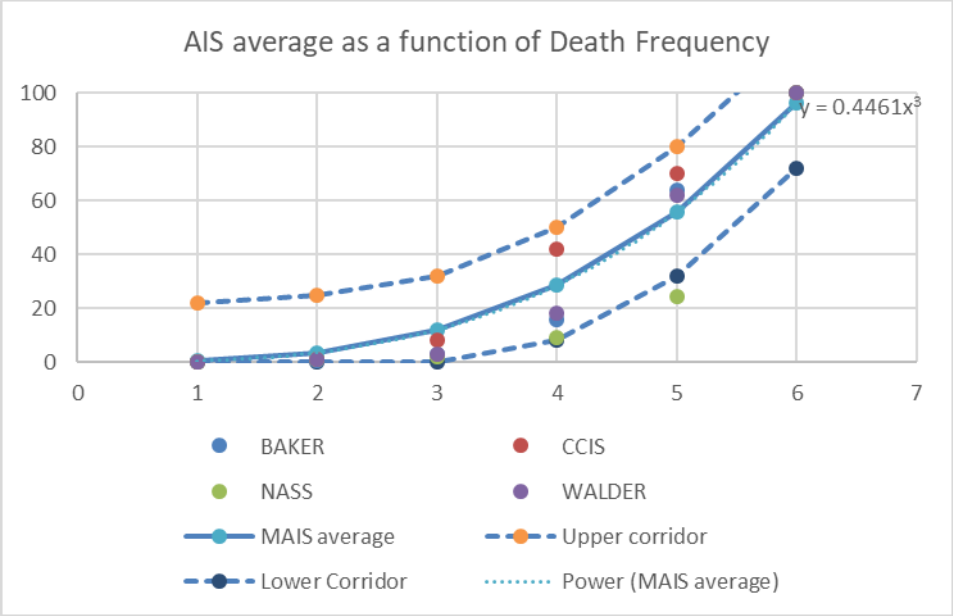

Figure 18 Curve fitting of MAIS and Probability of Fatality

In order to remove the bias from each study, all the results were averaged and interpolated with a cubic relationship as well as including a 95% confidence level corridor, as illustrated in Figure 18 (Neal-Sturgess, 2002). It was observed that the risk to life and the probability of death were related by a cubic ($R^2 > 0.95$). At this point it is important to note that the cubic fit does not aim at interpolating between the AIS values, which are ordinal values. The cubic relationship confirms that at the ordinal AIS values, the relationship between trauma levels is a cubic in the "frequency of death". Consequently, the relationship between the probability of fatality of MAIS level can be expressed as:

$$Probablity\ of\ fatality\ = a * MAIS^3$$

If the MAIS level is specified, then:

$$Probablity\ of\ fatality\ of\ MAIS5 = a * MAIS5^3$$

$$Probablity\ of\ fatality\ of\ MAIS4 = a * MAIS4^3$$

Consequently:

$$\frac{Probablity\ of\ fatality\ of\ MAIS5}{Probablity\ of\ fatality\ of\ MAIS4} = \frac{MAIS5^3}{MAIS4^3} = \frac{125}{64}$$

Hence, the ratios to extract AIS3, AIS2 and AIS1 from AIS4, as a reference, are 27/64, 8/64 and 1/64 respectively.

The AIS tolerance corridors based on the clinical studies illustrated in Figure 18, now tabulated in Table 8. This is then concluding the OTM trauma model generation (PHASE I).

MAIS level	Tolerance bound
1	+/- 21%
2	+/- 20%
3	+/- 20%
4	+/- 20%
5	+/- 23%

Table 8 Tolerance bounds of each MAIS level

Phase II will follow PHASEI and validate the OTM model using the real-world accident data provided by UKPF. The procedure is presented in Figure 19.

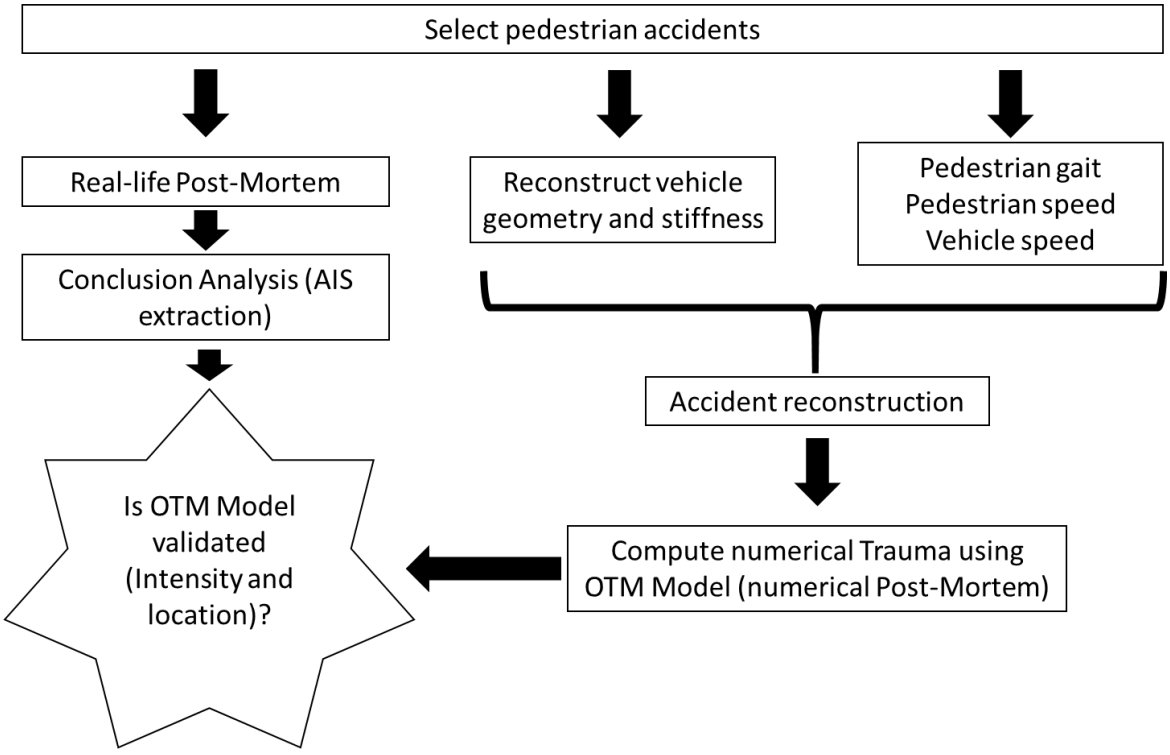

Figure 19 PHASE II. Validation of OTM trauma model

To do so, four accidents have been provided by the UKPF. For each accident, the real-life trauma is extracted from the Post-Mortem provided by the Coroner. The accident

is numerically reconstructed using Finite Element, using the THUMS 4.0 model, and the numerical trauma computed using the calibrated OTM model from Phase I.

In order to validate the OTM method, the trauma intensity (AIS level) and trauma location will be compared to the real-life trauma extracted by post-mortem (PM) to see if it is possible to predict real-life pedestrian trauma using an Engineering indicator which is PVP.

4.0 PVP Baseline Calibration

4.1 Convergence Investigation

Before the calibration tests start, a convergence study was performed in order to capture the most adequate output sampling rate to compute a consistent trauma injury

4.1.1 Explicit Finite Element Analysis (FEA) and Stress Wave Propagation

4.1.1.1 Fundamental of explicit computation

Explicit Finite Element codes were developed in 60s and 70s at DoE Lab in USA (Bastien, 2015). Explicit computing was invented by John Hallquist around 1987 (Department of Mechanical Engineering–Engineering Mechanics, 2018). The basic steps of the methods start with the base Newton's Second Law (Equation 3)

$$[M]\{\ddot{x}\} + [k]\{x\} = \{f_{ex}\}$$

Equation 3 Explicit method

The equation can be rearranged as:

$$[M]\{\ddot{x}\} = \{f_{ex}\} - [k]\{x\} = \{f_{ex}\} - \{f_{in}\}$$

Solution for the rearranged equation is:

$$\ddot{x} = \frac{(f_{ex}) - (f_{in})}{M}$$

Equation 4 Acceleration of explicit method

Using Equation 4, it is possible to extract the velocity and the displacements of all the nodes in the CAE model by integrating the acceleration. The integration constant is called the timestep and is noted Δt. Velocity and displacements are computed as per Equation 6.

Then the velocity and the displacements are computed as below:

$$\dot{x}_{n+1} = \Delta t \cdot \ddot{x}_{n+1} + \dot{x}_n$$

$$x_{n+1} = \Delta t \cdot \dot{x}_{n+1} + x_n$$

Equation 5 Velocity and displacement from explicit method

It can be observed that if the timestep Δt increases too much, hence producing quicker runtimes, then there is a risk of computation stability and accuracy (Bastien, 2015).

4.1.1.2 Model Computational Time Step; the influence of stress wave

In an impact scenario, the velocity of stress wave traveling in a structure is calculated as:

$$C = \pm\sqrt{\frac{E}{\rho}}$$

Equation 6 Stress wave velocity in explicit method

Where, E is Young's Modulus and ρ is density.

The stress wave velocity is constant until the yield stress is reached. The positive and negative sign indicates that the stress wave can travel in both direction (compression or elongation). According to the Coulomb criterion, the model computational time step of a structure is defined as:

$$\Delta t_{model} = \frac{l}{C}$$

Equation 7 Computing time step in explicit method

Where, l is the mesh element size in the structure, here the THUMS 4.0 human model

The model computational time step of THUMS pedestrian model is $4.44e^{-7}$s. In standard automotive crash simulations, the timestep Δt is around $10e^{-7}$s down to $8e^{-7}$s (Bastien, 2015), hence the timestep from the THUMS model is small for standard industrial applications but believable.

In order to compute an injury, computer output, based on a defined sampling rate, must be requested. The data extraction sampling rate cannot be less than $4.44e^{-7}$s as it would not make any sense. For optimised accuracy, the data extraction sampling rate does not need to be necessary to be too small, as it will affect runtime and output file size, which will make the post-processing unnecessary difficult. Therefore, it is

necessary to find out the optimised data extraction sampling rate which can achieve a balance between computational time, result accuracy and post-processing time.

4.1.2 Convergence Investigation

A convergence investigation was performed on the THUMS head. This choice was made because of the reduced size of the model, as well as containing many sub-components with a wide range of material properties. The THUMS' pedestrian head model was isolated and impacted against a rigid wall. In order to find the most suited sampling rate values, some sample rates between $1.0e^{-2}$s to $1.0e^{-5}$s were investigated. For each sampling rate, Von-Mises stress, Von Mises strain and Von Mises strain rate were calculated and plotted on a randomly chosen shell element (88139183), as presented in Figure 20 and Figure 21.

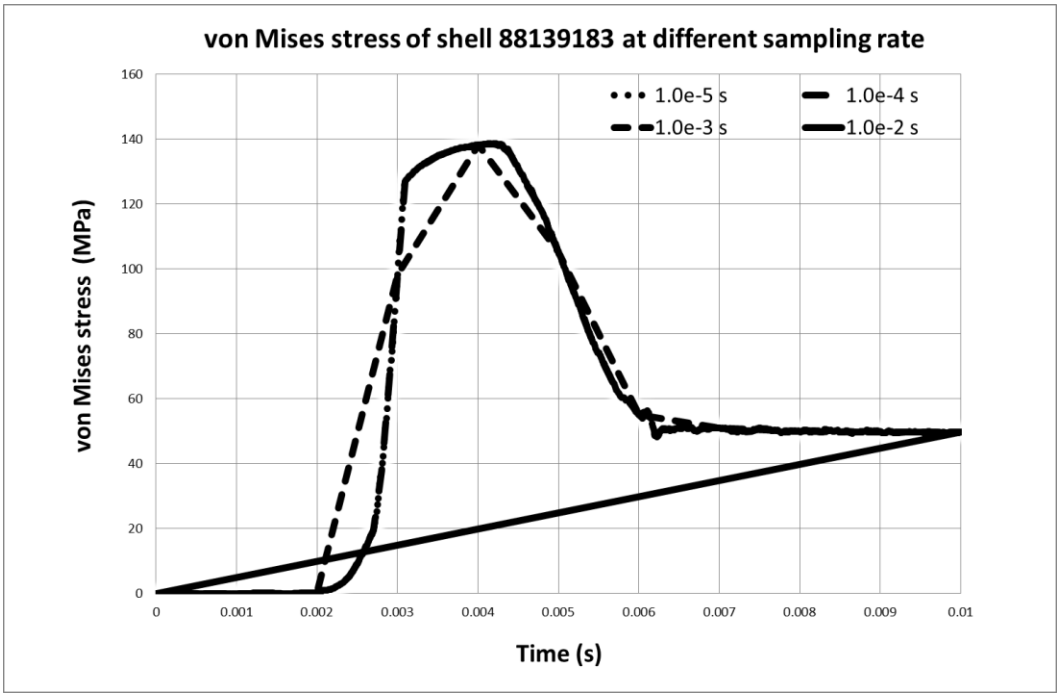

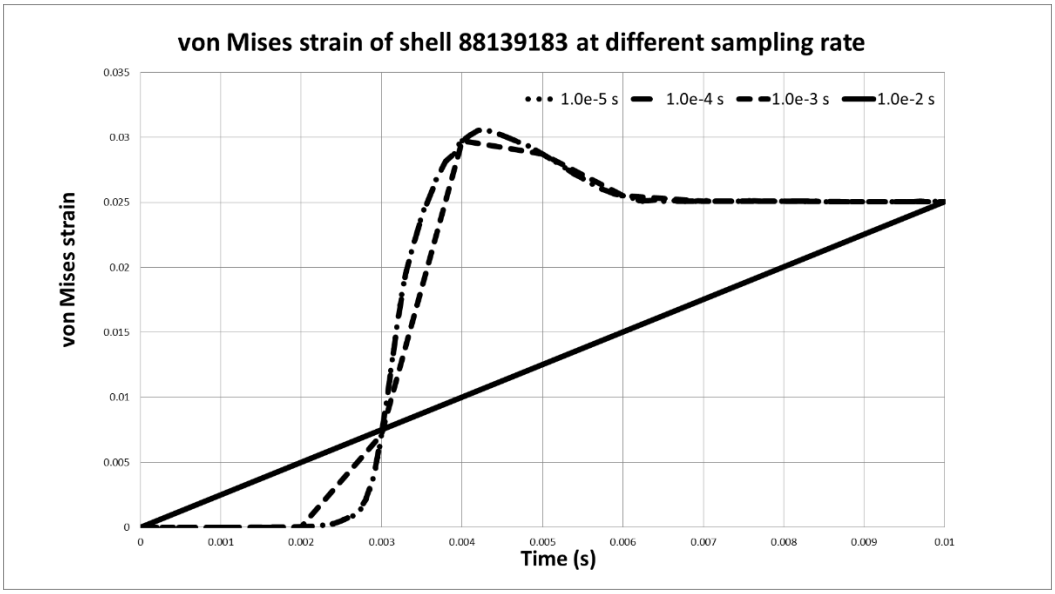

Figure 20 von Mises stress (upper) and strain (bottom) extracted on shell 88139183 at different sample rate

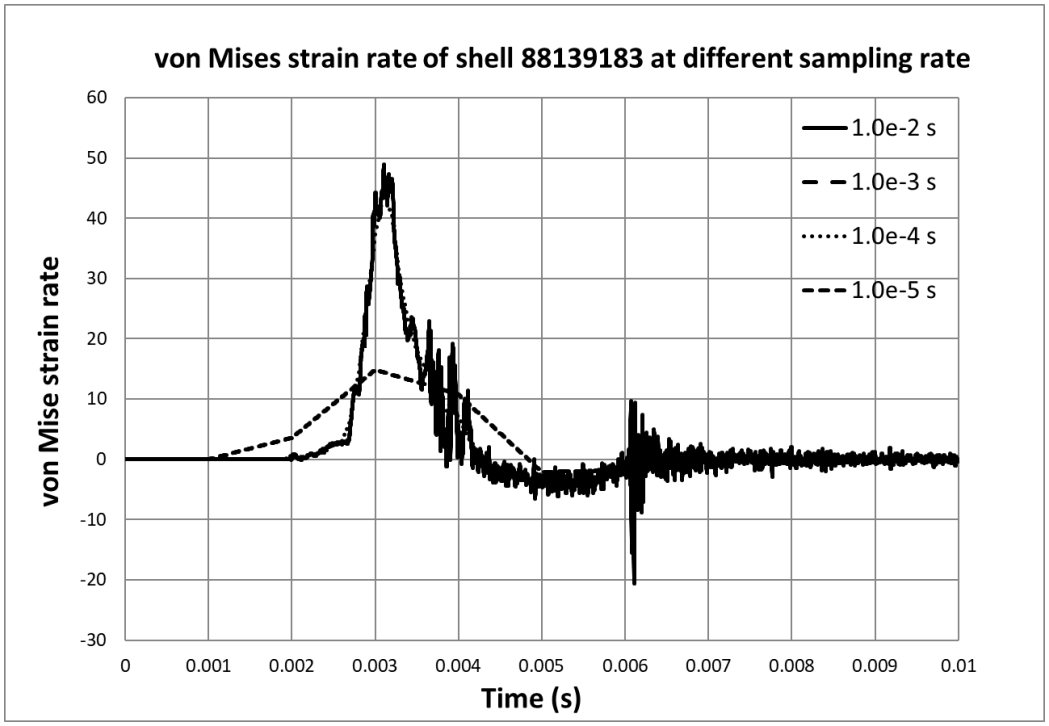

Figure 21 Von Mises strain rate of shell 88139183 at different sampling rate

In Figure 20, noticeable differences can be observed on the results for the sampling rates $1.0e^{-2}$s and $1.0e^{-3}$s. Von Mises stresses and strains overlap for a sampling rate of $1.0e^{-4}$s and $1.0e^{-5}$s therefore, four curves are displayed but only 3 curves are distinguishable. In the case of Figure 21, also noticeable differences can be observed on the results at sample rates of 1.0e-2s and 1.0e-3s. Strain rate at a sampling rate of $1.0e^{-5}$s is the finest curve. Strain rate at sampling rate of $1.0e^{-4}$s can represent most of features of the curve. The same procedure was performed on another shell element (88139193) which has same material property as 88138183. Data extracted on shell 88139193 at different sample rate is pictured in Figure 22.

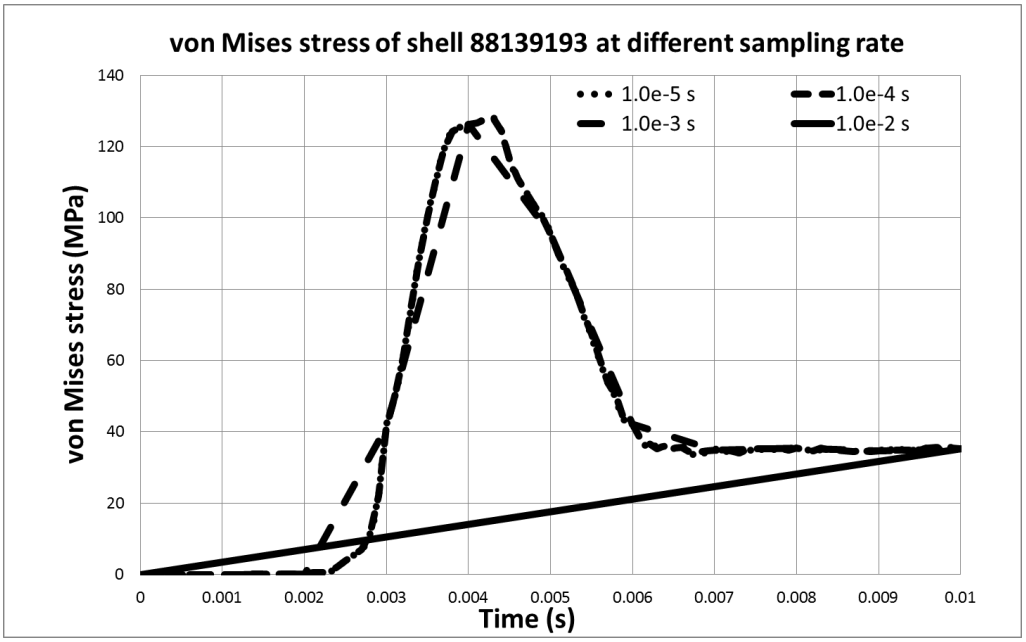

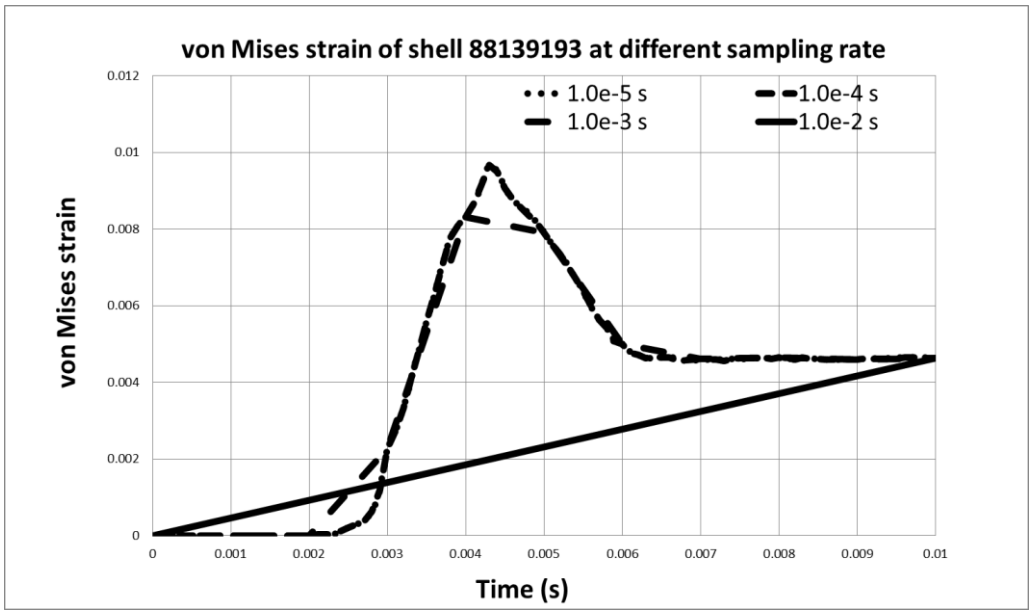

Figure 22 Von Mises stress (upper) and strain (bottom) extracted on shell 88139193 at different sample rate

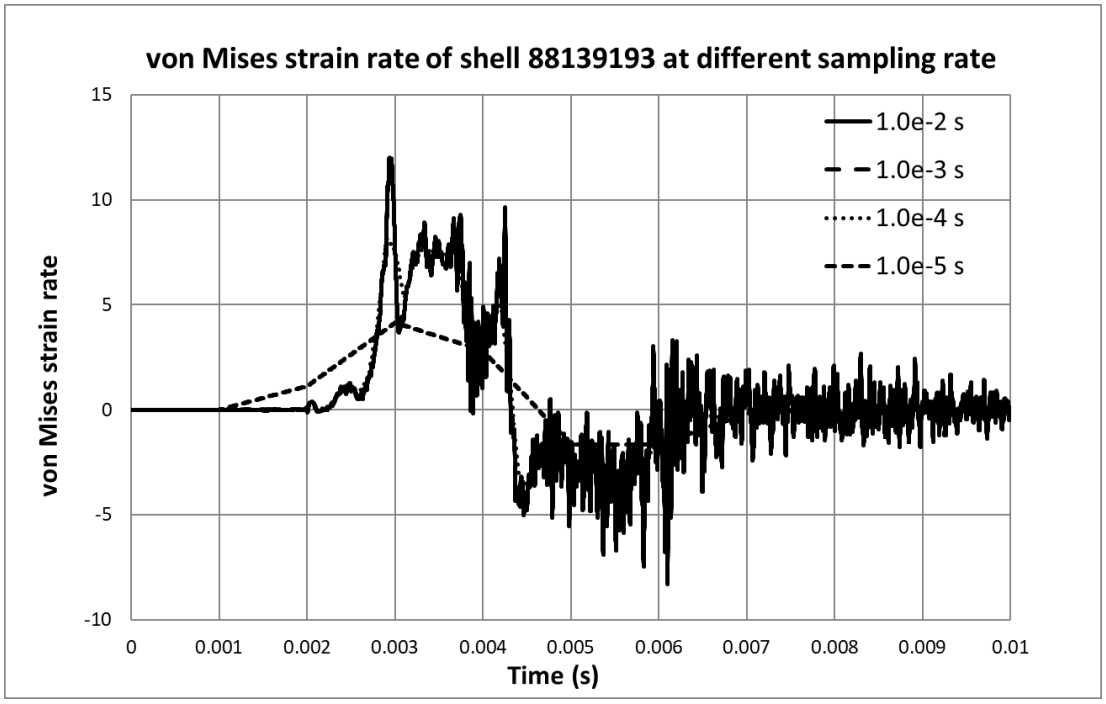

Figure 23 Von Mises strain rate of shell 88139193 at different sampling rate

In Figure 22, Von Mises stresses and strains of shell element 88139193 again show noticeable differences for sampling rates of $1.0e^{-2}$s and $1.0e^{-3}$s. Von Mises stress and strain overlap at sampling rates $10e^{-4}$s and $10e^{-5}$s;again only 3 curves can be identified. In Figure 23, as for shell 88139183, great differences can be observed on the results at sample rate of 1.0e-2s and 1.0e-3s. Strain rate at sampling rate of 1.0e-5s is the finest curve. Strain rate at sampling rate of 1.0e-4s can represent most of characters of the curve. The same procedure was applied under the sampling rate of $2.0e^{-4}$s and $5.0e^{-4}$s (Figure 24 and Figure 25) to refine the sampling rate estimation.

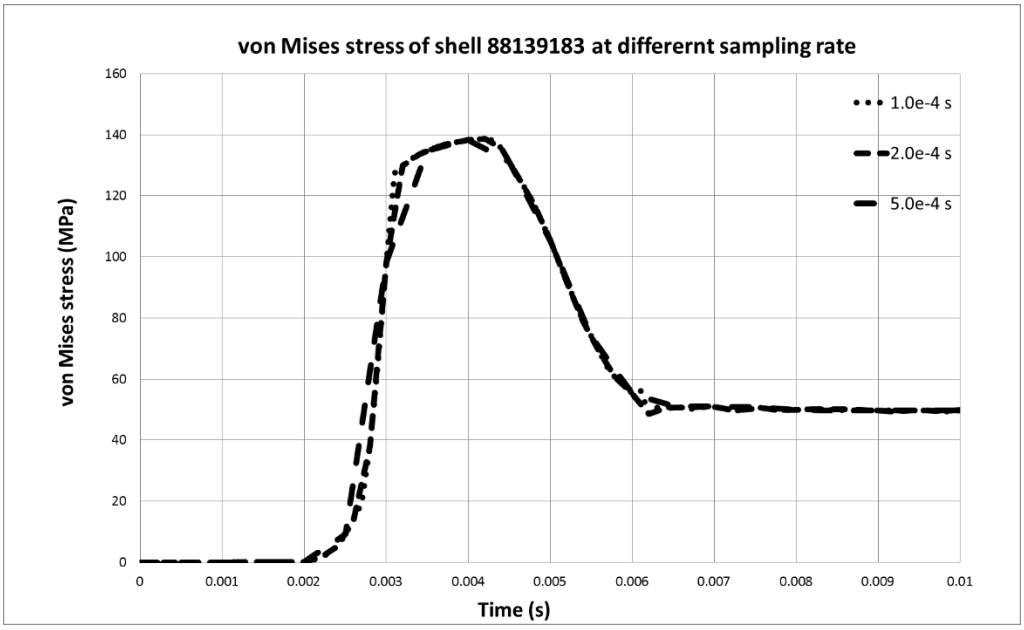

Figure 24 von Mises stress of shell 88139183 at different sample rate

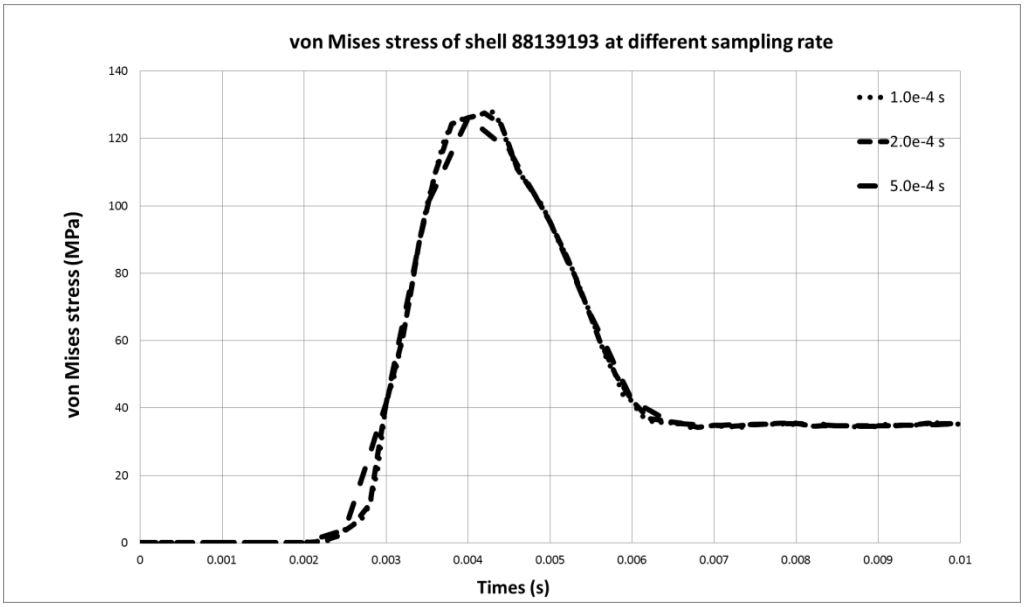

Figure 25 von Mises stress of shell 88139193 at different sample rate

In Figure 24 and Figure 25, results at sampling rate of $1.0e^{-4}$s, $2.0e^{-4}$s and $5.0e^{-4}$s are presented respectively. Differences can be observed at sampling rate of $2.0e^{-4}$s and $5.0e^{-4}$s compared with sample rate of $1.0e^{-4}$s. Again, considering the indicator PVP, strain rate under different sampling rate is also plotted (Figure 26 and Figure 27).

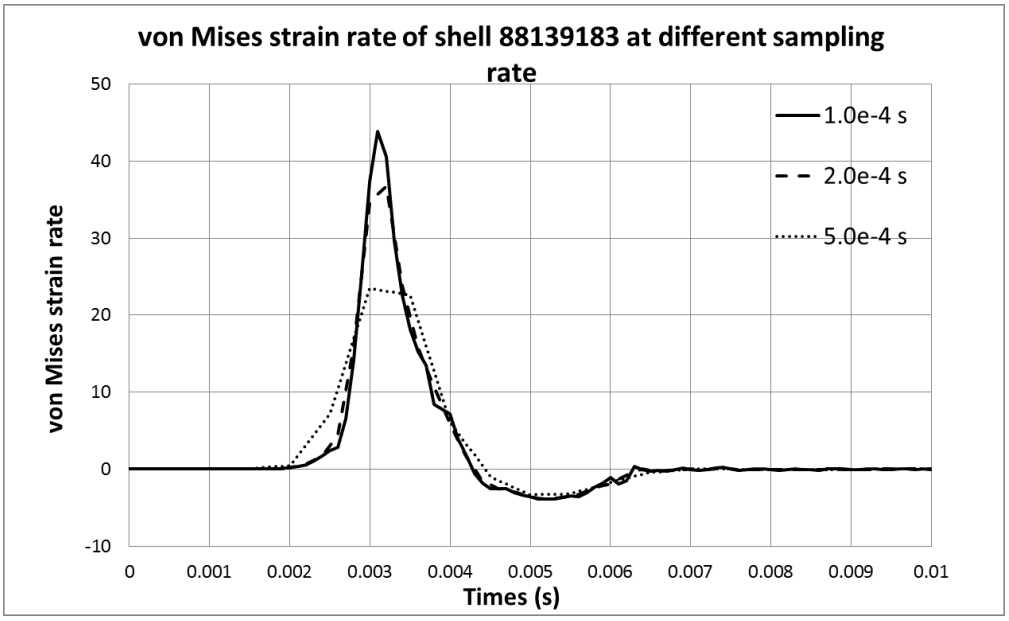

Figure 26 von Mises strain rate of shell 88139183 at different sampling rate

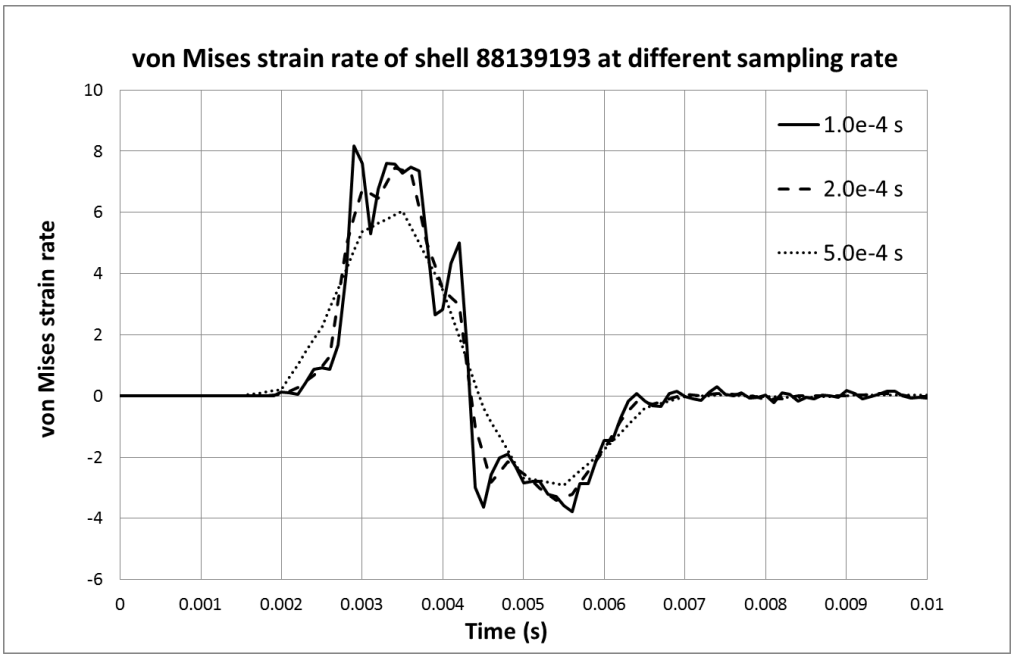

Figure 27 von Mises strain rate of shell 88139193 at different sampling rate

As presented in Figure 26 and Figure 27, great differences can be observed on Von Mises strain rate under different sampling rates. Strain rates under $2.0e^{-4}$s and $5.0e^{-4}$s is not accurate enough to output a consistent response.

As strain is material dependent, the same procedures were applied to a random selected solid element 88114302 with a different material property. The results are presented from Appendix A (Figure A 1 to Figure A 6). The conclusion is the same as

previous analysis. To conclude this study, the optimised suitable sampling rate used in this study is confirmed to be $1.0e^{-4}$s, considering computational time and size of output files for post-processing.

4.2 Peak Virtual Power (PVP) Baseline Threshold Calibration on THUMS Head

In order to investigate injury severity using PVP, the first step is to define the PVP threshold of injury on critical THUMS' body part or organs. As described in previous research (Chakravarthy et al., 2007), the head and chest are the most seriously injured body regions in adult pedestrian accidents, consequently the focus of injury calibration study will be on these organs. From an engineering perspective, the calibration study is required to determine the threshold of the material response under a specific load path. Therefore, a calibration study will be conducted at various locations on the head and the critical organs. This will be confirmed in section 4.2.2 "Calibration Method".

4.2.1 THUMS Head Model Analysis

The THUMS' head skull model was investigated for material properties.

Biologically, a cranial bone contains three layers including external (outer) table (1), internal (inner) table (3) and diploe (2) (Figure 28).

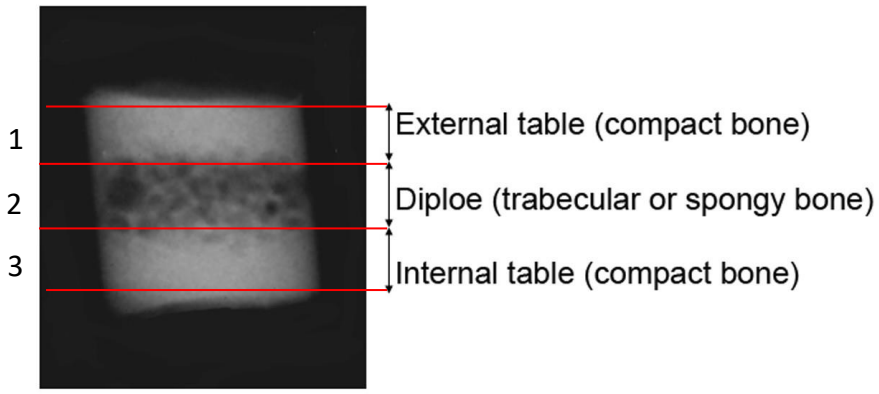

Figure 28 The three bone layers of the cranial vault (Niels Lynnerup, 2005)

In the cranial bones, the layers of compact cortical tissue are familiarly known as the tables of the skull; the external table is a compact bone, which is thick and tough; the internal table is also a compact bone, which is thin, dense and brittle. The intervening

cancellous tissue is called the diploe. Diploe is the spongy cancellous bone separating the inner and outer layers of the cortical bone of the skull (Niels Lynnerup, 2005). In the THUMS pedestrian model, the cranial bone is modelled with three layers of materials (Figure 29 and Figure 30), showing that THUMS is consistent with human anatomy.

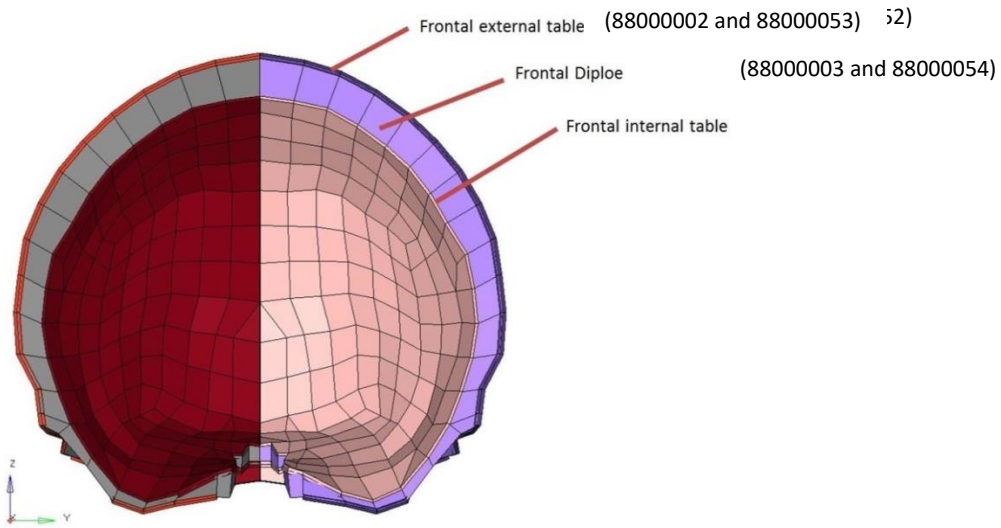

Figure 29 Frontal cranial bone of THUMS pedestrian model

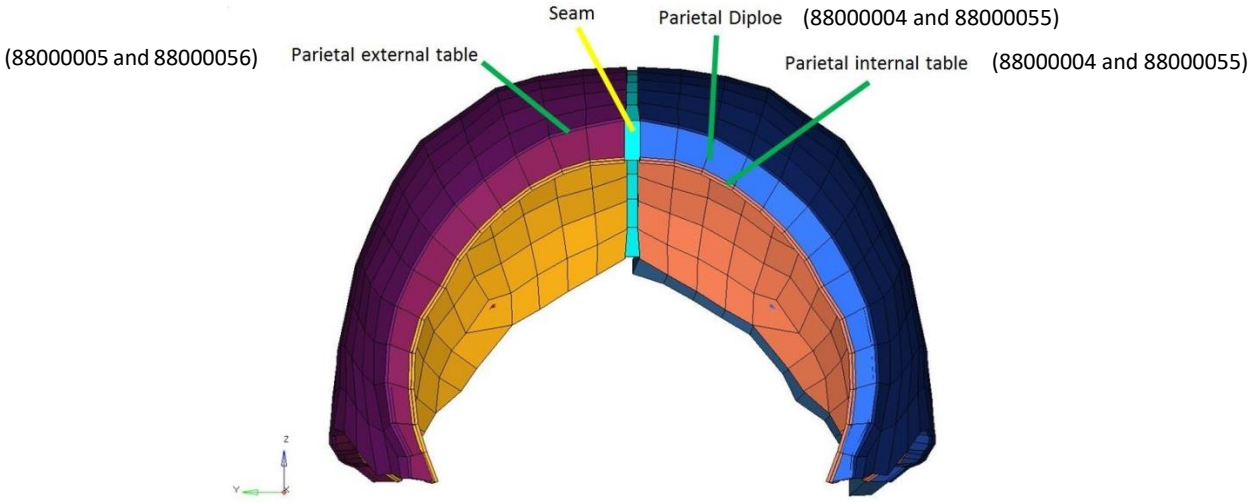

Figure 30 Parietal part of THUMS pedestrian model cranial bone

The external and internal tables are meshed using shell elements and the diploe is modelled using solid elements, as illustrated in Figure 29. In the THUMS model, different materials are applied to represent these distinctive characteristics. The

material properties used on the solid and the shell parts of cranial bone are summarised in Appendix II.

From the detailed material properties shown, three different materials were used on the THUMS skull. Differences can be observed on Young's modulus, yield stress and failure plastic strain (EPPF). Young's Modulus controls material stiffness, yield stress defined the stress at yield point and EPPF outline the plastic strain at failure point. Different material property affects material behaviour thus would affect the calibration result. The THUMS head is symmetrical, the geometry and material used on left side and right side are same (Figure 31).

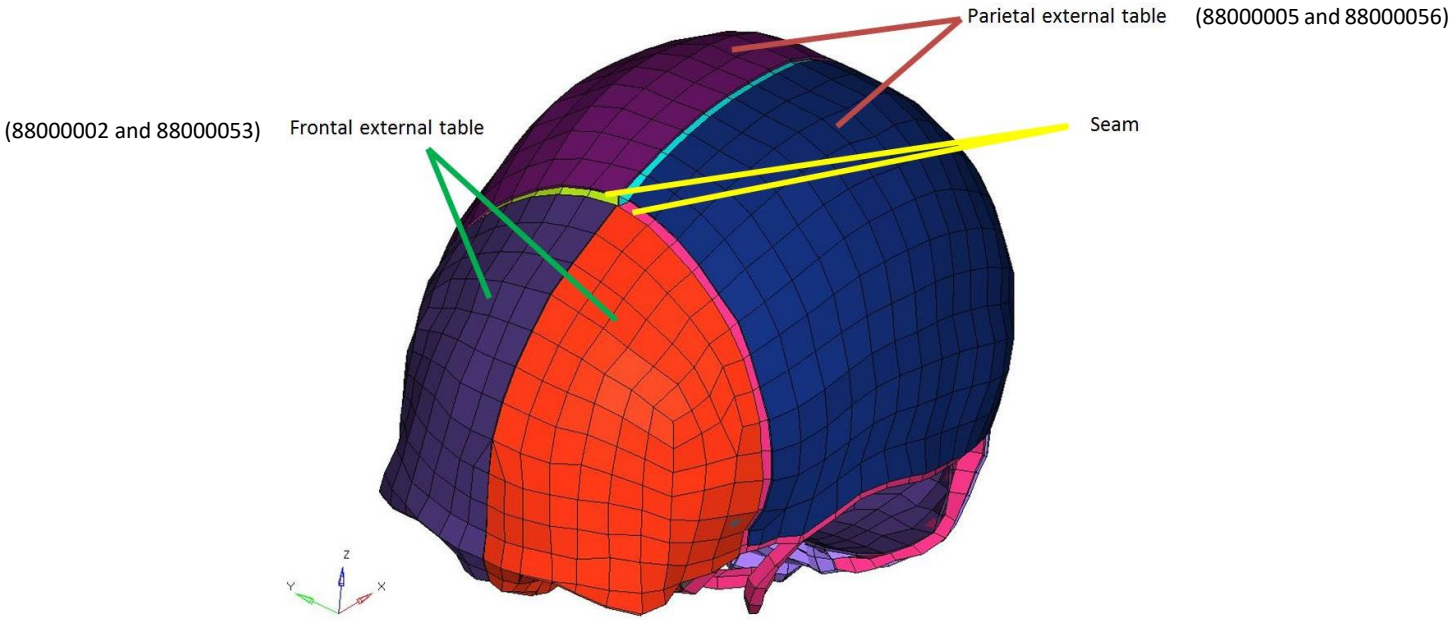

Figure 31 Cranial bones of THUMS head

Parts 88000001, 88000004 and 88000011 contain solid elements on the right side of the skull, representing the frontal diploe, parietal diploe and occipital diploe respectively. Part 88000002 represents the frontal external table. The same material is applied on all external tables of the skull. Part 88000003 and 8800006 represent the internal tables on frontal and parietal skull respectively. Differences can be observed on plastic strain of failure (EPPF) which defines the plastic strain limit at failure (as documented in Appendix III, Table A 1 and Table A 2). As the diploe is a spongy cancellous bone, its Young's modulus and yield stress are quite low on both frontal and parietal parts. On the other hand, the compact bone is the main component in

the skeleton to support and maintain the human body functions (Briers, 2012). Since the external and internal tables are made of compact bone which is a stable structure, an injury investigation should be performed on these tables instead of diploe. The occipital diploe has an extremely high density and yield stress, which makes it impossible to conduct any injury investigation using current properties. Consequently, the yield stress of the occipital diploe was changed to 30 MPa based on published study (Frankel and Burstein, 1970). Based on current findings, the injury investigation is performed on the frontal, parietal and occipital tables.

The THUMS' cranial bone is connected using seams. There are five seams used on whole skull, which are modelled using solids with damage material (MAT_105). The material property of the seams is different from the tables and the diploe of cranial bone; however, the seams will be also included in the calibration study to ensure the structural integrity of THUMS pedestrian head.

Different impact locations will result different contact areas between the pedestrian and the vehicle, thus, stress wave travels in different directions (See later section 4.2.2 "Calibration Method"). Consequently, three head impact locations will be investigated, representing the mostly encountered head impacts against a vehicle structure. These include a frontal impact with the contact location is the frontal external table, a side impact with the contact area on parietal external table and the impact on the occipital bone.

4.2.2 Calibration Method

4.2.2.1 Coupled (Occupant) System

Theoretically, PVP is power per unit mass and it also has a transient measure of impact pulse in milliseconds (Neal-Sturgess et al., 2001, Neal-Sturgess, 2010). Compared with a global description such as kinetic energy, PVP is impact mass independent. Mathematically, during and impact, the kinetic energy is transformed in strain energy.

Organ kinetic energy (T)= Organ strain energy (V)

Where $T = \frac{1}{2}mv^2$ is the kinetic energy released during the impact and , $V = \frac{\sigma^2}{2E}vol$ is the strain energy absorbed by the pedestrian head, for example (m is the mass of tissue/organ, v is impact velocity, σ is stress, E is Young's modulus and vol is volume of head).

Therefore, in a 1D medium

$$\frac{1}{2}mv^2 - \frac{\sigma^2}{2E}vol = 0$$

Equation 8 Non-relativistic Lagrangian

$$mv^2 = \frac{\sigma^2}{E}vol$$

But m=$\rho \cdot vol$ (ρ is the density, vol is the volume of tissue/organ), therefore,

$$\rho \cdot vol \cdot v^2 = \frac{\sigma^2}{E}vol$$

$$\sigma = \sqrt{\rho E}v$$

Rewriting the equation above, it is possible to express stress as a function of v.

$$\sigma = C_1 v$$

where $C_1 = \sqrt{\rho E}$. C_1 relates to the tissue/organ material properties

The next stage is to express the effect of strain rate. As mentioned in the thesis, at organ level:

$$PVP = maximum\ (\sigma \cdot \dot{\varepsilon})$$

Strain rate can be expressed as,

$$\dot{\varepsilon} = \frac{v}{L}$$

$$PVP = C_1 v \cdot \frac{v}{L}$$

$$PVP = \frac{1}{L}C_1 v^2$$

$$PVP = C_2 C_1 v^2$$

Equation 9 Relationship between PVP and impact speed in a coupled (occupant) system

Where: C_2 represents the tissue/organ geometry

$$C_2 = \frac{1}{L}$$

It can be noticed that PVP, for a coupled system, is a function of v^2. This is not the case for a pedestrian impact and will be expanded in the next section. It can be however observed that PVP is material property and geometry dependant as well as mass independent. Furthermore, PVP is mesh size dependant. In this project, PVP was calibrated using THUMS AM50 pedestrian model version 4.0, therefore the PVP threshold is based on the current THUMS 4.0 meshed model, with the material properties as given. If the research tool changes, the PVP threshold would need to be re-computed. This would be the case if the calibration had to be performed on the GHBMC.

4.2.2.2 Uncoupled (Pedestrian) System

In the case of pedestrian impacts, the PVP relationship needs to be adjusted as the system is uncoupled.

Impact energy is:

$$E_I = \frac{1}{2} m v^2 \propto v^2$$

Equation 10 Impact energy in an Uncouple (pedestrian) system

Where v= the initial velocity in the impact

Power is the time derivative of energy, consequently:

$$PVP \propto \frac{v^2}{\Delta t}$$

Now, in the case of a glancing impact, which the case was assumed as a minor injury case, then Δt will be small and could be considered to approximate to a constant value. Hence, for minor injuries:

$$PVP \cong Kv^2$$

Equation 11 PVP calculation on pedestrian

The ride-down can be ignored, because the pedestrian and the vehicle separate very quickly, consequently, the ride-down does not has any effect at all. Vehicle ride-down means crash distance (energy-absorption distance). However, if the body is in contact with the vehicle for a longer duration, then the ride-down of the vehicle needs to be considered. Assuming a simple Newtonian linear ride shown:

Let 'S' be the ride down, then:

$$S = \frac{v}{2}\Delta t \text{ or } \Delta t = \frac{2S}{v}$$

Equation 12 Vehicle ride down (crush distance)

Substituting Equation 12 into Equation 11 gives:

$$PVP \propto \frac{v^3}{S}$$

If S is now considered a constant for a given collision, then:

$$PVP \cong Kv^3$$

Equation 13 Relationship between PVP and impact velocity in an uncoupled (pedestrian) system

Real-life accidents have shown that PVP and v have a cubic relationship (Neal-Sturgess, 2001). Equation 13 has now suggested that this observation was theoretically correct.

From material perspective, for a given material, the energy absorbed at certain deformation value is the area under stress-strain curve (Vlack, 1959, Marcello Cammarata and Zummo, 2016, Unknown) (Figure 32).

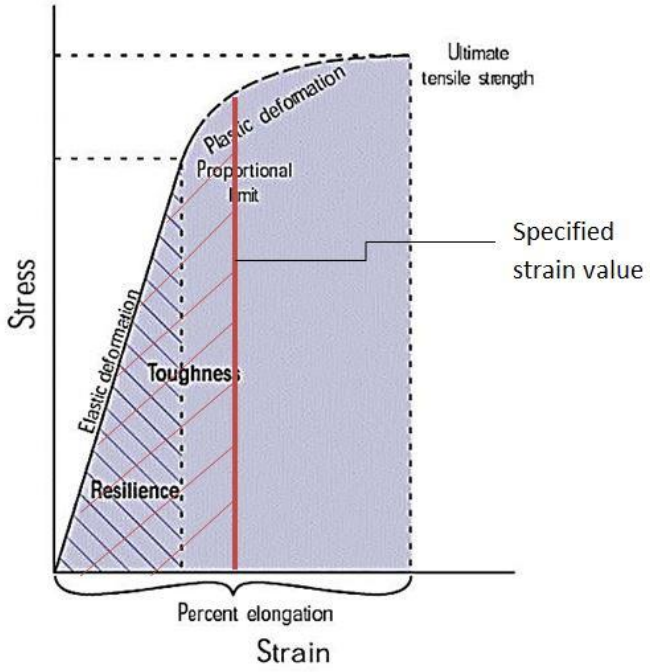

Figure 32 Energy absorbed of a material (Vlack, 1959)

If the strain value is specified, then the energy required is also confirmed. Based on this fact, if the failure strain is given, then the failure energy can also be obtained. Energy is the product of power and time. If the energy is specified, then power and time are in negative correlation. Higher power is resulted from shorter time and longer time results lower power for the same load. Similarly, in real-world accident, lower impact velocity produces longer contact time and higher impact velocity results shorted contact time. Based on this point, power is a positive correlation with impact velocity.

In summary, PVP will be calibrated on the head and the chest areas against mechanical threshold of brain tissue and main organs. The calibration will be conducted using different impact velocities. Once the current injury mechanical measure, listed in Table 9, is reached (corresponding to a set AIS level), then the corresponding PVP is extracted as threshold for the specific speed.

Tissue/Organ	Currently-used injury measurement	Injury description	AIS
Brain grey matter	30% maximum principal strain	Brain contusion	3-4
Brain white matter	21% maximum principal strain	Diffuse Axonal Injury (DAI)	4
Heart	30% maximum principal strain	Rupture	4
Liver	30% maximum principal strain	Rupture	4
Spleen	30% maximum principal strain	Rupture	4
Kidneys	30% maximum principal strain	Rupture	4

Table 9 Currently used injury criterion on brain and organs and corresponding AIS level(Toyota Motor Corporation, 2011)

The current injury criteria outline the threshold strain and the corresponding AIS level. The first element to reach the current injury criteria from Table 9 will be recorded and its PVP value calculated. At a different impact speed, the PVP of the same element will be extracted to derive the PVP threshold against impact speed. Since only current injury criteria's AIS levels are known, the PVP threshold derived will be the specific AIS level (mostly AIS 4 based from Table 9). In order to obtain other AIS levels, the scale factors presented later in Table 10 will be applied. By specifying the tolerance bound of each AIS level, a whole systematic PVP threshold under different impact speed is then obtained.

4.3 Brain tissue Calibration Results

From a mechanical point of view, the skull and the brain are of totally different structures, which require different scenario to obtain their PVP threshold. However, in real-world accident, the head is an assembly of skull and brain that undertake damage at the same time when the accident takes place. Consequently, the brain PVP threshold is also extracted in situ in scenarios of frontal impact, side impact and top impact. As previously described in Table 9, the injury criterion of Diffuse Axonal Injury (DAI) on the THUMS model is observed for a 21% maximum principal strain on the brain white matter. A 30% maximum principal strain was used as injury criterion for brain contusion in the brain grey matter. The first element reaching the injury criteria was documented and the PVP of that element was calculated. Then, PVP was plotted against impact speed and their relationship explored.

4.3.1 PVP Threshold of Brain Tissue in Frontal Impact

Using the described THUMS head validation process based on published cadaver test (Toyota Motor Corporation, 2011), a frontal impact numerical test was conducted using a cylinder impactor and the full THUMS head assembly (Figure 33). Impactor was positioned to contact the forehead.

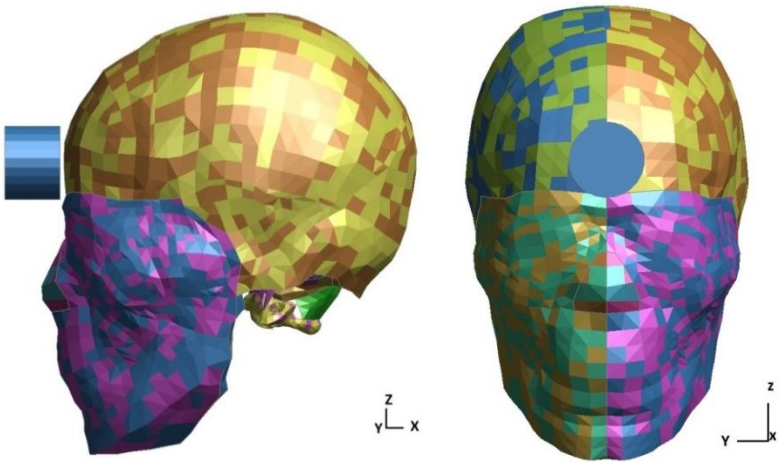

Figure 33 Frontal impact scenario using THUMS pedestrian head part

In a frontal impact scenario, the PVP threshold calibration results of AIS 4 DAI is shown in Figure 29 and the trauma result relating to an AIS 3 brain contusion is presented in Figure 30. In each figure, the polynomial fit as well as the regression value are provided.

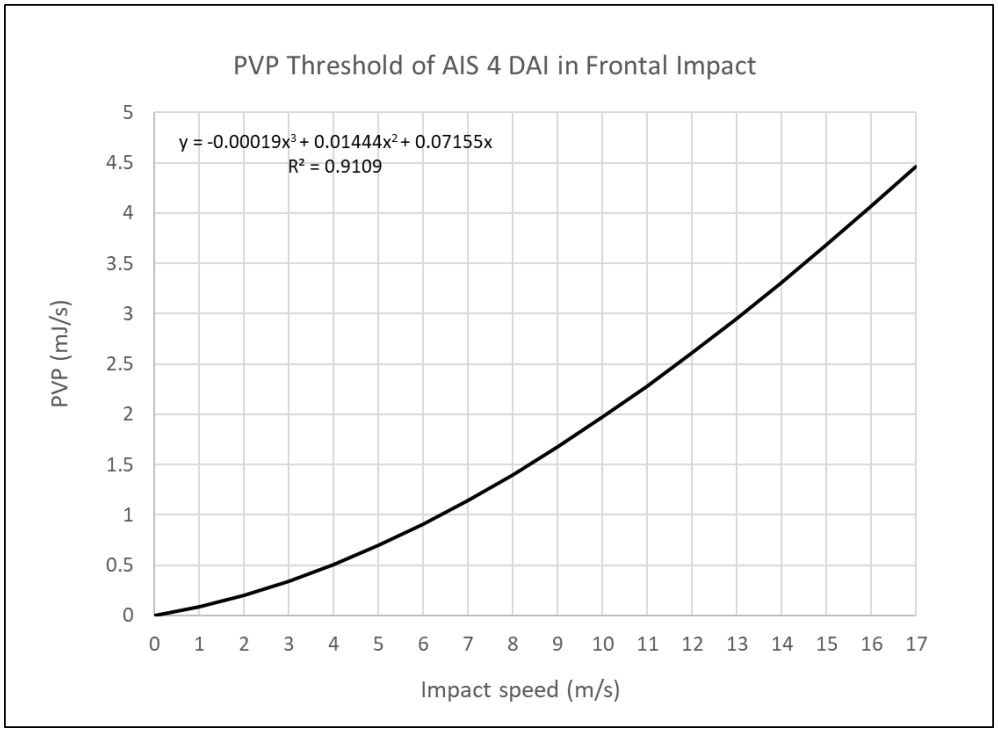

Figure 34 PVP threshold of AIS 4 DAI in frontal impact

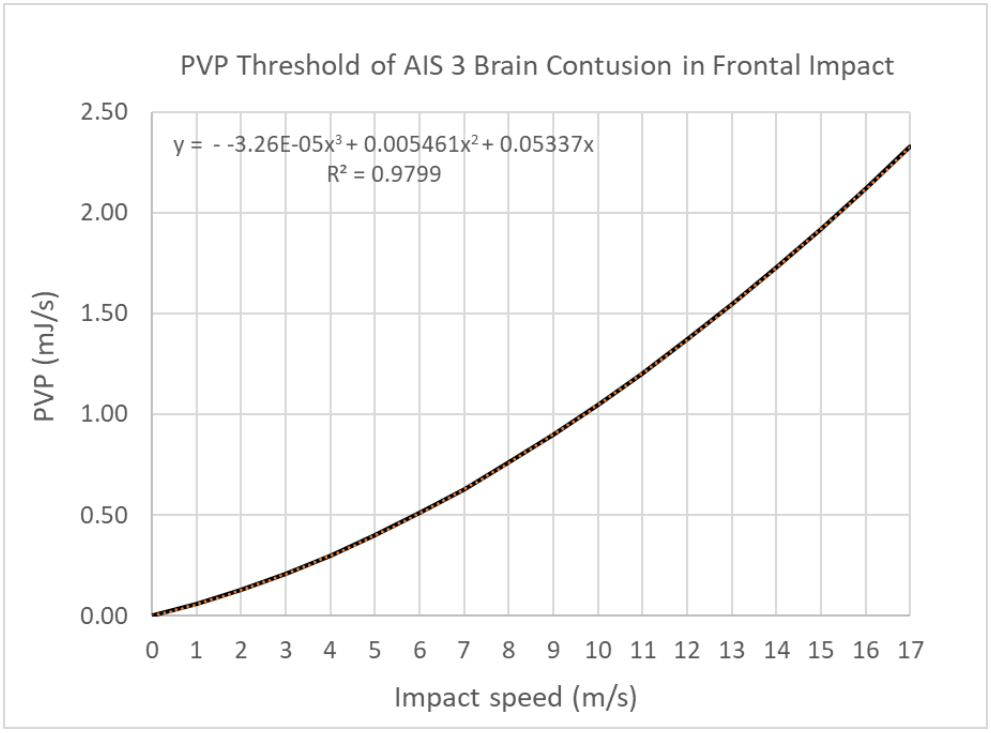

Figure 35 PVP threshold of AIS 3 brain contusion in frontal impact

In the DAI PVP threshold calibration (Figure 34), the first element reaching 21% maximum principal strain is solid 88128359, which is in the brain white matter. The PVP of this element was extracted and plotted against different impact speeds. DAI is

confirmed as an AIS 4 injury, which involved large area of haemorrhage occurring on the brain white matter only. Therefore, the PVP threshold at 21% maximum principal strain is the threshold of an AIS 4 injury. Regarding brain contusion, the PVP threshold calibration (Figure 35) is based on the first element reaching a 30% maximum principal strain (solid 88131788), which is in brain grey matter. The PVP value of this element was extracted and plotted against a range of impact speeds. Brain contusion is confirmed as an AIS 3 injury and it was not observed under 4m/s. By applying various fitting methods, a 3rd order polynomial with no constant was the best fit for all PVP threshold on brain in frontal impact scenario, as observed in section 4.2.2.2 “Uncoupled (Pedestrian) System”.

4.3.2 PVP Threshold of Brain Tissue in Lateral Impact

In order to keep the test setup consistent, a cylinder impactor was also used in lateral and later in occipital impact scenarios. The impact scenario is illustrated in Figure 36.

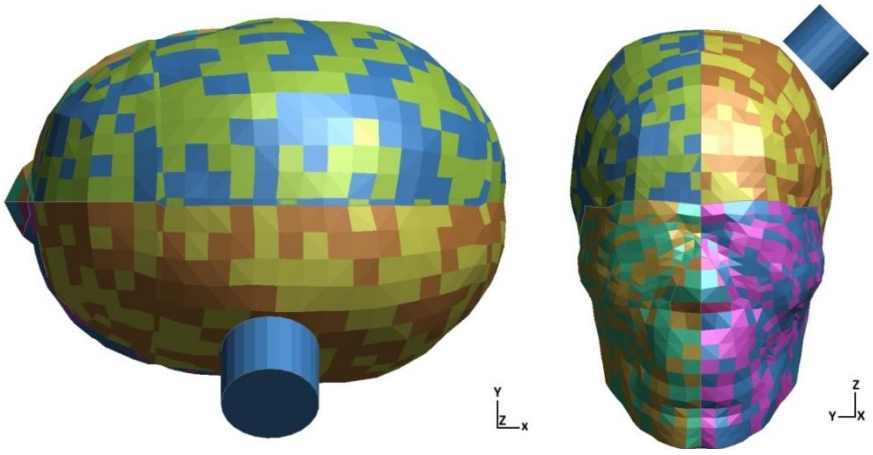

Figure 36 Left lateral impact scenario performing using THUMS pedestrian head part

As the THUMS head model is symmetrical, only one side needs to be impacted. The left side was arbitrary chosen. The results for DAI and brain contusion corridors are presented in Figure 37 and Figure 38 respectively.

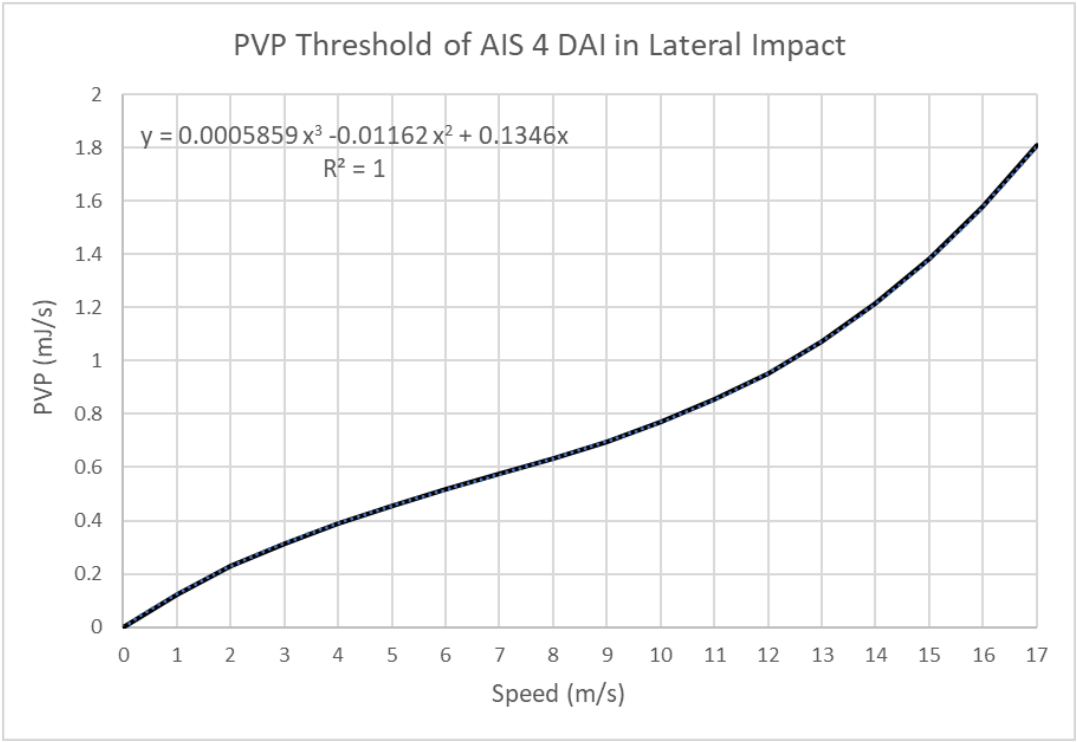

Figure 37 PVP threshold of AIS 4 DAI in lateral impact

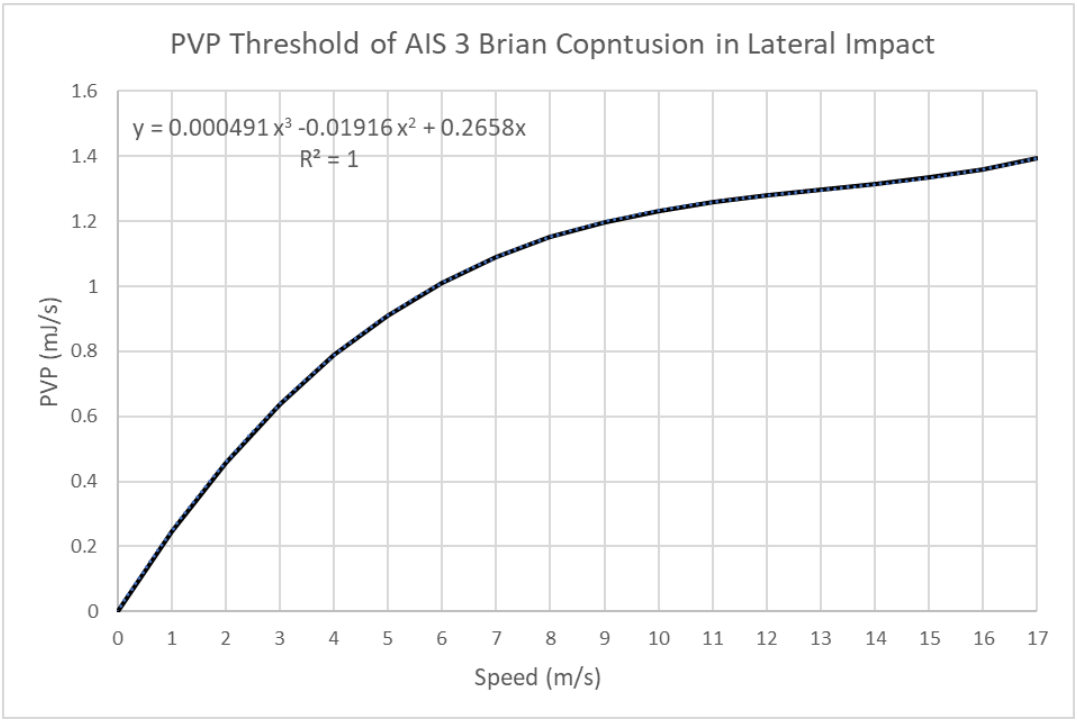

Figure 38 PVP threshold of AIS 3 brain contusion in lateral impact

Referring to the DAI calibration, the first element reaching 21% maximum principal strain is solid 88128366, which is different than in the frontal impact scenario. The PVP of this element was extracted and plotted against impact speed. DAI is confirmed as

an AIS 4 injury, therefore the PVP threshold with a 21% maximum principal strain is the threshold for AIS 4. On the brain grey matter, the first element reaching 30% maximum principal strain is solid element 88131788, which is the same as in the frontal impact scenario. The PVP of this element was extracted and plotted against impact speed. A best fitting interpolation was a 3rd order polynomial with no constant. Compared with the calibration results observed in the frontal impact scenario, the PVP threshold shows significant difference. Frontal impact and lateral impacts result in different contact angle and area, which both lead to differences in load paths. Different load paths result in different structure response, which leads to different PVP responses, hence calibration curve shapes.

4.4.3 PVP Threshold of Brain Tissue in Rear Impact

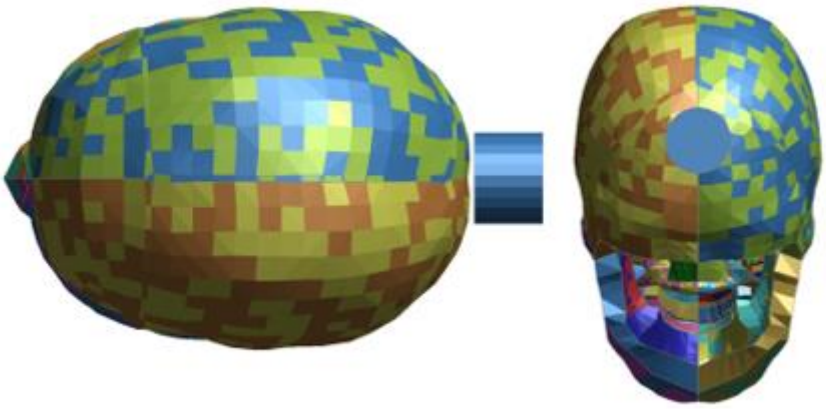

Figure 39 Occipital impact scenario of PVP threshold calibration

The third calibration scenario was a head occipital impact in which the same impactor contacts the occipital bone. The PVP threshold of DAI and brain contusion are shown in Figure 40 and Figure 41.

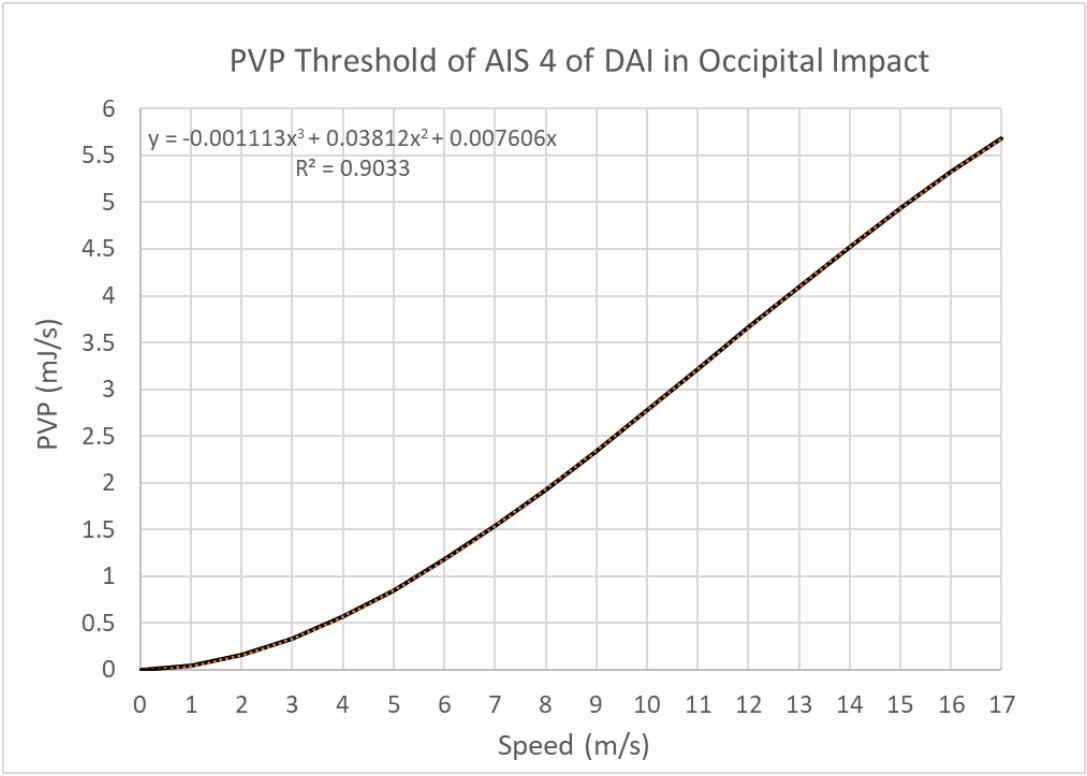

Figure 40 PVP threshold of AIS 4 DAI in occipital impact

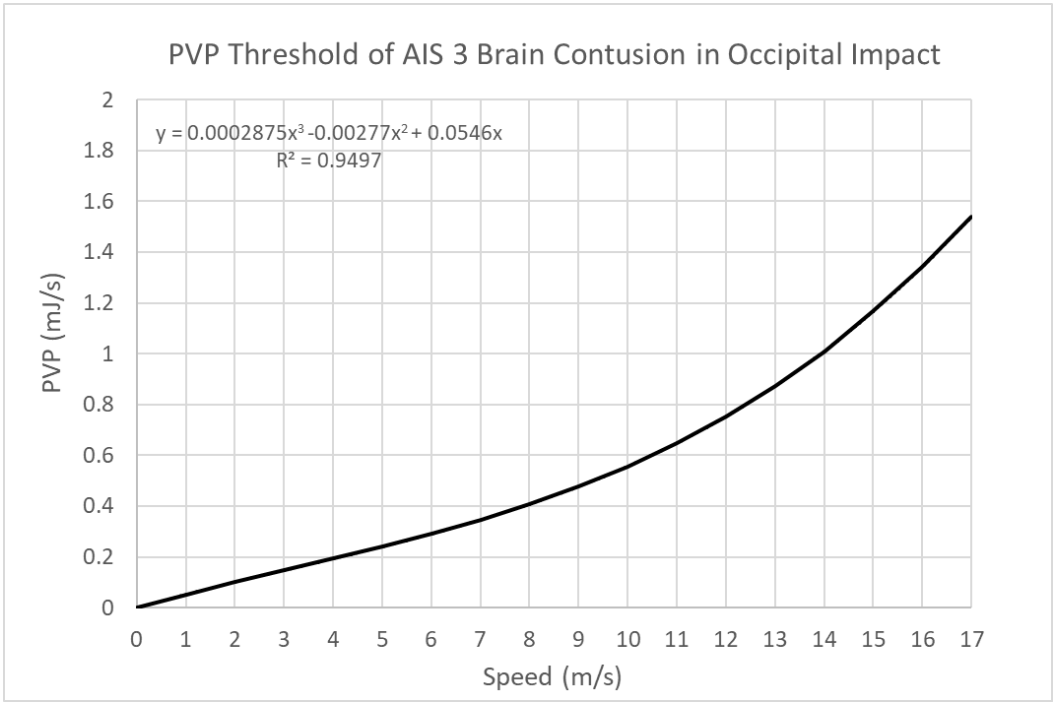

Figure 41 PVP threshold of AIS 3 brain contusion in occipital impact

Referring to DAI calibration, the first element reaching 21% maximum principal strain is solid 88128342, which is different than previous impact scenarios. The PVP of this

element was extracted and plotted against the impactor impact speed. DAI is confirmed as an AIS 4 injury, therefore PVP threshold of 21% maximum principal strain is the threshold for AIS 4. On the brain grey matter, the first element reaching 30% maximum principal strain is solid 88131788, which is the same as previous impact scenarios. The PVP of this element was also extracted and plotted against impact speed. Still the best fit is a 3rd order polynomial with no constant.

5.0 Peak Virtual Power (PVP) Calibration on THUMS Internal Organs

For the internal organs, injury can occur due to the impact of the vehicle structure, as well as inertial effects. In both cases organs contact with hard components or within themselves: both will cause injuries. Various materials are used on different organs, making organ calibration complex due to the limited physiological injury levels recorded in the literature.

In the case of serious (AIS 3+) injuries, the chest and abdomen region are important and take the second place after head injuries (Chakravarthy et al., 2007). Main organs such as heart, liver, spleen and kidney are also located in this region, therefore their respective PVP thresholds need to be determined. In the THUMS model, organs validation in frontal impact was conducted using a similar method (Kroell et al., 1971), as illustrate in Figure 42.

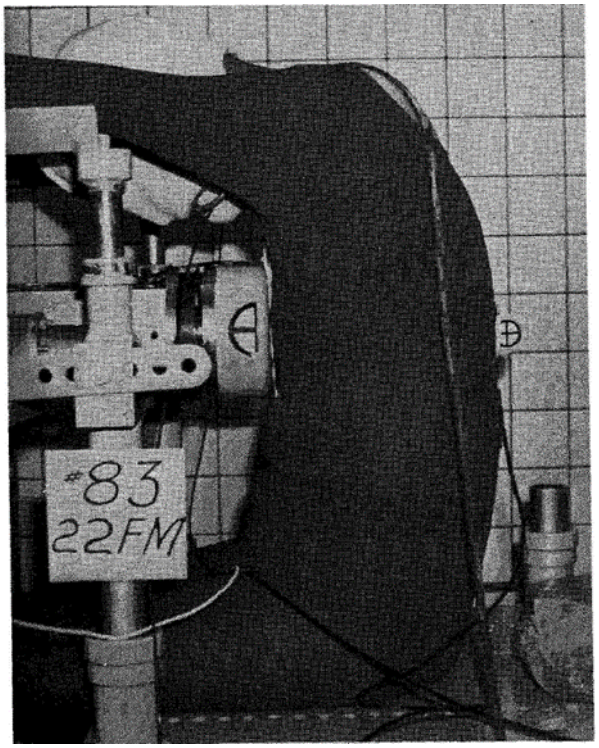

Figure 42 Cadaver organs validation scenarios (Kroell et al., 1971)

As shown in Figure 42, an impact force, using a mass of 52lb (23kg) (Kroell et al., 1971), was applied in the horizontal direction with a wooden contact block aligned vertically and centred mid-sagitally over the fourth costal interspace at the sternum. The

contacting interface was an unpadded, 6'' (15.24 cm) diameter wooden block, with a 0.5'' (12.77 mm) edge radius to prevent localized loading at the perimeter. According to this information, the scenario for PVP threshold calibration of the THUMS' internal organs are presented in Figure 43.

Figure 43 Scenario of PVP threshold calibration on THUMS internal organs

On the THUMS model, injury criterion used for main organs (heart, liver, spleen and kidney) is 30% strain (Yamada and Evans, 1970), however the type of strain was not specified. In Yamada's tests, a 30% Ultimate Tensile Strain (UTS) was proposed as the ultimate threshold on internal organ injury. Yamada's tests only determine the breaking point of the organ sample at AIS 4. THUMS model was also validated uses 30% UTS as organ injury threshold. UTS is a total strain, which is indicated in Figure 44.

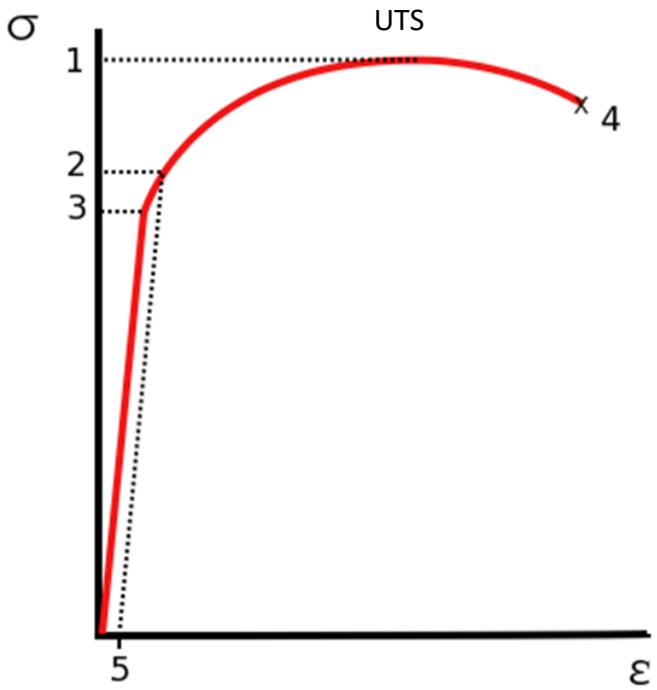

Figure 44 Stress-strain curve for ductile material (Degarmo et al., 1997)

In Yamada's test, the tensile strain or elongation occurring in a specimen was determined by measuring, with a reading microscope and a screw micrometre eyepiece, the increase in the width of a narrow gap between the ends of two thin flexible wires attached to each end of the specimen at the junction between the reduced and the expanded regions. The wires were in a straight line and parallel to the long axis of the specimen (Yamada and Evans, 1970). As the loading is uniaxial, no shear vector was involved. Furthermore, as illustrated in Figure 44, UTS is a total strain. Therefore, in organ calibration, 30% maximum principal strain was used as injury criterion.

Furthermore, in the Yamada's tests, the failure of biological structure was defined as rupture. From a medical perspective, rupture of the main organs such as heart and liver can be classified as AIS 3-4 (The American Association for the Surgery of Trauma, 2018), consequently, the PVP threshold calibration on the main internal organs can be also defined as PVP threshold of AIS 3-4 injury on main internal organs.

5.1 PVP Threshold Organ Calibration Results in Frontal Impact

In this section, the critical 'soft' organ calibration test will be discussed and will include the CAE setup procedure and the trauma calibration results.

Following the same procedure discussed in the previous section, the first element reaching 30% maximum principal strain was recorded, as well as the time of event. The relationship between PVP and impact speed was then plotted to define the threshold on each organ. It was notices that the whole THUMS model remained numerically stable up to 20m/s in frontal impact scenario. Therefore, the test speed was then extended to 20m/s (the maximum accident speed provided by UKPF was 16m/s) to improve the accuracy of the polynomial fit. Organ rupture is classified as an AIS 4 injury, therefore, the PVP threshold at 30% maximum principal strain is the threshold of AIS 4 organ rupture. Thresholds of other MAIS levels were scaled based on PVP threshold of AIS 4. The lung was not included because no test method was found in literature for PVP calibration. The results of PVP threshold calibration are illustrated from Figure 45 to Figure 49.

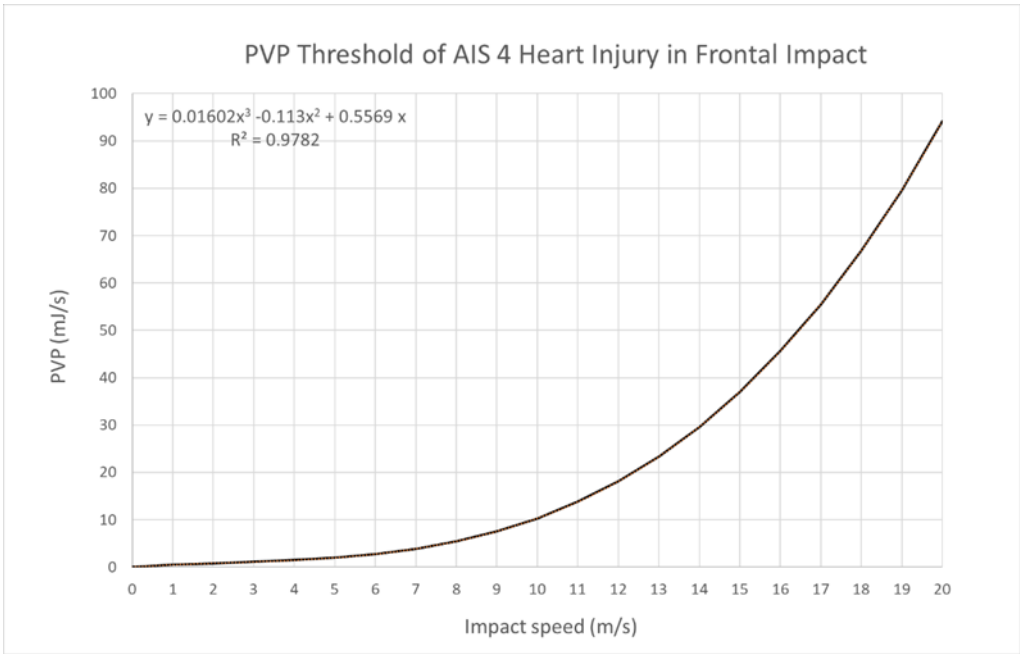

Figure 45 PVP threshold of AIS 4 heart injury in frontal impact

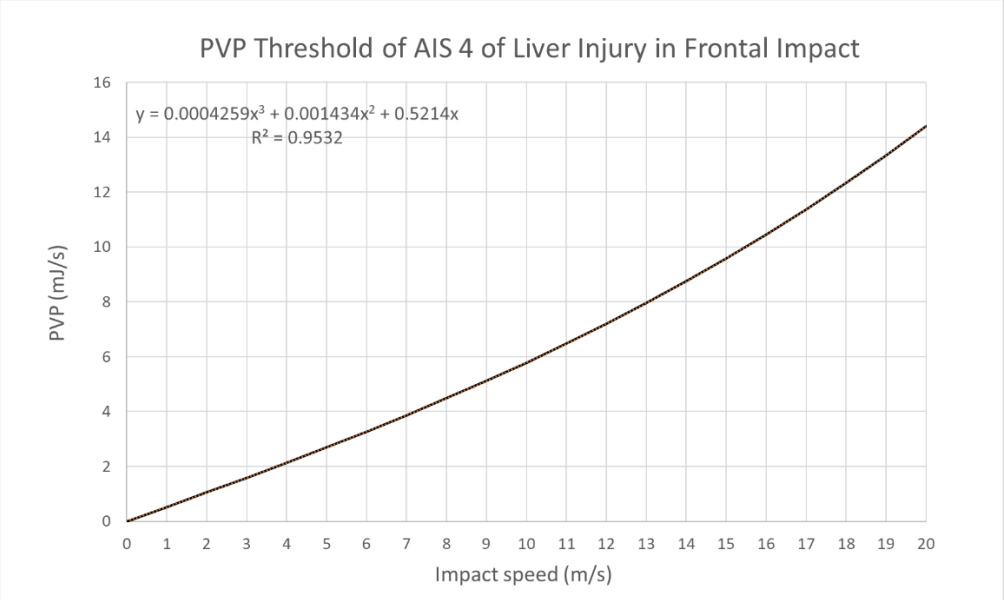

Figure 46 PVP threshold calibration on THUMS liver

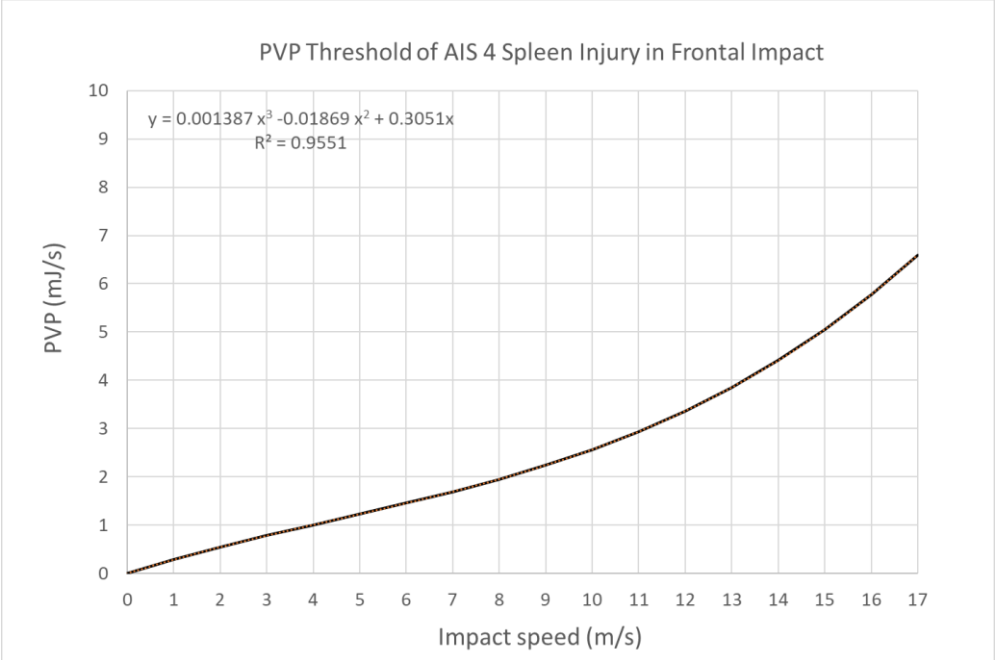

Figure 47 PVP threshold calibration on THUMS spleen

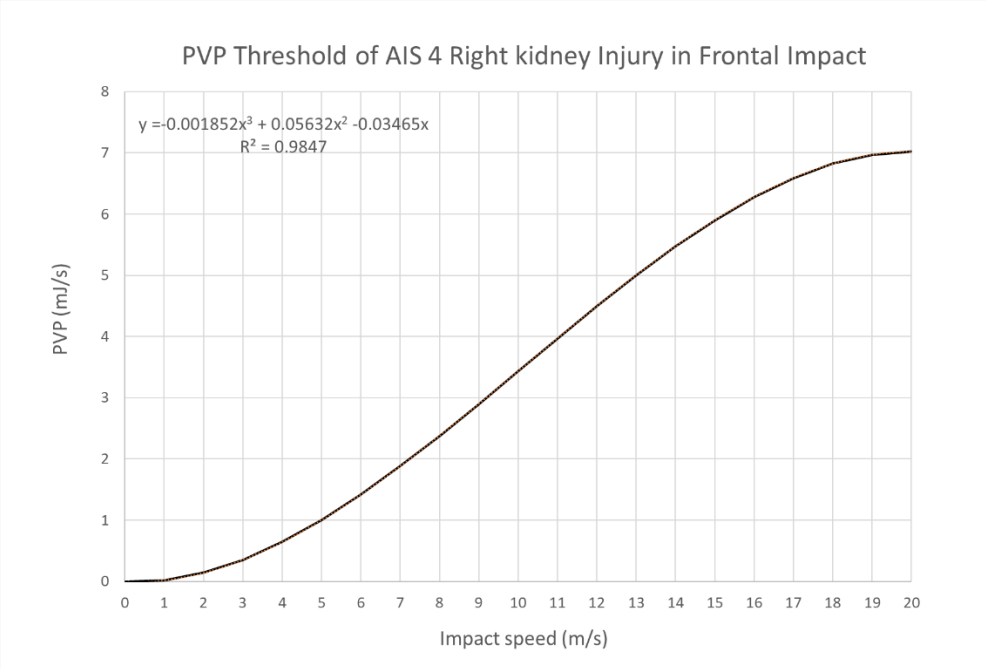

Figure 48 PVP threshold calibration on THUMS right kidney

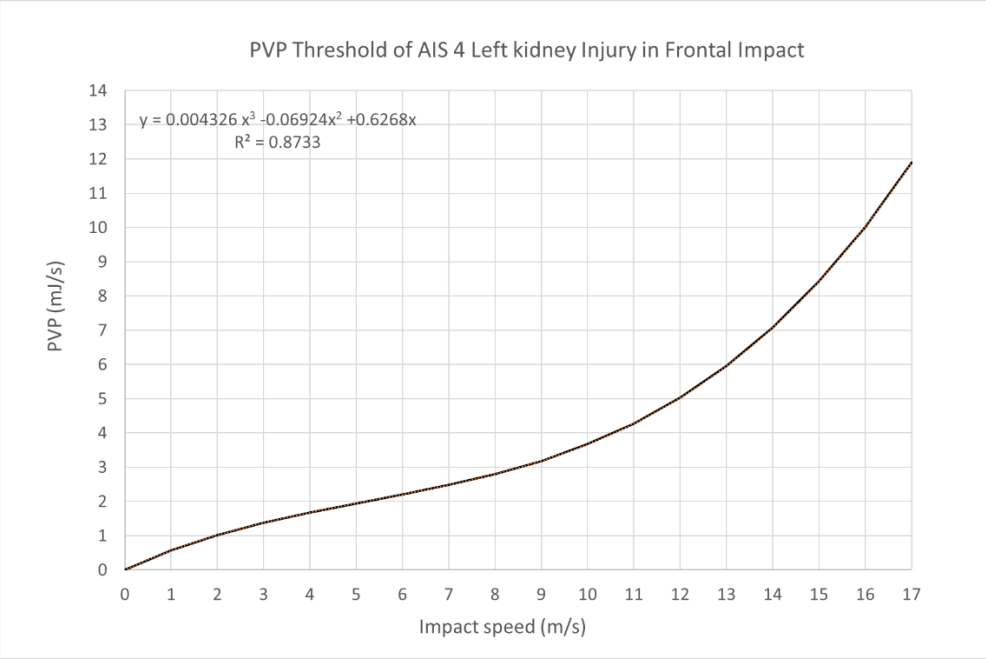

Figure 49 PVP threshold calibration on THUMS left kidney

In the organ PVP threshold calibration, the first element reaching 30% maximum principal strain was recorded and its PVP was calculated accordingly, as previously done. As organ rupture is classified as an AIS 4 injury, therefore a PVP threshold of 30% maximum principal strain is the threshold of AIS 4. PVP threshold depends on the organ shape. Due to the different load path during the impact, the stress wave travels

in different directions, organs with the same material also have different PVP threshold especially on the right and left kidneys.

5.2 PVP Threshold Calibration Organ Results in Left Lateral Impact

Side crashes are reported to have more serious injury and fatality rates compared to other crash types (Samaha and Elliott, 2003). Consequently, the PVP threshold calibration on organs was also conducted using lateral impact position. In this section, a side impact calibration is studied.

The impact scenario was reconstructed using same scenario given by Shaw (Shaw et al., 2006) (Figure 50).

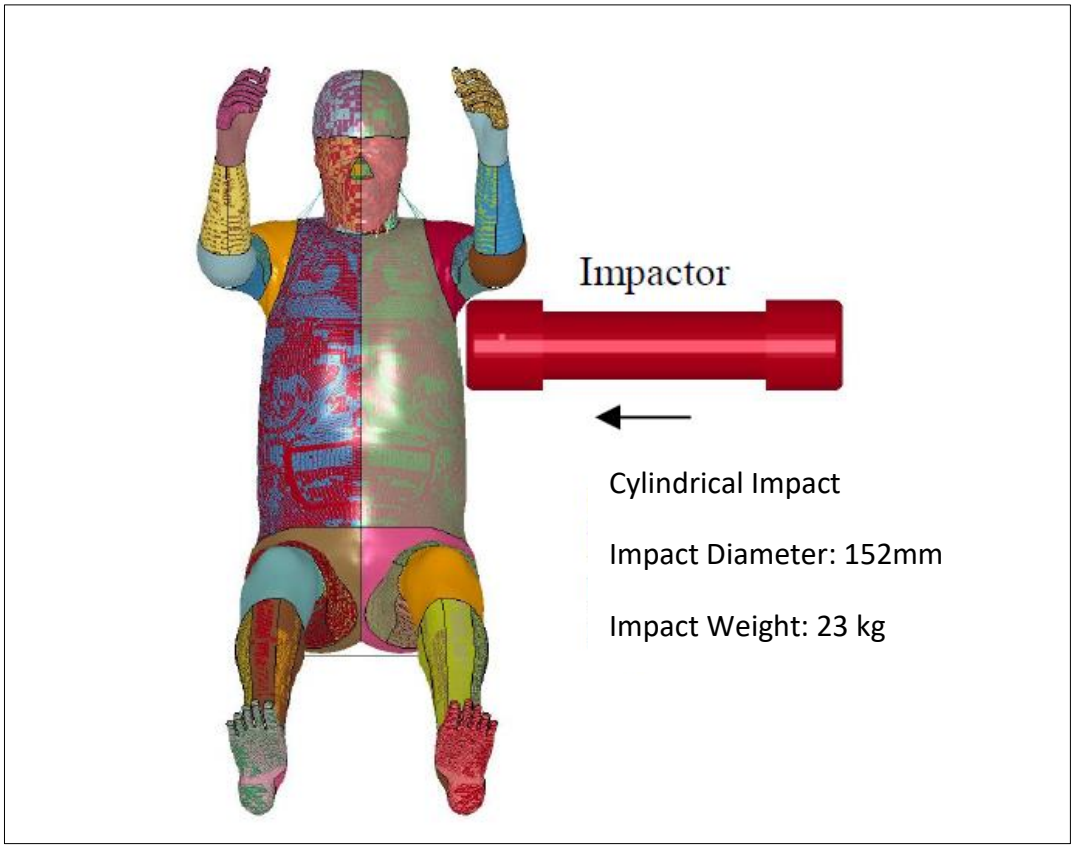

Figure 50 Organ left lateral impact scenario (Shaw et al., 2006)

The human body does not have a symmetrical organ layout, therefore the PVP threshold calibration should be conducted separately on each side. In this research, all the accidents provided by UKPF, which will be analysed later in the thesis, are left impact. Hence, the PVP threshold calibration study of left side of the pedestrian was

conducted first with the aim to extend this calibration in future work. The calibration test was only conducted using the validation setup shown in Figure 50. A sensitivity check with respect to different impact location was also included in further work, which will be discussed in the later chapter. In the left-lateral impact scenario, the THUMS model is numerically stable until 18m/s, therefore, the test speed was then extended to 18m/s (the maximum accident speed provided by UKPF is 16m/s) for more accurate curve fitting. The calibration results are shown from Figure 51 to Figure 55.

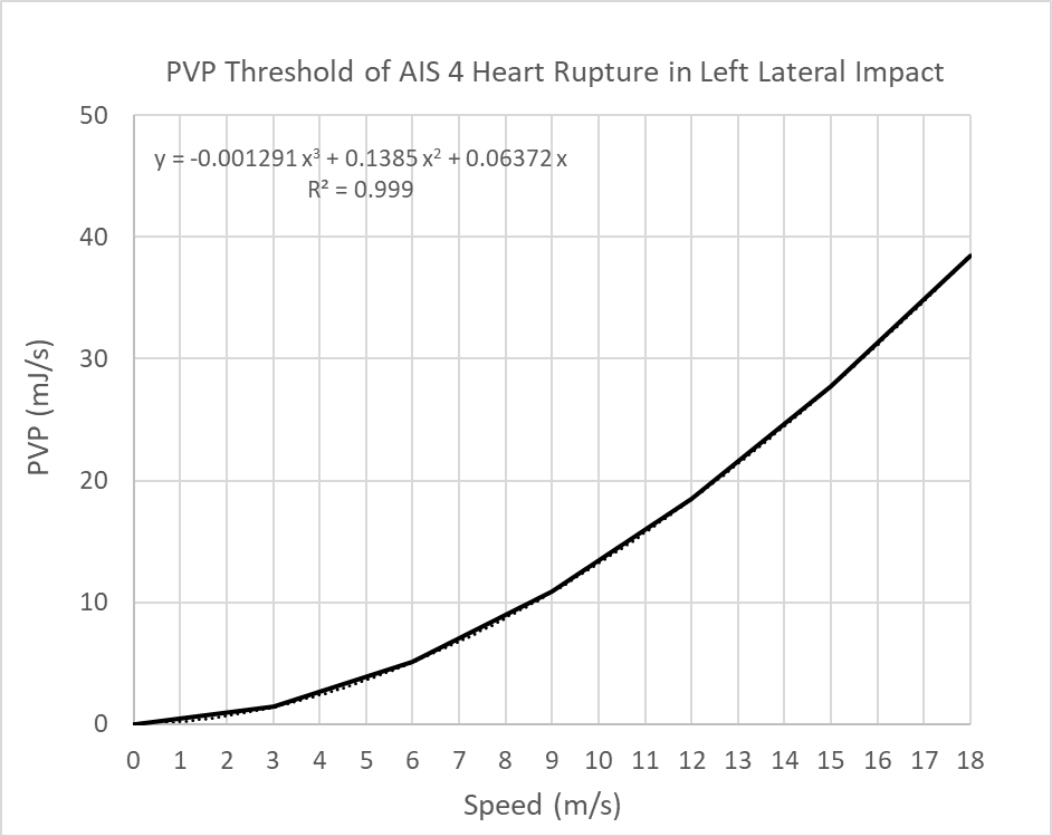

Figure 51 PVP threshold of AIS 4 heart rupture in left lateral impact

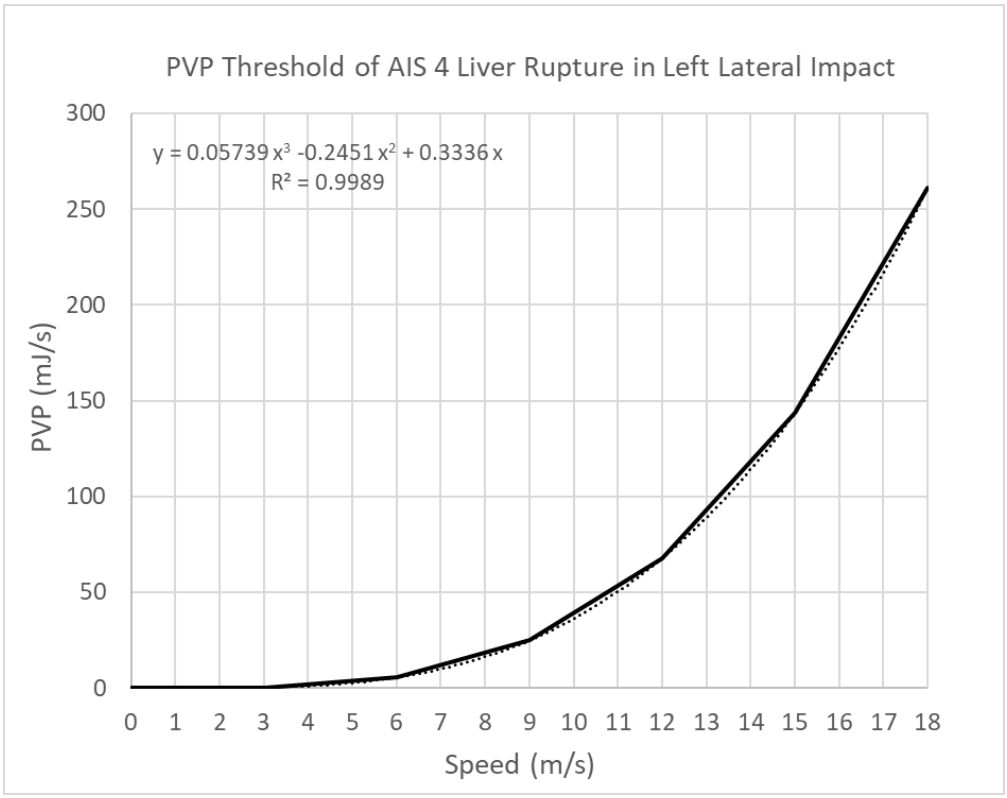

Figure 52 PVP threshold of AIS 4 liver rupture in left lateral impact

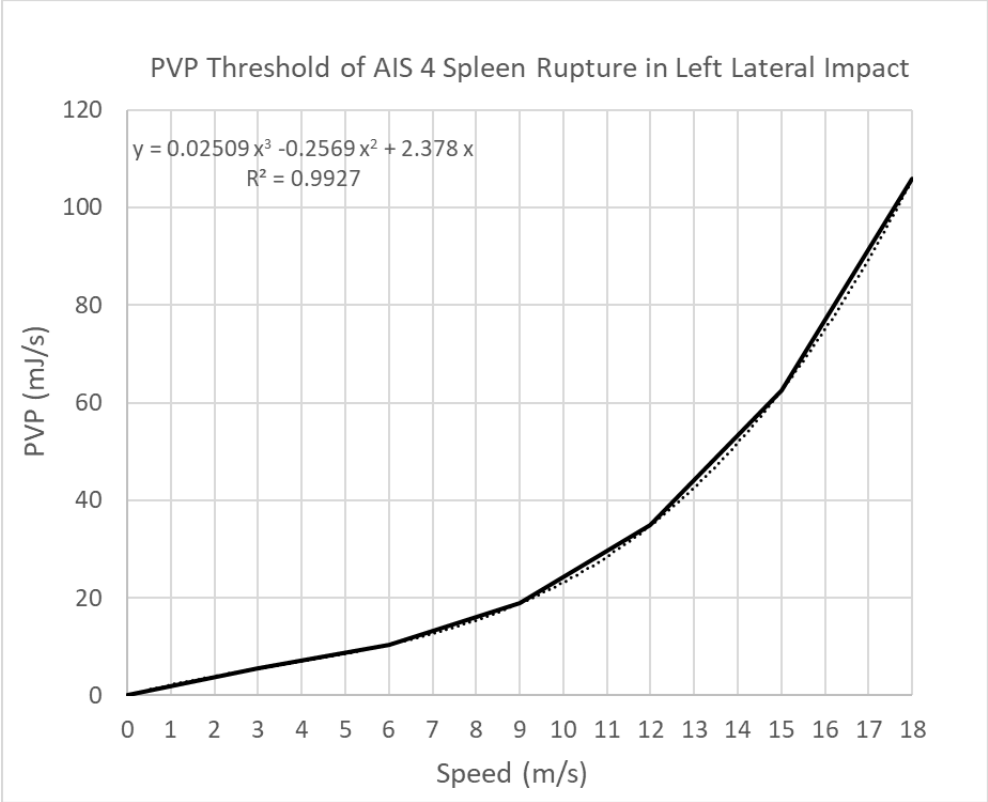

Figure 53 PVP threshold of AIS 4 spleen rupture in left lateral impact

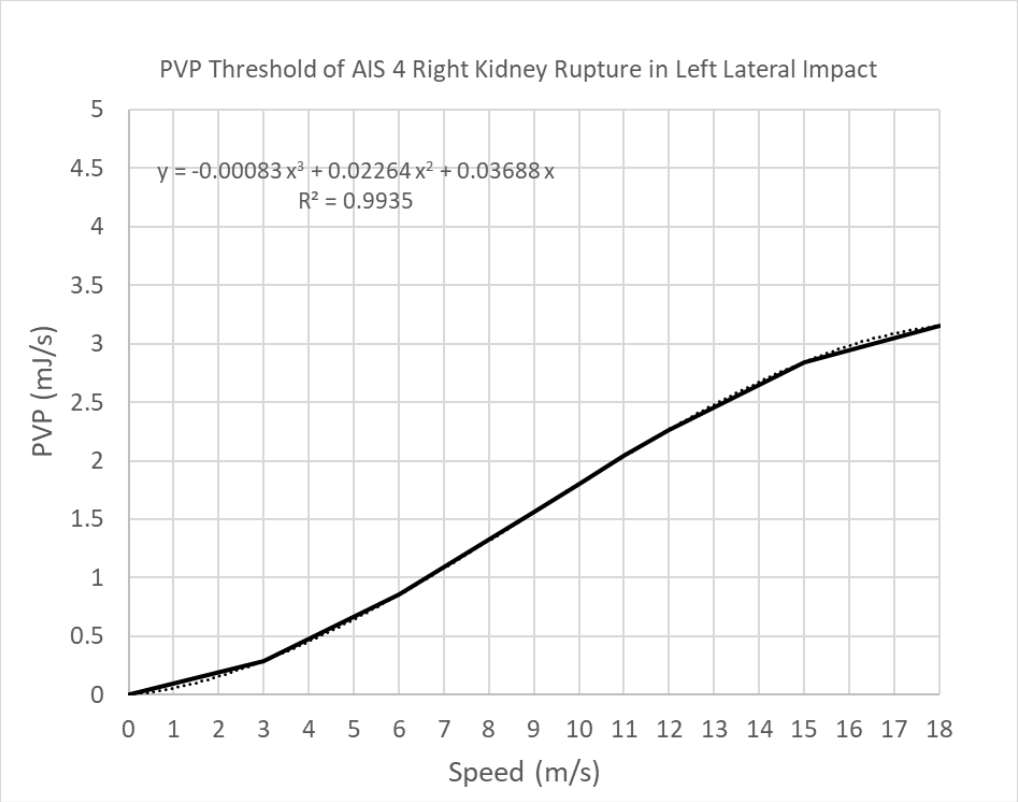

Figure 54 PVP threshold of AIS 4 right kidney rupture in left lateral impact

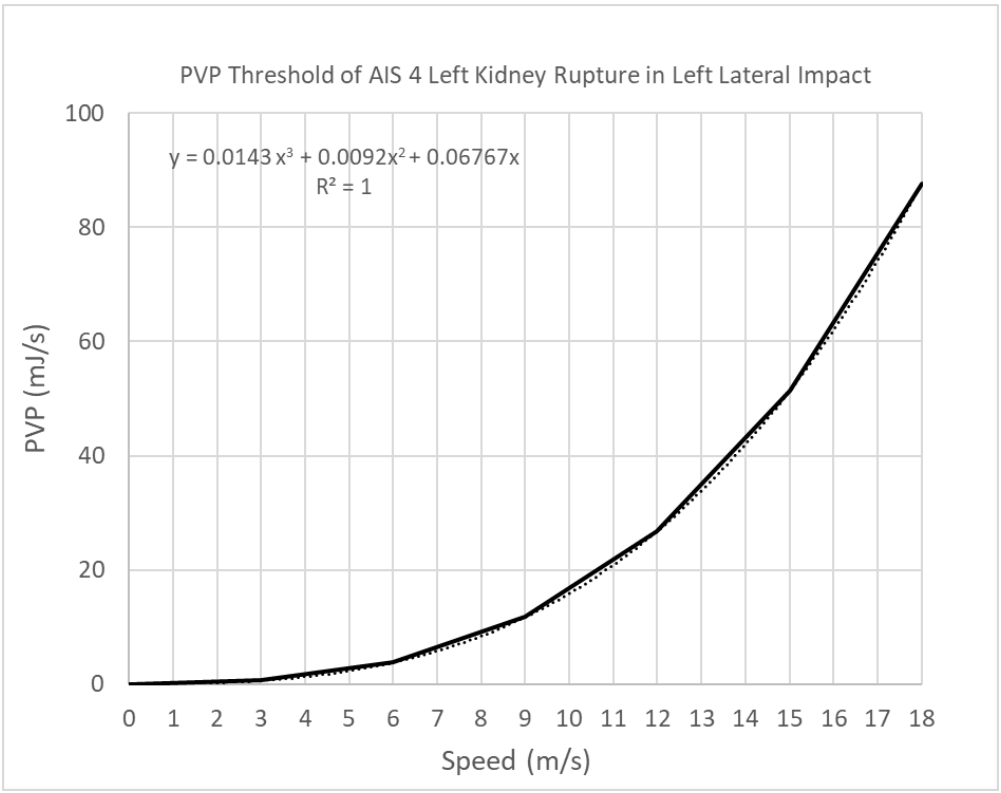

Figure 55 PVP threshold of AIS 4 left kidney rupture in left lateral impact

For the organ PVP threshold calibration, the first element reaching 30% maximum principal strain was recorded and PVP was calculated accordingly. The then PVP of this element was plotted against different impact speeds to represent the threshold of each organ. As organ rupture is classified as an AIS 4 injury, the PVP threshold for a 30% maximum principal strain is the threshold of AIS 4.

5.3 PVP Threshold Calibration Organ Result in Rear Impact

Following the previous calibration study, this section explains the calibration test procedure for the back (rear) impact scenario and demonstrates as well as the trauma threshold result

As the consequence of collision, human body could rotate on the bonnet during the impact. Rear contact is a common result of a lateral collision, therefore a. PVP calibration is necessary. The impact scenario was reconstructed as shown in Figure 56.

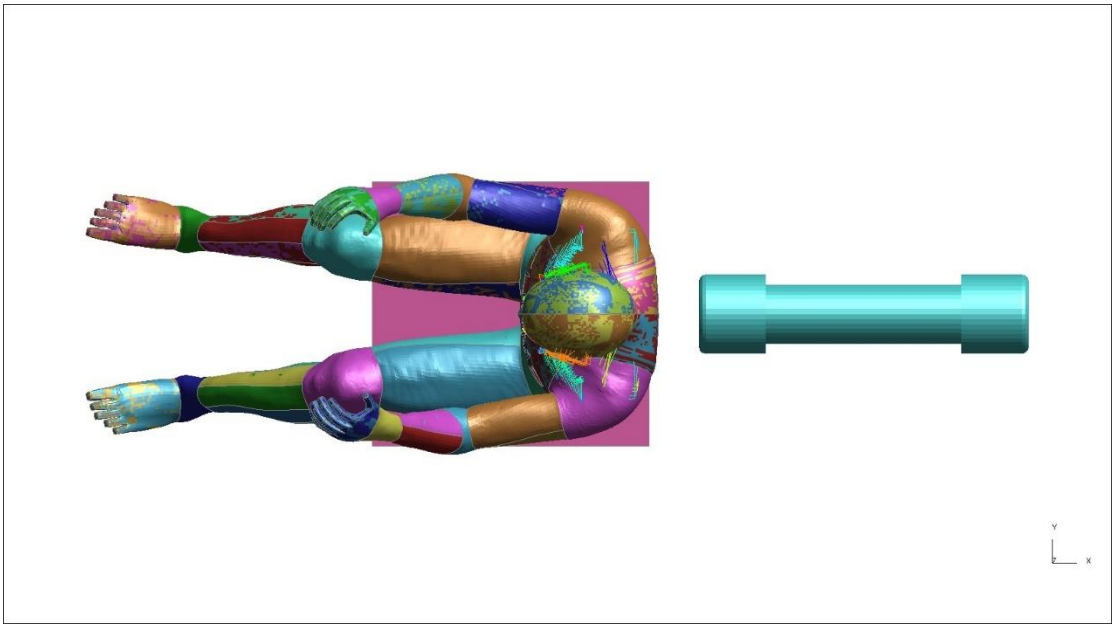

Figure 56 PVP calibration scenario in rear impact

In the back impact scenario, the THUMS model is numerically stable until 17m/s, therefore, the test speed range was set as 0m/s-17m/s (the maximum accident speed provided by UKPF is 16m/s) for more accurate curve fitting computation. The calibration results are shown from Figure 57 to Figure 61.

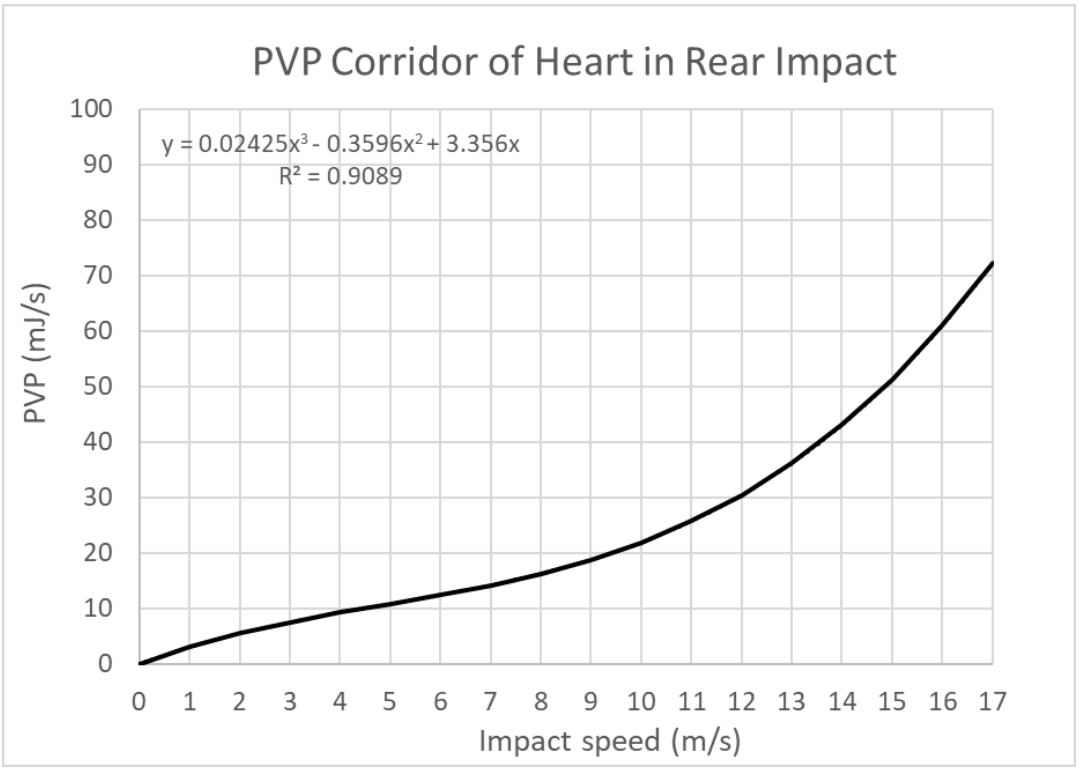

Figure 57 PVP threshold of AIS 4 heart rupture in rear impact

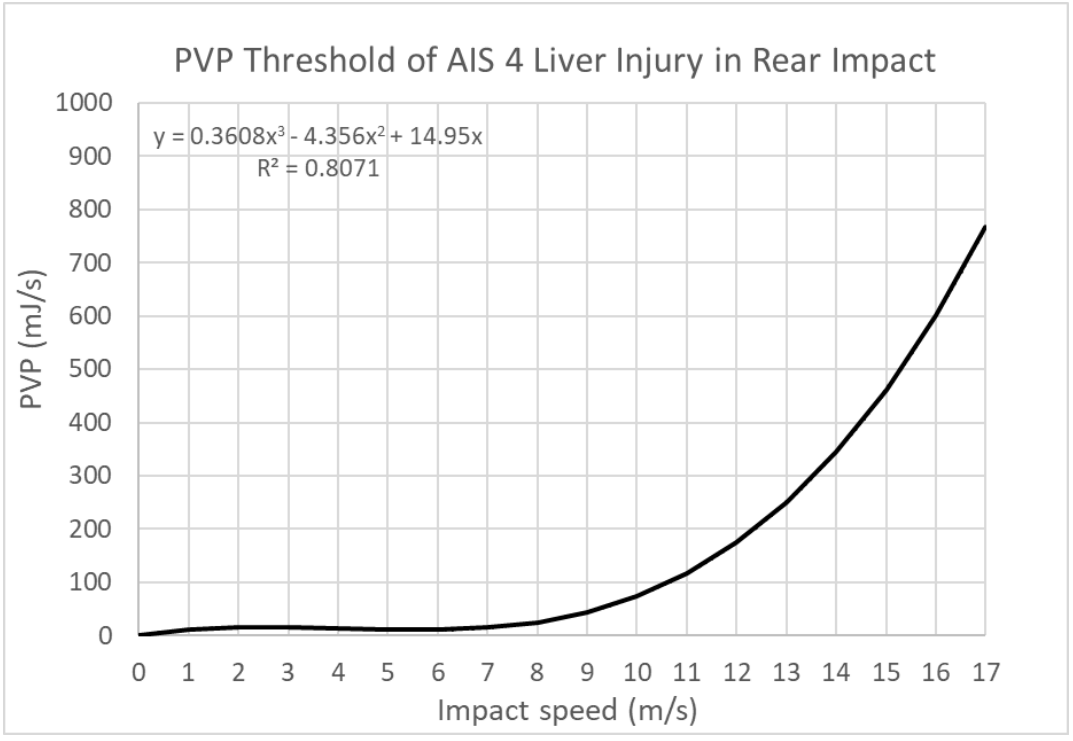

Figure 58 PVP threshold of AIS 4 liver rupture in rear impact

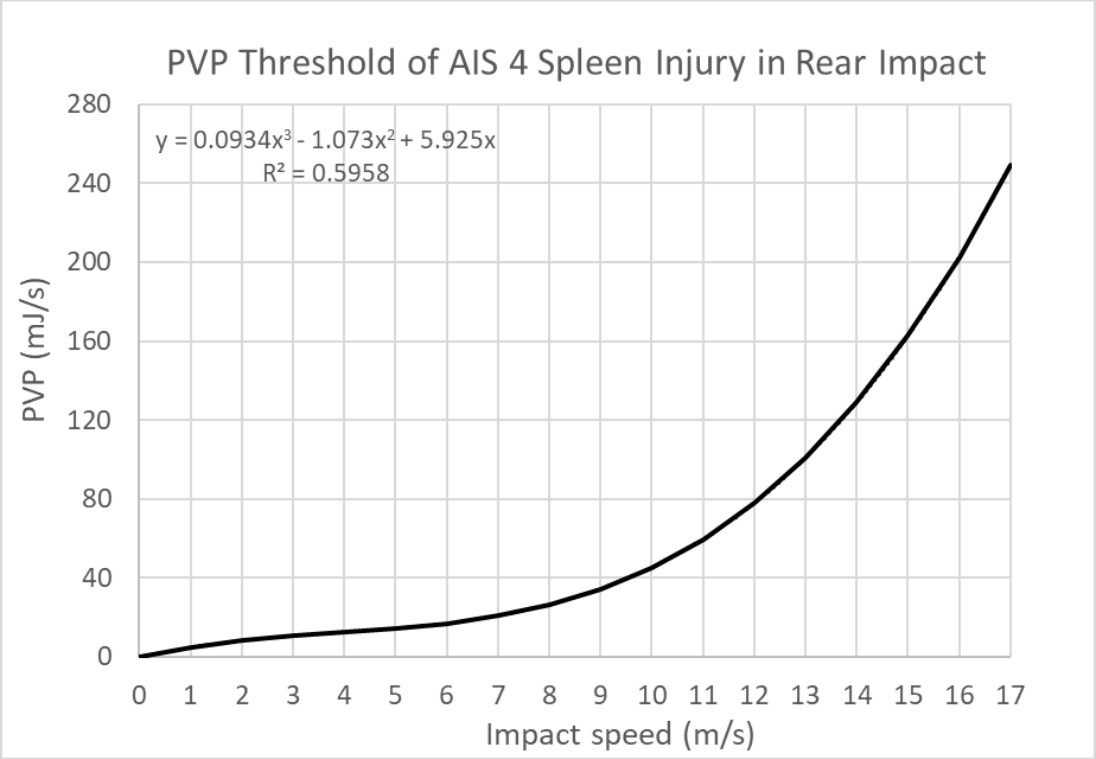

Figure 59PVP threshold of AIS 4 spleen rupture in rear impact

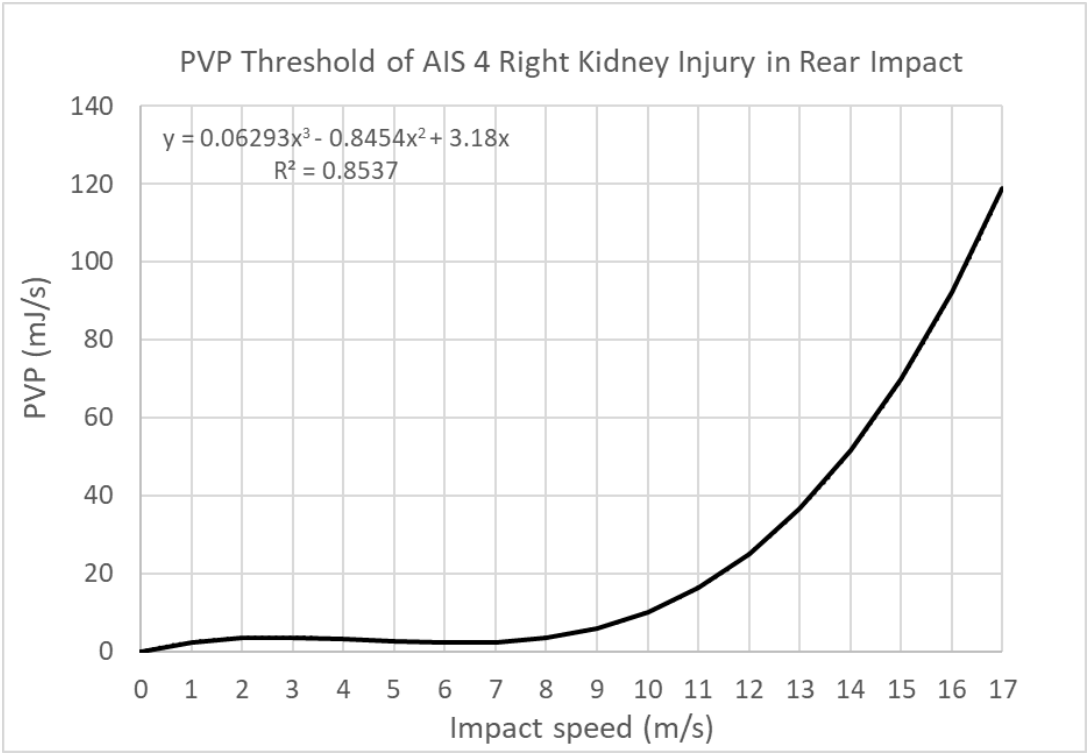

Figure 60 PVP threshold of AIS 4 right kidney rupture in rear impact

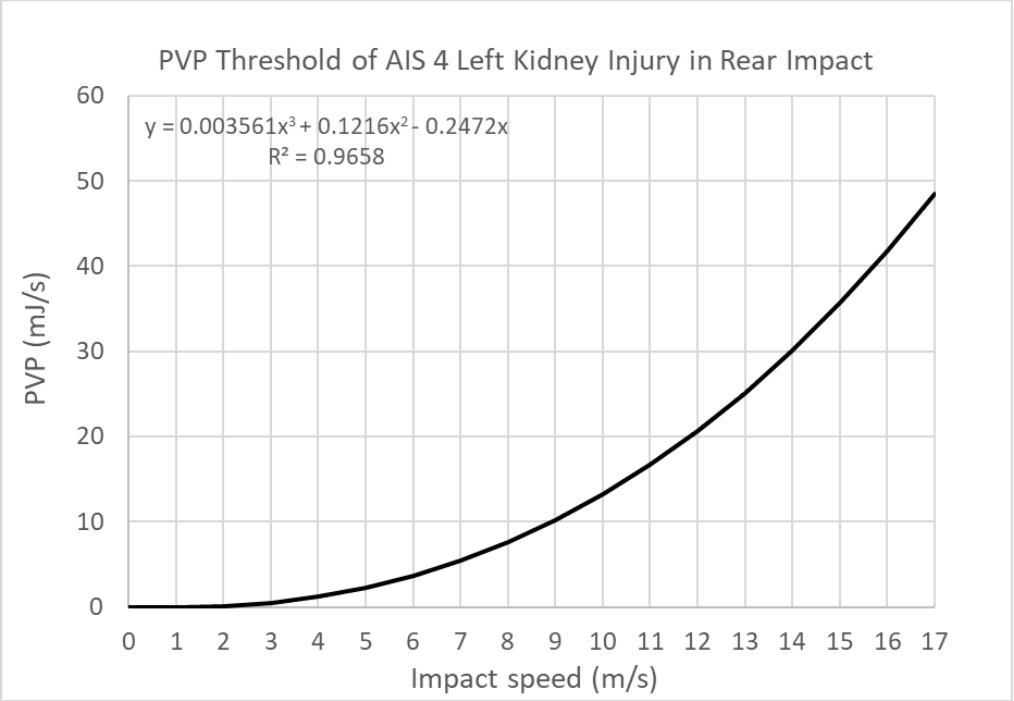

Figure 61 PVP threshold of AIS 4 left kidney rupture in rear impact

So far, all AIS 4 PVP thresholds for brain tissue and critical organs have been developed. Later on, in this thesis, these thresholds will be validated against real-world accident data and their ability to predict trauma injury answered.

6.0 PVP Threshold Corridor Investigation

The aim of this section is to propose a mathematical method to generate the complete systematic PVP threshold corridors. The curve fitting and scaling method will be explained, followed by the procedure to generate corridors of confidence.

6.1 Confirmation of the Curve Fitting Method

Curve fitting methods will be initially discussed. Several fitting parameters were applied and their correlation coefficients examined.

The original data of PVP threshold of different AIS level was extracted in the earlier section. If the relationship between PVP and impact speed on occupant is known to be correct (Neal-Sturgess et al., 2001), the relation of pedestrian still needs confirming. If real-life accident scenarios (Neal-Sturgess et al., 2001) and the theoretical derivations were performed in this thesis, another proof is needed to confirm this cubic relationship. It is proposed to use CAE and the PVP corridors defined in this thesis. In order to vindicate this, different polynomial fits will be applied on the PVP vs Velocity graphs and the order of the fit. To determine the relationship, several fitting methods were applied include 3rd order, 2nd order, 3rd order polynomial and 2nd order polynomial. During the polynomial fitting process, terms with and without constants were both tried. The correlation coefficient (R^2) of all polynomial fits were recorded to conclude the best fitting method (Table 10).

	$y=ax^3$	$y=ax^3+bx^2$	$y=ax^3+bx^2+cx$	$y=ax^3+bx^2+cx+d$	$y=a^2$	$y=ax^2+bx$	$y=ax^2+bx+c$
R^2 of Heart	0.9765	0.9777	0.9782	0.9782	0.9158	0.9638	0.9687
R2 of Liver	0.6494	0.9393	0.9532	0.9517	0.8706	0.9552	0.953
R2 of Spleen	0.2376	0.9108	0.9072	0.9024	0.6223	0.89	0.8887
R2 of Right kidney	0.6032	0.9845	0.9847	0.9848	0.8621	0.961	0.9702
R2 of Left kidney	0.9271	0.9273	0.9457	0.9481	0.8843	0.9028	0.9095

Table 10 Fitting results on organs in frontal impact

As presented in Table 10, the summary of the fitting results of pedestrian organ threshold are presented. The formula of each fitting curve was provided as well as the correlation coefficient (R^2). The correlation coefficient is a numerical measure relating to statistical relationship between two variables. The correlation coefficient ranges from −1 to +1, where +1 indicates the strongest possible agreement and −1 the strongest possible disagreement (Boddy and Smith, 2009). The best fitting terms for

each organ, i.e. with highest R^2 value, is highlighted in Table 10. On the heart, a 3rd order polynomial with and without constant gives the same R^2 value. On the Liver, a 3rd order polynomial without constant gives the best fit to the PVP calibration data. This result coincides with the theory explained in the previous chapter. On the kidneys, the best fit occurs with a 3rd order polynomial. On the spleen, the best fit is also a 3rd order polynomial only with cubic and square item. However, on this organ, there is slightly difference (0.9%) on the R^2 value between best fit and normal polynomial. Based on current findings, a normal 3rd order polynomial is the best fitting method giving best correlation. However, from a physical point, at 0m/s, there should be no PVP value on human body because no contact occurs. Using a 3rd order polynomial with constant will derive a non-zero PVP value when the impact speed is 0m/s, which is not physical. Therefore, in this case, a 3rd order polynomial without a constant term is proposed to be the best fitting method. The same procedure was applied to the brain tissue threshold (Table 11).

	$y=ax^3$	$y=ax^3+bx^2$	$y=ax^3+bx^2+cx$	$y=ax^3+bx^2+cx+d$
R2 of Brain contusion in side impact	-0.648	0.5336	1	0.6494
R2 of DAI in side impact	0.08923	0.6782	1	0.6953
R2 of Brain contusion in frontal impact	0.7808	0.9749	0.9799	0.982
R2 of DAI in frontal impact	0.7463	0.9086	0.9109	0.9115

Table 11 Fitting results on brain tissue

As shown in Table 11, the correlation coefficients of the different fitting methods of brain tissue threshold are presented. The same method was used as in organ the threshold fitting procedure, 3rd order, 2nd order, 3rd order polynomial and 2nd order polynomial. Negative correlation coefficient was found when using 3rd order fitting on threshold of brain contusion. This means that under a 3rd order fitting, the PVP and

the impact speed are moving in opposite directions. Overall, a 3rd order polynomial shows the best fitting on all thresholds of brain tissue. Since a 3rd order polynomial performed best fitting on threshold of organs (frontal impact) and brain tissue, therefore the same fitting method was then directly applied to thresholds of organs in the rear impact. The coefficients of a 3rd order polynomial (a, b, c) and correlation (R^2) are shown in Table 12.

	Heart	Liver	Spleen	Right kidney	Left kidney
a	0.009794	0.008927	-0.05674	-0.001677	-0.06117
b	0.2939	0.5195	0.9073	0.1074	1.323
c	-0.5991	-0.4883	-1.351	-0.2424	-3.216
R^2	0.9938	0.9939	0.9548	0.9993	1

Table 12 Fitting result of PVP threshold calibration in left lateral impact

As shown above, a 3rd order polynomial was applied to perform the curve fitting on threshold of organs in rear impact scenario. From the result of the correlation, coefficient (R^2), a 3rd order polynomial still gave the best fitting result.

6.2 PVP Corridor Scaling

The aim of this section is to apply the mathematical method derived in the methodology section (Figure 59) to generate the complete systematic PVP corridors covering all AIS levels. Due to the limited number of real-world accidents provided by UKPF, it is impossible to generate all AIS threshold directly. Consequently, the obtained AIS 4 thresholds will be scaled to obtained all the other ones.

At organ levels, PVP is the product of stress and strain rate. If it is a validated measure of injury severity, then it should be proportional to the maximum AIS (MAIS) score for body regions (Neal-Sturgess et al., 2001). Therefore, for a crash pulse, was proved that:

$$\text{Injury severity} \propto \text{PVP} \propto \text{MAIS (Neal-Sturgess et al., 2001)}$$

As MAIS is the numerical maximum value of AIS, therefore the proportional relationship shown above can be also presented as:

$$\text{Injury severity} \propto \text{PVP} \propto \text{MAIS} \propto \text{AIS}$$

Using medical data from previous research (Baker et al., 1974, Walder et al., 1995, Ulman and Stalnaker, 1986), the probability of fatality was plotted in Figure 18. An example of systematic PVP threshold corridor is presented in Figure 62.

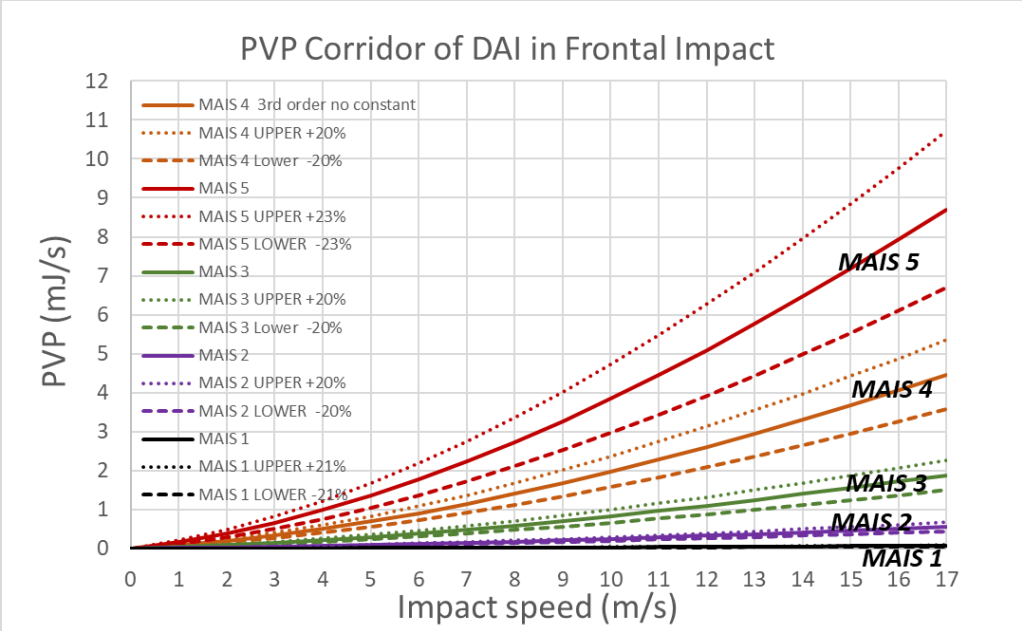

Figure 62 PVP corridor of DAI in frontal impact

Since the systematic PVP corridors have been determined, these corridors will be used as threshold indicators for trauma later in the thesis. By using accident data information provided from the UKPF, accident scenarios will be reconstructed accordingly, and their PVP on brain tissue and critical organs extracted. Trauma will be then computed by using PVP threshold corridors, as per Figure 18.

7.0 Real-world Accident Reconstruction

In this chapter, the real-world accidents provided by the UKPF will be reconstructed using the explicit CAE method discussed in the previous chapters. The first step was to filter real-world accident scenarios and select the ones providing the most chances for accurate reconstruction, including the vehicles involved in accidents, their geometry, stiffness, impact speed etc… as well as pedestrian information and PM results. All cases provided by the UKPF were factual cases. The pedestrians involved were also scaled to the given height and weight from the THUMS 4.0. Finally, the complete accident scenario was full replicated.

The best method to validate if PVP corridor enables to predict pedestrian injury is to duplicate real-world accident. The accident reconstruction focused in recreating the vehicle and the accident circumstances. In order to capture the pedestrian kinematics, the THUMS human model's geometry was scaled to match height and weight of the deceased using the scaling tool supported by Xiang Cheng from Coventry University to adjust height and mass. The THUMS model was then positioned in the most likely gait to replicate a comparable head landing position on the windscreen. The vehicle model was reconstructed with available data using its outside stylizing design surface whilst including a realistic stiffness locations acquired from the EuroNCAP vehicle assessment programme, using a similar methodology to the one used in APROSYS (Bastien, 2018).

Accidents used to validate were selected to include the detailed scene and the autopsy reports in order to reconstruct the impact scenario with realism. It was observed that the THUMS model had numerical instabilities for speeds greater than 40mph, hence any accident cases containing impact velocities exceeding 40mph were excluded from the study. It also has to be noted that the THUMS model does not include any fluid dynamics properties (SPH or ALE), injuries such as haemorrhage and swelling cannot be replicated. Based on these factors, the UKPF database was filtered and four relevant cases were selected to conduct the PVP trauma level calibration/ validation. The detailed selection filters are explained in the next section.

7.1 Real-life Accident Data Selection

•The accident data provided by the UKPF were released to the University, with the agreement of the Coroner and the agreement from the deceased families. From a statistical point of view, the size of the accident population was quite small. As discussed previously, due to the limitations of the THUMS human model and the simulations requirements, the following criteria were applied to filter the accidents into applicable cases

• The accident itself should have a precise police report with detailed description of the accident scene and detailed post-mortem report with detailed description of injuries withstood by the pedestrian and cause of death.

• Since the THUMS human model is a finite element human model with no separation mechanism to mimic human body organs when broken. High impact velocities can cause human body breakdown or separation, which the THUMS model cannot replicate. Therefore, to limit the amount body deformations, the impact speed cannot exceed 40mph (17.88m/s). Preferable impact speeds are in the range of 20mph (8.94m/s) to 30mph (13.41m/s).

• Due to the different body anthropometry, adult male scenarios are preferable (THUMS AM50 is a 50^{th} percentile male).

• It is ideal that vehicles involved in the accident should be a small sedan, not a truck or bus, because the limited choice of open source full finite element vehicle models. Also, in the cases of buses and trucks, the pedestrians tend to roll under the truck after the primary impact, which would make the reconstruction impossible. Vehicle models can be represented using a simple structure with different stiffness.

Due to the limited size of the database of the accidents available, the sample size is even smaller after applying the criteria, which is a limitation of this project. However, this is all the accident data available. Had enough data been available, then a statistical study on the validation on the applicability of PVP trauma prediction would have been more comprehensive. Consequently, this thesis will be based on these four cases.

7.2 Human Body Kinematics of Different Gait in Traffic Accident

As explained in this chapter, the gait of the pedestrian is very important, and it has a large influence on the pedestrian's kinematics during the accident.

Normally in the side impact scenario, the pedestrian has two walking gaits: left-leg forward or right-leg forward. Impact on different gait results in different trajectories, which will result different pedestrian rotation directions and contact area against the impacting vehicle (Appendix I). Different kinematics then produce differences injury patterns and severities (Figure 63).

Car colliding pedestrian from	Left			Right		
Leg contacting bumper (PM or video)	Left	Left	Right	Right	Right	Left
Location of windscreen impact head contact (PM)	Frontal	Occipital	Occipital	Frontal	Occipital	Occipital
Caused by	front of head hits windscreen	back of head hits windscreen	back of head hits windscreen	front of head hits windscreen	back of head hits windscreen	back of head hits windscreen
Head COG position prior to contact	Head forward of leg contact	Head rearward of leg contact	Head forward of leg contact	Head forward of leg contact	Head rearward of leg contact	Head forward of leg contact
Gait to consider	Rear Leg Hit	Front leg hit	Rear Leg Hit	Rear Leg Hit	Front leg hit	Rear Leg Hit

Figure 63 Different rotation direction and contact location due to different pedestrian gait (upper: left-leg forwarded, bottom right-leg forwarded) (Bastien et al., 2018)

The difference in kinematics due to pedestrian gait is highlighted in Figure 63. When the vehicle impacts from the right-hand side of a left-leg forward pedestrian, the upper torso rotates clockwise, resulting in a posterior head and torso contact against

the vehicle bonnet. When the vehicle impacts from the right side of a right-legged forward pedestrian, the upper torso rotates anticlockwise which results in a body contact on the anterior side of the head and torso. With this kinetic difference, it can be concluded that the pedestrian gait can be estimated from the body contact bruise locations and the damage marks observed on the vehicle during the pedestrian roll on the vehicle bonnet.

7.3 Vehicle Stiffness (Thickness) Reconstruction

In an accident, impact speed, contact geometry and contact stiffness are the dominant contributors to pedestrian injury severity (Bastien, 2018). Impact speed is given in the Police report. The vehicle frontal end was reconstructed with available data using its outside stylizing design surface and the contact stiffness modelled so that it replicates the same head impact injury location as Table 22 (Figure 64).

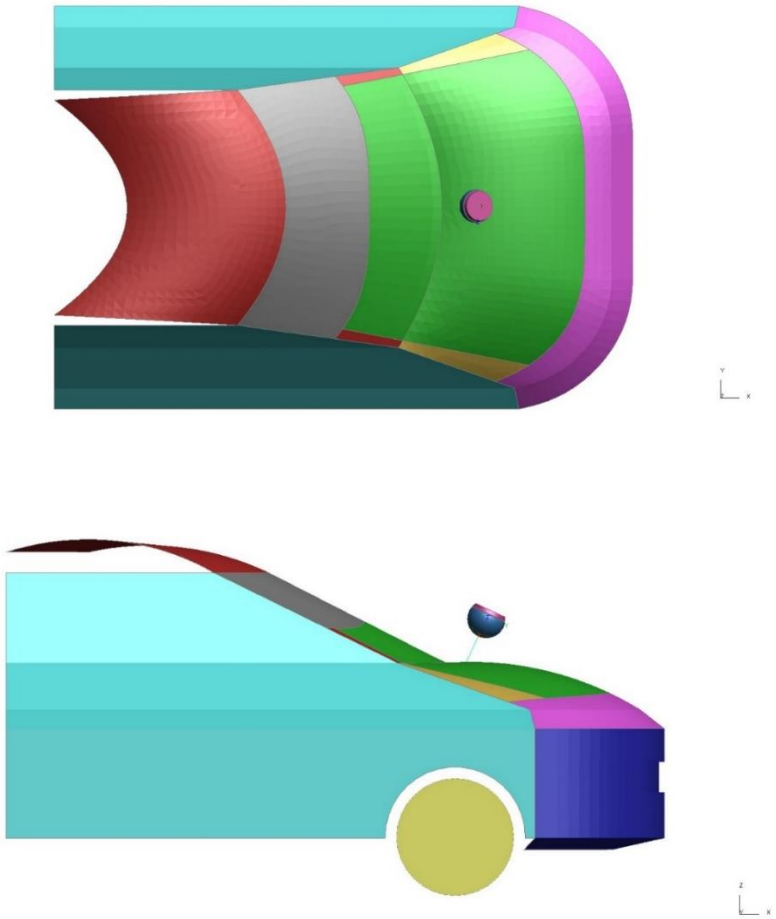

Figure 64 Stiffness test scenario

The stiffness of a vehicle bonnet is the combination of stiffness of the bonnet outer layer and inner supports. In this project, due to the lack of information, a CAD model with major geometry characteristics of the vehicle was derived. The vehicle model contains a single-layer bumper, bonnet and windscreen. The stiffness of the single-layer represents the whole structure stiffness of the actual vehicle. The stiffness of the bumper is created using comparable thicknesses.

Each stiffness is calibrated by changing the local thickness of the bonnet and correlating against an effective HIC value comparable to its EuroNCAP scoring. The HIC value is calculated using the accelerometer in the centre of the headform. In the EuroNCAP pedestrian protocol, the stiffness corresponding colour is listed in Table 13, each of them representing a stiffness level. Each stiffness range is represented using an assorted colour.

Green	<650
Yellow	650-1000
Orange	1000-1350
Brown	1350-1700
Red	>1700

Table 13 Stiffness and corresponding colour in EuroNCAP (EuroNCAP 2015)

From the literature review, in the EuroNCAP test, the vehicle bonnet is divided into child zones and adult zones. Therefore, in order to obtain a representative bonnet stiffness, a 3.5kg child head form and a 4.5kg adult head form were used to assess the local panel stiffness. Then corresponding thickness in each test was documented (Table 14)

	3.5kg		**4.5kg**	
	Thickness(mm)	HIC	Thickness(mm)	HIC
Green	1.47	650	1.8	649
Yellow	1.9	996	2.31	998
Orange	2.27	1325	2.8	1344
Brown	2.68	1692	3.05	1699
Red	2.69		3.06	

Table 14 Thickness and corresponding colour in EuroNCAP using child and adult head form (EuroNCAP 2015)

HIC value of each colour is given in a range, to fully duplicate the stiffness of the involved vehicle, maximum, average and minimum thickness of every colour will be applied in reconstruction (Table 15 and Figure 65).

	3.5kg			**4.5kg**		
	Max (mm)	Ave (mm)	Min (mm)	Max (mm)	Ave (mm)	Min (mm)
Green	1.47			1.8		
Yellow	1.9	1.69	1.47	2.31	2.06	1.8
Orange	2.27	2.09	1.9	2.8	2.56	2.31
Brown	2.68	2.5	2.27	3.05	2.93	2.8
Red	2.69			3.06		

Table 15 Thickness range of child and adult head form

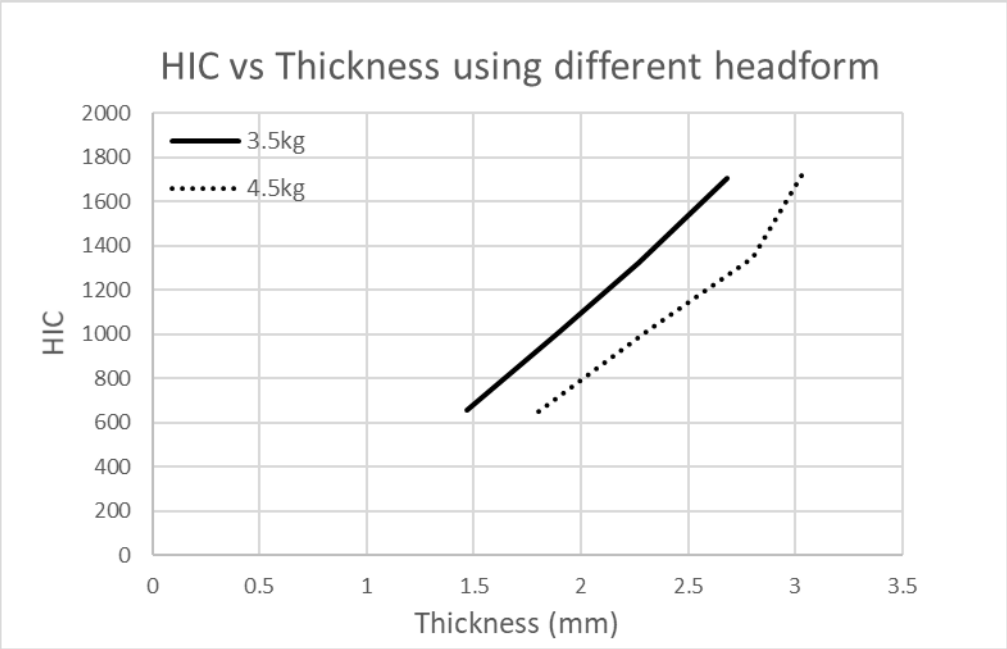

Figure 65 HIC vs thickness using different headform

As shown in Table 15 and Figure 65, the thickness necessary to generate the same HIC value varies with different headforms. Using the result of this investigation, the corresponding thicknesses were then applied to the designated area according to the EuroNCAP pedestrian test results of involved vehicle.

7.4 Real-world Accident Reconstruction Result

The selected UKPF cases meeting our requirements are listed in Table 16.

Case Id:	Vehicle	Pedestrian Mass (kg)	Pedestrian Height (cm)	Impact direction	Impact Speed (m/s)
1	Seat Leon	61.0	183	Left side impact (right leg forward)	16.0
2	Toyota Corolla	58.6	165	Right side impact (right leg forward)	11.2
3	Renault Clio	79.2	173	Side (left leg forward)	12.5
4	Benz B180	56.4	165	from driver's near to far side	12.5

Table 16 Case summary

As illustrated in Table 16, these four cases were filtered based on the criteria listed in section 7.1 from the UKPF database. These four cases are reconstructed accordingly. The stiffness reconstruction of vehicle frontal end for each selected case is shown in Table 17.

Case Id	EuroNCAP scoring	CAE model colour code
1(EuroNCAP, 2012a)	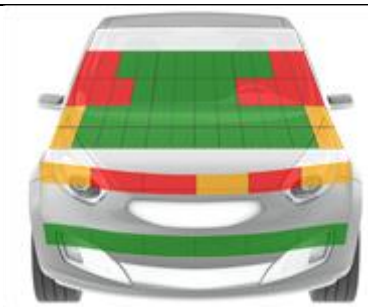	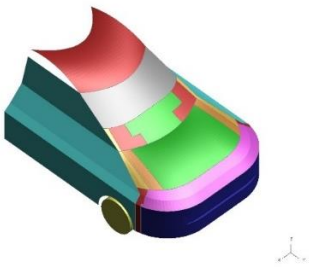
2(EuroNCAP, 2013)		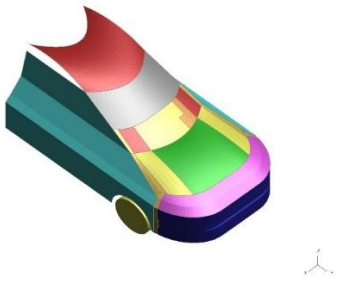
3(EuroNCAP, 2012b)		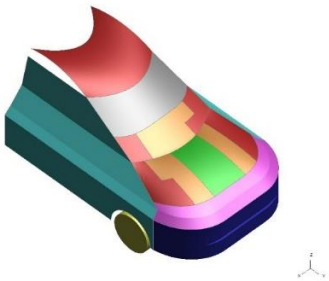
4(EuroNCAP, 2011)		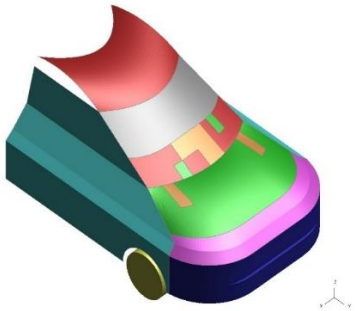

Table 17 Stiffness mapping for CAE models vs EuroNCAP

Using the stiffness investigation result from section 7.3, the corresponding thickness of the colliding vehicles was then applied to the designated areas according to the EuroNCAP scoring results shown in second column in Table 17. After adjusting for the

pedestrian height and weight, the four accidents were then replicated as shown in Table 18.

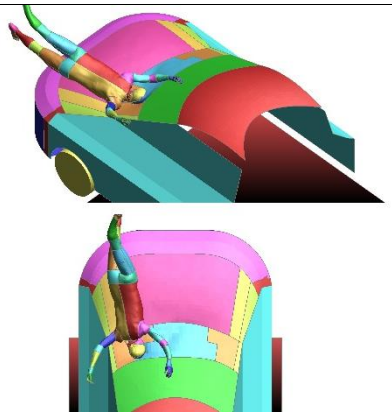	
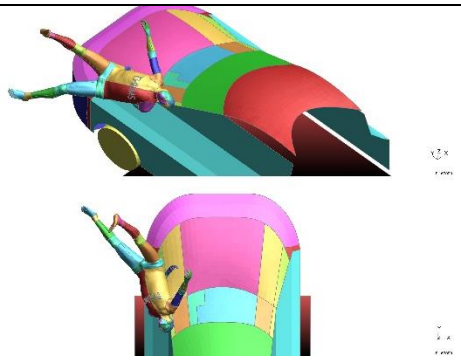	
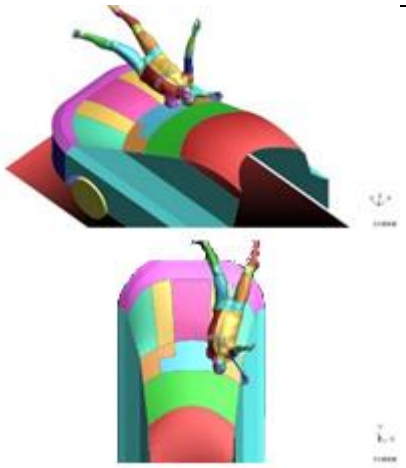	

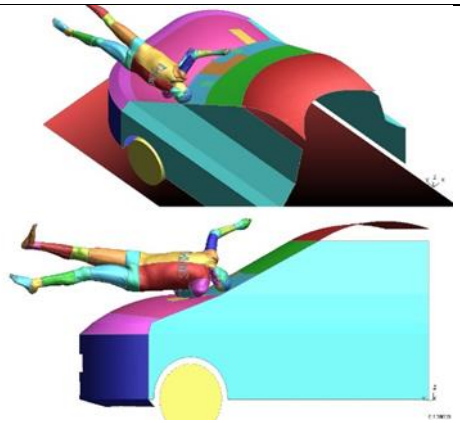	

Table 18 Landing area comparison between CAE and accident

In Table 18, the CAE reconstruction of every case was compared against the vehicle damage observable from the photographic evidence provided by the UKPF. Once the CAE simulation replicated the same kinematic behaviour and head strike landing position as the real-world accident, then PVP value was extracted.

8.0 Results

Following the accident reconstruction, the injury results of the pedestrian brain tissue and organs from the CAE simulations are extracted and the numerical trauma computed using the calibration curves extracted in chapter 4. In each case, the reconstructed scenario is initially commented upon, followed by the CAE global energy stability check, the contact forces observed on the vehicle and then the pedestrian kinetics. Finally, the PVP of the pedestrian brain tissue and the critical organs are extracted from the CAE computations.

8.1 Case 1: Accident scenario and Computation Setup

Accident 1 is a collision between an elderly male pedestrian and SEAT Leon (small sedan). The pedestrian was stuck when he was crossing the road (Figure 66). Based on the statement from the driver, due to parked vehicles to the nearside, he was driving closer to the centre of the road. The UKPF therefore drew an illustration of accident scenario based on the information (Figure 66).

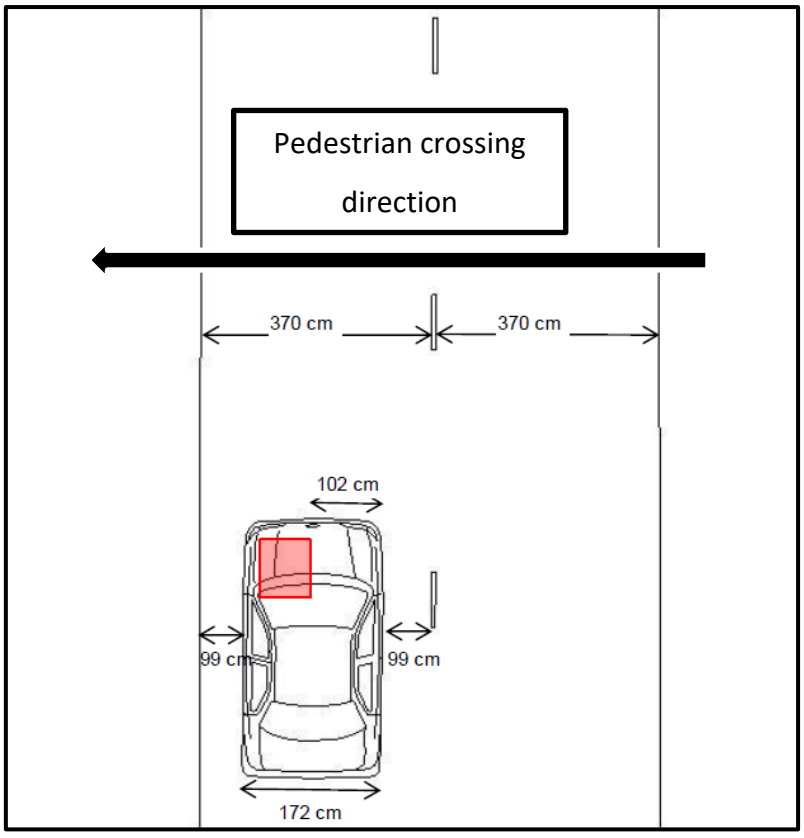

Figure 66 Accident location and pedestrian movement direction

The pedestrian was witnessed to run into the road and leave the driver no opportunity to stop. The UKPF concluded that the initial contact point between vehicle and pedestrian was on bumper, which is 102cm from the offside of the vehicle (point A in Figure 67).

Figure 67 Initial contact location on vehicle

The pedestrian was pronounced dead at the scene, and he sustained injuries above his right eye, under his chin and there was also a large area of grazing to the left side of his chest and abdomen. Based on the pedestrian kinematics investigated in section 4.2, it was concluded that the pedestrian was right-leg forward when the accident occurred. The windscreen was totally smashed in the accident and blood and human body tissue can be observed on A pillar (Figure 68, Figure 69 and Figure 70).

Figure 68 Vehicle damage locations

Some materials have been removed from this thesis due to Third Party Copyright. Pages where material has been removed are clearly marked in the electronic version. The unabridged version of the thesis can be viewed at the Lanchester Library, Coventry University

Figure 69 Blood on A pillar

Figure 70 Human body tissue on driver's door

All the information of the vehicle damage gave enough information to replicate the trajectory of the pedestrian landing process. This trajectory can be used to obtain pedestrian speed at the time of collision.

From the debris of the pedestrian belongings, the Police concluded that the vehicle speed was between 36mph and 44mph (16.09m/s-19.67m/s). Regarding the pedestrian speed, the UKPF used normal walking speed of 65+ years old (0.9m/s) as reference speed, which was questionable. Based on the reviewed human walking and running speed (Table 19 and Table 20), the running speed for 65+ year old male is 2.04m/s. Therefore, the pedestrian speed in simulation was assigned as 2.04m/s.

Pedestrian Age	Sample Size	Speed (m/s)		
		15th%	50th%	85th%
5-9	26	1.4	1.83	2.41
10-14	37	1.37	1.68	2.1
15-19	47	1.46	1.65	2.07
20-24	65	1.4	1.62	1.86
25-34	70	1.46	1.62	1.98
34-44	67	1.34	1.62	1.95
45-54	73	1.31	1.52	1.74
55-64	90	1.28	1.46	1.68
65+	67	1.07	1.28	1.46

Table 19 Pedestrian walking speeds for different age groups (Huang et al., 2006)

Pedestrian Age	Sample Size	Speed (m/s)		
		15th%	50th%	85th%
5-9	332	3.11	3.94	4.8
10-19	718	3.51	4.2	4.96
20-29	134	2.8	3.54	4.24
30-39	204	2.68	3.35	3.81
40-49	138	2.41	2.9	3.44
50-59	35	2.38	2.83	3.2
60+	30	2.04	2.47	2.71

Table 20 Pedestrian running speeds for different age groups (Huang et al., 2006)

The vehicle model was then reconstructed with available data using its outside stylizing design surface whilst including a stiffness location. As described in the previous section, the maximum, average and minimum thicknesses were applied to the vehicle exterior. It was observed that the maximum and minimum thicknesses did not alter the AIS level, (i.e. AIS prediction result did not change) only the PVP result changed numerically. Therefore, only the results of average thickness of reconstruction are presented in the thesis. The stiffness distribution of SEAT Leon was reconstructed as shown in Table 21.

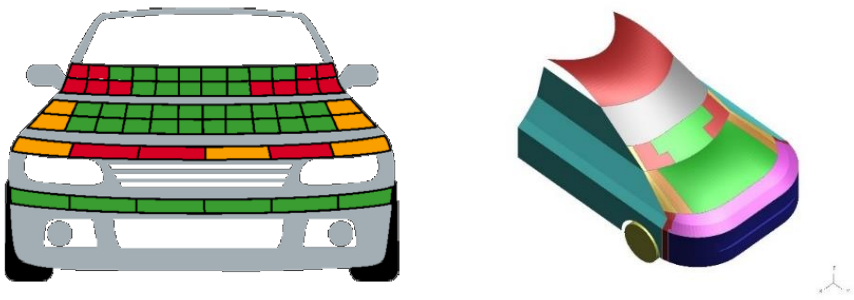

Table 21 Stiffness distribution of bonnet of SEAT Leon from EuroNCAP (EuroNCAP, 2012a)

Comparable stiffness of bumper and leading edge was used on the SEAT vehicle model. Also, a mass of 1.41 tonne was assigned to vehicle model according to actual curb weight of a SEAT Leon (Centre, 2012). In the autopsy report, the pedestrian mass was given as 61kg with a height of 183cm. The THUMS model was then scaled accordingly and positioned as right-led forwarded. Based on all the description of accident, the simulation scenario was reconstructed as illustrated in Figure 71.

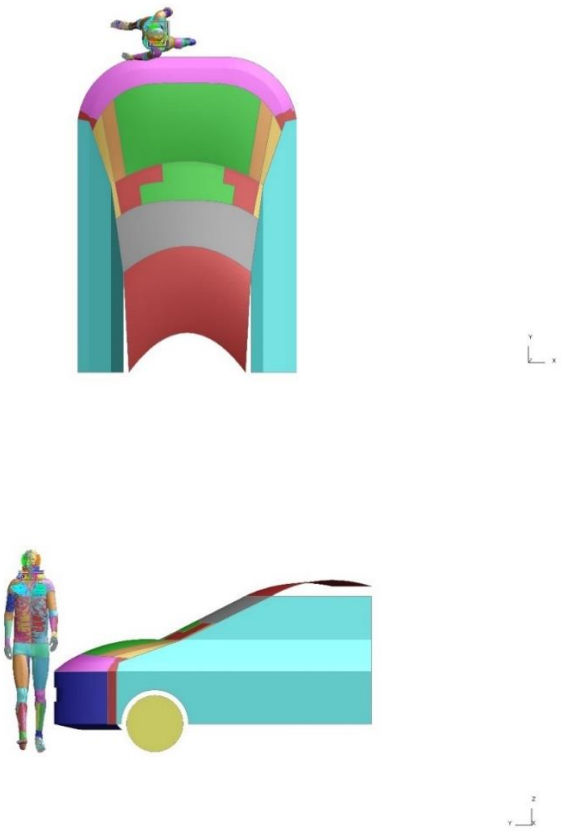

Figure 71 Simulation scenario

8.1.1 Pedestrian Kinematics

Different vehicle and pedestrian speed combinations were tested in this accident reconstruction. An initial simulation based on the UKPF accident report was performed (crossing speed of 0.9m/s), however the landing area (Figure 72) using computer simulation was very different compared to the vehicle damage evidence (Figure 68, Figure 69 and Figure 70).

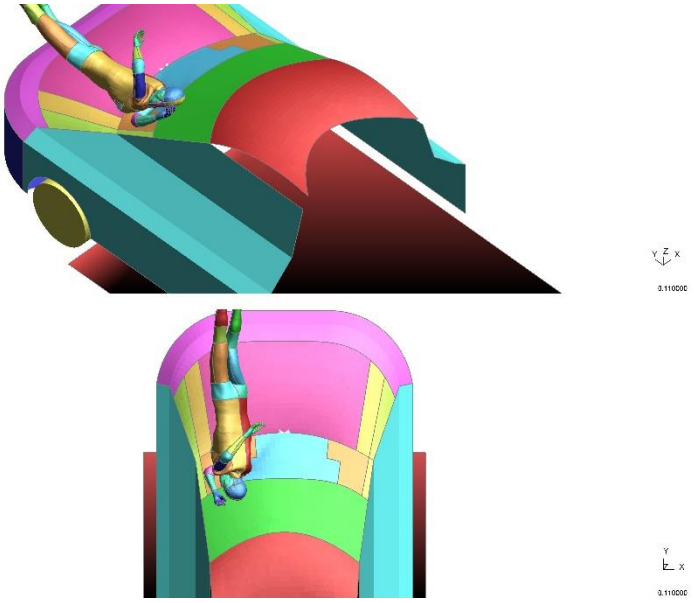

Figure 72 Pedestrian landing area of speed 0.9m/s

Considering the discrepancy in pedestrian landing zone, witness statement and pedestrian running speed, a 2.04m/s was applied in the simulation and the trajectory illustrated in Figure 73.

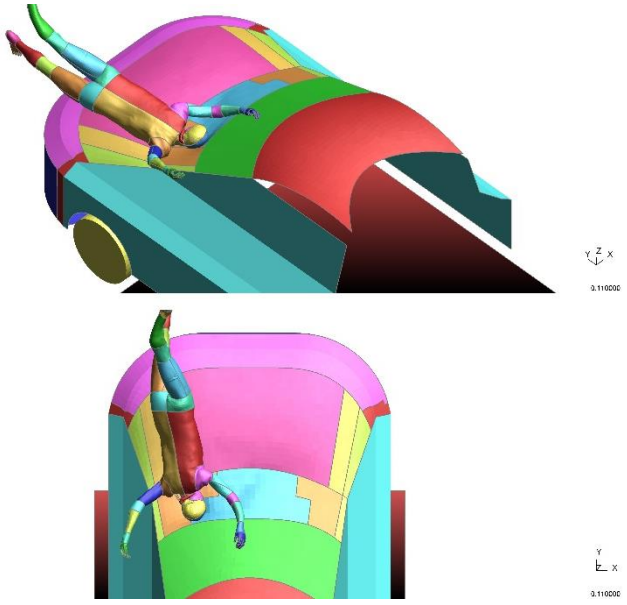

Figure 73 Pedestrian landing area of speed 2.04m/s. Vehicle speed 36mph (16.09m/s).

Again, by comparing the landing area against vehicle damage shown in Figure 68, Figure 69 and Figure 70, at speed of 2.04m/s, the pedestrian head landed on comparable area of windscreen. It was therefore concluded that a 2.04m/s crossing

speed was more likely to have had happened. The pedestrian kinematics during collision is presented in Figure 74.

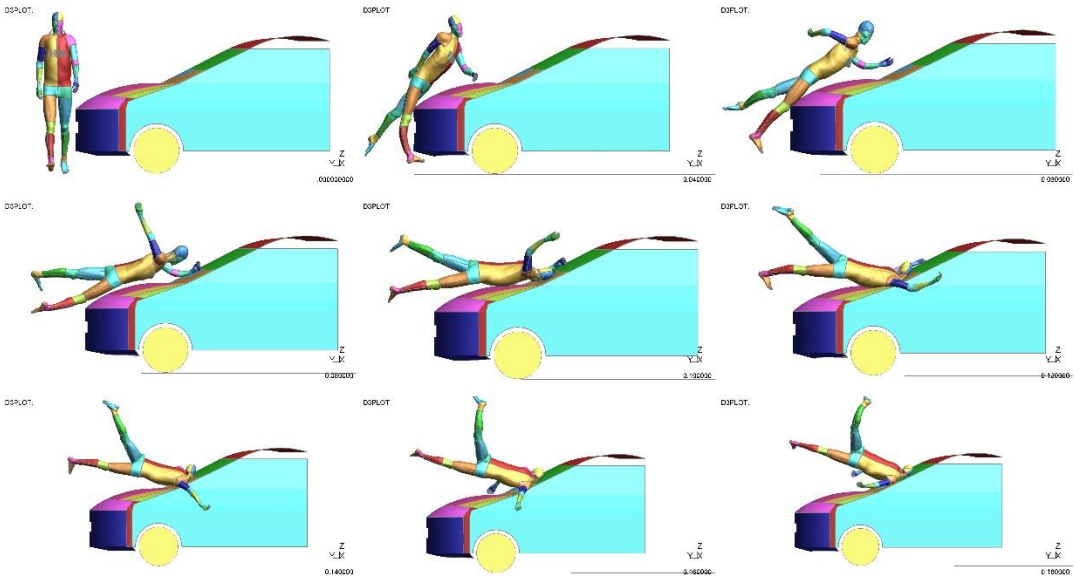

Figure 74 Pedestrian kinematics during impact at vehicle speed of 36mph

The pedestrian was right-leg forward at running speed of 2.044m/s when the collision occurred. The pedestrian lower extremities impacted with the bumper at the initial stage of the collision. Regarding the autopsy report, the injury was observed on the right thigh and patella. In the simulation, the right thigh contacted with the bonnet leading edge and the right ankle contacted with lower bumper. When the pedestrian landed on the windscreen, the frontal area of head contacted with the glass with coincided with damage observed on the vehicle. Also, the anterior area of the torso contacted with the bonnet which coincides with the injury location described on chest and abdomen in the autopsy report. To ensure the model is numerical stable, the energy curves of whole simulation isshown in Figure 75 and the contact forces between pedestrian and vehicle is shown in Figure 76.

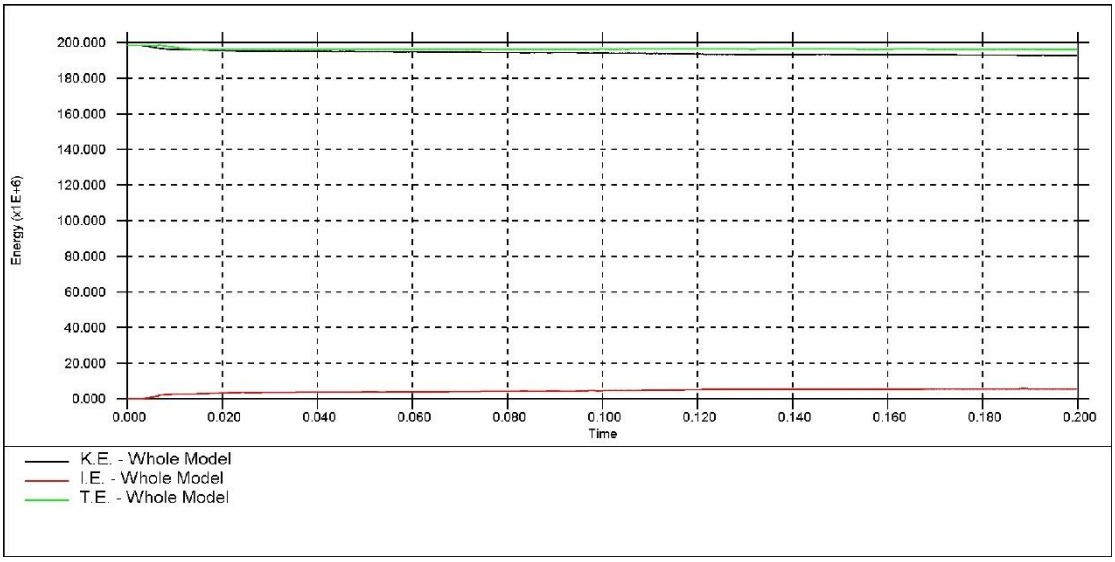

Figure 75 Energy curve of case 1

As shown in Figure 75, the total energy curve remains constant throughout the whole time history. There is no energy loss and no hourglassing, therefore, the whole simulation is numerically stable.

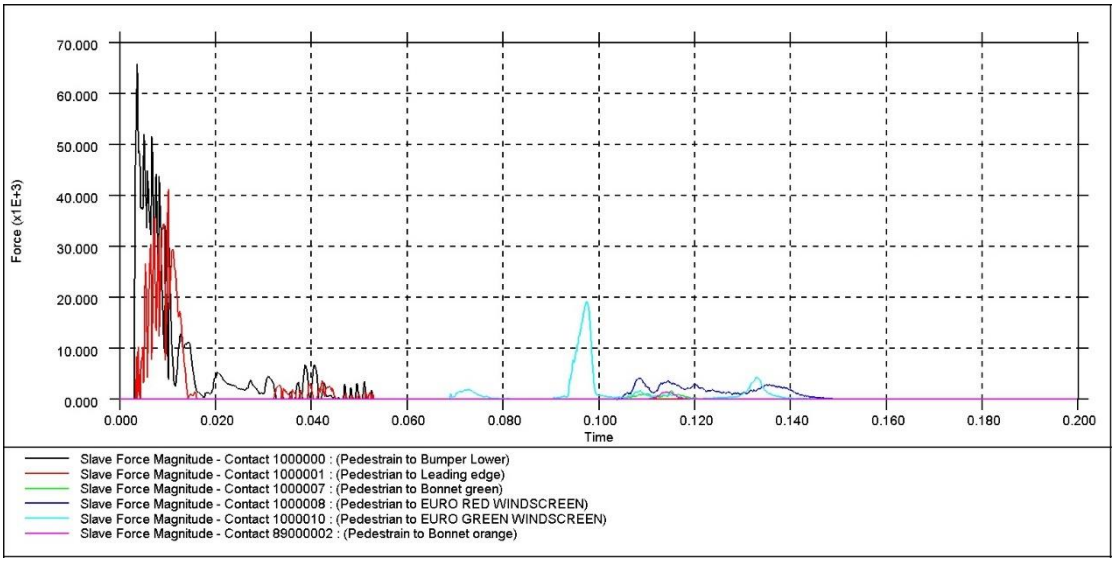

Figure 76 Contact force of case 1

As shown in Figure 76, pedestrian lower extremities contacted with lower bumper at first showing as the first peak around 0.01s. Then the pedestrian started to rotate due to the impact: thigh, pelvis and lower abdomen started to contact with bonnet leading edge shown as peak around 0.04s. The pedestrian landed on the windscreen around 0.1s and the contact lasted until 0.14s.

8.1.2 Injury Results using PVP

The pedestrian was frontally impacted against vehicle windscreen. Therefore, the PVP corridors of frontal impact calibration corridors were used as injury threshold indicators as shown in Table 22

Organs (Injury)	AIS level	PVP Threshold at 36mph (mJ/s)
white matter (DAI)	4	4.46
Grey matter (Brain contusion)	3	2.33
Heart (Rupture)	4	46.44
Liver (Rupture)	4	10.54
Spleen (Rupture)	4	4.42
Right kidney (Rupture)	4	6.31
Left kidney (Rupture)	4	11.47

Table 22 PVP threshold of AIS 4 injury at impact speed of 36mph

The PVP values and distributions of brain tissue and critical organs were then extracted to display the pedestrian trauma injuries. The PVP and its distribution on the brain white matter are highlighted in Figure 77. The PVP and its distribution on the brain grey matter in Figure 78. The PVP value and distribution on the critical organs highlighted from Figure 79 to Figure 82.

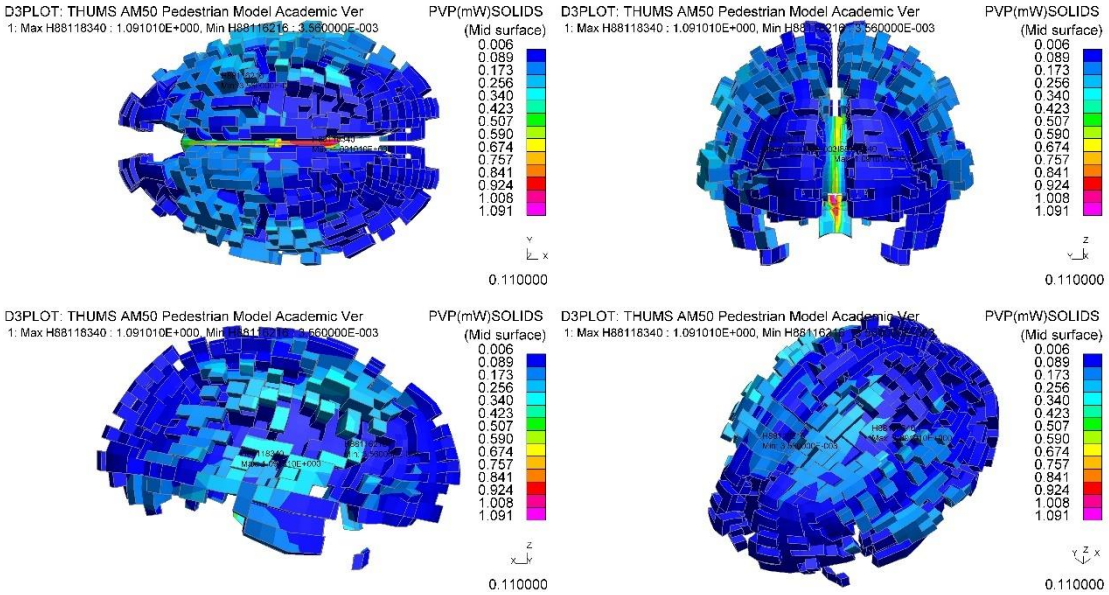

Figure 77 PVP on brain white matter at 0.11s (110ms) of case 1

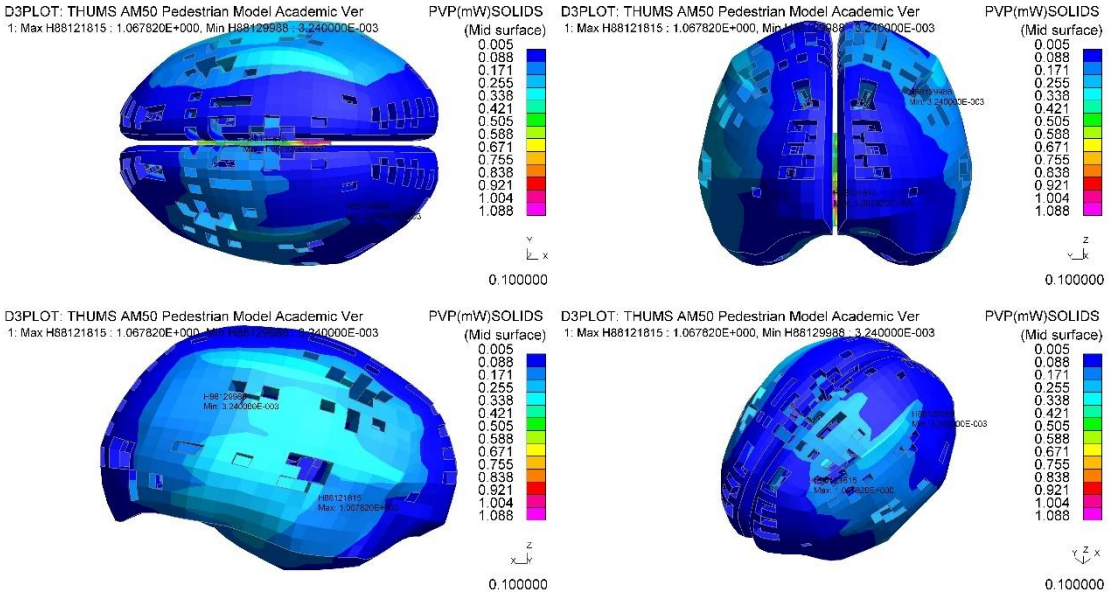

Figure 78 PVP on brain grey matter at 0.1s (100ms) of case 1

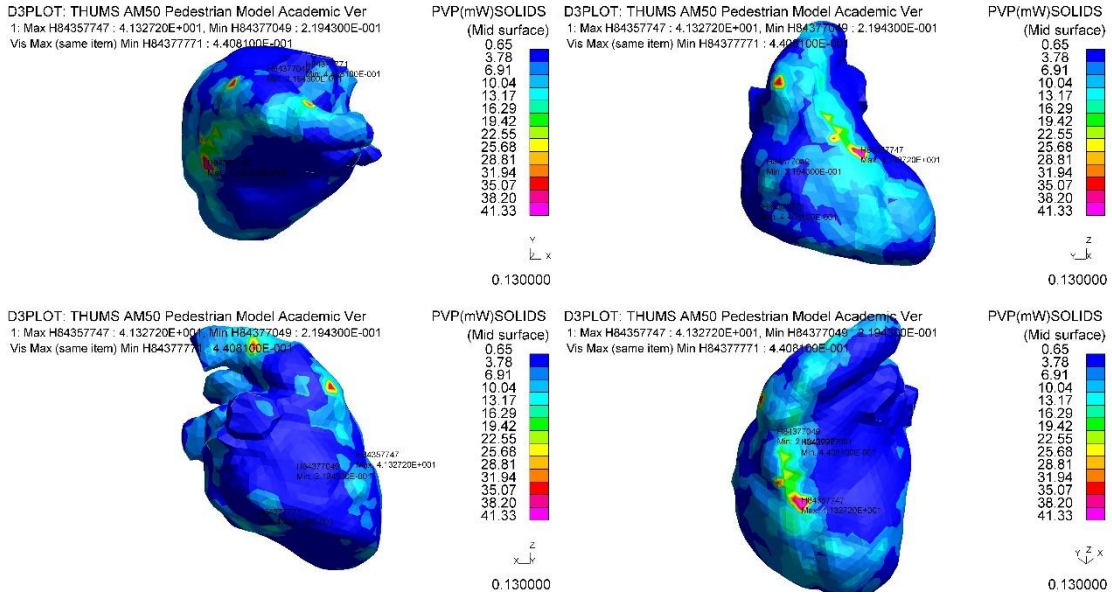

Figure 79 PVP distribution on heart at 0.13s (130ms) of case 1

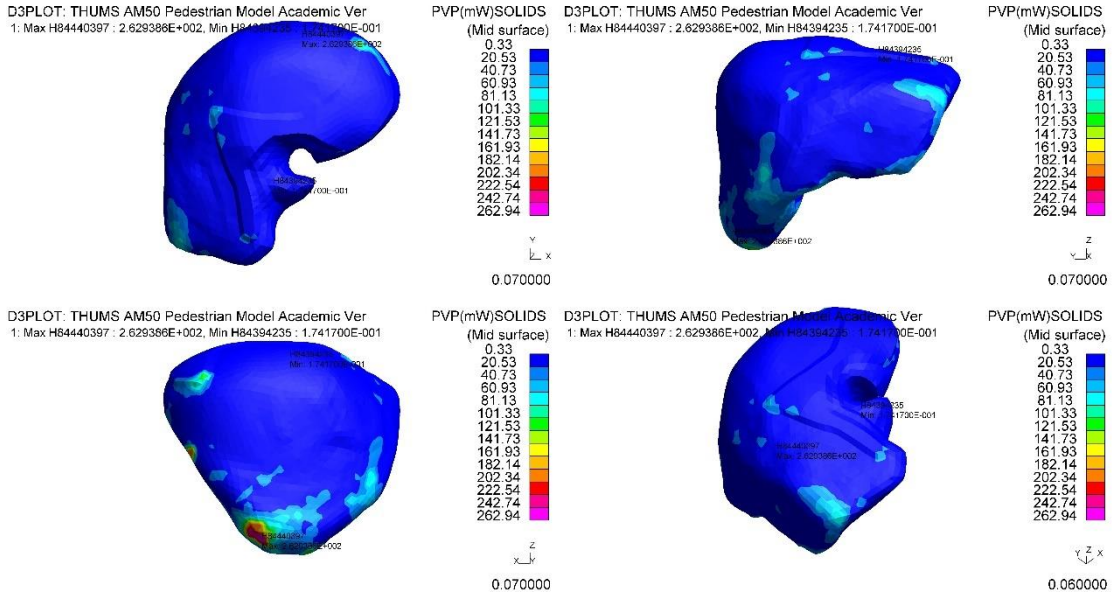

Figure 80 PVP distribution on liver at 0.06s (60ms) of case 1

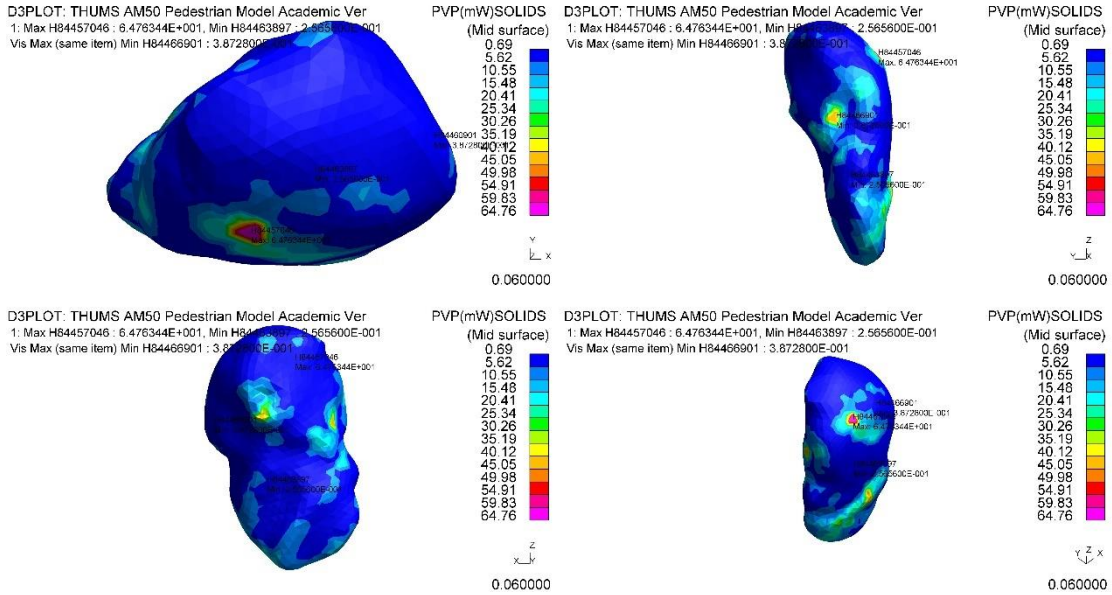

Figure 81 PVP distribution on spleen at 0.06s (60ms) of case 1

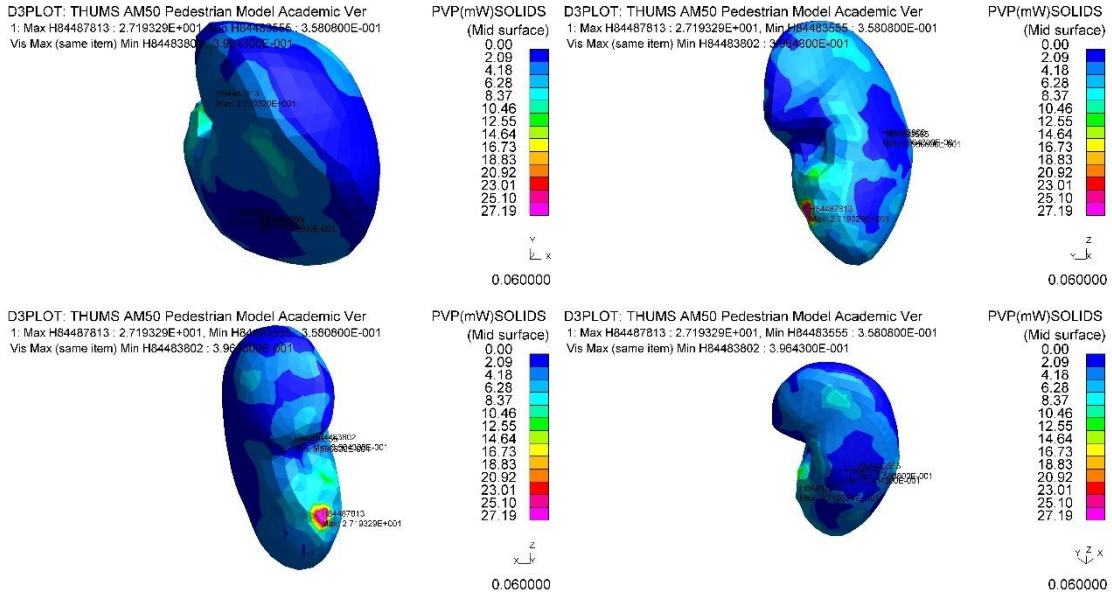

Figure 82 PVP distribution on left kidney at 0.06s (60ms) of case 1

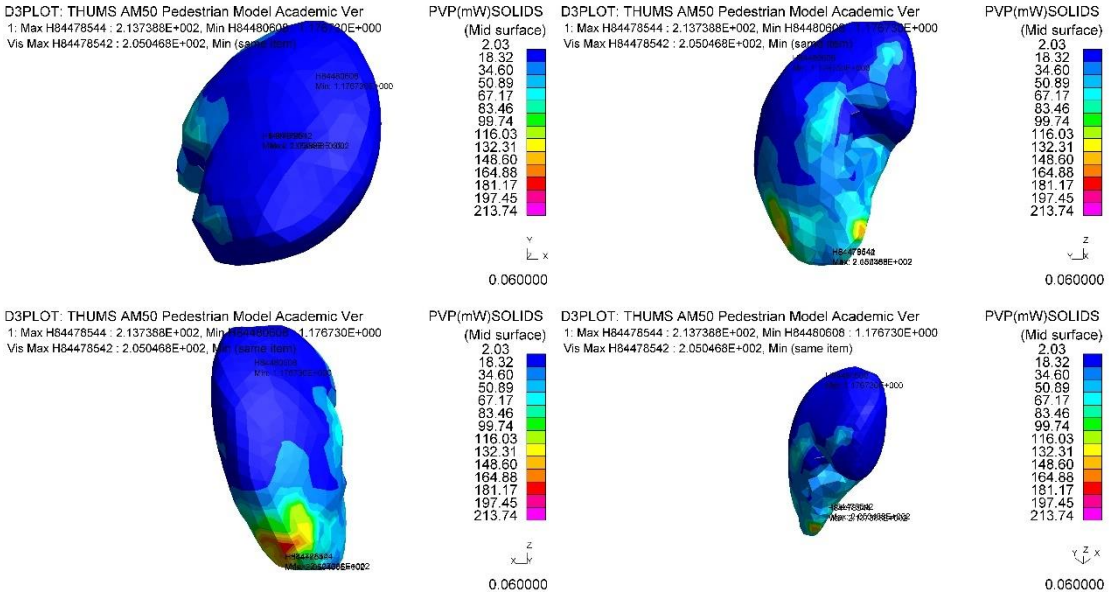

Figure 83 PVP distribution on right kidney at 0.06s (60ms) of case 1

In summary, The PVP values of accident 1 at vehicle speed of 36mph are listed in Table 23.

Organs/Location	36mph (mJ/s)	Time (ms)
White matter (DAI)	1.09	110
Location (ID)	88118340	
Grey matter	1.07	100
Location (ID)	88121815	
Heart	41.33	24
Location (ID)	84357747	
Liver	262.94	37
Location (ID)	84440397	
Spleen	64.76	57
Location (ID)	84457046	
Left kidney	27.19	32.7
Location (ID)	84487813	
Right kidney	213.74	15.4
Location (ID)	84478544	

Table 23 PVP result of accident 1

8.1.3 Result of Case1

The summary of injury results of case 1 is listed in Table 24, as well as the comparison between CAE prediction and PM report. The comparison of individual injury is also presented from Figure 84 to Figure 90.

Organs/Tissue	Injury	AIS of PM	AIS of CAE	MAIS of PM	MAIS of CAE	ISS of PM	ISS of CAE
Brain white matter	DAI	4	2-3	4	3	48	54
Brain grey matter	Brain contusion	0-2	2				
Heart	Rupture	4	4	4	3+		
Liver	Rupture	4	6+	4	6		
Spleen	Rupture	2-3	6+				
Right kidney	Rupture	4	6+				
Left kidney	Rupture	4	5+				

Table 24 Injury summary of Case 1

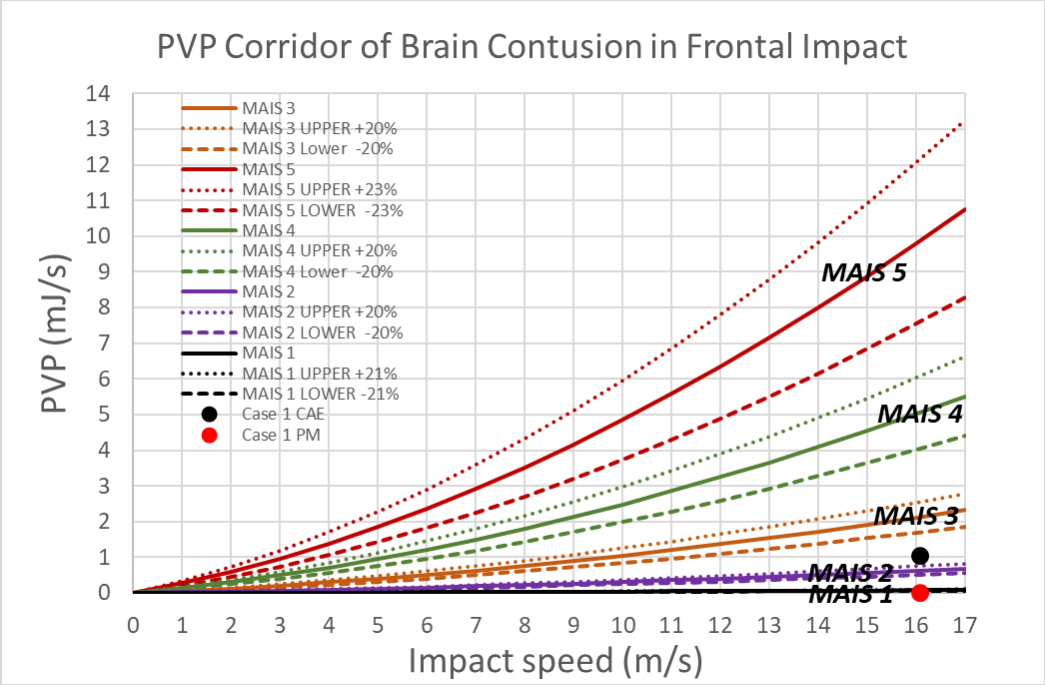

Figure 84 Brain contusion result of case 1 from CAE and autopsy report

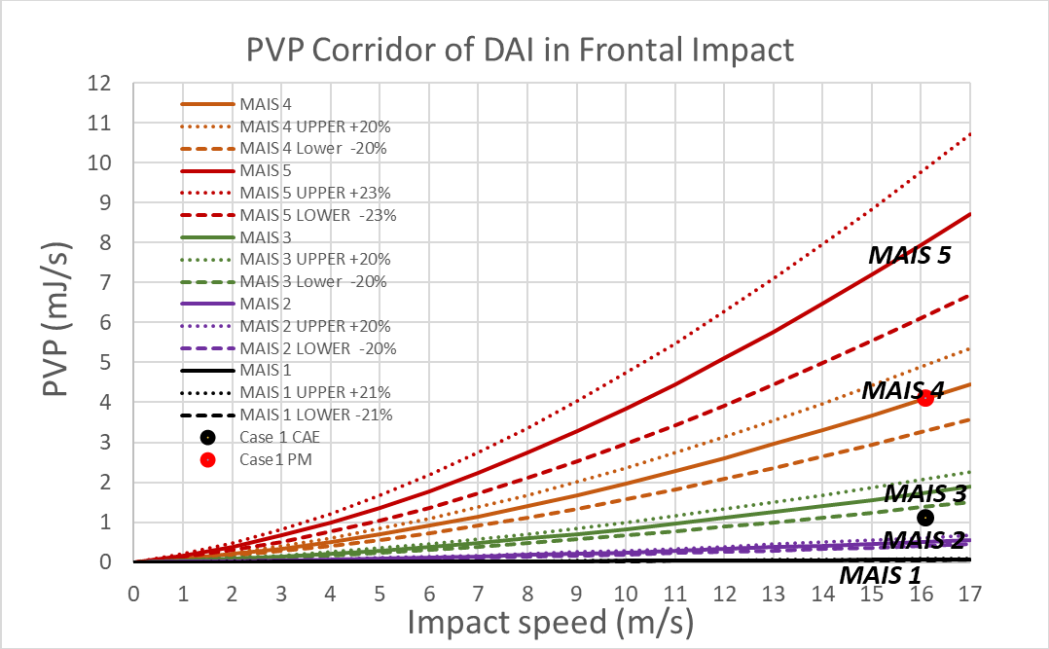

Figure 85 DAI result of case 1 from CAE and autopsy report

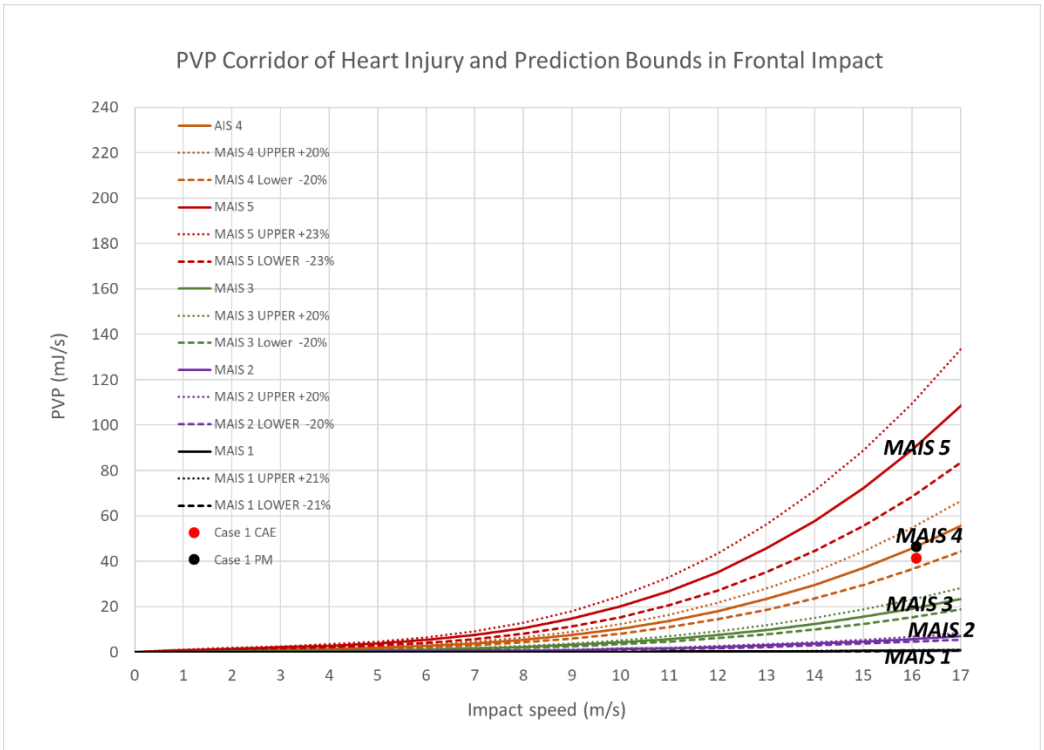

Figure 86 Heart injury result from CAE and Post-mortem report of case 1

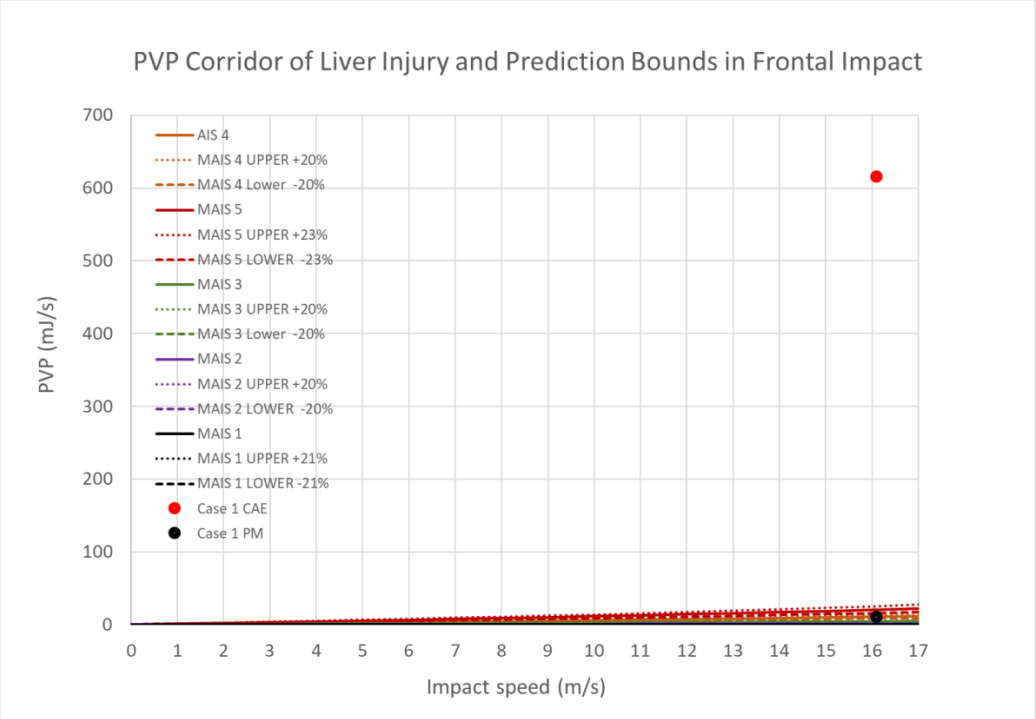

Figure 87 Liver injury result from CAE and Post-mortem report of case 1

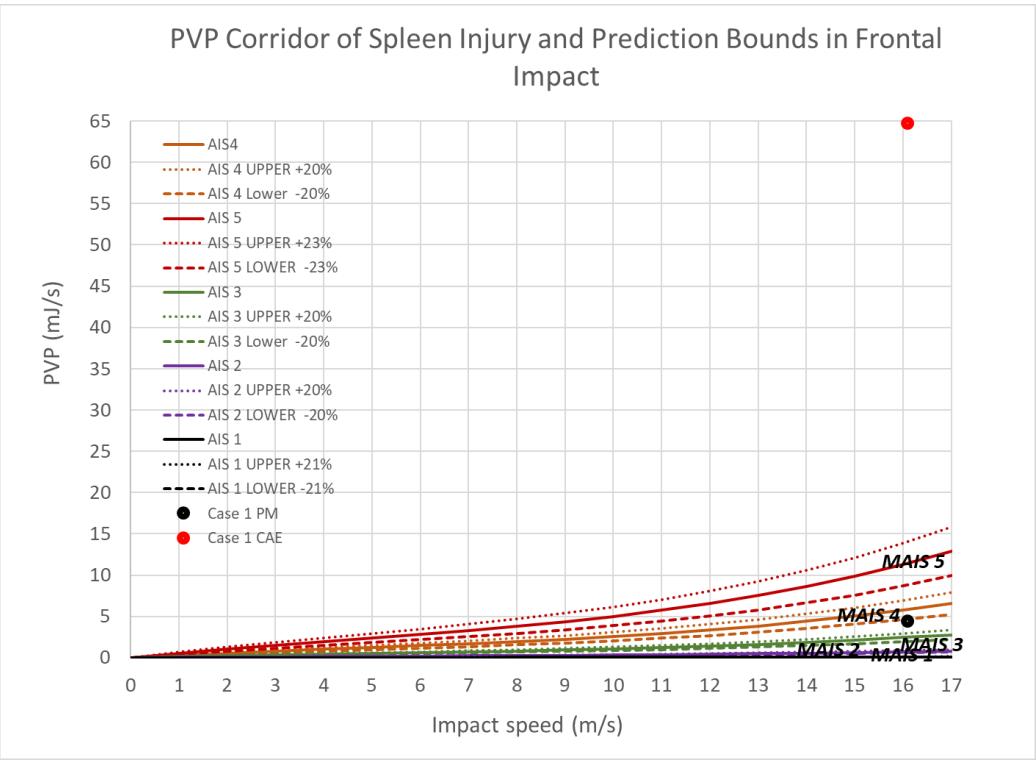

Figure 88 Spleen injury result from CAE and Post-mortem report of case 1

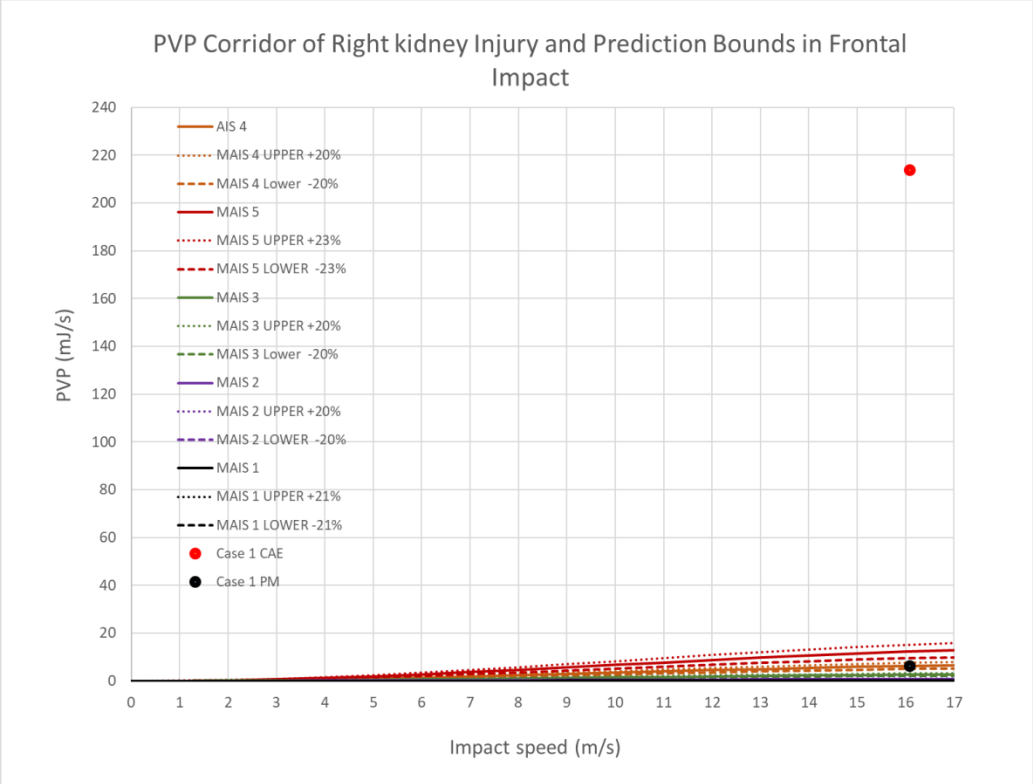

Figure 89 Right kidney injury result from CAE and Post-mortem report of case 1

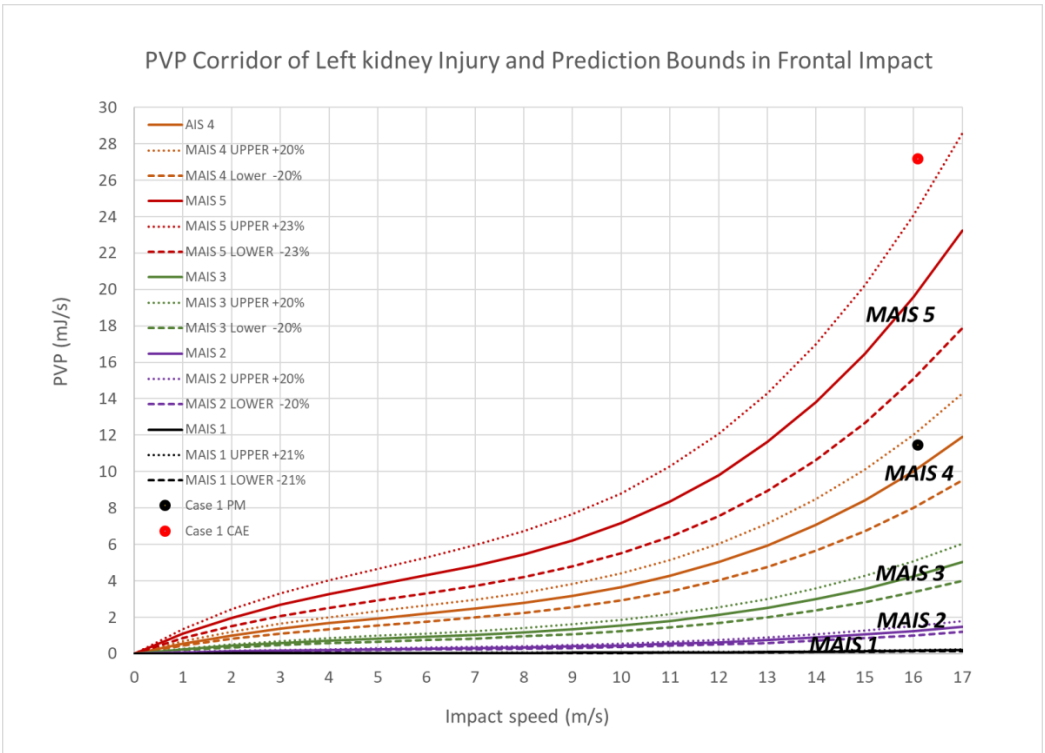

Figure 90 Left kidney injury result from CAE and Post-mortem report of case 1

The initial results suggests that the CAE predictions are in the same order of magnitude as the PM report on brain tissue injury. At an early stage of the impact, the pedestrian lower extremities contacted with vehicle lower bumper, and then the thigh, then the pelvis and the lower abdomen contacted with the bonnet leading edge. The pedestrian's head landed on the windscreen at the last stage. Based on the contact force graph (Figure 76), the head contacts with windscreen lasted from 0.09s (90ms) to 0.15s (150ms). Low values of PVP were observed before 0.09s (90ms). As the head rotated on the windscreen, the PVP spreads on both the parietal lobe and the temporal area. Before 0.09s, very low PVP were observed on the centre area of the brain white matter. After contacting with the windscreen, the PVP was visible on the parietal lobe, the temporal area and the centre area. On the grey matter, before 0.09s, very low PVP was observed on centre area brain grey matter. After contacting with the windscreen, the PVP was visible on the parietal lobe, the temporal area and the centre area. Compared with left side of the head, the PVP distribution area on the parietal lobe is larger on right side of grey matter. The maximum PVP value was observed at 0.11s (110ms) on white matter and 0.1s (100ms) on grey matter. The Solid element with highest PVP value on white matter is number 88118340, which is in centre area of right white matter (Figure 91 - left). The solid element with the highest PVP value on grey matter is 88121815, which is located in the centre area of right grey matter (Figure 91 - right), while in the PM report, the brain showed an area of subdural haemorrhage over the right parietal lobe, also over the cerebellum in the midline and over right cerebella hemisphere. A cut surface of the brain showed some small petechial haemorrhage present in the right cerebella peduncle. No other brain injury was identified. The pedestrian died however of a brain haemorrhage. The CAE model can only predict mechanical damage, it is not able to predict the blood loss, which is a dynamic, post-accident fluid problem. As a side symptom, haemorrhage can be considered as a clue to DAI. Nevertheless, as a mechanical indicator it is predicted in the correct damage area.

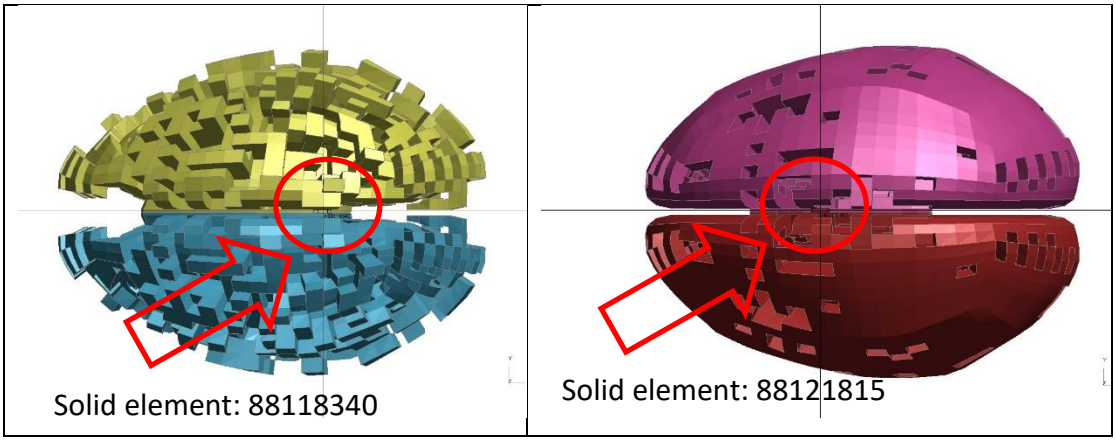

Figure 91 Injury location of brain white matter (left) and grey matter (right) of case 1

On the heart, both CAE and PM indicated an AIS 4 heart rupture. A low value PVP was visible before the pedestrian contacting the bonnet leading edge. The PVP increased as the pedestrian rotated on the bonnet. A large PVP distribution was observed at the anterior and the top of the heart. The maximum PVP value was visible on the anterior portion of the heart.

As the liver is located in the middle of the abdomen area, the PVP is identified at the early stage of collision. A low PVP value was visible when the pedestrian started to land on bonnet leading edge. As the pedestrian started to contact with the bonnet, a large PVP distribution was observed on frontal bottom area of the liver.

The kidneys are located in the lower abdomen at the back of human body. A rise of PVP can be noticed in the early stage of collision. A large PVP distribution area was observed on the lower part of right kidney. The maximum PVP was also located in lower part of right kidney.

On the liver, the PM shows obvious rupture over the anterior surface, which was also observed in the CAE result. In addition, the CAE simulation indicates a higher AIS level injury than the PM outcome. The liver showed obvious rupture over the anterior surface in the PM report, which was also observed in the CAE result. CAE results highlight that the damage location is on the bottom anterior surface of liver. However, the PM report just specifies the damage location as anterior surface. On the spleen, the CAE suggested a high AIS level injury while the PM concluded an AIS 4 rupture. In the PM report, there was a marked perinephric haemorrhage around both kidneys, which is out of the prediction scope of THUMS model.

8.2 Case 2: Accident scenario and Computation Setup

Accident 2 is a collision between a female pedestrian and a TOYOTA Corolla (small sedan). The female pedestrian had been crossing the road (from offside to nearside) to use a telephone kiosk. Upon reaching lane two of the inter-city carriageway, the pedestrian wasstruck by the vehicle. As the vehicle involved in the accident is a TOYOTA Corolla, the provided CAD vehicle model wasscaled to the dimensions according Corolla's blue print (Figure 92).

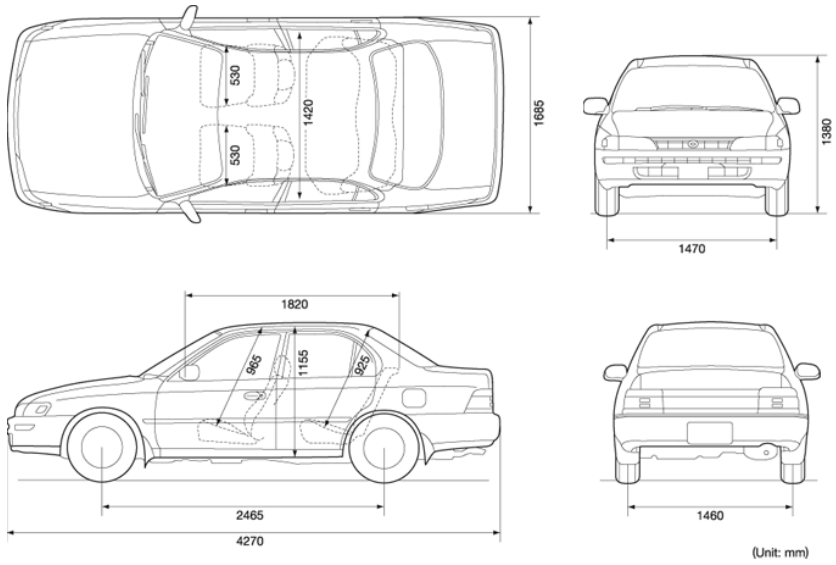

Figure 92 TOYOTA Corolla blue print (Tomil, 2007)

The stiffness of the vehicle was adjusted by using average the thickness of the bonnet corresponding to the HIC value. The stiffness distribution was remapped using the location of the EuroNCAP assessment result (Figure 93).

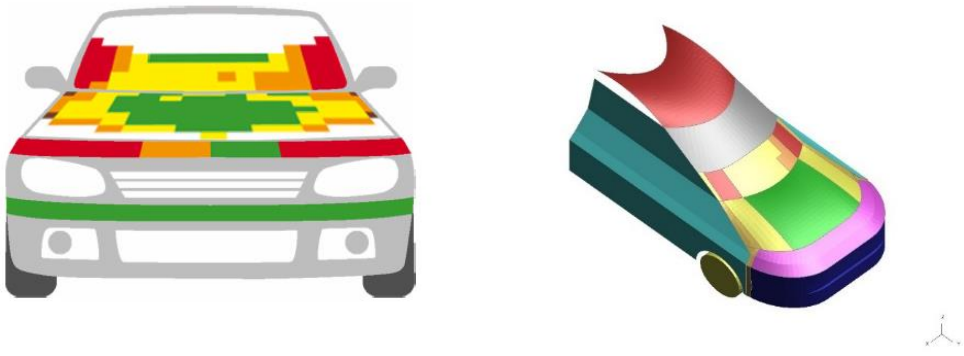

Figure 93 Thickness distribution of Toyota Corolla from EuroNCAP (EuroNCAP, 2013)

Regarding the stiffness of the bumper and the bonnet leading edge, comparable stiffness were applied as the previous vehicle in Case 1. A real Toyota Corolla mass of 1.1 tonne was assigned to the vehicle model (Toyota, 2013). In the PM report, it was noted that the pedestrian was a 162cm 34-year old female weighing 58.6kg. The pedestrian occipital area was injured. Based on investigation in section 4.2, the most likely position of pedestrian is left-leg forward.

From the debris and belongings of the pedestrian, the UKPF concluded that the vehicle was travelling with a speed ranging from 25mph-30mph (11.18m/s-13.41m/s). From the driver's statement, the pedestrian was running from his offside across the path of his vehicle providing him with no opportunity to avoid the collision. The pedestrian walking and running speed of different age group is listed in Table 19 and Table 20. A 34-year-old female, normal running speed is 3.35m/s, normal walking speed is 1.62m/s, fast walking is 1.98m/s and slow walking is 1.46m/s. As the exact pedestrian and vehicle speed in accident is unknown, all these speed combinations were applied in the accident reconstruction simulations. The vehicle damage situation (Figure 94 and Figure 95) was used as the reference to determine the actual pedestrian and vehicle speed in the accident.

Figure 94 Damage observed on vehicle

Figure 95 Damage observed on A pillar and windscreen

In the UKPF report, the pedestrian's first contact point and landing area were recorded by the A pillar, as shown in Figure 94 and Figure 95. The first marks were scuffs to the leading edge of the bumper near to the nearside edge of the number plate, which measured to be approximately 60cm in from the nearside edge and at a height of 43cm from the ground. This is commonly the initial impact point between the car and a pedestrian's leg. The line of damage is indicative of the vehicle striking a pedestrian who upon impact folded on to the bonnet and then struck the windscreen / 'A' pillar with their head before being projected forwards by the impact with the vehicle. Based on this information, the accident scenario was reconstructed as Figure 96.

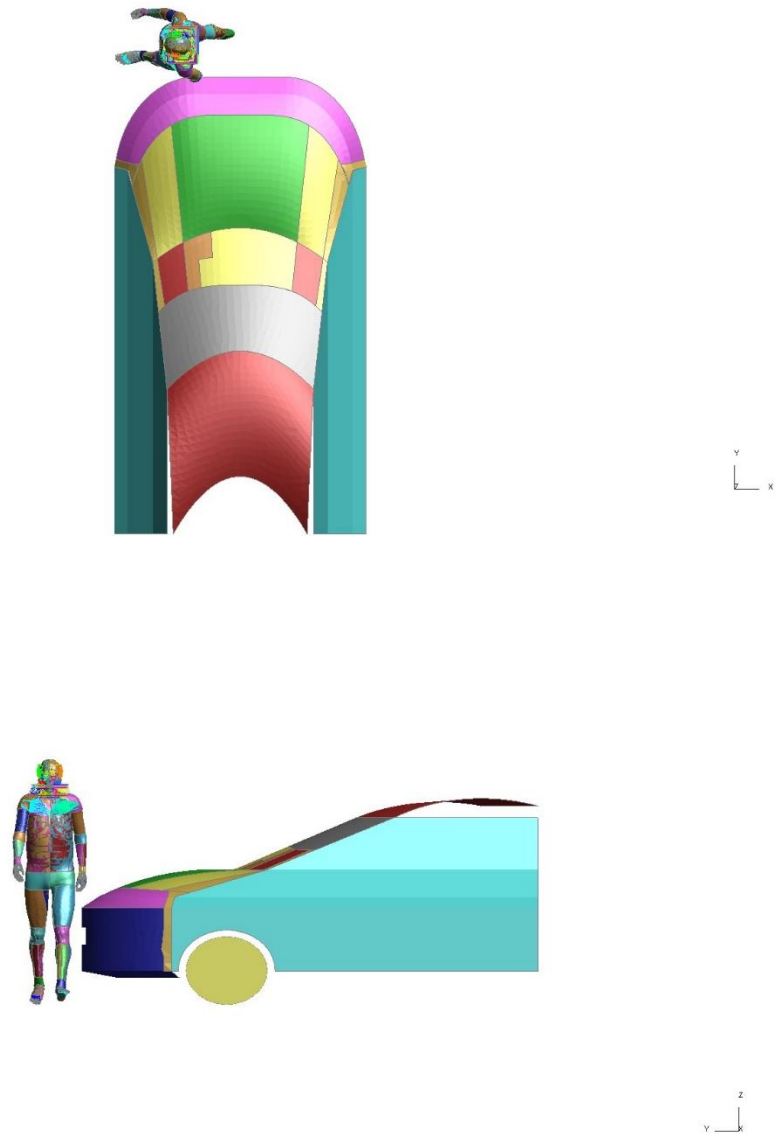

Figure 96 Accident 2 scenario reconstruction

8.2.1 Pedestrian Kinematics

A 1.0m/s crossing pedestrian speed and 25mph vehicle speed replicated the same landing area and damage as in the real-life accident (Figure 97).

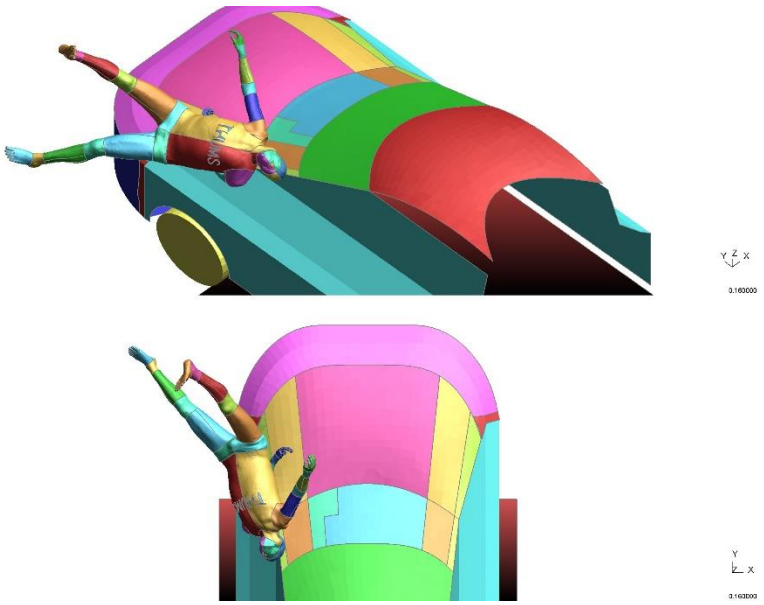

Figure 97 Pedestrian landing area at speed of 1m/s while vehicle speed is 25mph

The pedestrian kinematics of whole collision is presented in Figure 98.

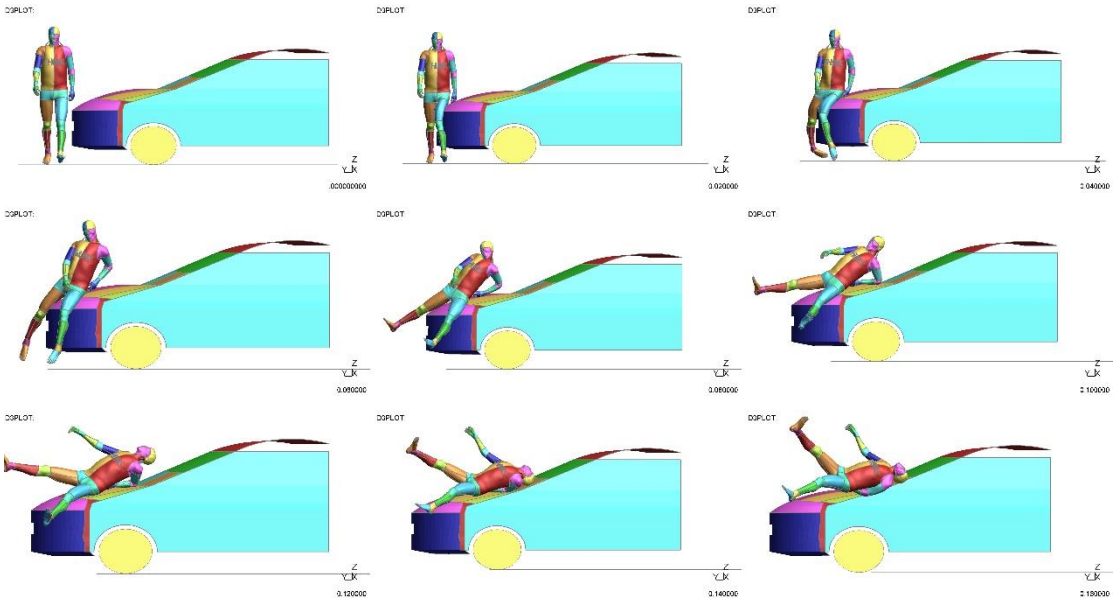

Figure 98 Pedestrian kinematics during impact at vehicle speed of 25mph

The pedestrian was left-leg forward at a speed of 1m/s when the collision occurred. The pedestrian lower extremities impacted with the bumper at the initial stage of the collision. Regarding the autopsy report, an injury was observed on the left ankle. In the simulation, the left ankle deflection was also observed. When the pedestrian landed on the windscreen, the occipital area contacted with the A pillar which coincided with the damage on the vehicle as well as on the autopsy report. To ensure that the simulation is numerically stable, the energy balance is presented in Figure 99. The contact forces between the pedestrian, the bonnet and the windscreen are also captured in Figure 100.

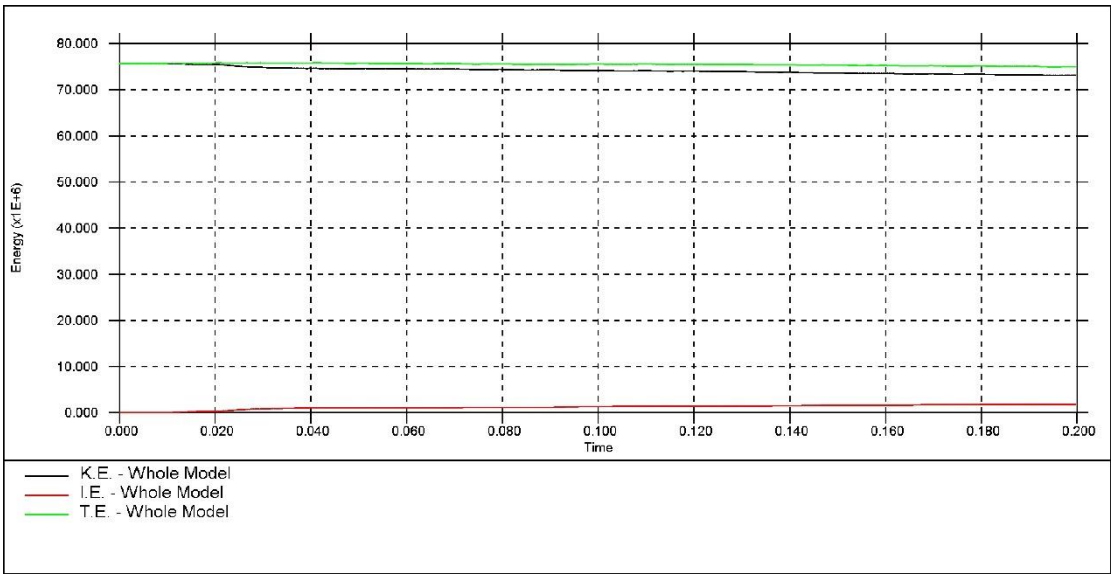

Figure 99 Energy curve of case 2

As shown in Figure 99, the total energy curve remains constant through the whole time history of the accident. There is no energy loss and no hourglassing, therefore, the whole simulation is numerically stable.

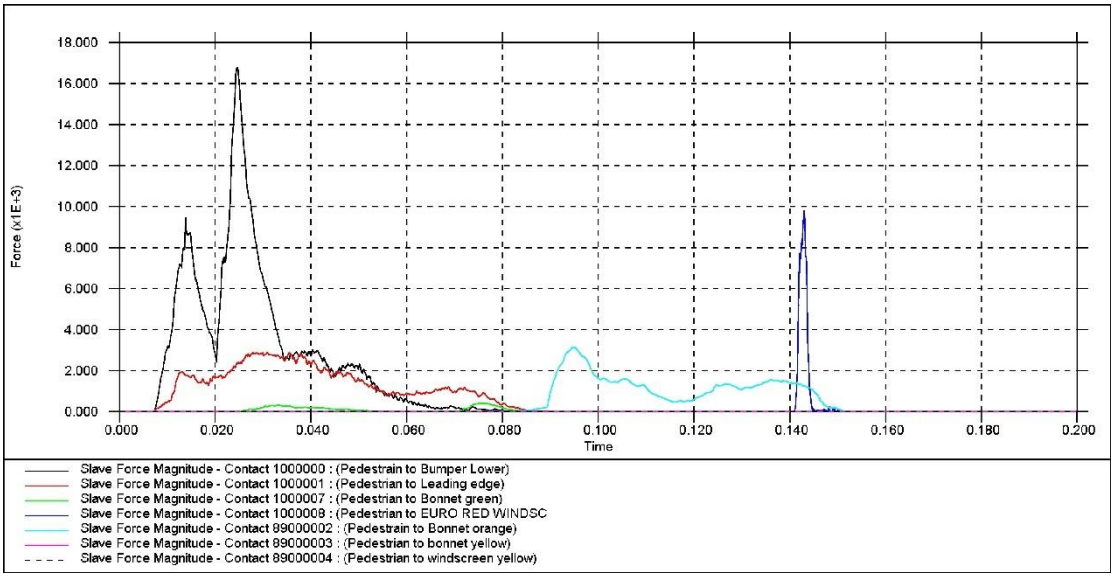

Figure 100 Contact force between pedestrian, bonnet and windscreen

As shown in Figure 100, the pedestrian lower extremities contacted with the lower bumper from approximate 0.01s (10ms). This contact lasted 0.08s (80ms) as the two legs rotated on the vehicle bumper. The contact between the pedestrian and the bonnet leading edge started at the same time and lasted a bit longer to approximate 0.09s (90ms). The pedestrian contacted then with bonnet starting from 0.03s (30ms) to 0.15s (150ms) approximately. During this period of time, the pedestrian rotated on the vehicle bonnet. The pedestrian head contacted with the A pillar started from 0.14s (140ms) and ended at 0.15s (150ms) which is shown as a quick peak in Figure 100.

8.2.2 Injury Results using PVP

As the pedestrian occipital location contacted with the A pillar, the PVP relating with the occipital corridor was used to calculate the AIS injury. From the description in the PM report, the PVP value for brain tissue and the critical organs at the impact speed 25mph was interpolated using the trendline inserted (Table 25).

Organs (Injury)	AIS Level	PVP threshold at 25mph (mJ/s)
White matter (DAI)	4	1.39
Grey matter (Brain contusion)	3	0.67
Heart (Rupture)	4	0-0.15

Liver (Rupture)	4	0-15.86
Spleen (Rupture)	4	0-7.83
Right kidney (Rupture)	4	0-2.23
Left kidney (Rupture)	4	0-2.18

Table 25 PVP threshold for accident 2

The PVP distribution on brain white matter is shown on Figure 101.

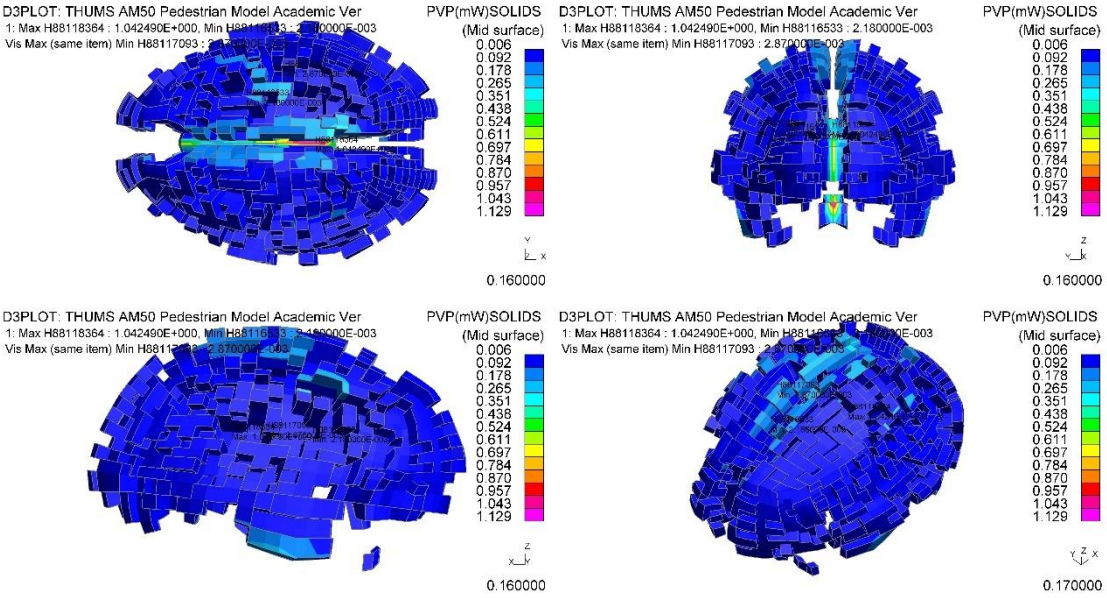

Figure 101 PVP on brain white matter at 0.16s (160ms) at vehicle speed of case 2

Regarding the grey matter, the PVP distribution is highlighted in Figure 102.

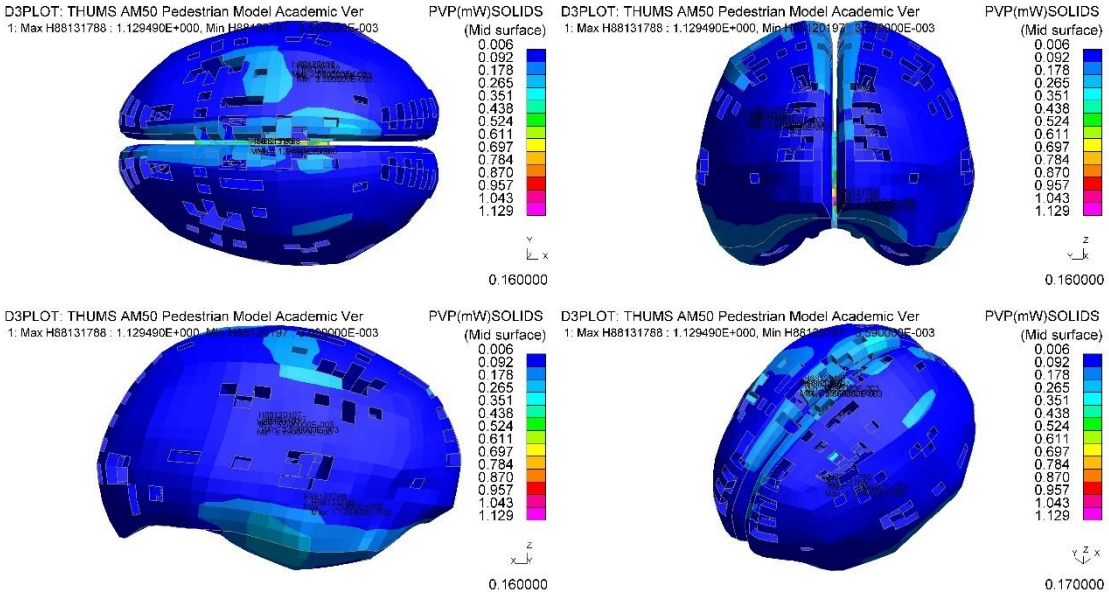

Figure 102 PVP on brain grey matter at 0.16s (160ms) at vehicle speed of case 2

PVP results of critical organs are illustrated from Figure 102 to Figure 107.

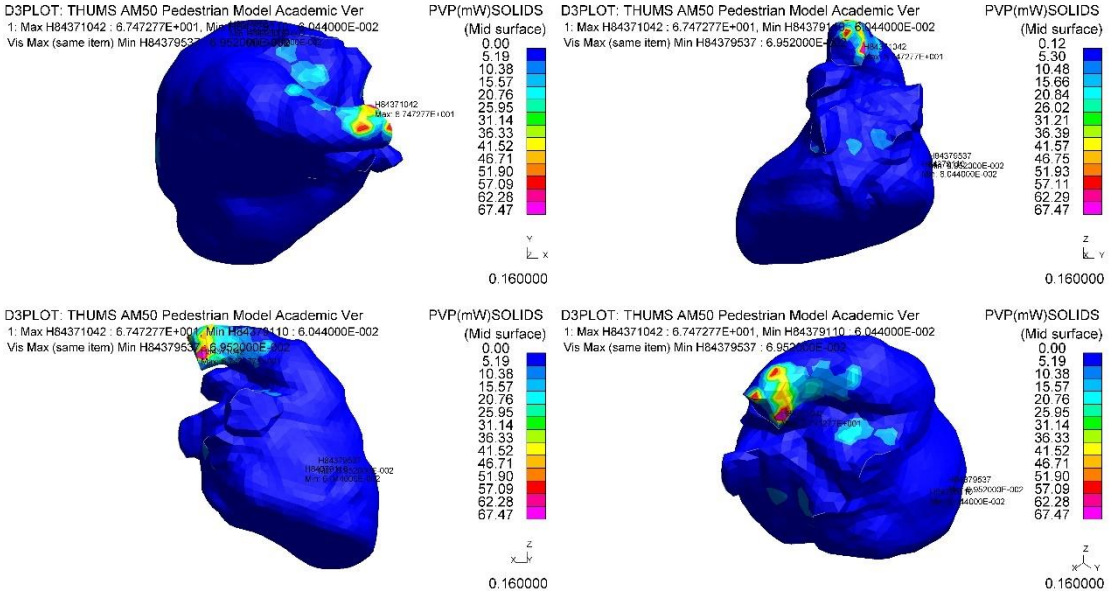

Figure 103 PVP of heart at 0.16s (160ms) at vehicle speed of case 2

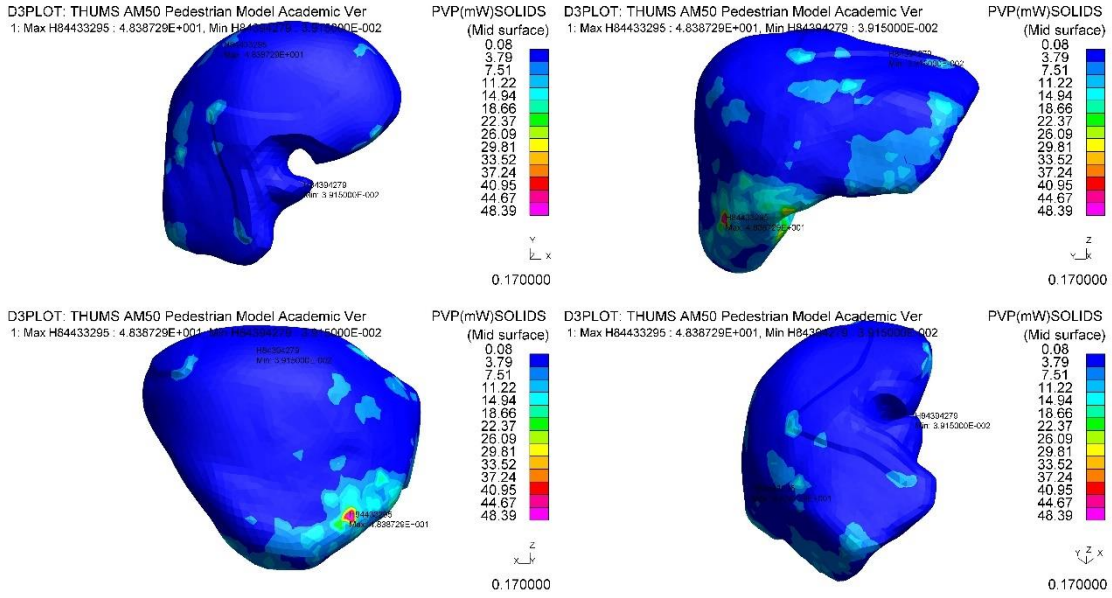

Figure 104 PVP of liver at 0.17s (170ms) at vehicle speed of case 2

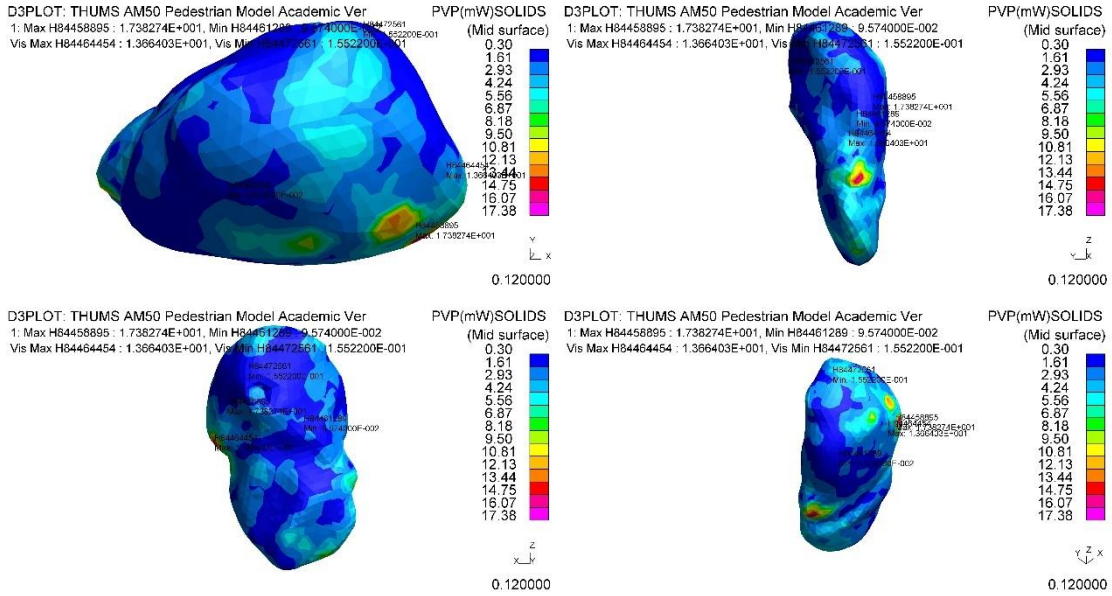

Figure 105 PVP of spleen at 120ms at vehicle speed of case 2

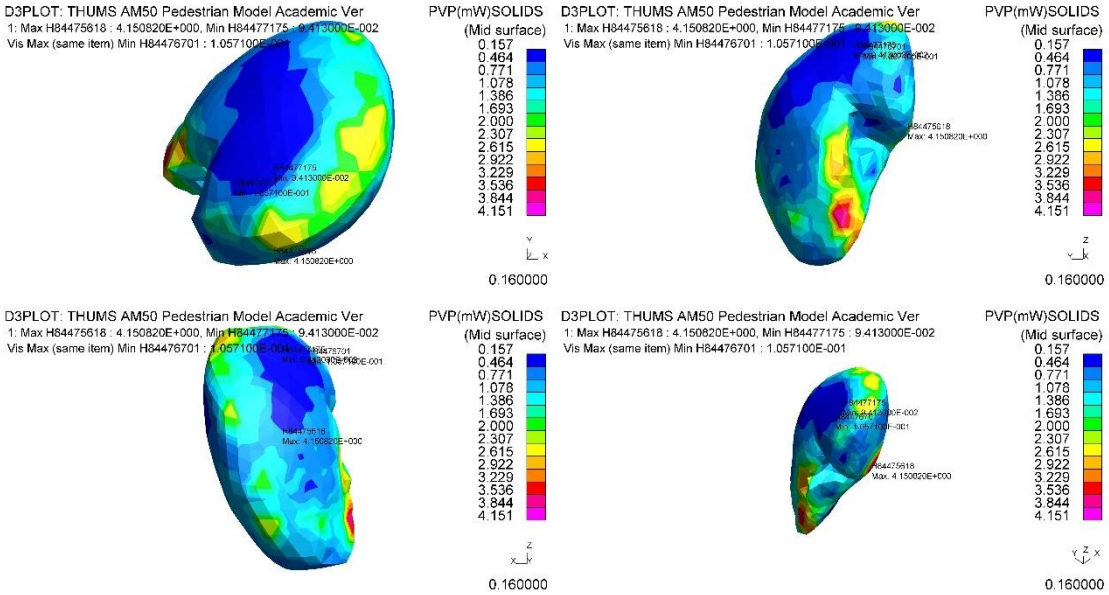

Figure 106 PVP of right kidney at 160ms at vehicle speed of case 2

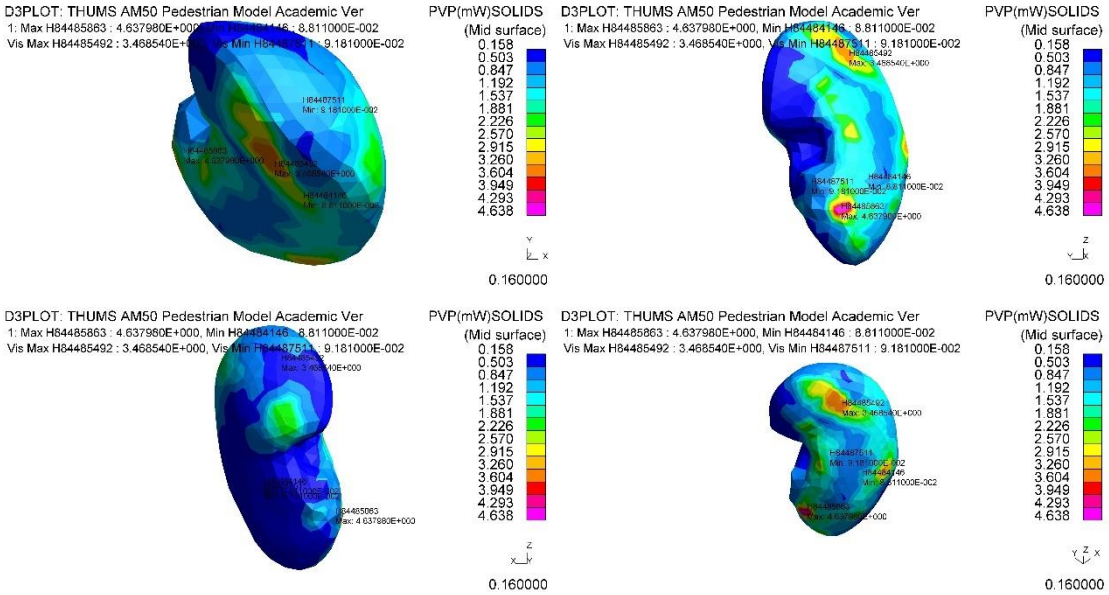

Figure 107 PVP of left kidney at 160ms at vehicle speed of case 2

A summary of the PVP results for case 2 is provided in Table 26.

Organs/Location	25mph (mJ/s)	Time (ms)
PVP value of white matter (DAI)	1.04	142
Location (ID)	88118364	
PVP value of grey matter (brain contusion)	1.13	145
Location (ID)	88131788	
PVP value of Heart	67.47	149
Location (ID)	84371042	
PVP value of Liver	48.39	125
Location (ID)	84433295	
PVP value of Spleen	17.38	112
Location (ID)	84458895	
PVP value of Left kidney	4.64	120
Location (ID)	84485863	
PVP value of Right kidney	3.01	65.5
Location (ID)	84477752	

Table 26 PVP results of case 2 CAE simulation

8.2.3 Results of Case 2

A comparison between PM report and CAE simulation of injury is presented in Table 27.

Organs/Tissue	Injury	AIS of PM	AIS of CAE	MAIS of PM	MAIS of CAE	ISS of PM	ISS of CAE
Brain white matter	DAI	3	3	3	3	17	54
Brain grey matter	Brain contusion	3	3				
Heart	Unremarkable	0-2	4	2	6		
Liver	Unremarkable	0-2	3	2	3		
Spleen	Congested	0-2	2+				
Right kidney	Unremarkable	0-2	2+				
Left kidney	Unremarkable	0-2	2+				

Table 27 Injury result summary of accident 2

The individual comparison of tissue/organ is presented from Figure 108 to Figure 114.

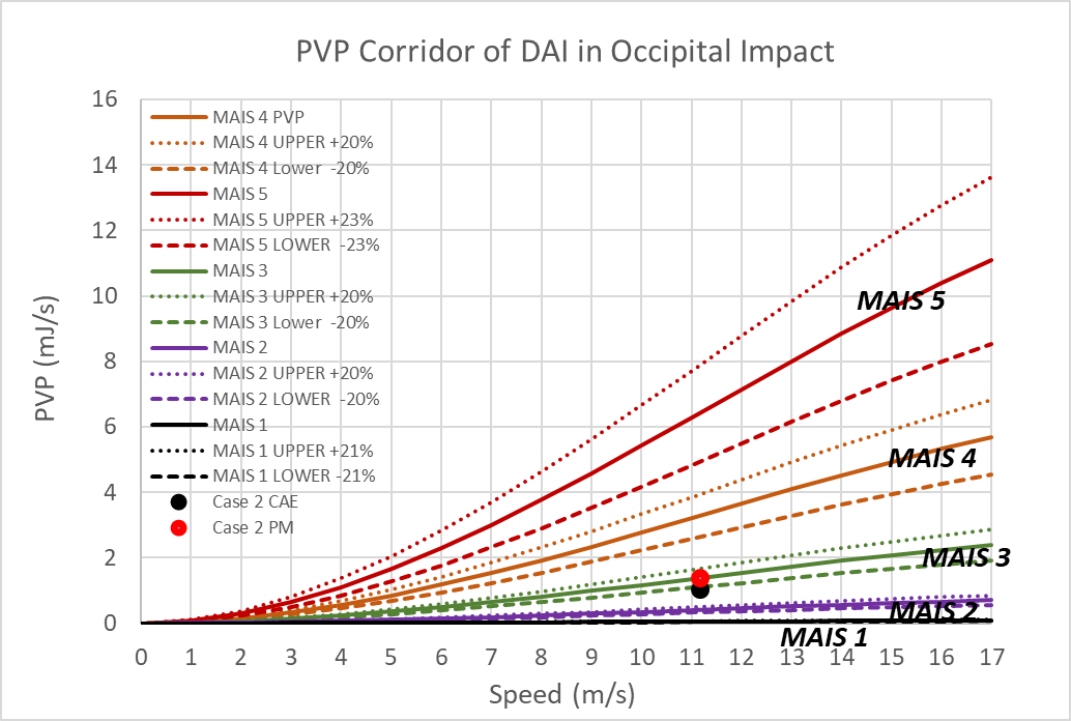

Figure 108 DAI result of case 2 from CAE and autopsy report

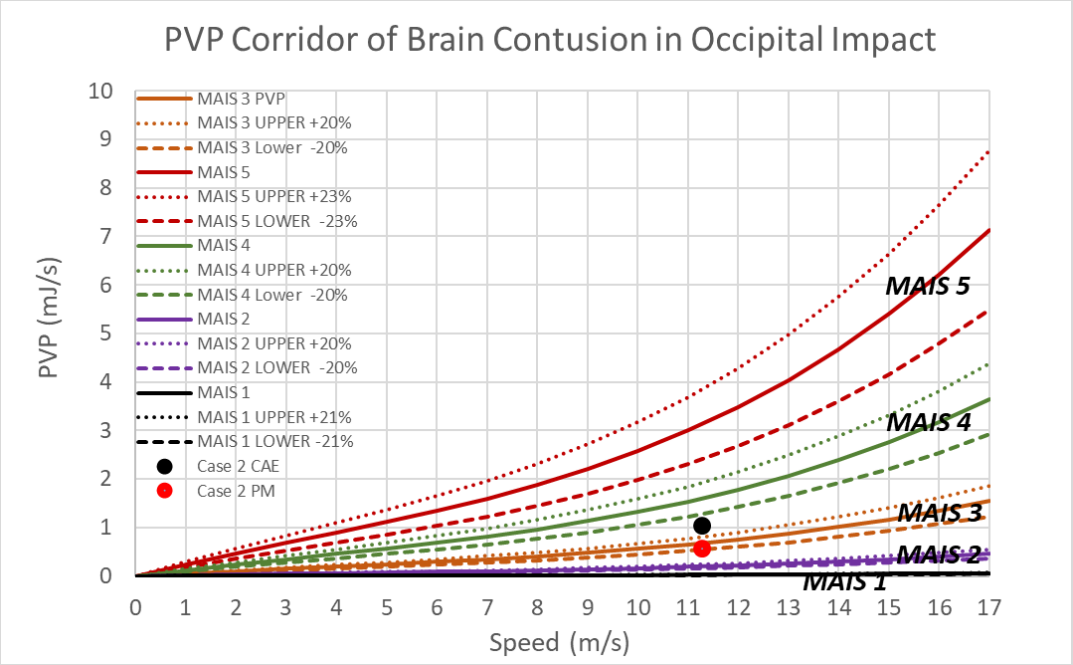

Figure 109 Brian contusion result of case 2 from CAE and autopsy report

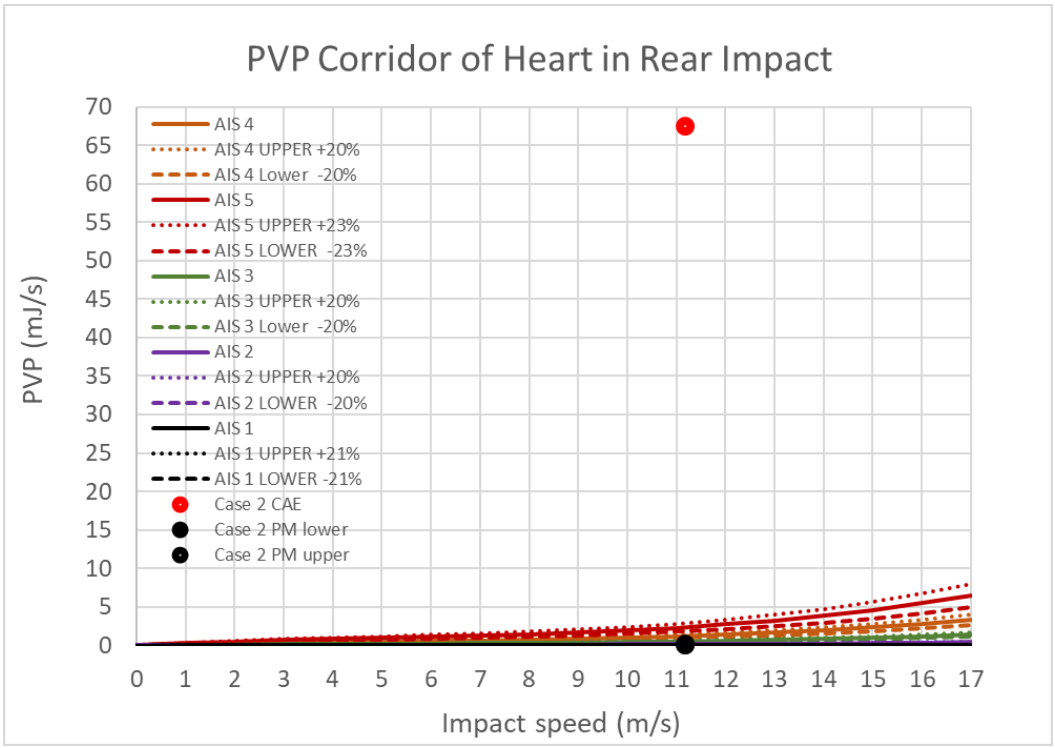

Figure 110 Heart result of case 2 from CAE and autopsy report

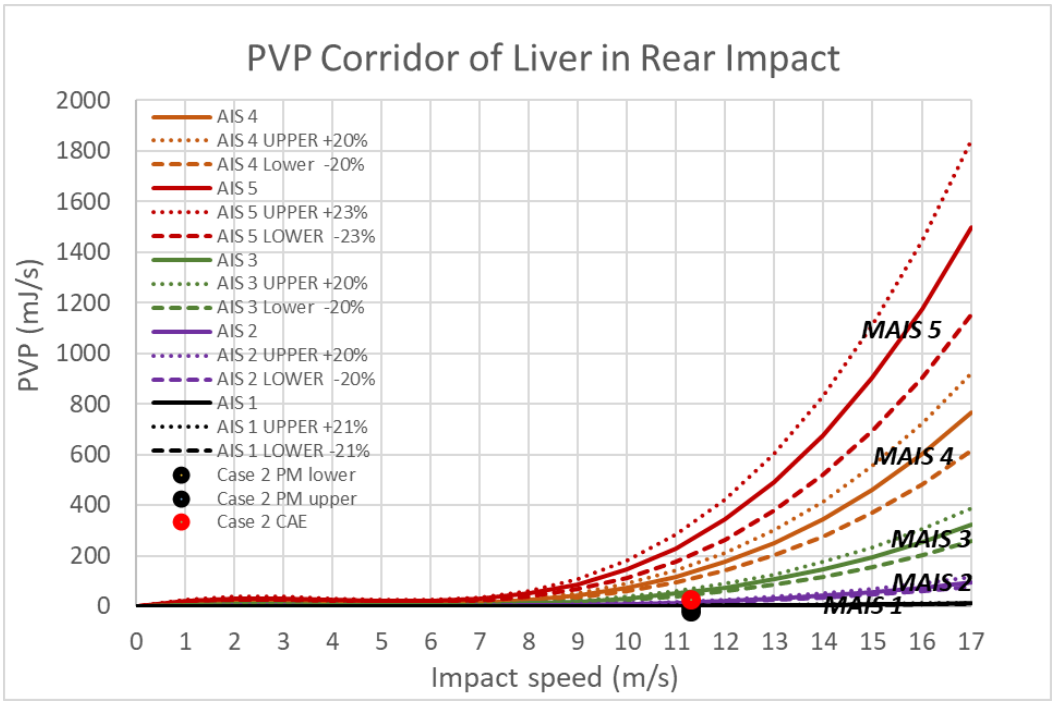

Figure 111 Liver result of case 2 from CAE and autopsy report

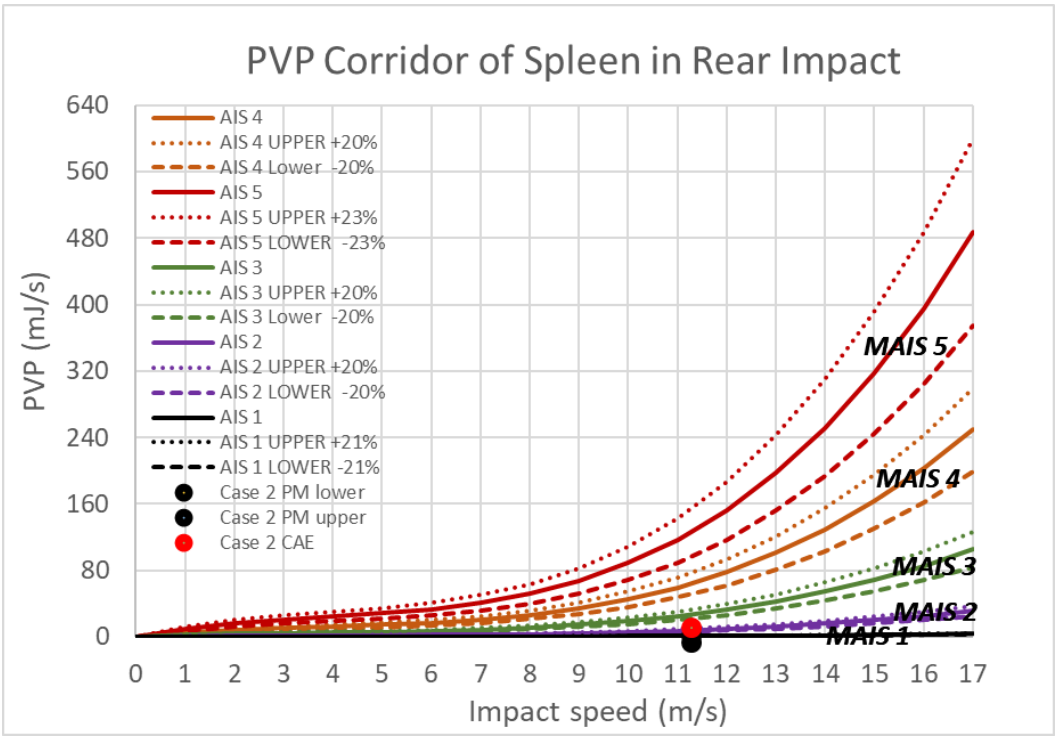

Figure 112 Spleen injury result of case 2 from CAE and autopsy report

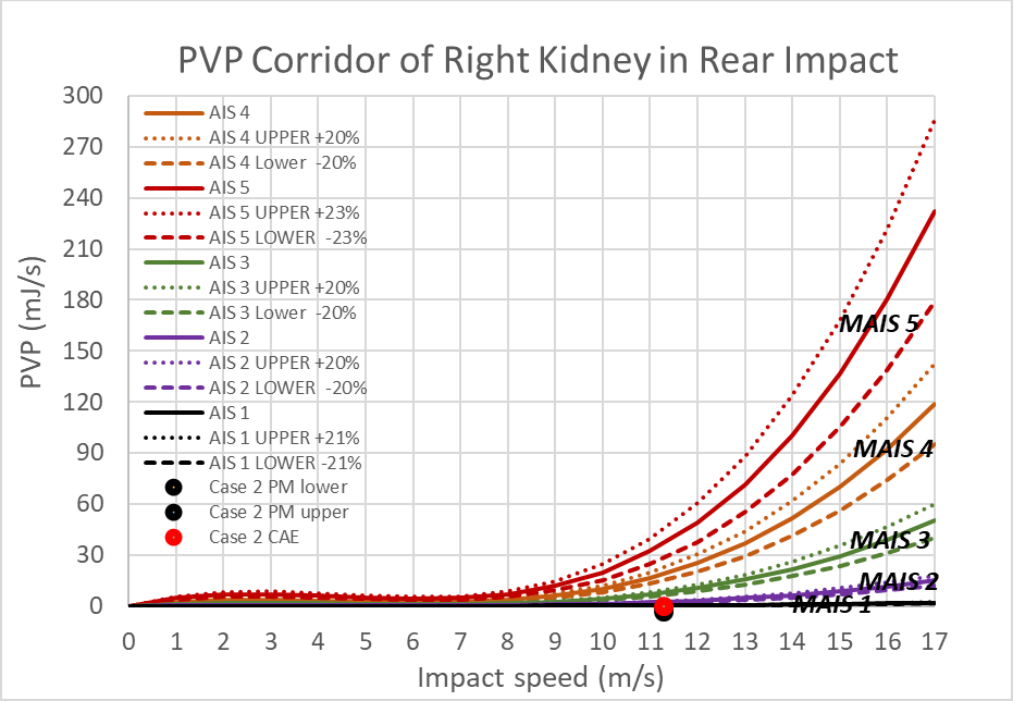

Figure 113 Right kidney injury result of case 2 from CAE and autopsy report

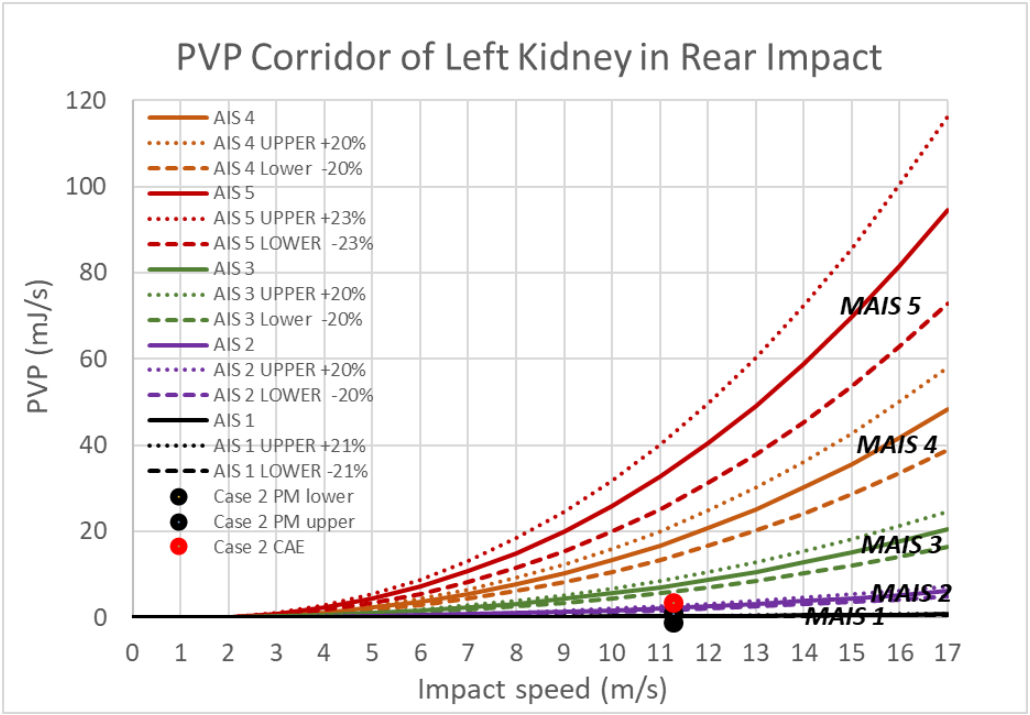

Figure 114 Left kidney injury result of case 2 from CAE and autopsy report

At the initial stage, the pedestrians left lower extremity impacted against the lower bumper. Then the pedestrian contacted and rotated on the bonnet. The pedestrian's head landed on the A pillar at the late stage of the impact from 0.14s (140ms) to 0.15s

(150ms). Before the head impact, no PVP was observed on the brain white matter. After contacting with the A pillar, the PVP was visible on parietal lobe as well as the centre area. PVP was also observed on the stem area on both side of white matter. Compared to left side, the PVP was distributed more on right side of white matter, on brain grey matter. PVP was not visible before the head contacting with windscreen. After the collision, the PVP was observed largely on right parietal lobe, temporal area and central area. No PVP was visible on the stem area. The solid element with the highest PVP value on the white matter is 88118364 (Figure 115 - left), which is in the central area of right white matter. The solid element with the highest PVP value on the grey matter is 88131788 (Figure 115 - right), which is located in centre area of left grey matter.

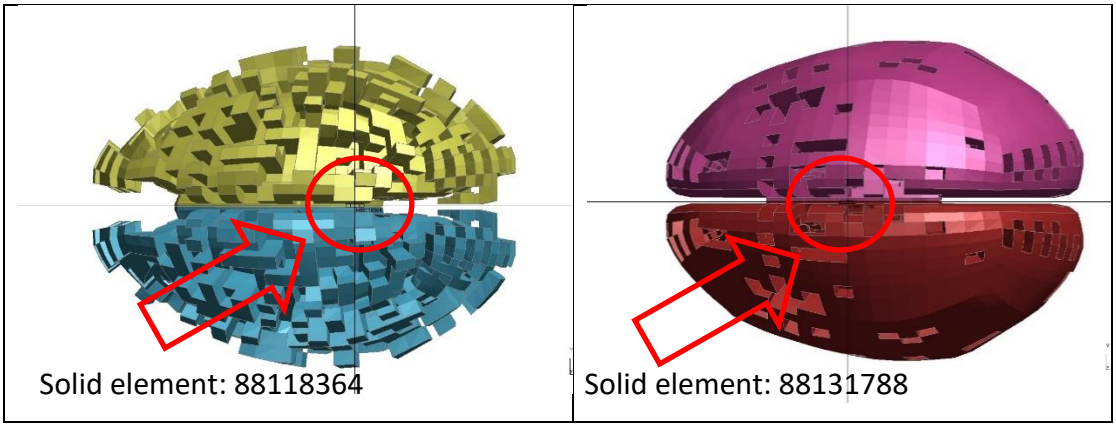

Figure 115 Injury location of brain white matter (left) and grey matter (right) of case 2

In the PM report, a subarachnoid haemorrhage was recorded. The brain appeared diffusely swollen to a mild degree and there were contusions on the inferior aspect of the right temporal lobe. CAE and PM both predicted an AIS of 3 on the brain, which is a serious injury. In CAE result, PVP was also observed largely on the temporal area on right grey matter.

Regarding the critical organs, the PM report did not conclude any obvious injuries. The critical organs were described as unremarkable. Based on the AIS classification definition described in the introduction, AIS 2 is moderate injury with low fatality probability. No AIS level given in PM report is then assumed as AIS 0-2 injury, which is not necessary to record or even to observe. On the heart, the CAE indicated an AIS 4 injury while the PM report described it to be unremarkable. On the other organs, the

CAE results coincide with the PM report, i.e. AIS 2 injuries. ISS is different compared with PM report due to the over-estimation on the heart.

8.3 Case 3: Accident scenario and Computation Setup

The third accident is an impact between a male and a Renault Clio. The pedestrian was believed to try to pick up his hat situated in the middle of the road when impacted by the vehicle. The front offside of the vehicle collided with the pedestrian, as illustrated in Figure 116, which is providing the road layout.

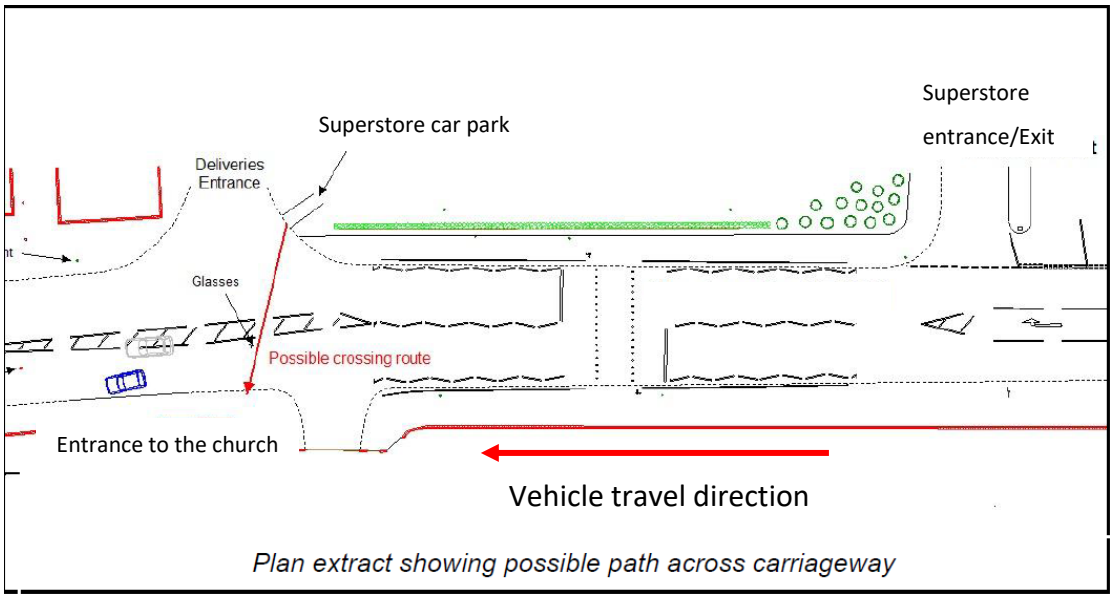

Figure 116 Scenario of accident 3

As shown in Figure 116, the pedestrian was trying to cross from the offside of the driver to the nearside. As provided in the autopsy report, the pedestrian‘s height was 1.73m and 79.2kg in weight. The THUMS model was scaled accordingly to represent the pedestrian anthropometry. The external injuries provided by the PM were recorded as brusing on the right side of the back and fracture to the left ankle. From the pedestrian kinematics investigation, only the left-legforward stance can result in injuries on back of the left ankle.

From the damage location of the vehicle is can be proposed that the pedestrian was most likely standing still when the collision happened, as there impact direction was straigth, as illustretd in Figure 117.

Figure 117 Frontal damage on vehicle

In the witness statement, the pedestrian stopped for “some reason when he was trying to cross the road”. It was raining very heavily, and the pedestrian was believed to pick up his hat when he was impacted by the vehicle. Pedestrian hair was found on board the windscreen and the roof (Figure 118), consequently the pedestrian must have been standing in from of the vehicle at the moment of impact and not in a crouching or bending stance.

Figure 118 Damage on roofline

It is noticeable that there is an obvious dent at the centre of the bonnet as illustrated in Figure 117, as per the rest of the damage. As previous explained, the weather was very bad and the pedestrain had an ambrella in his hand. Therefore, it is very likely that the dent present at the centre of the bonnet was caused by the umbrella.

The involved vehicle, a Renault Clio, was scaled from baseline model. The stiffness distribution was remapped according to the EuroNCAP assessment results (Figure 119) and the angle of the windscreen and bumper height were also adjusted to ensure that the updated CAE model represented the correct geometry (Figure 120).

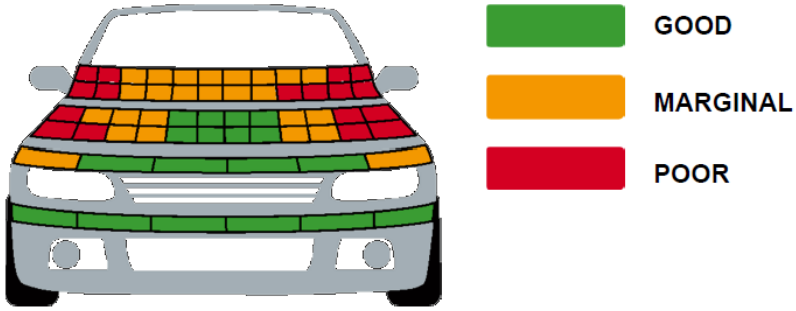

Figure 119 Stiffness distribution of Clio (EuroNCAP, 2012b)

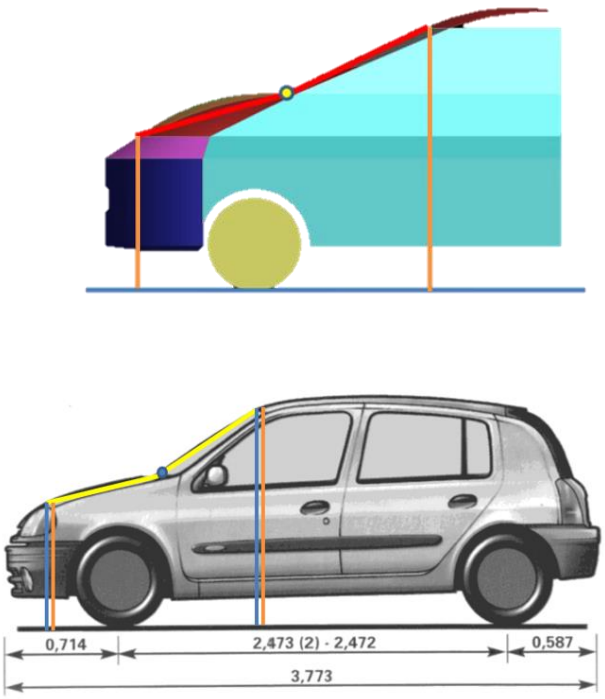

Figure 120 Windscreen angle of CAE model and Renault Clio

8.3.1 Pedestrian Kinematics

Due to the weather factor, the UKPF could not duplicate the impact scenario exactly. The speed test performed could only provide a very rough estimation of the impact speed from vehicle. The estimated impact speed was between 30 and 36mph. The CAE simulation was tried for both speeds. By comparing the kinematics and the head landing area of pedestrian, it was observed that at 36mph, the pedestrian reached the edge of the windscreen and the roof of the Renault Clio (Figure 121), which coincides with the photographics evidence from accident report (Figure 118).

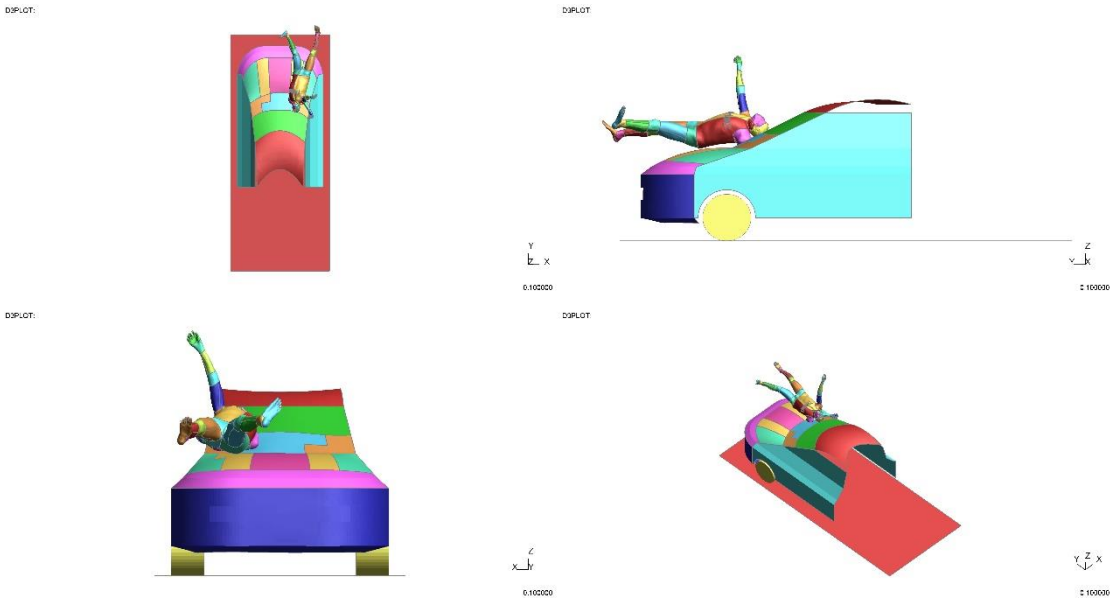

Figure 121 pedestrian landing area at impact speed of 36mph

The kinematics of the pedestrian is illustrated in Figure 122.

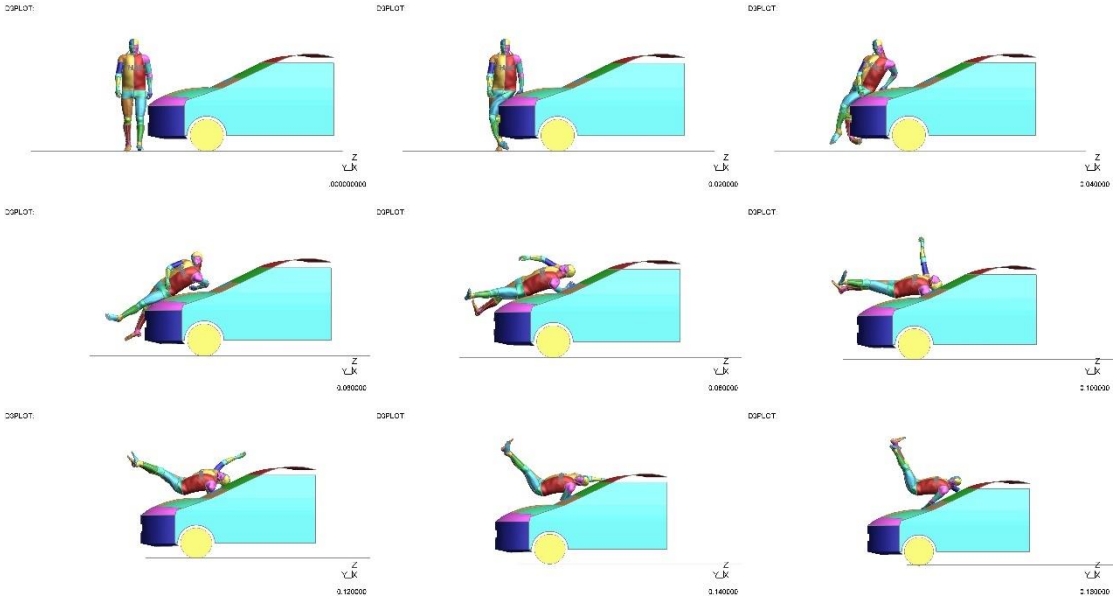

Figure 122 Pedestrian kinematics of case 3

The pedestrian was placed with his left-leg forward in a standing position as per the accident boundary conditions. At the initial stage of the impact, the pedestrian lower extremities contacted with the bumper. Then the pedestrian rotated and the back of his torso contacted with the bonnet. The pedestrian head occipital area landed on the roofline in the late stage of accident. In order to ensure that the simulation was numerical stable, an energy balance was performed, as shown in Figure 123. The

contact forces (Figure 124) were also extracted to understand in more detailed the sequence of scenarios of the accident

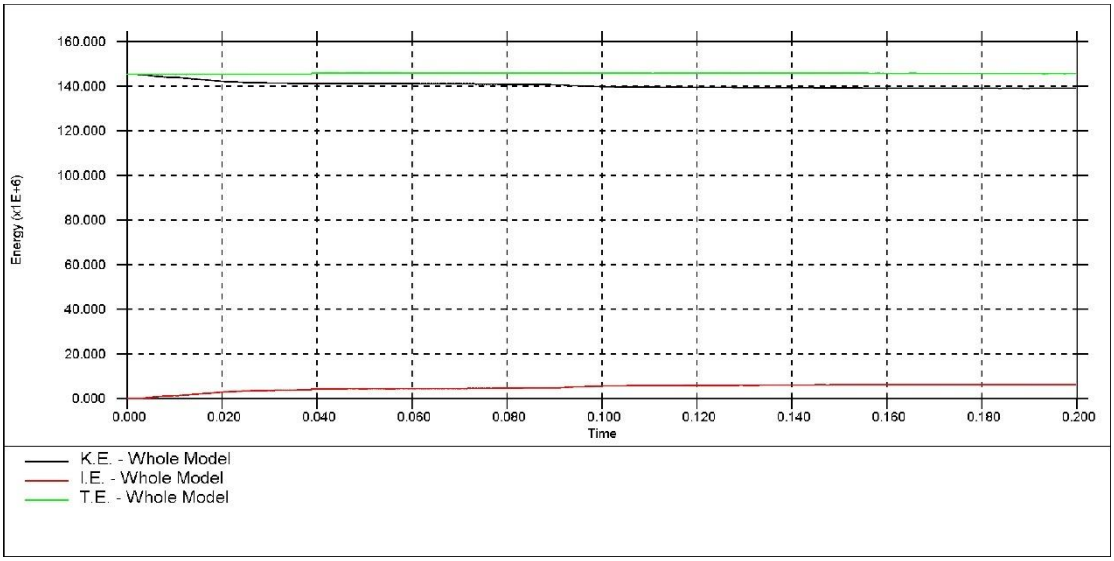

Figure 123 Energy curve of case 3

As shown in Figure 123, the total energy curve remains constant through the whole-time history. There is no energy loss and no hourglassing, therefore, the whole simulation is numerically stable.

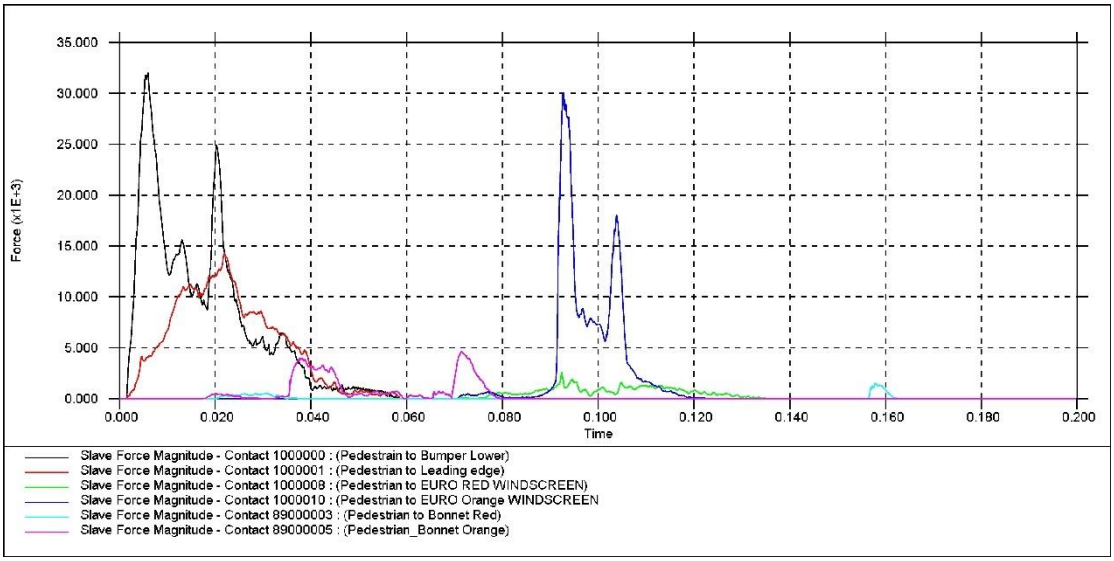

Figure 124 Contact force of case 3

As shown in Figure 124, the pedestrian lower extremities contacted with the lower bumper very soon after the impact. This contact lasted 0.06s (60ms) as the two legs rotated on the vehicle bumper. The contact between the pedestrian and the bonnet

leading edge started at the same time and lasted to approximately 0.06s (60ms). The pedestrian contacted with the bonnet from time 0.02s (30ms) to 0.08s (80ms) approximately. During this time, the pedestrian rotated on the vehicle bonnet. The pedestrian head contacted then with the windscreen from time 0.07s (70ms) until 0.12s (120ms) which is shown as the double peak in Figure 124.

8.3.2 Injury Results using PVP

The pedestrian occipital was impacted against the vehicle roofline. Therefore, the PVP corridor of head occipital impact was used as injury threshold predictor. Based on the PM report, the PVP threshold at speed of 36 mph (16.09m/s) is shown in Table 28.

Organs (Injury)	AIS Level	PVP Threshold at 36mph (mJ/s)
White matter (DAI)	4	5.35
Grey matter (Brain contusion)	3	1.36
Heart (Rupture)	4	0-0.36
Liver (Rupture)	4	0-76.97
Spleen (Rupture)	4	0-25.82
Right kidney (Rupture)	4	0-11.8
Left kidney	4	0-6.35

Table 28 PVP threshold at 36mph (16.09m/s)

The PVP values and distributions on the brain tissue and the critical organs were extracted to evaluate the injury results. The PVP results of brain tissue and critical organs are illustrated in Figure 125 and Figure 126.

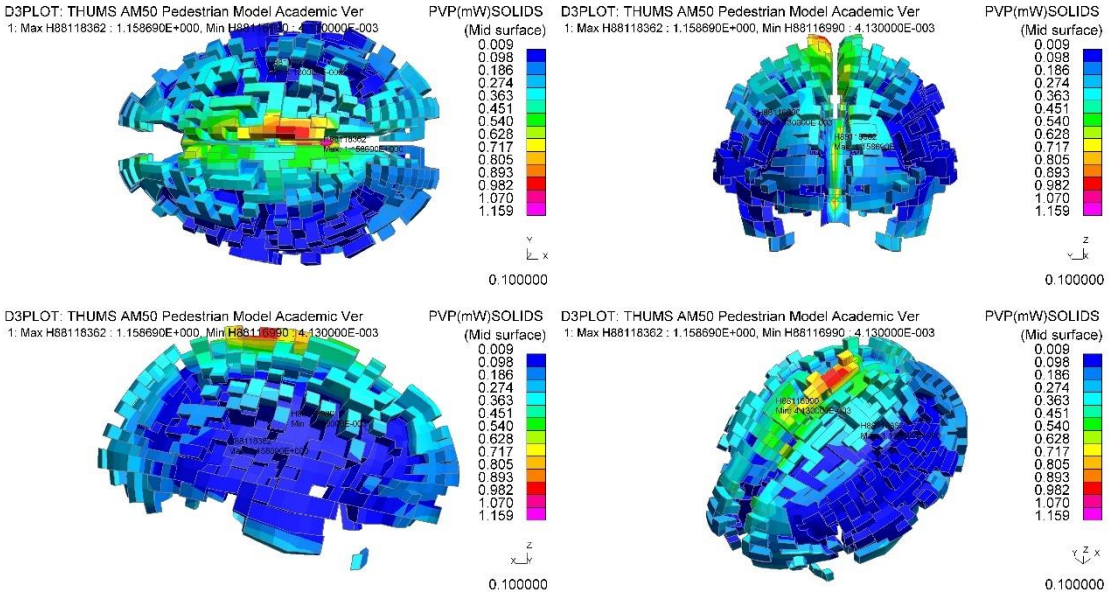

Figure 125 PVP on brain white matter at 0.1s (100ms) of case 3

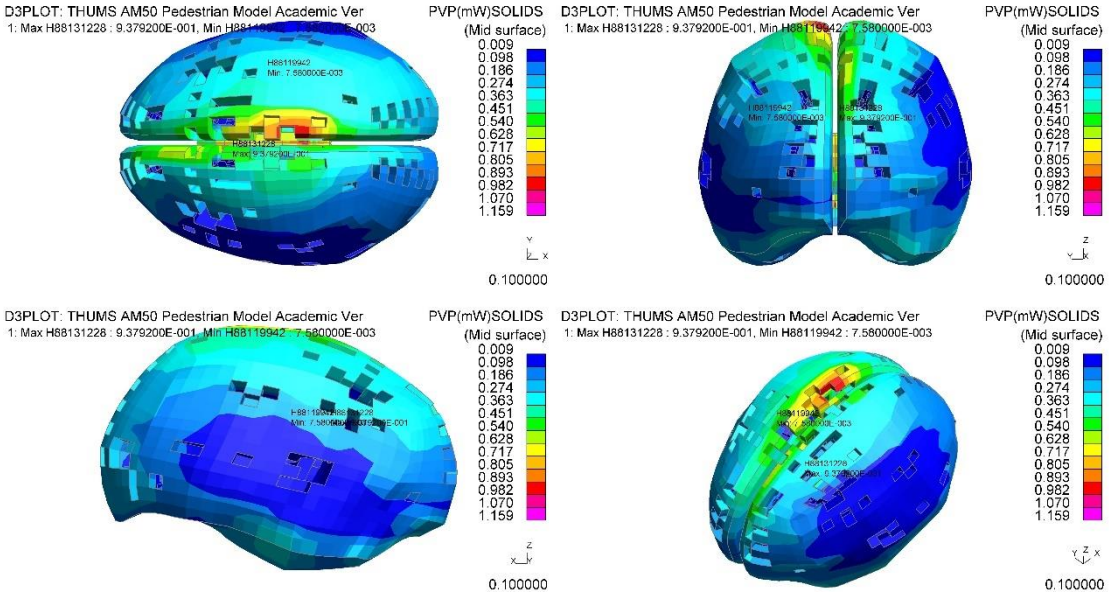

Figure 126 PVP on brain grey matter at 0.1s (100ms) of case 3

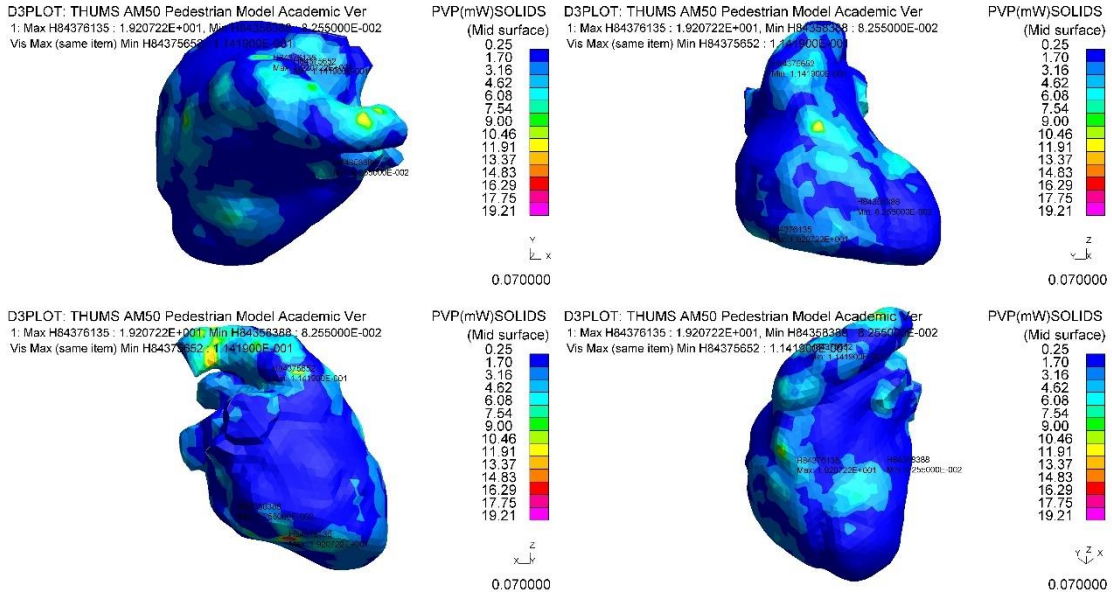

Figure 127 PVP on heart at 0.07s (70ms) of case 3

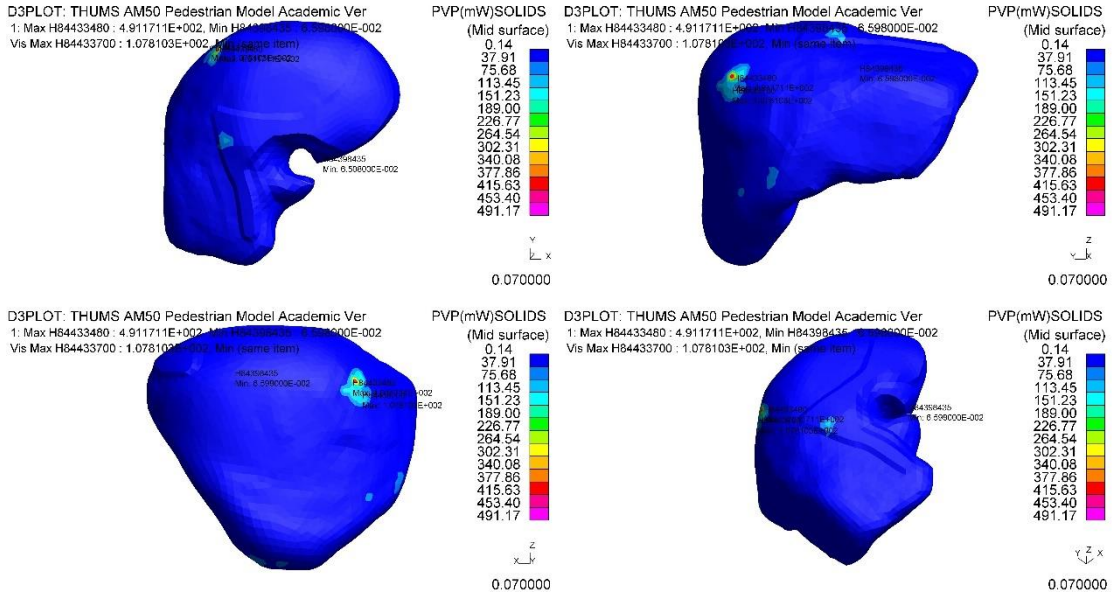

Figure 128 PVP liver at 0.07s (70ms) of case 3

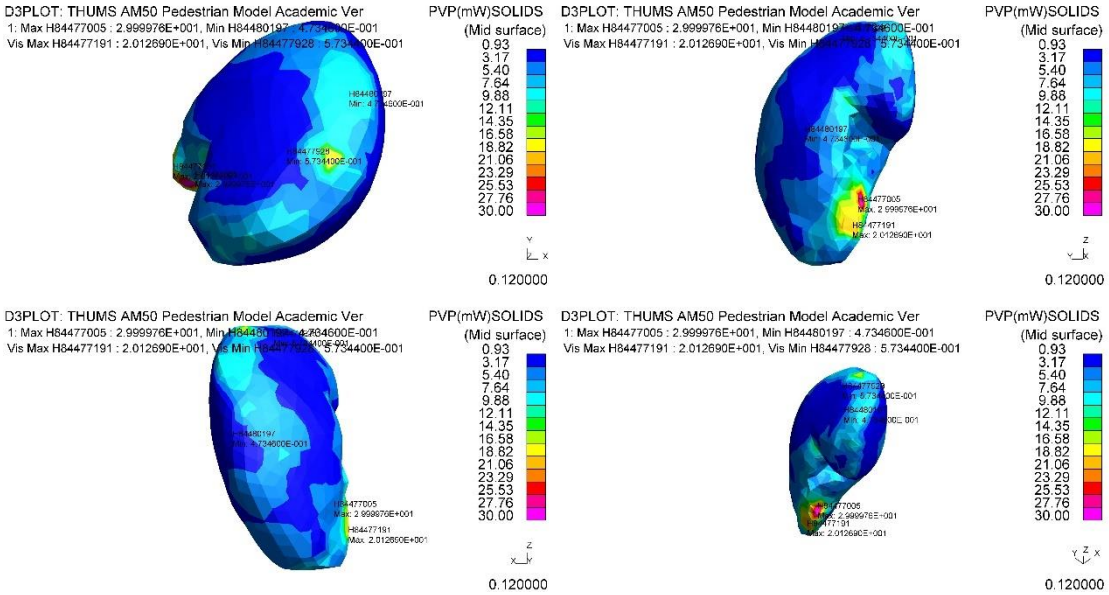

Figure 129 PVP on right kidney at 0.12s (120ms) of case 3

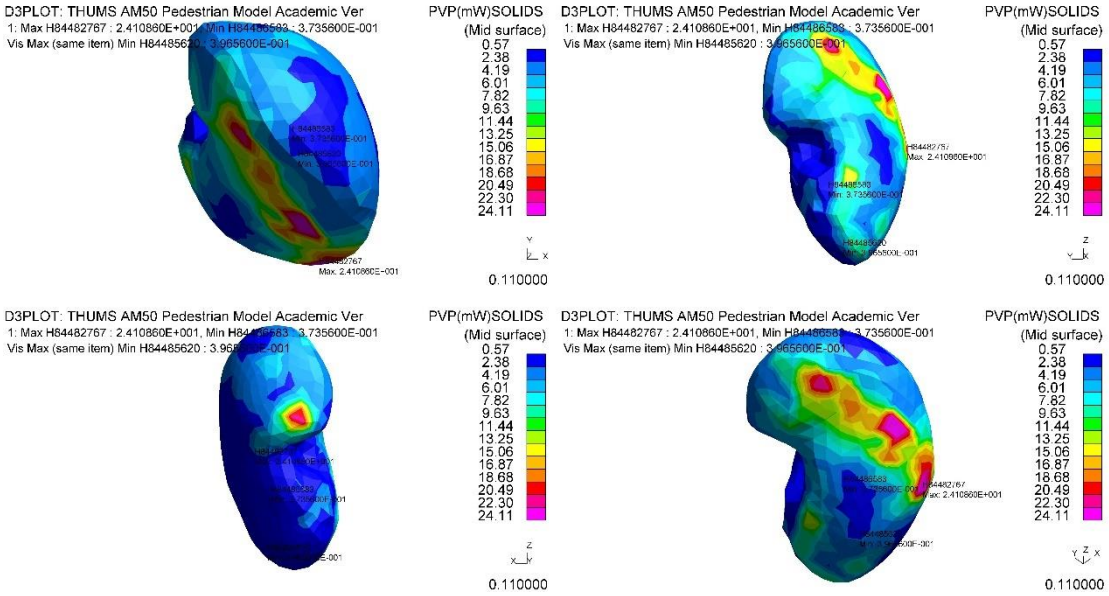

Figure 130 PVP on left kidney at 0.11s (110ms) of case 3

A summary, the maximum PVP results are presented in Table 29.

Organs/Tissue	PVP from CAE simulation (mJ/s)	Location (ID)	Time (ms)
White matter (DAI)	1.16	88118362	94
Grey matter (brain contusion)	0.94	88121824	100
Heart	19.21	84376135	41.5
Liver	491.17	84433480	63
Spleen	68.24	84461263	32
Right kidney	30	84477005	111
Left kidney	13.07	84485593	36.8

Table 29 Injury summary of case 2

8.3.3 Result of Case 3

The comparison between CAE injury result and PM outcomes is shown in Table 30.

Organs/Tissue	Injury	AIS of PM	AIS of CAE	MAIS of PM	MAIS of CAE	ISS of PM	ISS of CAE
Brain white matter	No evidenced	0-2	3	2	3	12	54
Brain grey matter	No contusion	0-2	3				
Heart	No abnormality	0-2	6+	2	6		
Liver	Congested	0-2	3+	2	3		
Spleen	Congested but no laceration	0-2	2+				
Right kidney	No focal lesion	0-2	2+				
Left kidney	No focal lesion	0-2	2+				

Table 30 Injury comparison between CAE simulation and PM report

Comparison of individual injury is also presented from Figure 131 to Figure 137.

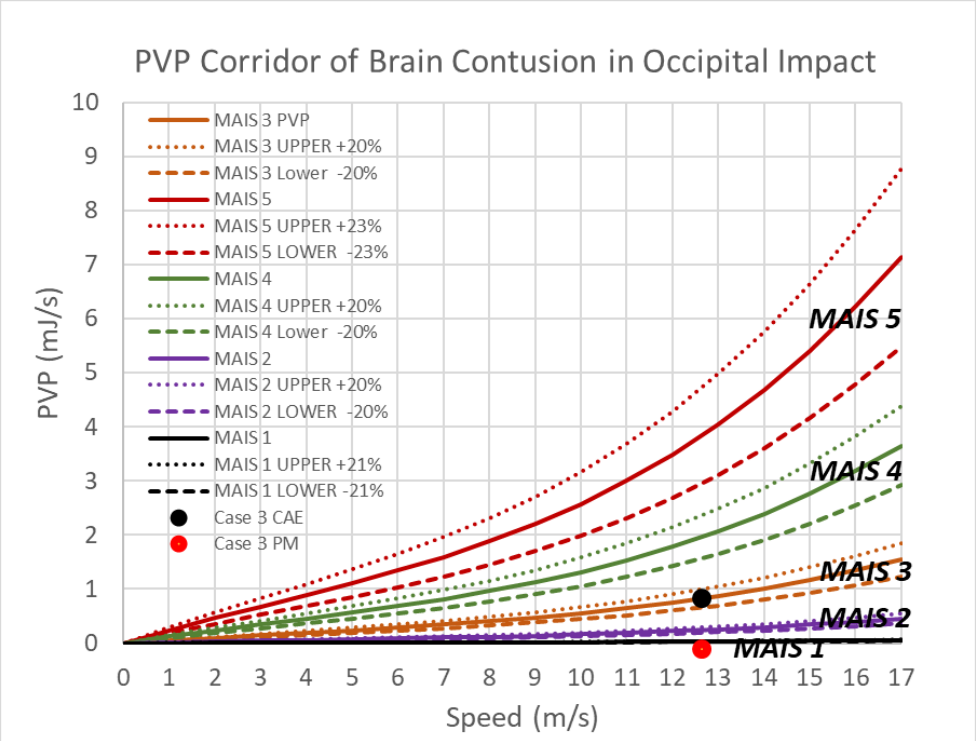

Figure 131 Brian contusion result of case 3 from CAE and autopsy report

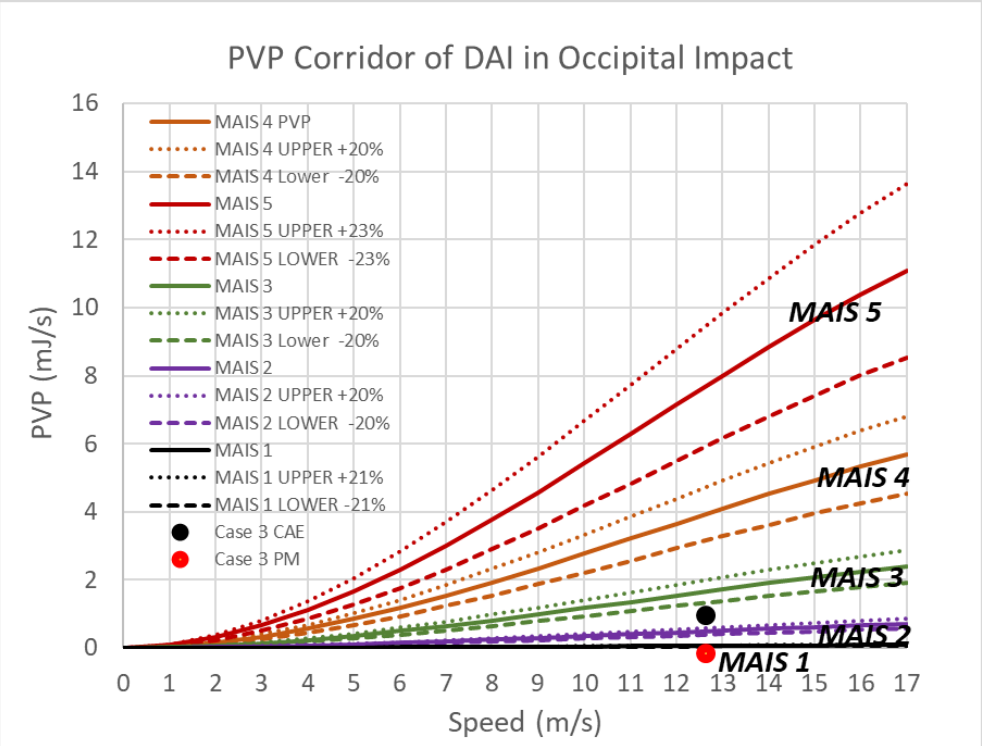

Figure 132 DAI result of case 3 from CAE and autopsy report

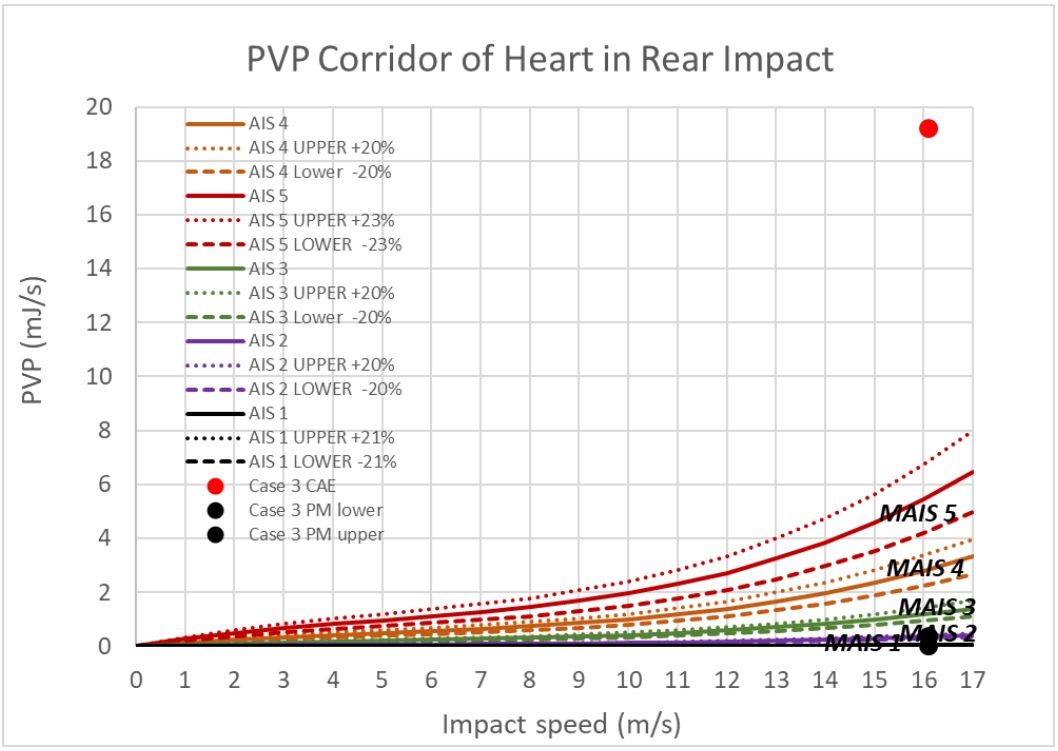

Figure 133 Heart injury result from CAE and Post-mortem report of case 3

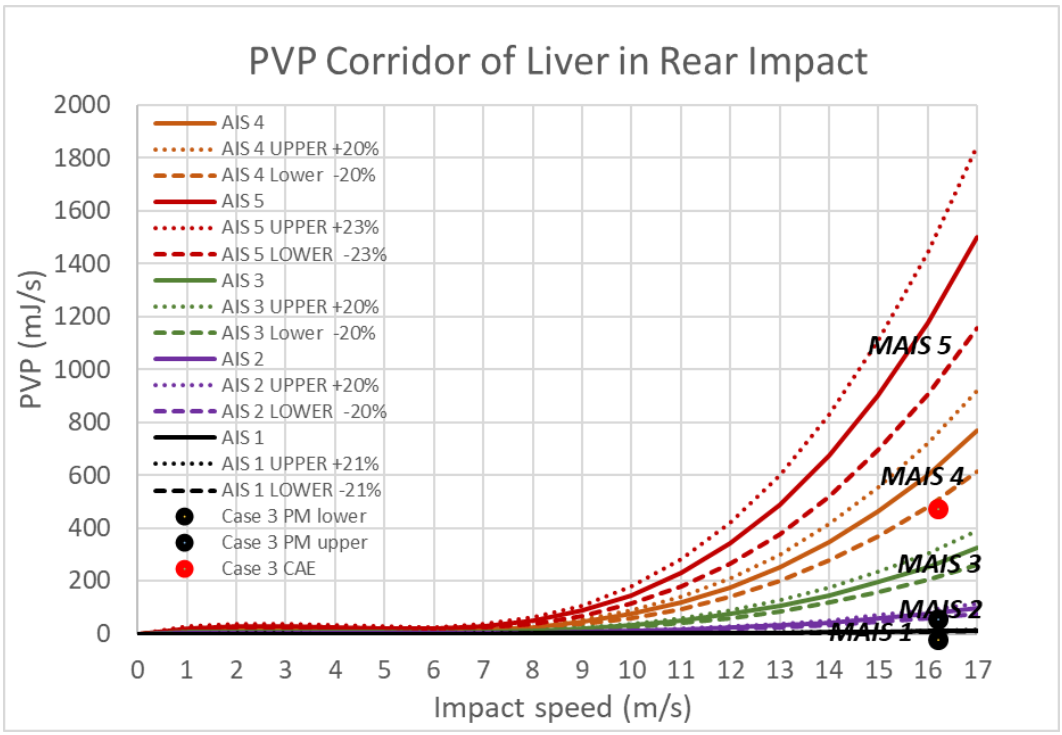

Figure 134 Liver injury result from CAE and Post-mortem report of case 3

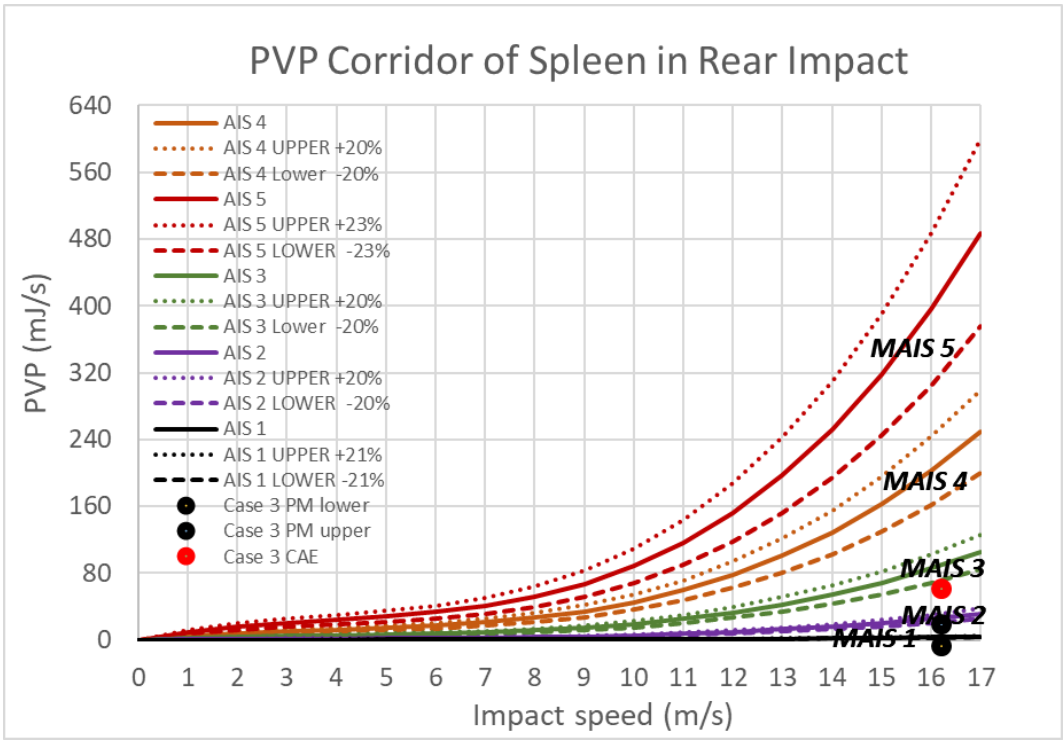

Figure 135 Spleen injury result from CAE and Post-mortem report of case 3

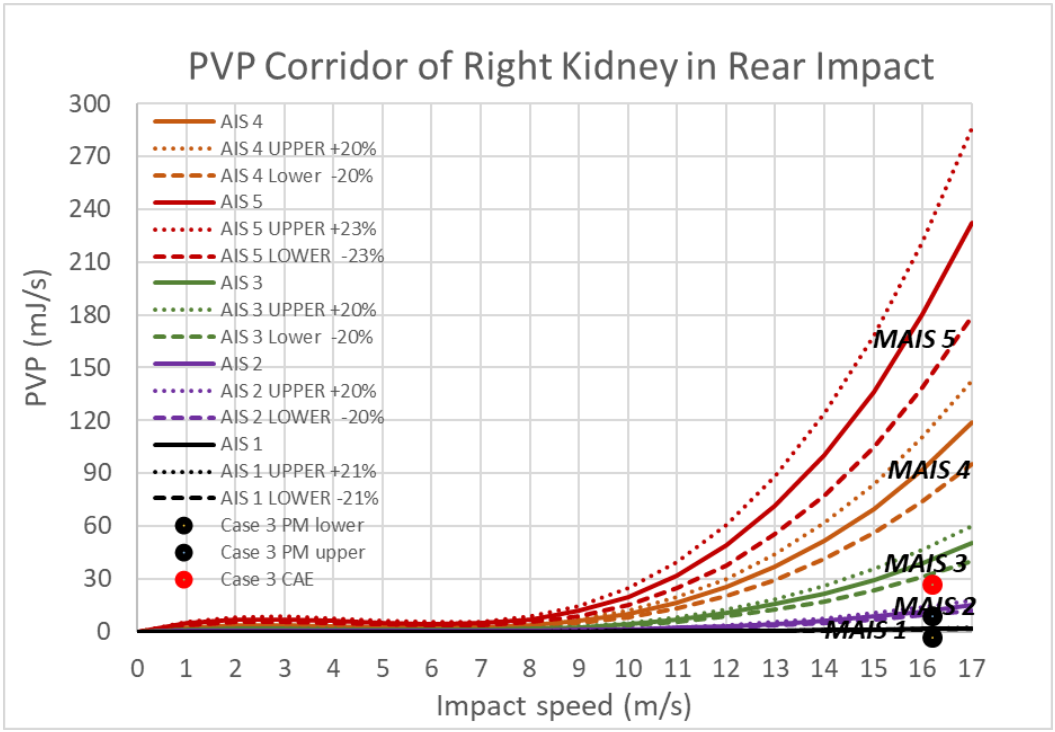

Figure 136 Right kidney injury result from CAE and Post-mortem report of case 3

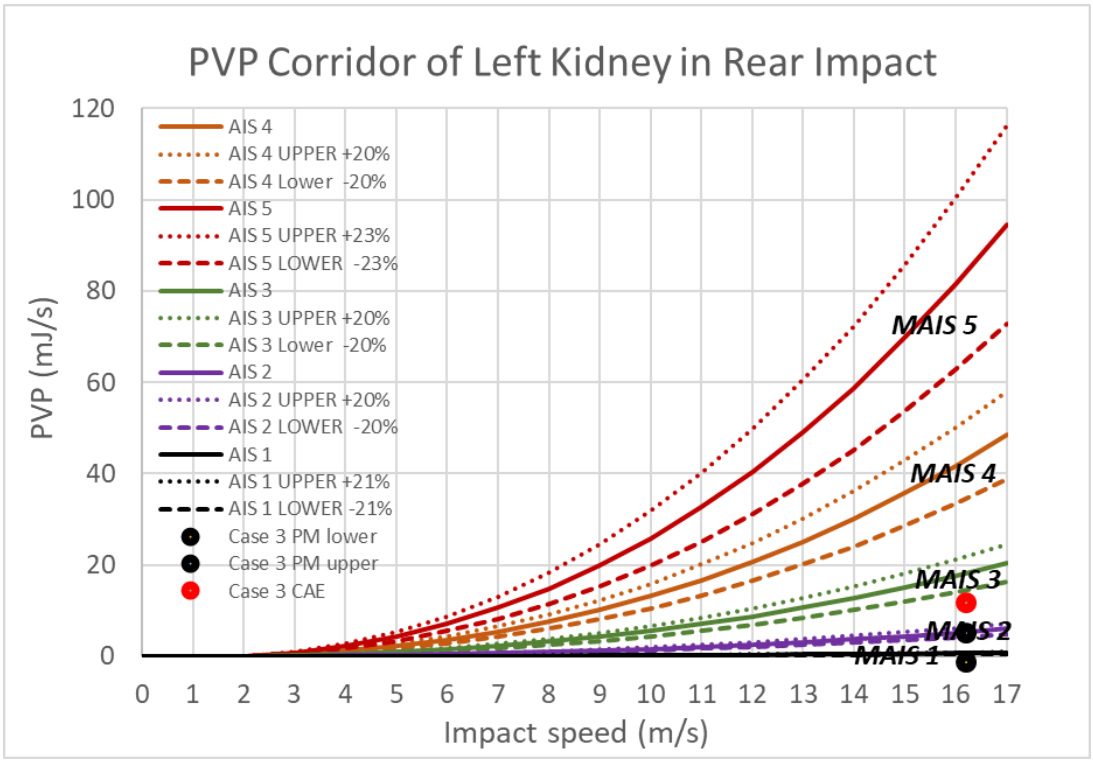

Figure 137 Left kidney injury result from CAE and Post-mortem report of case 3

The initial results suggest that the CAE predictions are in the same order of magnitude as the PM report on brain tissue injury. The PVP value on the brain white matter is 1.16 mJ/s which occurs on element 88118362. This element is located at junction area of brain but on right white matter. The PVP value on the brain ghite matter is 0.94 mJ/s which occurs on element 88121824. The element is also located at junction area of the brain but on right grey matter. On the white matter, no injury was given from the PM report, for which an AIS 0-2 was recorded by the Coroner. In the CAE simulation, an AIS 3 serious injury has been computed on the grey matter, however no contusion was concluded on the grey matter PM report.

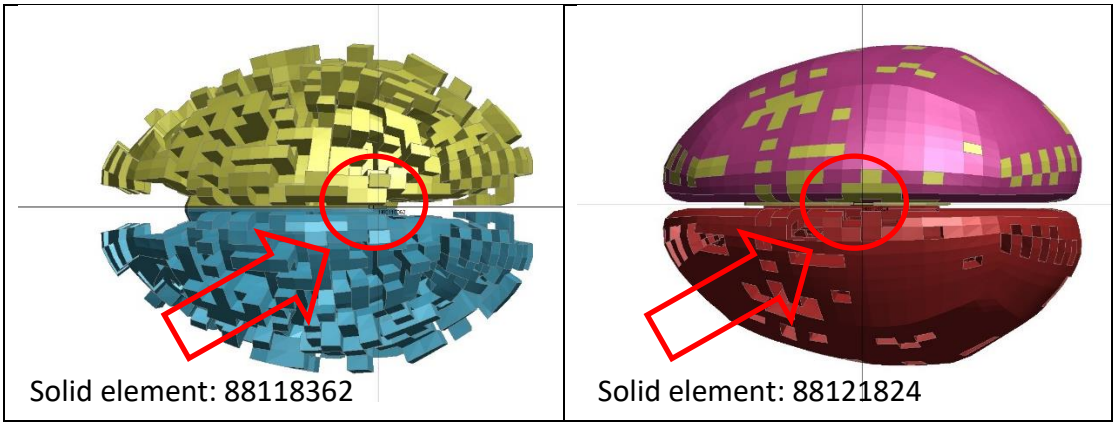

Figure 138 Injury location of brain white matter (left) and grey matter (right) of case 3

On the critical organs, no AIS level was given in the PM report. An AIS 0-2 was assumed, because of the difficulty to locate such injuries in the autopsy. On the heart, the CAE indicated an untreatable injury while the PM described no abnormality. On the liver, the PM concluded congestion. Referring to an AIS rating explanation in the introduction section, the liver congestion is not included, then AIS 0-2 can be assumed. The CAE indicated on the contrary an AIS 3+ injury on liver. On the other organs, the CAE predictions coincided with the PM injury severity.

8.4 Case 4: Accident scenario and Computation Setup

Accident 4 is a collision between a 25-year old male and a Mercedes Benz B180. The pedestrian was crossing from the driver's nearside to the far side when impacted (Figure 139).

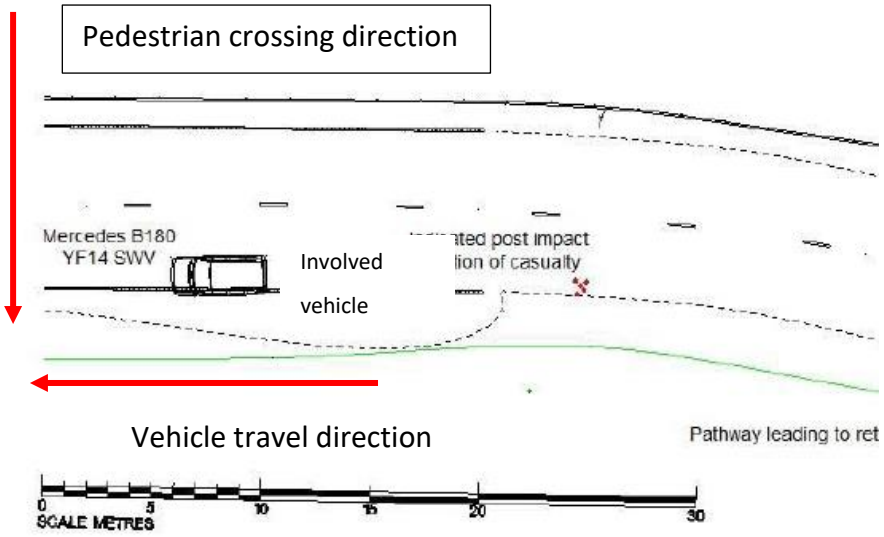

Figure 139 Scenario of case 4

The involved vehicle is a Mercedes Benz B180. It was scaled according to the available dimensions blue print of the vehicle. The stiffness distributed was then remapped based on the assessment information provided by EuroNCAP (Figure 140).

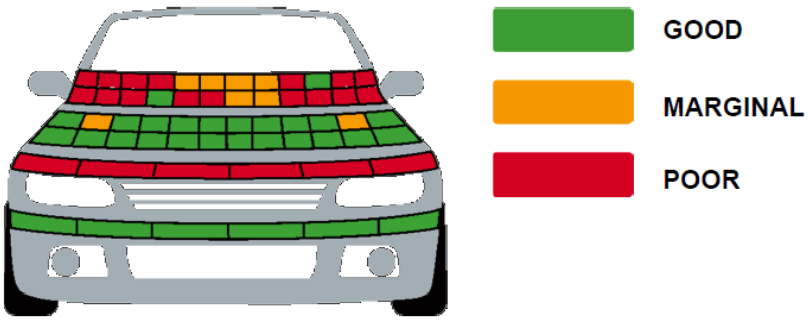

Figure 140 Stiffness distribution of Mercedes Benz B180(EuroNCAP, 2011)

The windscreen angle was also measured to ensure the correct geometry (Figure 141).

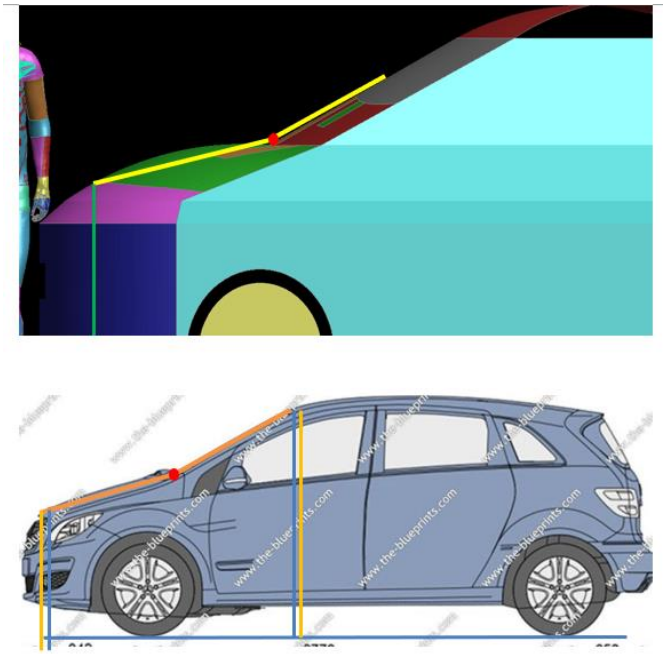

Figure 141 Geometry comparison between CAE model and vehicle blue print

8.4.1 Pedestrian Kinematics

As described in the autopsy report, a large number of brusing and fracture was observed on the left side of the body (left knee, left forearm). An obvious fracture was also observed at the base on the left hand side of the skull. From all the information

provided, the pedestrian was most likely left leg forward. As stated in the autopsy report, the pedestrian was 1.65m in height and 56.4 kg in weight. The THUMS model was then scaled accordingly. From a witness statement, the pedestrian was running into the road giving no opportunity for the driver to react. According to the information given in Table 19 and Table 20, a high running speed for a 25-year old male is 4.24m/s and slow running speed 2.8m/s. The vehicle impact speed range given in th UKPF report is 28-35mph. All speeds were applied in the CAE simulation, however the pedestrian missed the windscreen area in all the cases. Using an impact speed of 28mph with the pedestrian running at 2.6m/s, pedestrain landed in an area comparable with the accident photo provided (Figure 142 and Figure 143).

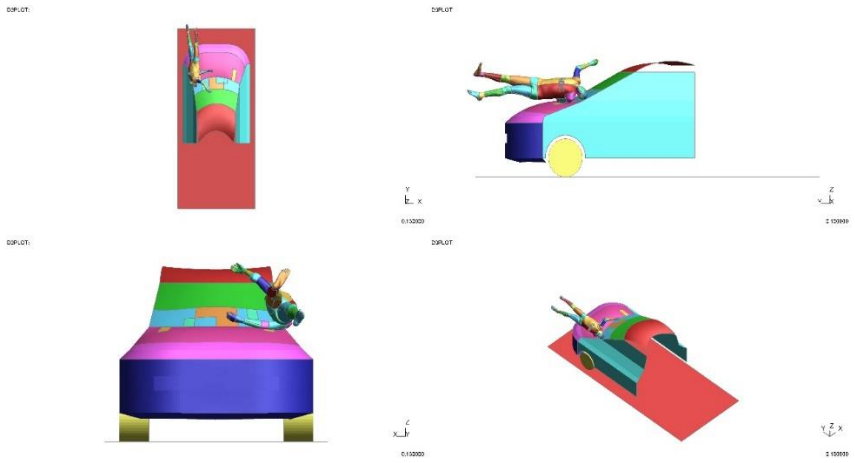

Figure 142 Pedestrian landing area of case 4

Figure 143 Damage on windscreen in case 4

The kinematics of the pedestrian is shown in Figure 144.

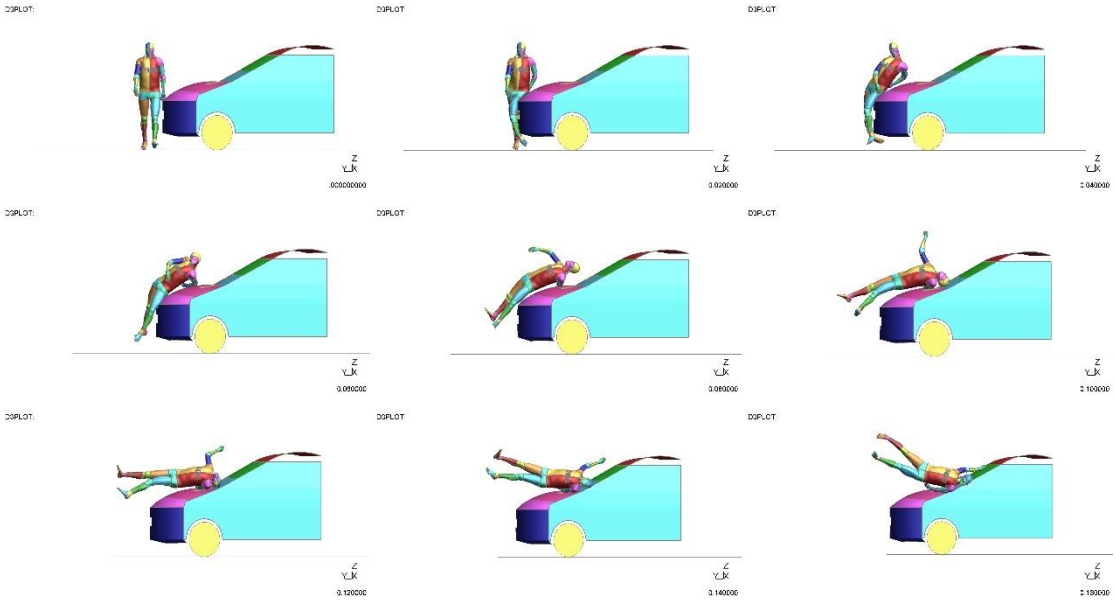

Figure 144 Kinematics of pedestrian of case 4

The pedestrian was positioned with his left-leg forward. At the initial stage, the pedestrian's lower extremities contacted with the bumper. Then the upper torso started to rotate and land on the bonnet. At a later stage, the pedestrian's head landed on the corner of the windscreen. To ensure the model was numerically stable, an energy balance of whole simulation is provided in Figure 145 and contact forces between the pedestrian and the vehicle is shown in Figure 146.

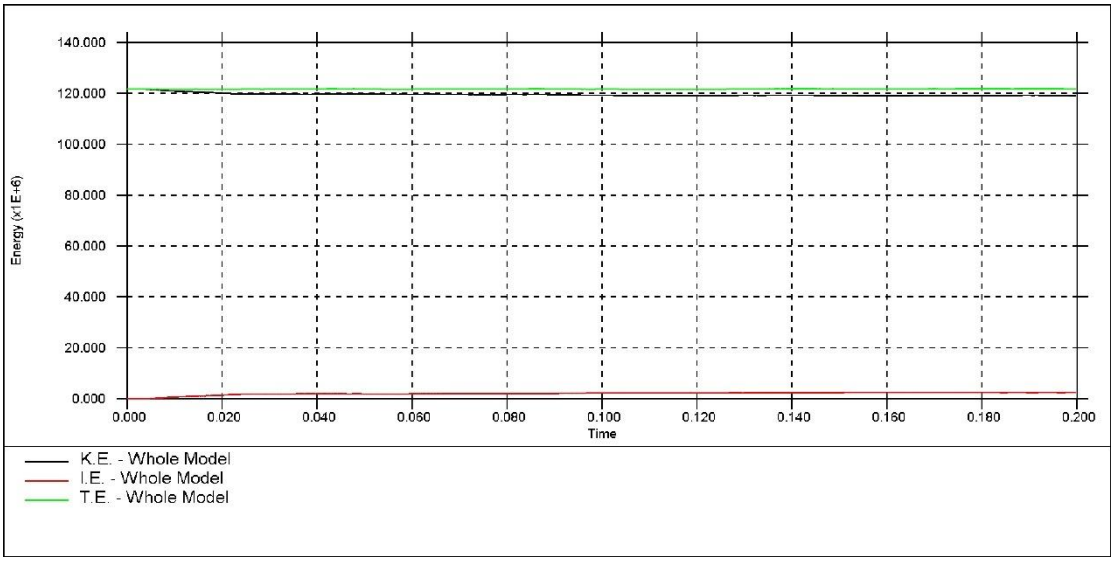

Figure 145 Energy curve of case 4

As shown in Figure 145, the total energy curve remains constant through the whole time history. There is no energy loss and no hourglassing, therefore, the whole simulation is numerically stable.

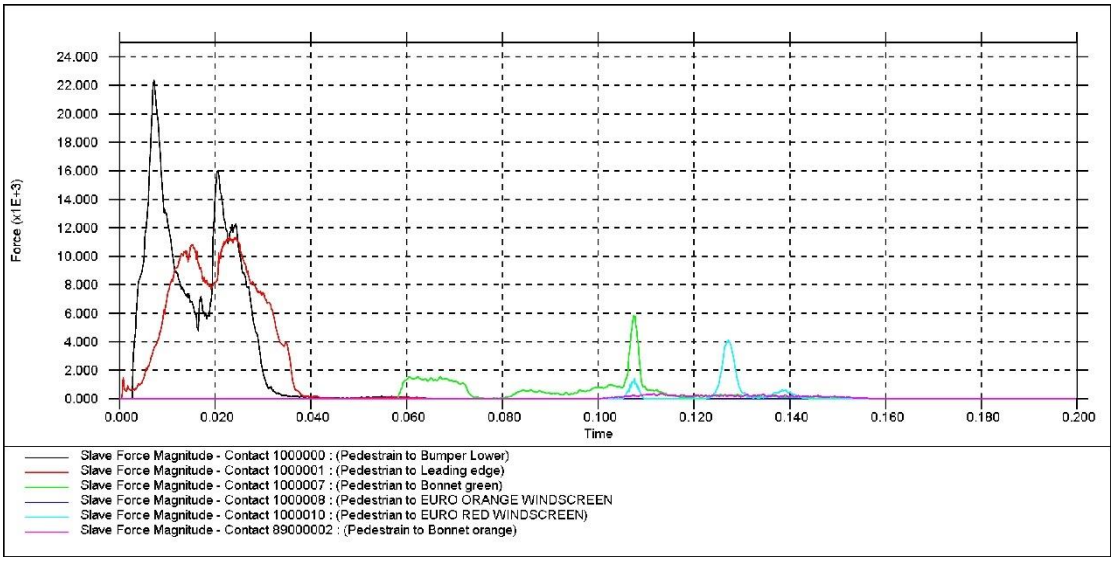

Figure 146 Contact force between pedestrian and vehicle of case 4

As shown in above, the contact started between pedestrian lower extremities and bumper instantaneously. The pedestrian then started to contact with the bonnet leading edge. These contacts lasted until 0.06s (60ms). The contact between the pedestrian and the bonnet lasted from 0.06s (60ms) to 0.12s (120ms) approximately. During this period of time, the pedestrian rotated on the bonnet. The pedestrian head contacted then with windscreen starting from 0.12s (120ms) to 0.14s (140ms) which is illustrated with the peak in Figure 146.

8.4.2 Injury Results using PVP

The pedestrian was impacted on his left against vehicle windscreen, consequently the PVP corridor from the lateral impact was used as injury threshold predictor. Based on the PM report conclusions, the PVP threshold at speed of 28mph (12.52m/s) in pedestrian rear impact is shown in Table 31.

Organs (Injury)	AIS Level	PVP Threshold at 28mph (mJ/s)
White matter (DAI)	4	1.01
Grey matter (Brain contusion)	3	1.29
Heart (Rupture)	4	0-0.19
Liver (Rupture)	4	0-31.87
Spleen (Rupture)	4	0-11.16
Right kidney (Rupture)	4	0-3.85
Left kidney (Rupture)	4	0-2.87

Table 31 PVP threshold at impact speed of 28mph (12.52m/s)

The PVP values and distribution on brain tissue and critical organs were then extracted. The PVP distribution on the brain white matter and the grey matter illustrated in Figure 77 and Figure 78 respectively, while the critical organs injuries are shown from Figure 79 to Figure 82.

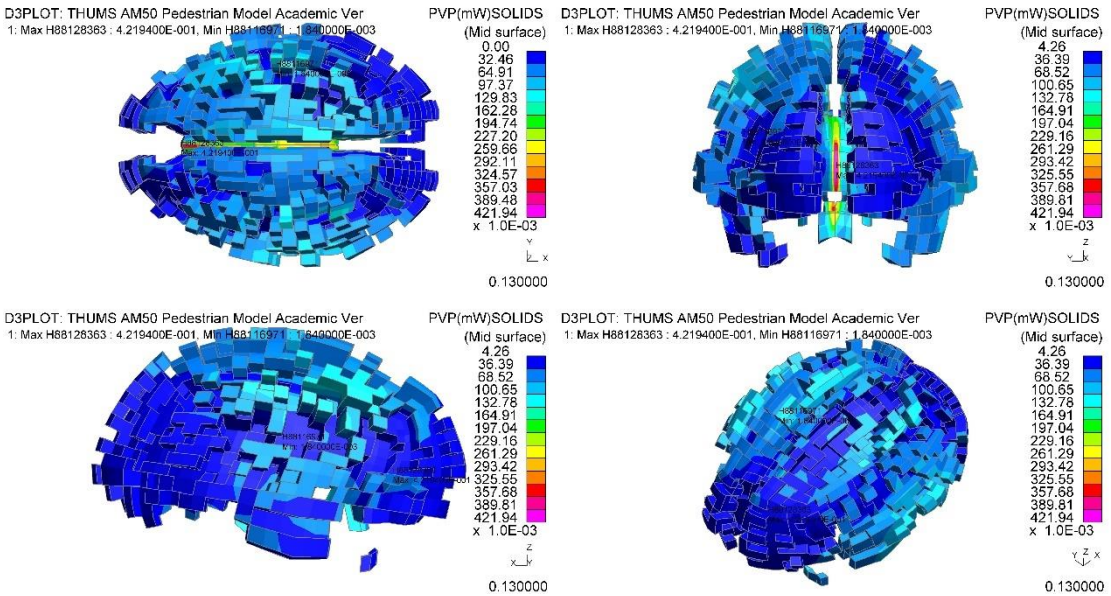

Figure 147 PVP on brain white matter at 0.13s (130ms) of case 4

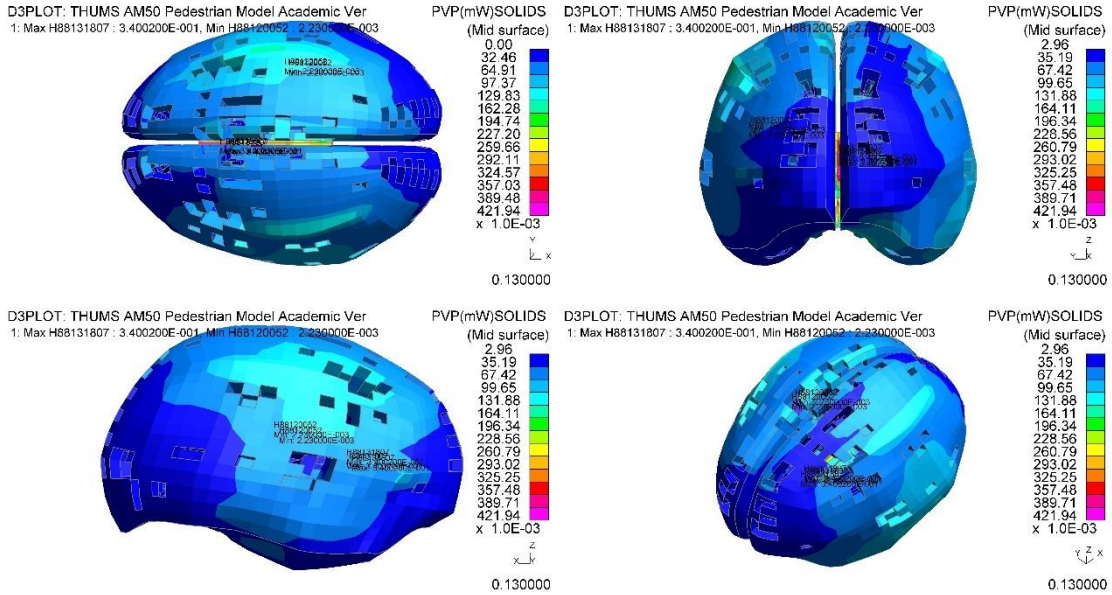

Figure 148 PVP on brain grey matter at 0.13s (130ms) of case 4

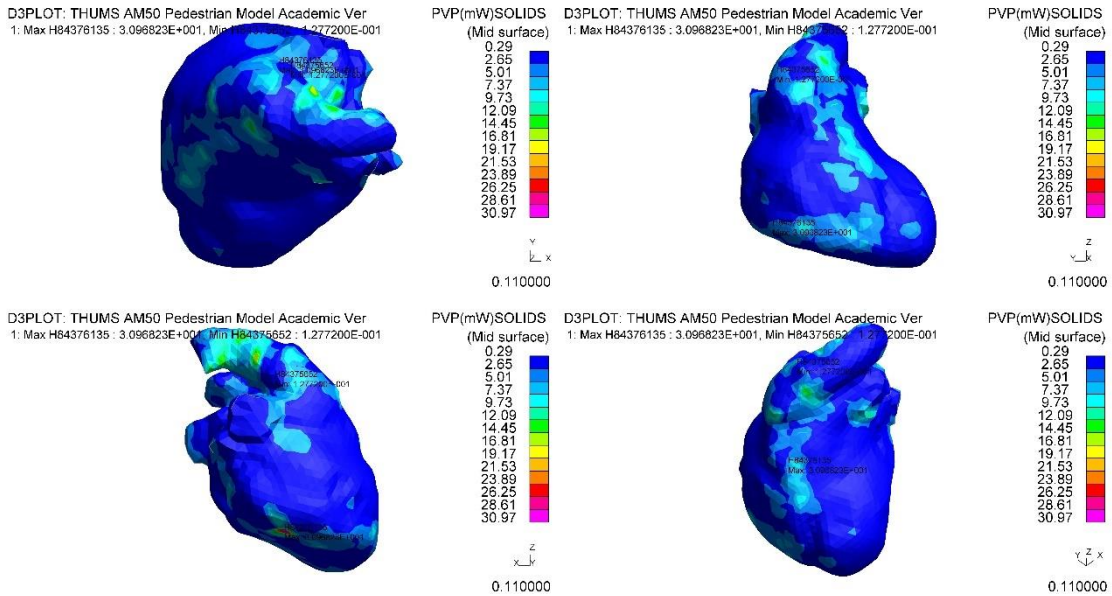

Figure 149 PVP on heart at 0.11s (110ms) of case 4

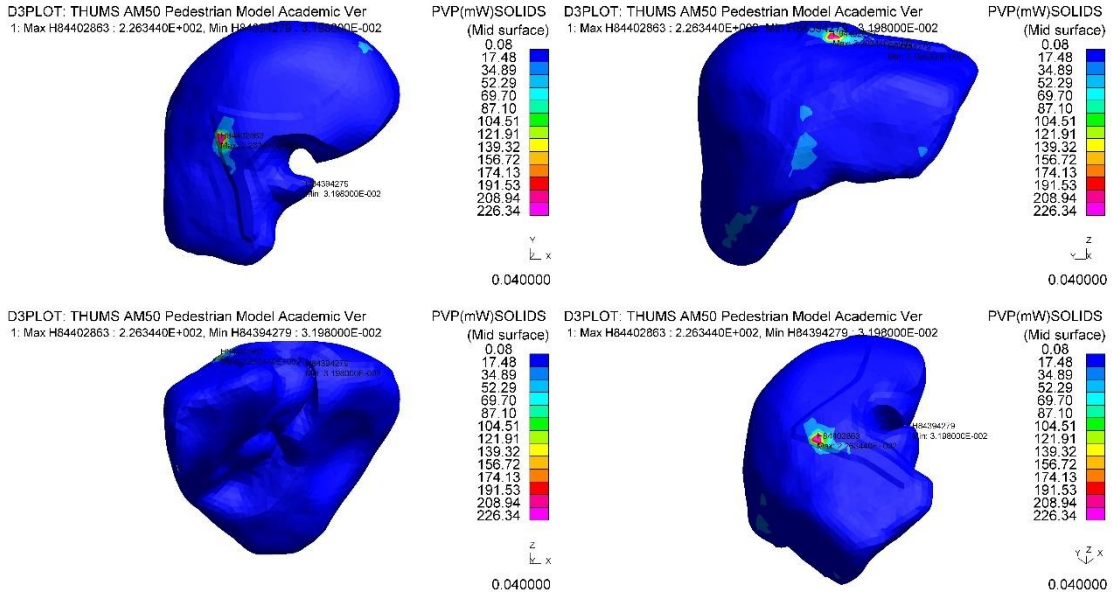

Figure 150 PVP on liver at 0.04s (40ms) of case 4

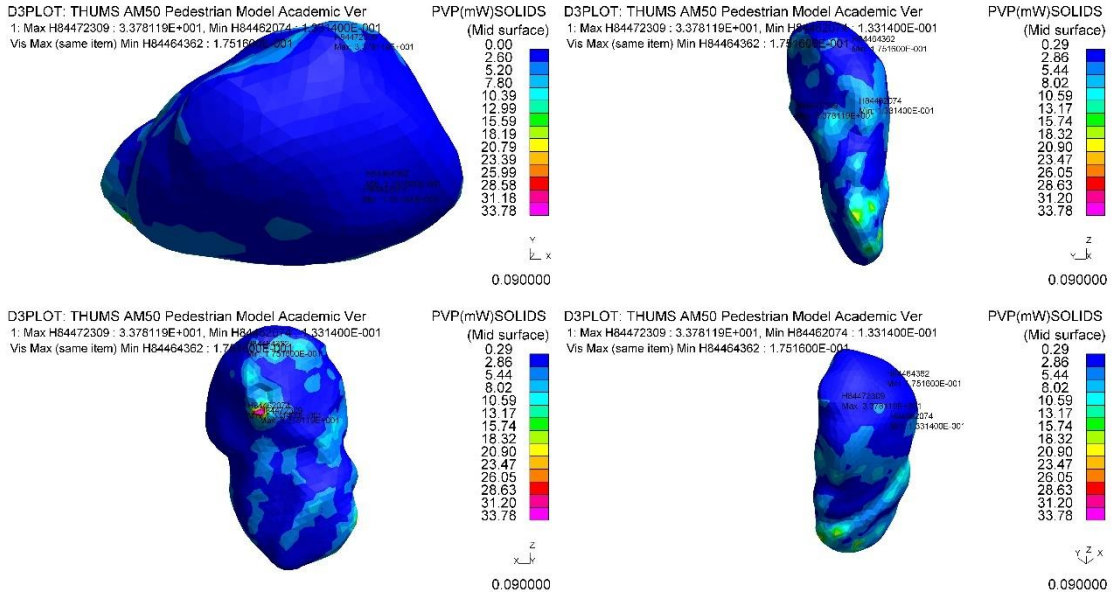

Figure 151 PVP on spleen at 0.09s (90ms) of case 4

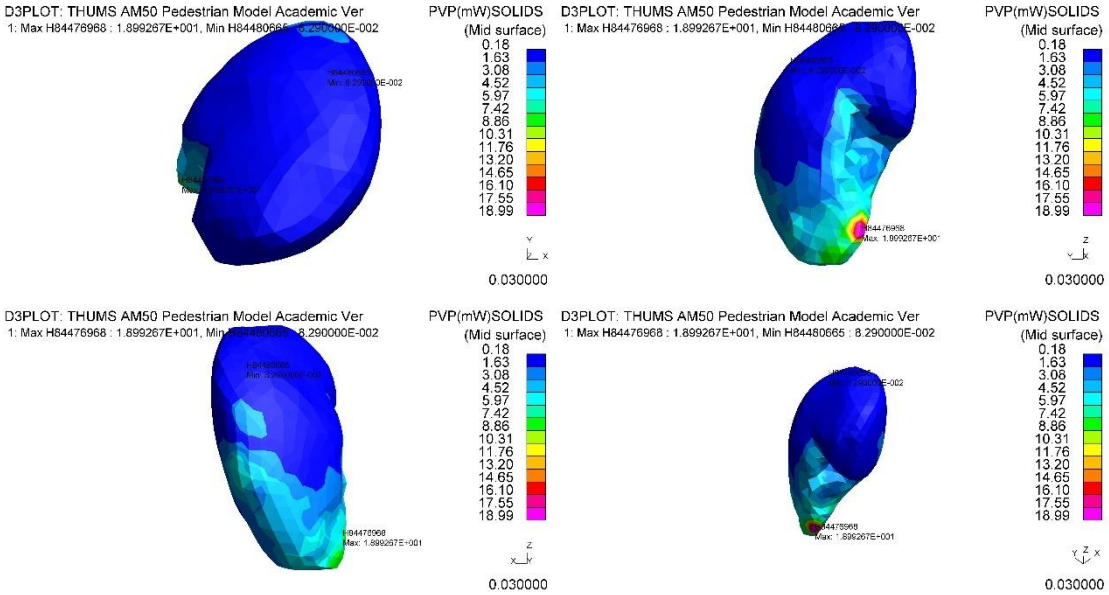

Figure 152 PVP on right kidney at 0.03s (30ms) of case 4

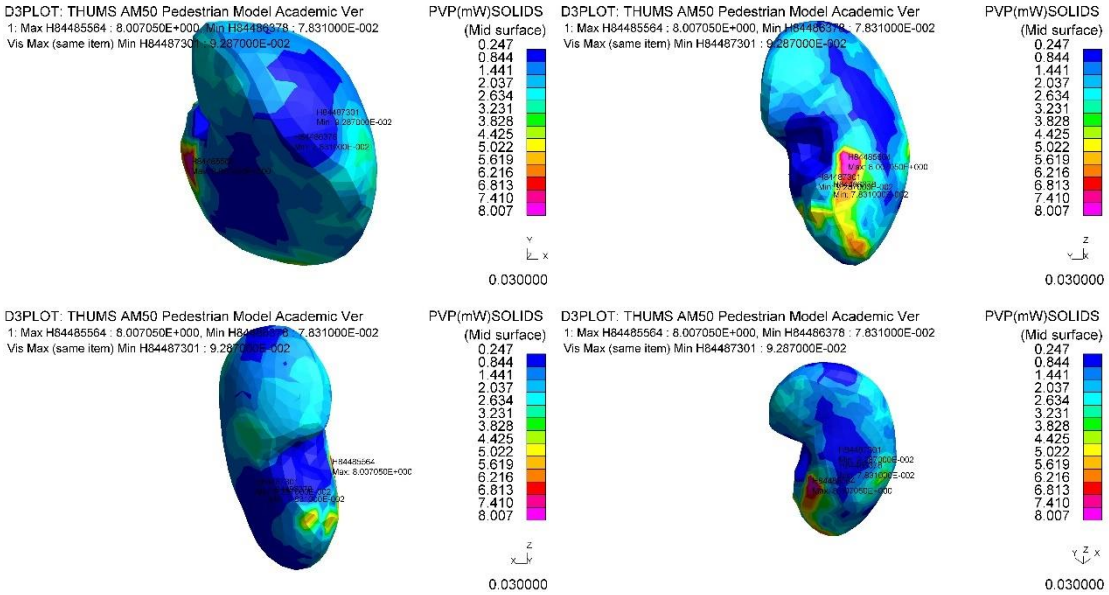

Figure 153 PVP on left kidney at 0.03s (30ms) of case 4

In summary, the PVP injury results of case 4 is listed in Table 32.

Organs/Tissue	PVP from CAE simulation (mJ/s)	Location (ID)	Time (ms)
White matter (DAI) in side impact	0.42	88128363	84
Grey matter (brain contusion) in side impact	0.34	88131807	84
Heart	30.97	84376135	35.4
Liver	226.34	84402863	31
Spleen	33.78	84472309	80
Right kidney	19	84476968	26
Left kidney	8.01	84485564	25.5

Table 32 PVP injury result of case 4

8.4.3 Result of Case 4

The comparison between the CAE prediction and the PM report of case 4 is presented in Table 33. The comparison of individual injuries are also presented from Figure 154 to Figure 160.

Organs/Tissue	Injury	AIS of PM	AIS of CAE	MAIS of PM	MAIS of CAE	ISS of PM	ISS of CAE
Brain white matter	Subarachnoid haemorrhage	4	3	4	3	24	61
Brain grey matter	No evidenced	0-2	0-2				
Heart	Normal	0-2	6+	2	6		
Liver	Unremarkable	0-2	4	2	4		
Spleen	Normal	0-2	2+				
Right kidney	Normal	0-2	3				
Left kidney	Normal	0-2	3+				

Table 33 Injury result comparison between CAE and PM report of case 4

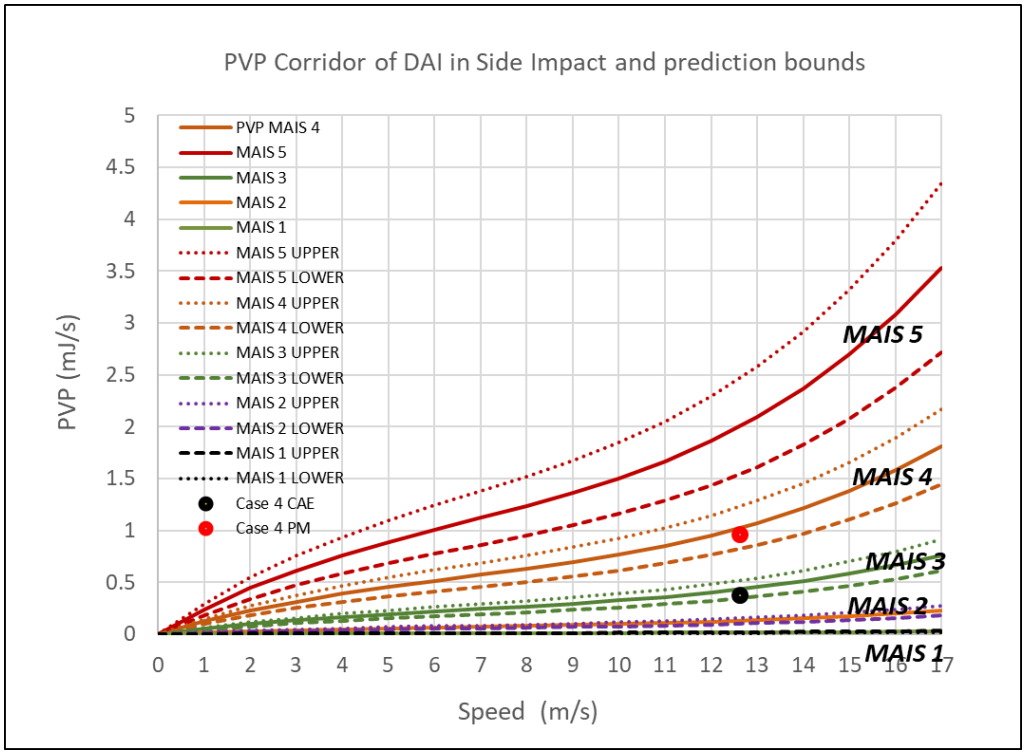

Figure 154 Brian DAI result of case 4 from CAE and autopsy report

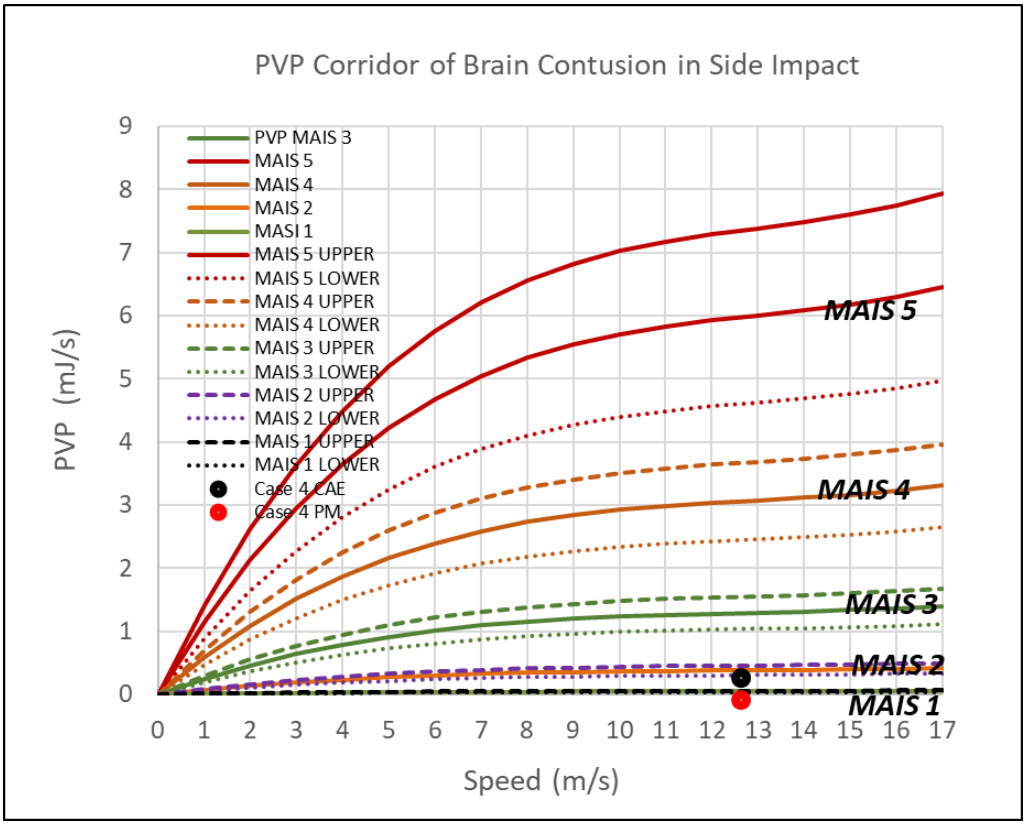

Figure 155 Brian contusion result of case 4 from CAE and autopsy report

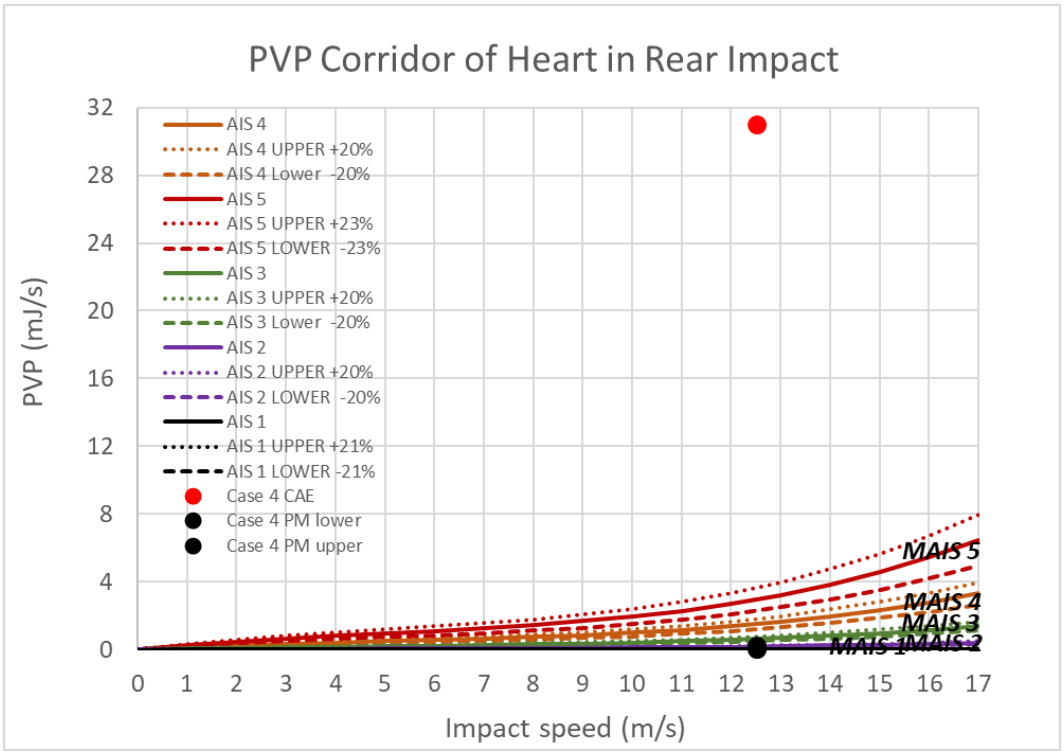

Figure 156 Heart injury result from CAE and Post-mortem report of case 4

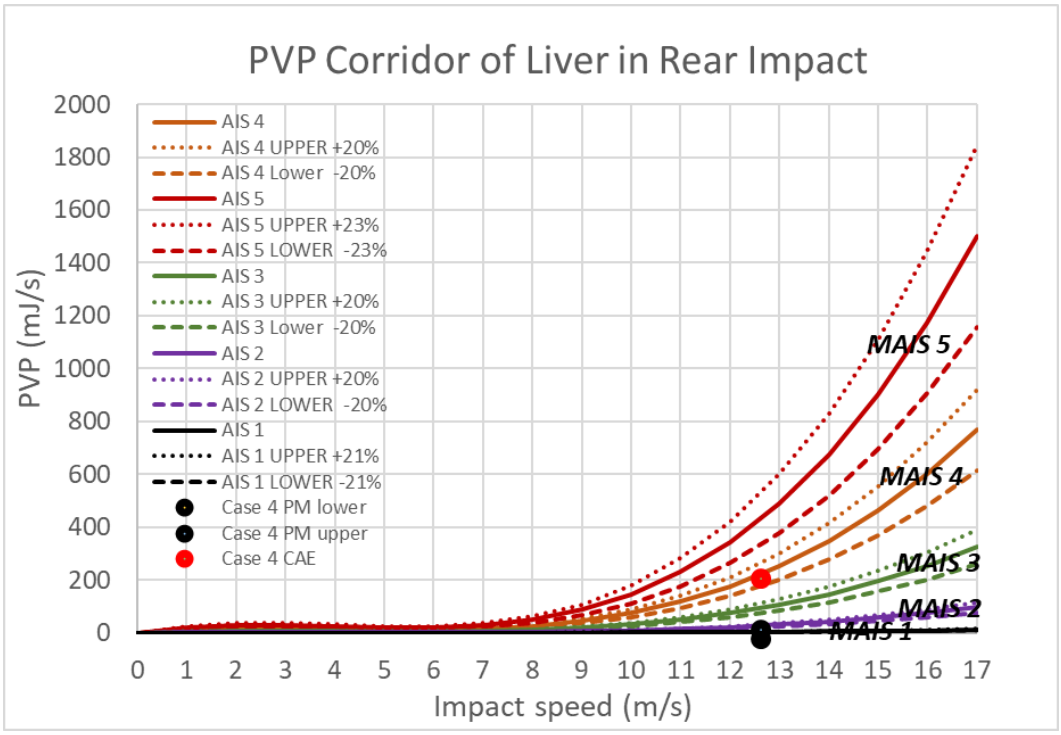

Figure 157 Liver injury result from CAE and Post-mortem report of case 4

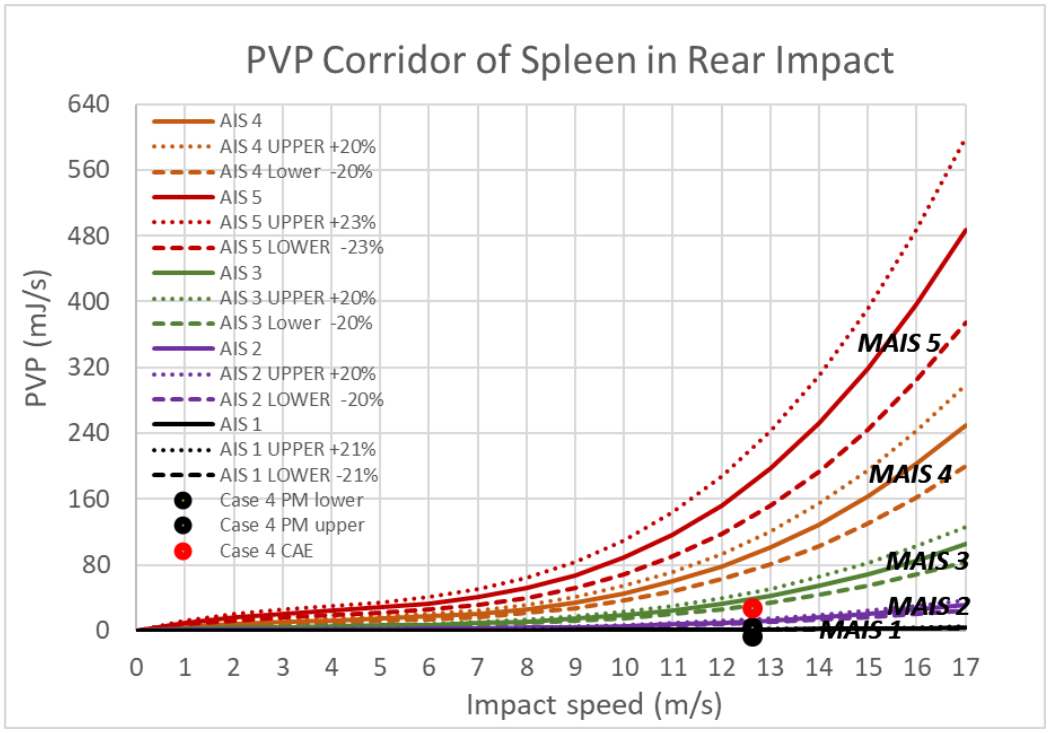

Figure 158 Spleen injury result from CAE and Post-mortem report of case 4

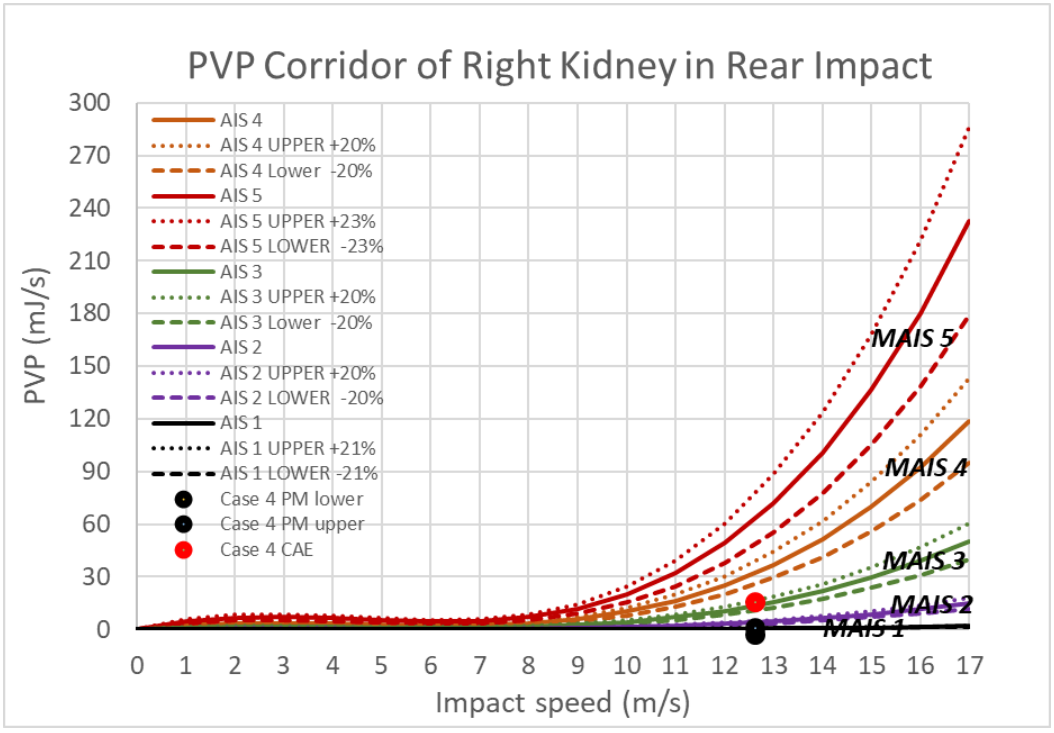

Figure 159 Right kidney injury result from CAE and Post-mortem report of case 4

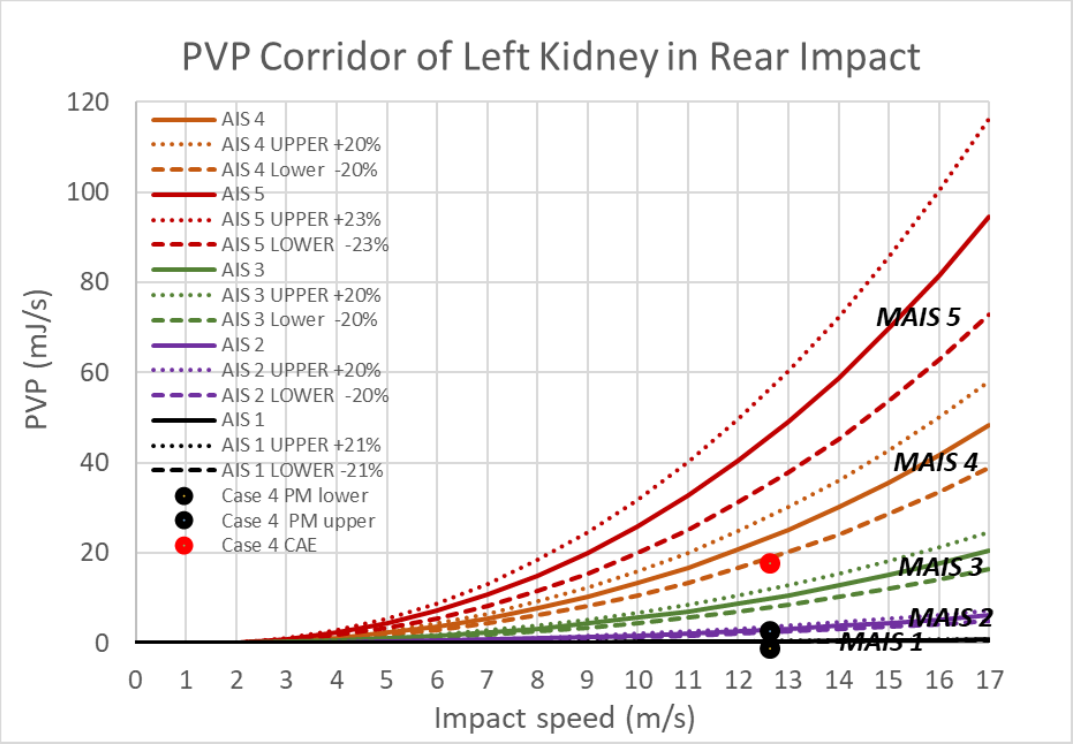

Figure 160 Left kidney injury result from CAE and Post-mortem report of case 4

The initial results show that the CAE predictions are in the same order of magnitude as the PM report on brain tissue injury. However, noticeable differences can be observed on heart injury predictions. As stated in the PM report, a subarachnoid haemorrhage was identified on the pedestrian head, which makes the AIS level for white matter injury a 4. Furthermore, the PM report concluded an extensive haemorrhage within the left cerebral hemisphere with peripheral haemorrhage within both cerebral lobes. In the CAE simulation, an AIS 3 on the white matter injury was predicted. As shown in Figure 147, the injury spread on both cerebral lobes. However, post-accident dynamic injury such as haemorrhage is out of the prediction scope of numerical FE human model, as the THUMS model is only able to predict mechanical injuries. Consequently, post-accident injuries cannot be simulated in the CAE model. No brain contusion was identified in the PM report while the CAE simulation concludes an AIS 2 minor injury.

On the critical organs, no injuries were reported in the PM report. Again, an AIS 0-2 was assumed. On the liver, the CAE predictions indicated an AIS 4 injury while in the

PM report, it was noted that the liver to be unremarkable. On the other organs, the CAE over-predicted the PM report by 1 AIS level

9.0 Discussion

This section aims to further explore and discuss the injury results from the CAE simulations and compare them with Post- Mortem (PM) findings. The ISS score of the PM and CAE simulation are presented from Figure 161 to Figure 164. In order to compute the ISS, the sum of the squares of the head, the chest and the abdomen are considered.

As the heart AIS predictions are off scale, the ISS was also calculated separately.

Organs/Tissue	Injury	AIS of PM	AIS of CAE	MAIS of PM	MAIS of CAE	ISS of PM	ISS of CAE
Brain white matter	DAI	4	2-3	4	3	48	54
Brain grey matter	Brain contusion	0-2	2				
Heart	Rupture	4	4	4	3+		
Liver	Rupture	4	6+	4	6		
Spleen	Rupture	2-3	6+				
Right kidney	Rupture	4	6+				
Left kidney	Rupture	4	5+				
Except heart						32 (48-16)	45 (54-9)

Figure 161 Overall prediction result from CAE and PM of case 1

Organs/Tissue	Injury	AIS of PM	AIS of CAE	MAIS of PM	MAIS of CAE	ISS of PM	ISS of CAE
Brain white matter	DAI	3	3	3	3	17	54
Brain grey matter	Brain contusion	3	3				
Heart	Unremarkable	0-2	4	2	6		
Liver	Unremarkable	0-2	3	2	3		
Spleen	Congested	0-2	2+				
Right kidney	Unremarkable	0-2	2+				
Left kidney	Unremarkable	0-2	2+				
Except heart						13 (17-4)	18 (54-36)

Figure 162 Overall prediction result from CAE and PM of case 2

Organs/Tissue	Injury	AIS of PM	AIS of CAE	MAIS of PM	MAIS of CAE	ISS of PM	ISS of CAE
Brain white matter	No evidenced	0-2	3	2	3	12	54
Brain grey matter	No contusion	0-2	3				
Heart	No abnormality	0-2	6+	2	6		
Liver	Congested	0-2	3+	2	3		
Spleen	Congested but no laceration	0-2	2+				
Right kidney	No focal lesion	0-2	2+				
Left kidney	No focal lesion	0-2	2+				
Except heart						8 (12-4)	18 (54-36)

Figure 163 Overall prediction result from CAE and PM of case 3

Organs/Tissue	Injury	AIS of PM	AIS of CAE	MAIS of PM	MAIS of CAE	ISS of PM	ISS of CAE
Brain white matter	Subarachnoid haemorrhage	4	3	4	3	24	61
Brain grey matter	No evidenced	0-2	0-2				
Heart	Normal	0-2	6+	2	6		
Liver	Unremarkable	0-2	4	2	4		
Spleen	Normal	0-2	2+				
Right kidney	Normal	0-2	3				
Left kidney	Normal	0-2	3+				
Except heart						20 (24-4)	25 (61-36)

Figure 164 Overall prediction result from CAE and PM of case 4

In the instance of Case 1, it can be observed that the CAE predictions are in the same order of magnitude as the PM on the brain trauma. On brain tissue, the CAE prediction coincides with the PM conclusion of all cases. On the critical organs, the CAE predictions suggest a significant difference on the heart. On the rest of the organs, the CAE simulations calculate a good correlation. Regarding the injury location, the comparison was also made between the PM report and the CAE simulations (Table 34).

Case No.	PM description	CAE location	Reason
1	Right parietal lobe (Haemorrhage)	88118340 (Centre of parietal lobe, not surface)	Haemorrhage is ot of the preditcion scope of THUMS. Thums can only predict mechanical damage on white matter which is DAI. The side effect of DAI is haemorrhage.
2	The inferior aspect of the right temporal lobe (Swollen)	88131788 (Left grey matter, but in midlineof whole grey matter)	The maximum PVP is not located on the description of PM, but PVP distribution can be clearly observed on right temporal lobe. Also, swollen is a post-accident injury which cannot be shown using THUMS
3	No eveidence of skull fracture and brain showed no evidence of contusion	88118362 (Centre of right white matter parietal lobe) 88121842 (Centre of right grey matter parietal)	
4	Extensive haemorrhage within the left cerebral hemisphere with peripheral haemorrhage within both cerebral lobes.	88128363 (Left white matter frontal lobe)	

Table 34 Injury location from PM report and CAE simulations

In case 1, the PM report and CAE simulation indicated the same injury location. The CAE simulation indicated that the location of maximum PVP was at the centre of the parietal lobe, not in the surface, while the PM report did not give any details. Haemorrhage, as a dynamic post-accident trauma, is out of the prediction scope of THUMS model. In Case 2, the PVP was largely observed on the inferior aspect of the

right temporal lobe of right grey matter (Figure 102), which is the injury location indicated by the PM report. Numerically, the maximum PVP is on the left grey matter located in the connection of the two sides. Again, PVP, as a mechanical indicator, cannot predict post-accident result. Regarding Case 3, no brain injury was identified from the PM report, while the PVP indicated an AIS 3 brain trauma. In Case 3, it has to be noted that the pedestrian died later in hospital. In Case 4, the PM report indicated extensive haemorrhage within both cerebral lobes, while the PVP was largely distributed on both lobes (Figure 147 and Figure 148). The maximum PVP value is located on the frontal lobe of left the white matter, while the PM report did not provide any details.

In the instance of Case 1, on the white matter, the CAE prediction was an AIS 3 while the PM predicted AIS 4. In the PM report, it was observed that the skull and the cranial cavity were normal. The brain showed an area of subdural haemorrhage over the right parietal lobe, as well as over the cerebellum in the midline and over right cerebella hemisphere. No other brain injury was identified. It can be observed from that that the PVP is located in exactly the same area as the PM report. On the brain grey matter, the PVP observed an AIS 2 moderate injury while no grey matter injury was indicated in the PM report. The pedestrian died however of a brain haemorrhage, or bleeding. The CAE model can only predict mechanical damage, and as it is using a Lagrangian formulation, it is not able to predict the blood loss, which is a fluid problem. As a post-accident injury, haemorrhage is out of the prediction scope of the THUMS model and it is promising that PVP is underestimating the white matter injury. Nevertheless, as a mechanical indicator, it predicted the correct damage area which maximum principal strain failed to do, as illustrated in Figure 165.

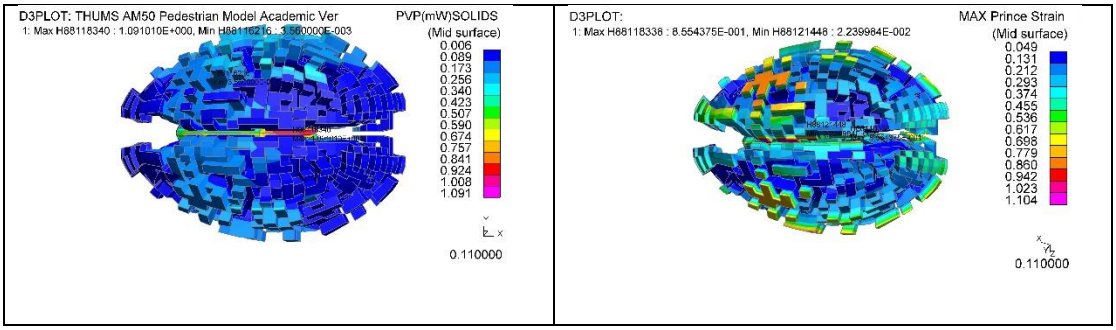

Figure 165 Injury comparison between PVP and maximum principal strain of case 1

From the PVP distribution, the injury location can be clearly identified. On the contrary, the Maximum principal strain cannot indicate injury location, because DAI threshold, which is 21% maximum principal strain, covers nearly all the white matter. Referring to the PM report, the PVP is a better indicator in both injury severity and location.

Regarding the organ expectation of Case 1, the CAE predictions of the heart are in the same order of magnitude as the PM prediction. In the PM report, the pericardial cavity was concluded as ruptured. The pericardium is a tough double layered fibroserous sac which covers the heart (Combs, 1995) (Figure 166). In the THUMS model, the heart is modelled as a whole solid tetrahedron meshed part which does not contain enough details of biological structure i.e. cavities and fluid. Also, the heart of THUMS model has significant geometric differences compared with human heart (Figure 166), consequently, the CAE simulation cannot accurately mimic real human heart behaviour using this model. An AIS 4 heart injury was still identified on heart in CAE simulation.

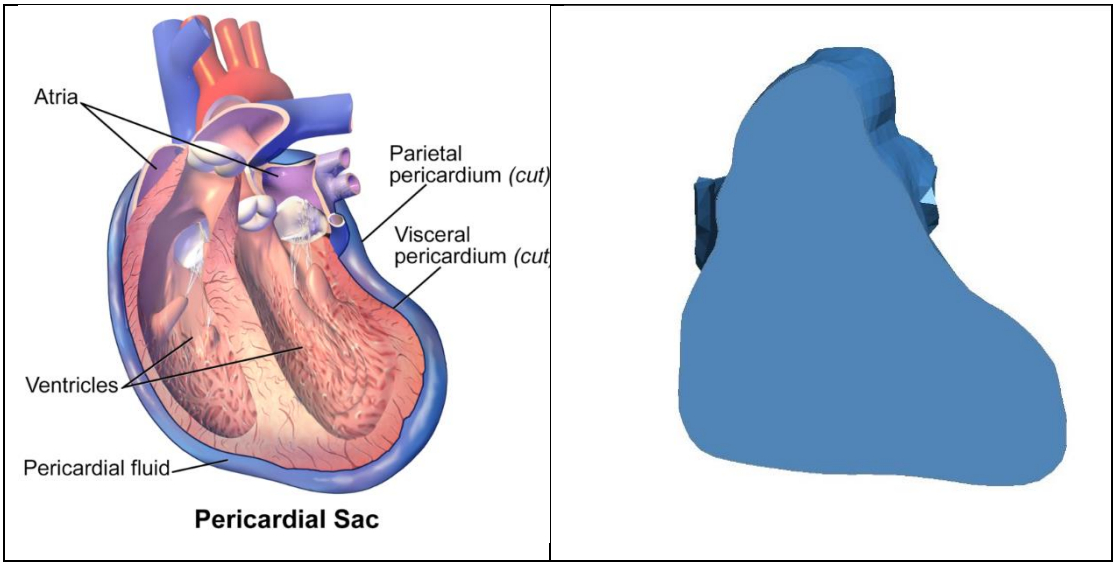

Figure 166 Heart structure (Combs, 1995)

On the liver, the CAE confirmed an AIS 4 liver rupture while the PM indicated an AIS 4 liver rupture. The PM report identified that the liver showed obvious rupture over the anterior surface, which is the exact area highlighted by the PVP (Figure 80). On the spleen, the PM report concluded an AIS 4 spleen rupture, however the injury location was not evidenced. The CAE simulation indicated an untreatable spleen injury on the upper anterior surface of spleen. On the right kidney, the PM report identified a perinephric haemorrhage around both kidneys. No AIS level was reported in the PM. Based on the AIS rating explanation explained in previous chapter, a perinephric haemorrhage is classified as AIS 2-3 at different blood loss level. On the contrary, the CAE indicated an untreatable injury on the right kidney. Compared with the other organs, the kidneys are located at the back of the upper torso, while the heart and the liver are located in the anterior of upper torso. The heart is protected by the ribcage. Regarding material properties, all organs of the THUMS are modelled using material of simplified rubber with different bulk modulus (Table 35).

	Heart	Liver	Spleen	Kidney
Material ID	MAT 181	MAT 182	MAT 183	MAT 184
Material type	Simplified rubber	Simplified rubber	Simplified rubber	Simplified rubber
Density (ρ, t/mm^3)	1.00E-10	1.00E-10	1.00E-10	1.00E-10
Bulking modulus (K, MPa)	100	4.59	4.59	4.59

Table 35 Material used on organs of THUMS pedestrian model

As illustrated in Table 35, high bulk modulus means high resistance in compression. Therefore, comparing with other organs, heart can remain stable in compression load. The impact speed for Case 1 is 36mph (16.09m/s). Under high impact speed, kidneys behave unstably compared to the heart and liver due to differences in load path. Different material properties also generated different reaction under impact. All these factors influence the injury result of different organs. Case 1 is a left lateral impact in

which the pedestrian landed on his front. The right side of torso rolled over on bonnet throughout the impact, explaining why the. PVP on right kidney is higher than the one on the left.

In Case 2, the CAE and the PM both predicted an AIS of 3 on the brain tissue, which is a serious injury. The PM listed that there was some subarachnoid haemorrhage. The brain appeared diffusely swollen to a mild degree and there were contusions on the inferior aspect of the right temporal lobe. These contusions were captured, however, it was not possible to predict the haemorrhage and the swellings, which are post impact injuries. Nevertheless, as a mechanical indicator, it predicted the correct damage area which maximum principal strain failed to do so (Figure 167).

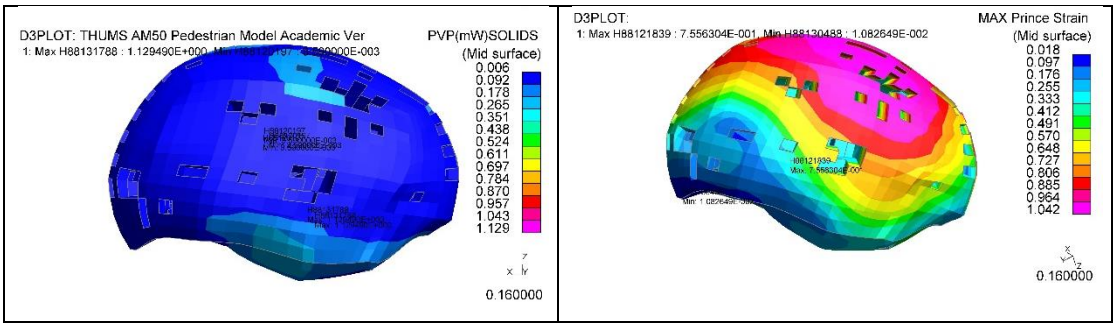

Figure 167 Injury comparison between PVP and maximum principal strain of case 2

As previous stated, currently a 30% maximum principal strain is used as brain contusion threshold. As shown above, the maximum principal strain concluded a brain contusion nearly on all right grey matter. The PVP distribution is more localised which makes the injury location clearly.

On the organs, the PM report did not indicate any AIS level of organ injury. As explained in the previous chapter, a low AIS such as AIS 0-2 injury might not be recorded in the PM report, as it may not clearly visible by the coroner. Therefore, such trauma level were assumed between 0 and 2. For the heart, the CAE is two levels higher than the PM report. As shown in Figure 97, case 2 is a left lateral impact in which the pedestrian's back landed on the vehicle. The pedestrian left body side landed on the line of A-pillar and edge of the bonnet, which has an extremely high stiffness compared with other parts of the vehicle. The heart located on the left side of the chest sustained dramatic higher PVP compared with other organs.

Case 3's PM was unremarkable, as no trauma was observed in the deceased ("No evidence of skull fracture and brain showed no evidence of contusion"). The CAE model predicted an AIS of 2, which is a moderate trauma. Again, maybe such trauma level is quite complicated to observe, as being low risk. On the organs, no trauma was indicated in the PM report. On the contrary, the CAE suggested untreatable injury on the heart. On the liver, CAE over-prediction one level compared with the PM report. The CAE predictions of other organs coincide with the PM report. Detailed PM report is listed below in Table 36.

Injury location	Description
Cardiovascular system	The great vein was unremarkable. Examination on cardiac valves showed no abnormality
Respiratory system	The mouth, tongue and oesophagus were unremarkable
Gastrointestinal system	Stomach appeared unremarkable. The small and large intestines appeared unremarkable. The liver, 1316g, appeared congested. The gallbladder and pancreas were unremarkable.
Lymphoretlcular system	The spleen was terminally congested but with firm pulp. No indication of laceration
Genitourinary system	The kidneys showed no focal lesion on the cut surface.
Central Nervous system	No evidence of skull fracture and brain showed no evidence of contusion
Cause of death	**Multiple injuries and Road traffic injuries**

Table 36 Case 3 PM report

No trauma was identified on each organ and tissue; however, it was still concluded that the pedestrian died of multiple injuries and road traffic injuries, suggesting that the CAE prediction is plausible. Also, regarding the research on the accuracy of PM report (Ncepod, 2006a), accuracy of autopsy report is shown in Table 37.

Quality of the history as presented in the autopsy report		
	n=	%
Good	242	18
Satisfactory	957	71
Unsatisfactory	141	11
TOTAL	*1340*	*100*
Not answered	351	

Table 37 Quality of the history as presented in the autopsy report (Ncepod, 2006b)

Overall, among all the PM reports, the good or satisfactory rate is 89% (Ncepod, 2006b). From the study, the PM report cannot be treated as the unique validation standard in injury investigation.

Case 4 had some similarity with Case 2, except that there was some “significant” skull fracture. The model used in this study is based on THUMS4.01C, which does not contain any fracture/ damage capabilities. This fracture was extending from the right temporal area coronally to the left temporal region. There was also a fracture of the base of skull on the left-hand side. A subarachnoid haemorrhage was identified, and upon slicing through the brain, there was extensive haemorrhage within the left cerebral hemisphere with peripheral haemorrhage within both cerebral lobes. A 1cm haematoma was also noted in the right cerebellum. The computer model predicted an AIS 3 while the PM suggested an AIS 4. Again, it was not possible to predict the haemorrhage, which is a post trauma effect, which requires an Eulerian solving method to extract. Again, PVP, as a mechanical indicator, has predicted the correct damage area while maximum principal strain is more confused (Figure 168).

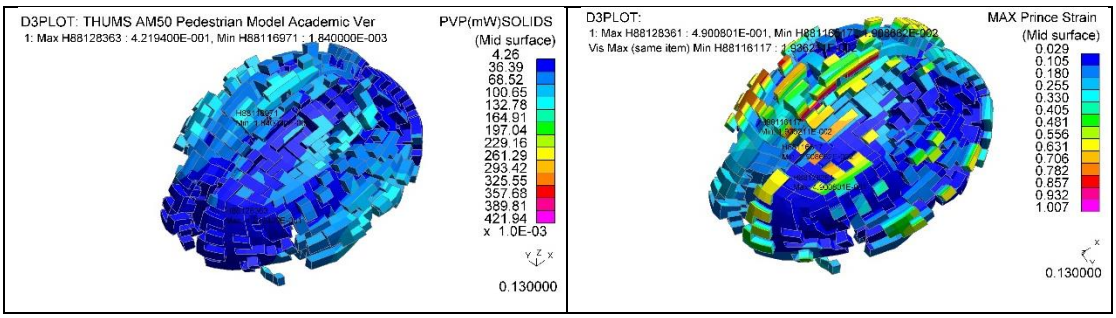

Figure 168 Injury comparison between PVP and maximum principal strain of case 4

As indicated in the PM report, extensive haemorrhage was identified on both lobes. No detailed injury locations were given. Both PVP and maximum principal strain were largely distributed on both lobes. Maximum PVP was observed in the centre of white matter while the peak value of maximum principal strain spread on the surface of the white matter.

On the organs, again, no trauma was suggested in the PM report while the CAE simulation overestimated on all critical organs except for the spleen. The PVP was calibrated on organs in frontal, left lateral and rear impact scenario. Case 4 is not a direct rear impact, which may lead to errors in prediction. Other calibration scenarios need to be investigated.

Overall, it can be observed that the comparison between PVP prediction result of pedestrian injury and the autopsy report shows a promising correlation of the risk to life applied to the pedestrian head. This observation would suggest that it could be proposed to complement the standard pedestrian head impactor numerical process with a human computer head model to assess the real trauma level of a pedestrian. With the current safety assessment processes which are using a head impactor, in ECE 127 (United Nations, January 2013) and EuroNCAP (EuroNCAP, November 2017), which just evaluate HIC, it is only possible to evaluate the likelihood of skull linear damage. This new method can go beyond the current limitations and would predict the trauma outcome in the head white and grey matter. In the case of EuroNCAP, as the bonnets are validated using calibration tests and then scaling of CAE prediction results, it is possible to add this PVP method to simulate alongside the EuroNCAP protocol. As the human head's response is direction dependent this complementary method could investigate different brain trauma risks for all likely head impact directions

10.0 Conclusions

A Finite Element method, using Peak Virtual Power (PVP), was used to successfully extract AIS in pedestrian impact scenarios from CAE computation. The method calibrated PVP using a human computer model (THUMS) which was impacted in specific locations observed in pedestrian accidents, i.e. frontal, lateral and occipital on head and frontal, left lateral and rear on chest. PVP was then extracted in local areas once the critical maximum principal strain known to cause risk to life was observed. As PVP is impact location and speed dependent, this process was repeated to extract a known risk to life (AIS) response as a function of impact velocity. The known AIS response curve was then scaled and corridor bounds computed to create a full spectrum trauma response. A 95^{th} percent confidence interval was used to create these trauma corridor bounds The corridor trauma curves, extracted for head white, grey matter, heart, liver, spleen and kidneys, were then tested against four real-life accident scenarios for which PM data was available.

The selected real-life accidents were reconstructed according to data provided by the UKPF. The vehicle model was modelled with available data using its outside stylizing design surface and including a realistic stiffness location acquired from the EuroNCAP vehicle assessment programme. Pedestrian head forms (diameter 165mm, mass 3.5kg and 4.5kg) were impacted against plates representing sections of the bonnet for child and adult areas. Corresponding thickness was then remapped on the vehicle bonnet. Pedestrian involved was scaled to the recorded height and weight provided. Pedestrian gait was duplicated as the most likely position when accident occurred according to the police report description.

The PVP of the critical organs was calculated from CAE simulations and the corresponding AIS level was concluded using the PVP corridors obtained. This prediction result was then compared with the PM conclusions provided by the coroners. If no AIS level was observed in the PM report, then the AIS rating of 0 to 2 was then proposed as possible trauma outcomes which were too small for the coroner to capture. By comparing with PM report, the trauma prediction result from CAE simulation was then verified.

Case 1 overestimated on the spleen, liver and kidneys by one AIS level. Case 2 provides a reasonable correlation. Case 3 and 4 overestimated on the heart trauma. The PVP prediction of brain trauma shows well correlation and appears consistent.

PVP correctly predicts the AIS level and location which principal strain does not. PVP gives a better correlation on head. This may be due to the double-convex skull structure, giving a well-defined contact, and the suitability of a cylindrical impactor for the calibration. However, the other results seem to suggest the discrepancies are not systematic, but maybe due to a combination of calibration. It is suggested that future work would consider possibly a plate impactor to mimic the contact between vehicle and pedestrian. A plate impactor would give a more realistic loading when the upper body rolls over the bonnet. The THUMS's heart has a significant geometry difference compared with the human heart, which would likely lead to differences in injury predictions. The cubic relationship between the risk of life and impact speed in pedestrian scenarios is confirmed to work properly.

In conclusion, PVP is a good candidate to predict AIS in a Finite Element head model, and that head trauma under-predictions were due to haemorrhage, which is post-impact injury. This method brings however some benefits, as it would allow the assessment of head white and grey matter injuries, which are currently not measured, and may live alongside the current EuroNCAP test protocol to enhance the protection of pedestrian head injuries. By using PVP, numerical AIS level of brain injury can be read directly as well as injury location. With such method, poor vehicle design can be also identified and hence used to improve pedestrian safety and vehicle design dramatically. Results on critical organs, except the heart, show some promising potential, however much more research is necessary to improve their validation

11.0 Limitations and Further Works

The investigation tool used in this research is the THUMS v4 50th male pedestrian model, which is based on a 39 y/o male, with a defined set of anthropometric data. Age and gender may have some effect in material human biological properties (Yamada and Evans, 1970). Also statistically, elderly pedestrians are more vulnerable to AIS 3+ injuries (Carter et al., 2014). Due to the limited number of accident cases, pedestrian age and gender is not considered when filtering the cases. Also, THUMS, as covered in the thesis, is a dynamic Lagrangian CAE model which cannot be used to predict post-accident like swelling and bleeding, but the material damage: in this case trauma. Consequently, a means to extract the post-impact trauma will require a fundamental rebuild of the computer model and include maybe SPH or ALE formulations to evaluate bleeding and swelling.

On the head, a cylinder impactor was used to conduct calibration study, which successfully mimicked the impulse head impact during an accident. It is important to investigate in the future the effect of head impact location sensitivity on AIS predictions.

The torso kinematics in pedestrian accident is a complex procedure. The pedestrian upper torso's rotation might be a combination of different rolling directions. A simple frontal or lateral calibration scenario may not represent pedestrian kinematics in real-world accidents. Differences in calibration may lead to differences between trauma prediction and PM report results. Compared with cylinder impact, which is more localised, real-world accident may be presented using plate impactor. Model errors in structure and material also have a significant influence on the discrepancy between the CAE and PM result. In order to decrease this discrepancy, a better organ calibration and further model improvements are needed. In the future, this study will continue and focus on internal organs, and investigate whether the same level of correlation can be achieved, leading eventually to the CAE calculation of ISS.

12.0 Reference

Association for the Advancement of Automotive 2015. Association for the Advancement of Automotive Medicine.

Bain, A. C. & Meaney, D. F. 2000. Tissue-Level Thresholds for Axonal Damage in an Experimental Model of Central Nervous System White Matter Injury. *Journal of Biomechanical Engineering,* 122**,** 615-622.

Baker, S. P., O'neill, B., Haddon Jr, W. & Long, W. B. 1974. The injury severity score: a method for describing patients with multiple injuries and evaluating emergency care. *Journal of Trauma and Acute Care Surgery,* 14**,** 187-196.

Bastien, C., Wellings, R. & Burnett, B. 2018. An evidence based method to calculate pedestrian crossing speeds in vehicle collisions (PCSC). *Accident Analysis & Prevention,* 118**,** 66-76.

Bastien, C., Wellings, R., Burnett, B. 2018. An Evidence Based Method to Calculate Pedestrian Crossing Speeds in Vehicle Collisions.

Bastien, D. C. 2015. Application of Finite. *Coventry University* [Online]. Available: https://cumoodle.coventry.ac.uk/pluginfile.php/709508/mod_resource/content/1/M55MAE_Crashworthiness_Finite_Element_Analysis.pdf [Accessed 1 20].

Bell, C. 2018. THOR-50M Frontal Impact ATD.

Boddy, R. & Smith, G. 2009. *Statistical methods in practice: for scientists and technologists*, John Wiley & Sons.

Briers, D. 2012. *Difference Between Compact Bone and Spongy Bone Simplified* [Online]. Available: http://www.dbriers.com/tutorials/2012/12/difference-between-compact-bone-and-spongy-bone-simplified/ [Accessed].

Carter, P. M., Flannagan, C. A., Reed, M. P., Cunningham, R. M. & Rupp, J. D. 2014. Comparing the effects of age, BMI and gender on severe injury (AIS 3+) in motor-vehicle crashes. *Accident Analysis & Prevention,* 72**,** 146-160.

Centre, S. M. 2012. *The new SEAT Leon – the car for the heart and the head* [Online]. Available: http://seat-mediacenter.com/en-content/static-content/model-range/seat-leon-2/seat-leon/press-kit-2/the-new-seat-leon-the-car-for-the-heart-and-the-head?backUrl=%2F%2Fen-content%2Fproc%3Flocale%3Den_HQ%26nav%3D1%26tag%255BTopics%255D%3D2%26tag%255BBasic%2BInformation%255D%3DALL%26formats%3DFORMATS_ALL%26timescale%3DPAST_TIME_178 [Accessed 20/08 2017].

Chakravarthy, B., Lotfipour, S. & Vaca, F. E. 2007. Pedestrian injuries: emergency care considerations. *Western Journal of Emergency Medicine,* 8.

Christensen, J. 2012. Introduction to Finite Element Method Theory and Application.

Combs, D. 1995. Dorland's Illustrated Medical Dictionary. *Journal of Family Practice,* 40**,** 191-192.

Crandall, J. R., Bhalla, K. S. & Madeley, N. 2002. Designing road vehicles for pedestrian protection. *BMJ: British Medical Journal,* 324**,** 1145.

Degarmo, E. P., Black, J. T., Kohser, R. A. & Klamecki, B. E. 1997. *Materials and process in manufacturing*, Prentice Hall.

Deng, Z. 2014. *Injury Evaluation and Examples* [Online]. Available: http://wenku.baidu.com/link?url=-

0l6mtqMlfzUCimf2jk9QwoAmT1vl2f0IL_ROndUtoNs37CBYHG3jVTKqTPTe23jP563ya000iC0kOWdNn9n1yDNHGjTPgl4WlzRrLyoGx3 [Accessed].

Department of Mechanical Engineering–Engineering Mechanics 2018. John O. Hallquist. *Department of Mechanical Engineering–Engineering Mechanics.*

Dynamore 2016. Human Model. DYNAmore.

EuroNCAP 2011. Test result of MERCEDES-BENZ B-class.

EuroNCAP 2012a. SEAT Leon 1.6TDI 'Reference', LHD, Test Results.

EuroNCAP 2012b. Test result of RENAULT Clio.

EuroNCAP 2013. Toyota Corolla, 1.6 Mid grade, LHD Test Results. 2.

EuroNCAP 2015. Pedestrian Testing Protocol.

EuroNCAP 2019. *Vulnerable Road User (VRU) Protection* [Online]. Available: https://www.euroncap.com/en/vehicle-safety/the-ratings-explained/vulnerable-road-user-vru-protection/ [Accessed].

EuroNCAP Nov 2017. European New Car Assessment Programm Pedestrian Testing Protocol Version 8.4.

EuroNCAP November 2017. European New Car Assessment Programm.

European Union 2018. European Commission - Fact Sheet: 2017 road safety statistics.

Frankel, V. H. & Burstein, A. H. 1970. *Orthopaedic biomechanics: the application of engineering to the musculoskeletal system*, Lea & Febiger Philadelphia.

Gayzik, F. S., Moreno, D. P., Vavalle, N. A., Rhyne, A. C. & Stitzel, J. D. Development of the global human body models consortium mid-sized male full body model. International Workshop on Human Subjects for Biomechanical Research, 2011.

Got, C., Patel, A., Fayon, A., Tarriere, C. & Walfisch, G. 1978. Results of experimental head impacts on cadavers: the various data obtained and their relations to some measured physical parameters. SAE Technical Paper.

Harris, J. Proposals for test methods to evaluate pedestrian protection for cars. Proceedings: International Technical Conference on the Enhanced Safety of Vehicles, 1993. National Highway Traffic Safety Administration, 293-302.

Hayes, W. C., Erickson, M. S. & Power, E. D. 2007. Forensic injury biomechanics. *Annu. Rev. Biomed. Eng.,* 9**,** 55-86.

Hodgson, V. R. & Thomas, L. M. 1972. Effect of long-duration impact on head. SAE Technical Paper.

Huang, S., Yang, J. & Eklund, F. 2006. Analysis of car-pedestrian impact scenarios for the evaluation of a pedestrian sensor system based on the accident data from Sweden. *Bundesanstalt für Straßenwesen. Die Reihe,* 136.

Humanetics Innovative Solutions 2016. History of Crash Test Dummies. Humanetics Innovative Solutions.

Insurance Institute for Highway Safety and Highway Loss Data Institute. 2018. *Pedestrians and bicyclists* [Online]. Available: https://www.iihs.org/iihs/topics/t/pedestrians-and-bicyclists/fatalityfacts/pedestrians [Accessed].

John Combest, J.-T. W. 2016. Status of The Global Human Body Models Consortirm. Washington, DC, US.

Kimpara, H. & Iwamoto, M. Mild Brain Injury Predictors Derived From Dummy 6DOF Motions. 40th International Workshop on Human Subjects for Biomechanical Research, 2012.

Kroell, C. K., Schneider, D. C. & Nahum, A. M. 1971. Impact Tolerance and Response of the Human Thorax. SAE International.

Kroell, C. K., Schneider, D. C. & Nahum, A. M. 1974. Impact Tolerance and Response of the Human Thorax II. SAE International.

Kuehn, M., Froeming, R. & Schindler, V. 2005. An advanced testing procedure for pedestrian-car collisions. *International journal of vehicle safety,* 1**,** 85-99.

Kurczewski, N. 2011. *Smarter Crash Test Dummies* [Online]. Available: https://www.roadandtrack.com/car-culture/a16755/smarter-crash-test-dummies/ [Accessed].

Lau, I. V. & Viano, D. C. 1986. The viscous criterion-bases and applications of an injury severity index for soft tissues. SAE Technical Paper.

Lawrence, G. & Hardy, B. Pedestrian safety testing using the EEVC pedestrian impactors. 16th ESV Conference, 1998.

Livermore Software Technology Corporation. 2011. *Total Human Model for Safety - THUMS* [Online]. Livermore Software Technology Corporation. Available: http://www.lstc.com/thums [Accessed].

Lobdell, T., Kroell, C., Schneider, D., Hering, W. & Nahum, A. 1973. Impact response of the human thorax. *Human Impact Response.* Springer.

Marcello Cammarata , F. N., Mario Di Paola , Antonino Valenza , Giovanni & Zummo 2016. Mechanical behavior of human bones with different

saturation levels.

Marjoux, D., Baumgartner, D., Deck, C. & Willinger, R. 2008. Head injury prediction capability of the HIC, HIP, SIMon and ULP criteria. *Accident Analysis & Prevention,* 40**,** 1135-1148.

Mchenry, B. G. 2004. Head injury criterion and the ATB. *ATB Users' group***,** 5-8.

Melvin, J., Stalnaker, R. L., Roberts, V. & Trollope, M. 1973. Impact injury mechanisms in abdominal organs. SAE Technical Paper.

Mertz, H. J., Prasad, P. & Irwin, A. L. 1997. Injury risk curves for children and adults in frontal and rear collisions. SAE Technical Paper.

Mertz, H. J., Prasad, P. & Nusholtz, G. 1996. Head injury risk assessment for forehead impacts. SAE Technical Paper.

Nahum, A. M., Schneider, D. C. & Kroell, C. K. 1975. Cadaver skeletal response to blunt thoracic impact. SAE Technical Paper.

Ncepod 2006a. The Coroner's Autopsy: Do we deserve better?

Ncepod 2006b. The Coroner's Autopsy: Do we deserve better?(A report of the National Confi dential Enquiry into Patient Outcome and Death (2006)).

Neal-Sturgess, C. 2010. The Entropy of Morbidity Trauma and Mortality. *arXiv preprint arXiv:1008.3695*.

Neal-Sturgess, C., Carter, E., Hardy, R., Cuerden, R., Guerra, L. & Yang, J. 2007. APROSYS European in-depth pedestrian database. *Age,* 91**,** 95.

Neal-Sturgess, C. E. 2001. A Thermomechanical Theory of Impact Trauma.

Neal-Sturgess, C. E., Hassan, A. & Cuerden, R. The relationship of AIS to peak virtual power. Annu Proc Assoc Adv Automot Med, 2001. 141-157.

Newman, J. A. & Shewchenko, N. 2000. A proposed new biomechanical head injury assessment function-the maximum power index. SAE Technical Paper.

Niels Lynnerup, J. G. A., Birgitte Sejrsenbio 2005. Thickness of the human cranial diploe in relation to age, sex and general body build.

Samaha, R. R. & Elliott, D. S. NHTSA side impact research: motivation for upgraded test procedures. Eighteenth International Technical Conference on the Enhanced Safety of Vehicles, Paper, 2003.

Schmitt, K.-U., Niederer, P. F., Muser, M. H. & Walz, F. 2013. *Trauma biomechanics: Introduction to accidental injury*, Springer Science & Business Media.

Schmitt, K.-U., Zürich, P. F. N. E., Muser, M. H. & Walz, F. 2009. *Trauma Biomechanics: Accidental injury in traffic and sports*, Springer Science & Business Media.

Shanahan, D. F. 2004. Human tolerance and crash survivability. *Pathological Aspects and Associate Biodynamics in Aircraft Accident Investigation*.

Shaw, J. M., Herriott, R. G., Mcfadden, J. D., Donnelly, B. R. & Bolte, J. H. 2006. Oblique and lateral impact response of the PMHS thorax. SAE Technical Paper.

Sievert, W. 2000. European New Car Assessment Programme (Euro NCAP). *Berichte der Bundesanstalt für Straßenwesen*.

Stürtz, G. 1984. Global-und Komponentenversuche zur Fußgängersicherheit. *Forschungsvereinigung Automobiltechnik eV (FAT) No,* 22.

Takhounts, E. G., Craig, M. J., Moorhouse, K., Mcfadden, J. & Hasija, V. 2013. Development of brain injury criteria (BrIC). SAE Technical Paper.

Takhounts, E. G., Hasija, V., Ridella, S. A., Rowson, S. & Duma, S. M. Kinematic rotational brain injury criterion (BRIC). Proceedings of the 22nd enhanced safety of vehicles Conference. Paper, 2011. 1-10.

Tass International. 2016. *MADYMO Product Suite* [Online]. Available: https://www.tassinternational.com/madymo [Accessed 01-11-2016 2016].

The American Association for the Surgery of Trauma. 2018. *Injury Scoring Scale* [Online]. Available: http://www.aast.org/Library/TraumaTools/InjuryScoringScales.aspx#heart [Accessed].

The Automobile Association. 2016. *Euro NCAP's tests: The tests behind the new car safety ratings* [Online]. Available: http://www.theaa.com/motoring_advice/euroncap/crash_tests.html [Accessed 02-11-2016 2016].

Tomil. 2007. *Toyota Corolla AE100 Sedan* [Online]. Available: http://www.smcars.net/threads/toyota-corolla-ae100-sedan-1992-95.25294/ [Accessed 19/08/2017 2017].

Tomoyuki , M. & Junji , H. 2011. Development of An Finite Element Model of The Total Human Model for Safety and Application to Car-Pedestrian Impacts.

Toyota. 2013. *Corolla Axio specs in Japan* [Online]. Available: http://toyota.jp/corollaaxio/ [Accessed 20/08 2017].

Toyota Motor Corporation 2011. Documentation of Total Human Model for Safety (THUMS_AM50_V4AC_Document).

Transport for London 2004. Making London a walkable city.

Transport for London 2010. Pedestrian Sfaety Action Plan.

Trauma.Org. 2016. *Injury Severity Score* [Online]. Available: http://www.trauma.org/archive/scores/iss.html [Accessed].

Ulman, M. & Stalnaker, R. Evaluation of the AIS as a measure of probability of death. 1986 International IRCOBI Conference on Biomechanics of Impacts, 1986. 2-4.

United Nations 2012. Uniform provisions concerning the approval of motor vehicles with regard to their pedestrian safety performance.
United Nations January 2013. Regulation No. 127

Uniform provisions concerning the approval of motor

vehicles with regard to their pedestrian safety performance.
United Nations Economic Commission for Europe 2016. Consolidated Resolution on the Construction of Vehicles (R.E.3) ECE/TRANS/WP.29/78/Rev.4.
Unknown. *Plastics. Ceramic masses and sitalls* [Online]. Available: http://intranet.tdmu.edu.ua/data/kafedra/internal/stomat_ortop/classes_stud/en/stomat/ptn/Propaedeutics%20of%20orthopedic%20stomatology/2/08.%20Plastics.%20Ceramic%20masses%20and%20sitalls..htm [Accessed].
Viano, D. 1978. Thoracic injury potential. *Proc. 6th International Research Council on the Biomechanics of Impact***,** 142-156.
Vlack, V. 1959. *Elements Of Material Science And Engineering, 6/E*, Pearson Education India.
Walder, A., Yeoman, P. & Turnbull, A. 1995. The abbreviated injury scale as a predictor of outcome of severe head injury. *Intensive care medicine,* 21**,** 606-609.
Ward, C., Chan, M. & Nahum, A. 1980. Intracranial pressure–a brain injury criterion. SAE Technical Paper.
World Health Organisation 2015. Global Status Report on Road Safety 2015.
World Health Organization 2018. Global status report on road safety 2018.
Yamada, H. & Evans, F. G. 1970. *Strength of biological materials,* Baltimore,, Williams & Wilkins.

Appendix I Stability and Sensitivity of THUMS Pedestrian Model and its Trauma Response to a Real Life Accident

Lianjie Wen[1], Christophe Bastien[1], Michael Blundell[1], Clive Neal-Sturgess[1], Kambiz Kayvantash[2]

[1] Coventry University

Faculty of engineering and Computing

Coventry, CV1 5FB, UK

[2] CADLM

43 Rue de Saule Trapu

91300 Massy, France

1 Introduction

With dramatically rapid development of computing and modelling technology, occupant and pedestrian safety models went through the development of crash test dummies and multi-body mathematical dynamic modelling to finite element pedestrian human model (THUMS 4.0). THUMS 4.0 is a state of art human model which includes a skeleton structure, as well as internal organs and soft tissues, which makes it a suitable candidate to analyze accident trauma.

The THUMS model has been correlated at the limbs level [1], as well as successfully validated against rigid impactor tests, in frontal [1][2], lateral and oblique [3]. Nevertheless, the responses capture during these tests were overall force-displacement characteristics, not at the trauma and injury level [1][3], consequently more research is needed to investigate whether human models are accurate enough and adequate to capture trauma injury levels.

The THUMS human model is based on finite element analysis and the injury threshold levels are captured using a plastic strain tensor and only a kinematics computation was undertaken as a mean of validating the model [1]. Little to no research has documented trauma correlation to real-life accidents, but only the kinematics [4] using accident data from the APROSYS database [5]. The APROSYS relates to pedestrian and cyclists fatalities and is limited in the detail photographic evidence on

the damage vehicle and the deceased [5], as well as a computation of the thrown away distances and objective measurements of the accident scene. Consequently, Coventry University has approached UK Police Force (UKPF) in order to access best in class accident data, used in criminal courts, in order to investigate the accuracy and adequateness of the THUM human model.

This paper investigates the stability of the THUMS pedestrian model in different impact scenarios, as well as performing an initial injury response comparison against a real-life pedestrian collision which occurred in Coventry (UK). The study will use a dataset of a fatal accident which has been recorded by UK Police Force (UKPF) and will focus on the ability for the THUMS model to relate to the pedestrian injury and trauma autopsy results.

2 THUMS Model Stability and Sensitivity

2.1 Stability

The purpose of this section is to investigate whether the THUMS model is stable against a vehicle impact when its position is changed from centreline. In order to investigate this, a generic sedan model was chosen (Toyota Yaris [6]), travelling at the legal limit of a European city of 30km/h and setup to collide with a pedestrian.

Three positions were selected including:

- the exact centre in front of vehicle – scenario 1
- 45 degree rotated back to vehicle and aligned with the centre of the vehicle – scenario 2
- 45-degree rotated back to vehicle and aligned with the outside edge of the vehicle – scenario 3

The Toyota Yaris model was validated against a frontal crash test and comprises of deformable structure and non-linear material properties card. The scenarios studied included a vertical gravity filled in the vertical Z direction and a ground defined as a

planar **`*RIGIDWALL`** to provide a non-deformable surface used to position the vehicle and the pedestrian (Fig.1:).

Fig.1: Simulation scenarios used in stability check. Scenario 1 (Left), Scenario 2 (Middle), scenario 3 (Right)

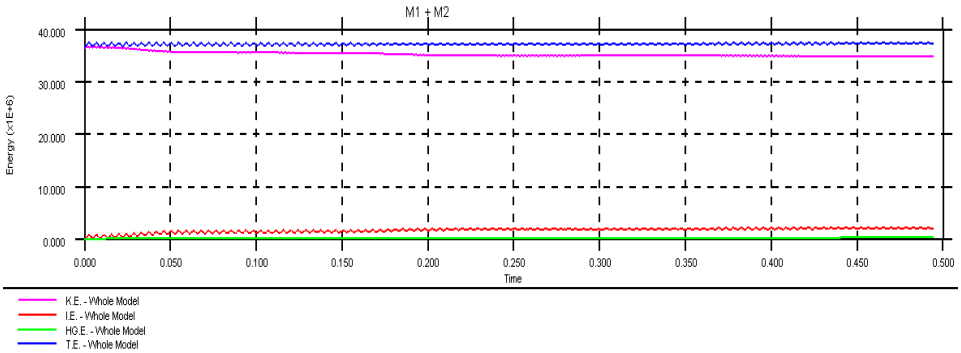

Fig.2: Typical energy curves reposnses for all the 3 models

Looking at Fig.2: it can be noted that the total energy stays stable, which relates to a conservative system. The small oscillations in the total Energy relate to the Toyota Yaris‘ tyre contacting and interacting with the **`rigidwall`**, and the drop of kinetic energy to the change of vehicle speed when the pedestrain is impacted.

In head impact location of each scenario is depicted in Fig.3:

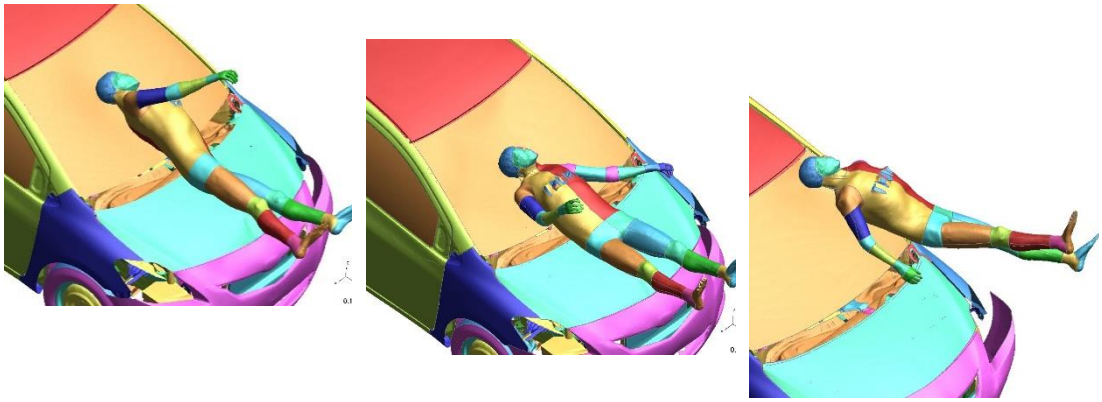

Fig.3: Head to vehicle contact zone. Scenario 1 (Left), Scenario 2 (Middle), scenario 3 (Right)

It can be concluded from this section that for a European city impact speed (30km/h), the THUMS human model is numerically stable.

2.2 Kinematics and Sensitivity of THUMS Pedestrian Model

In order to capture the kinematics sensitivity of the THUMS human model, 3 contacts were generated including pedestrian to bumper, pedestrian to bonnet and pedestrian to windscreen interactions, as well as 1 node output located on the cranial bone (node 87000222).

Two new simulations based on scenario 1, previously studied, were performed to investigate the kinematics and sensitivity of pedestrian model, including 2 offset scenarios of ±100mm from the centre of the vehicle, as depicted in Fig.4:. The value on 100mm was chosen to minimise the effect of the bumper, bonnet and windscreen geometrical curvatures and stiffness changes.

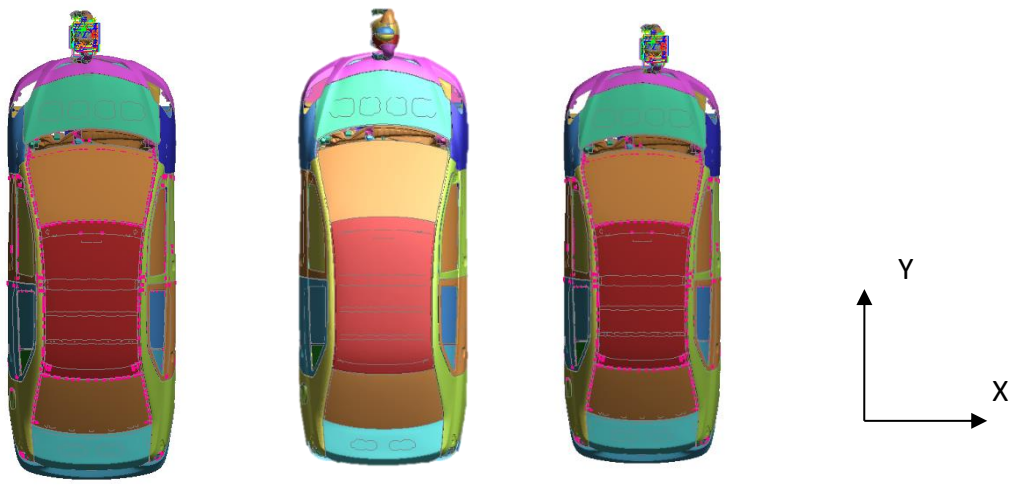

Fig.4: Sensitivity study (-100mm Left, centre and +100mm Right)

The head kinematics have generally the same trend until impact, which takes place around 180ms to 190ms (Fig.5:).

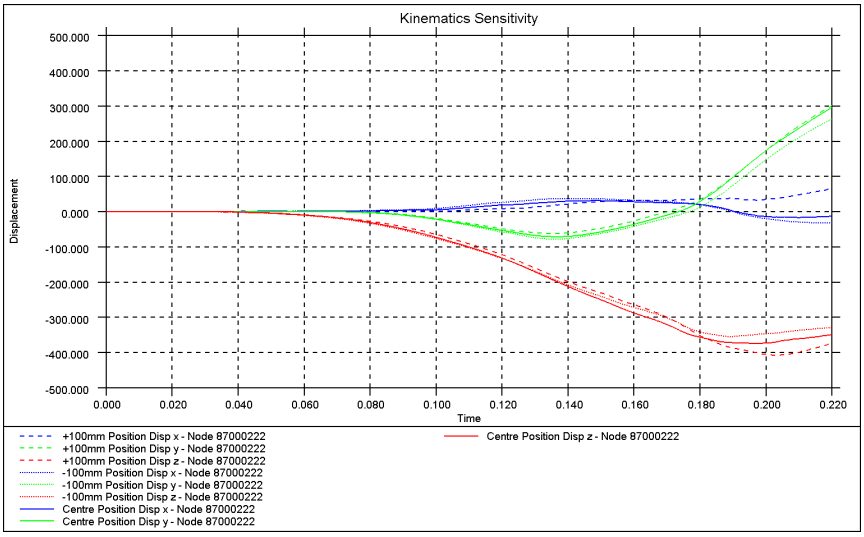

Fig.5: Displacement of node 87000222 (cranial bone in all 3 scenarios)

It can be noted from Fig.5: that the head displacement along and across the vehicle is consistent for the 3 models and start to diverge from 0.2s, which is the time of head contact to the windscreen. Looking at the X axis, which is across the vehicle, it can be noticed that the head, when the pedestrian is at rest and hit sideways, travels along the direction of the vehicle which minor lateral excursions.

Looking at Fig.6:, the pedestrian presents however different overall body kinematics. Visible changes can be observed early in the impact at around 0.06s. This change

seems to initiate a change of kinematics at the very beginning of the impact and initiate a body rotation which can be observed observing the legs motion (Fig.6:).

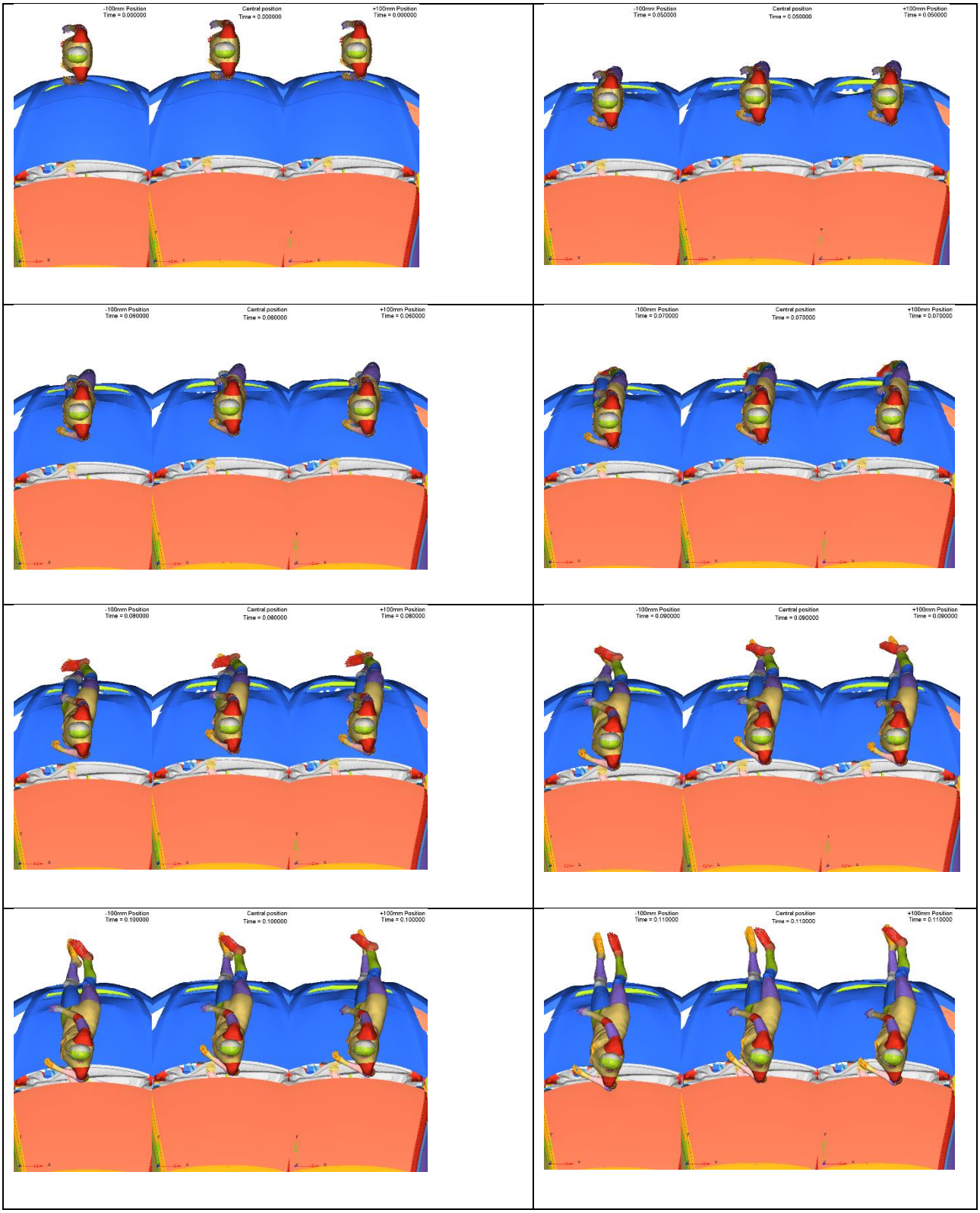

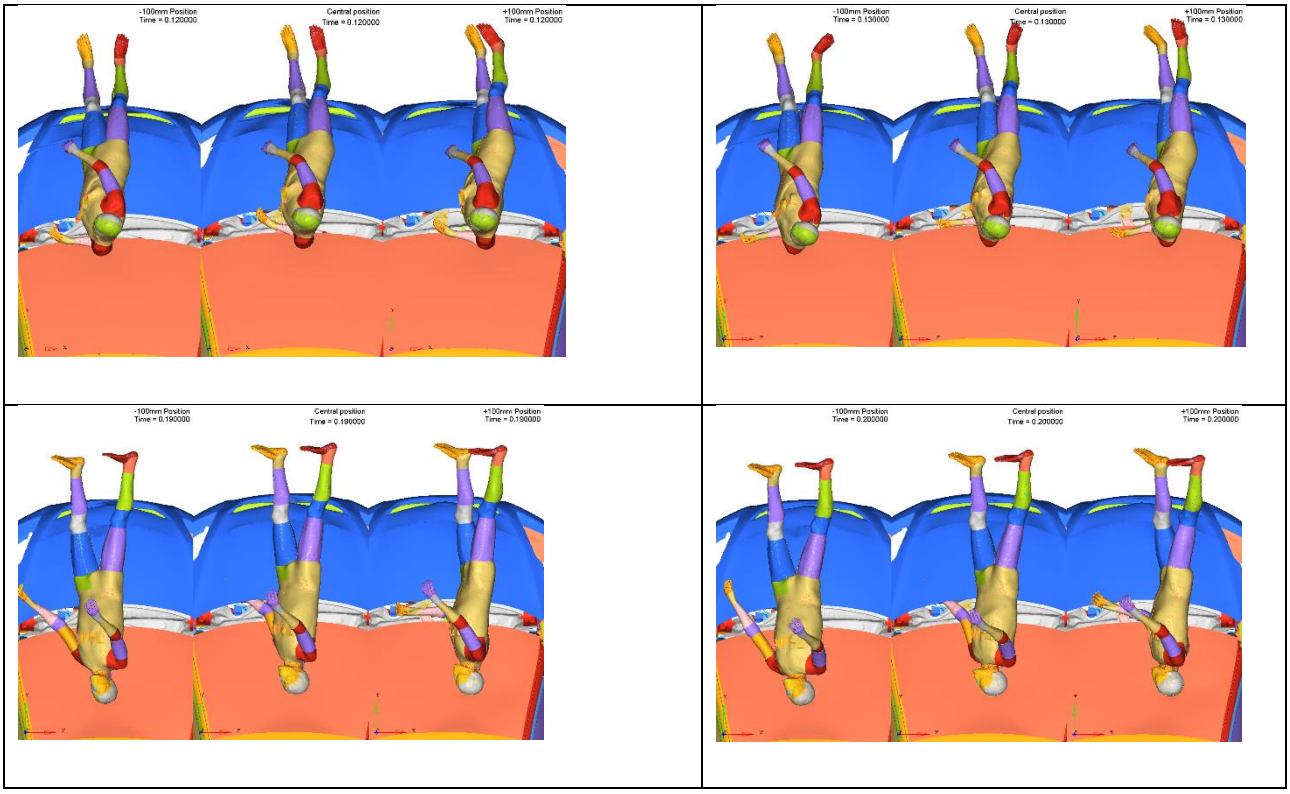

Fig.6: Sensitivity study – pedestrain kinematics (focus on early human body rotation). (-100mm Left, centre and +100mm Right)

It can be noted that the contact force between on the bumper and the pedestrian varies between the three simulations (Fig.7:), especially at time 0.03s, looking at the pedestrian to bumper impact and the bonnet edge contacts curves. At time 0.03s, the contact force drops, which means that there is a local structure collapse (Fig.8:), then the force is transferred to the bonnet. The difference in force magnitude at 0.03s between the +100mm and the two other position is 1kN.

In each run, all the computer parameters are the same except the pedestrian starting X position across the vehicle. As the offset is small (100mm), the overall vehicle stiffness change of the vehicle is likely to be minimal, consequently local collapse must have generated this force change. It is suggest that early impact events have created this body rotation.

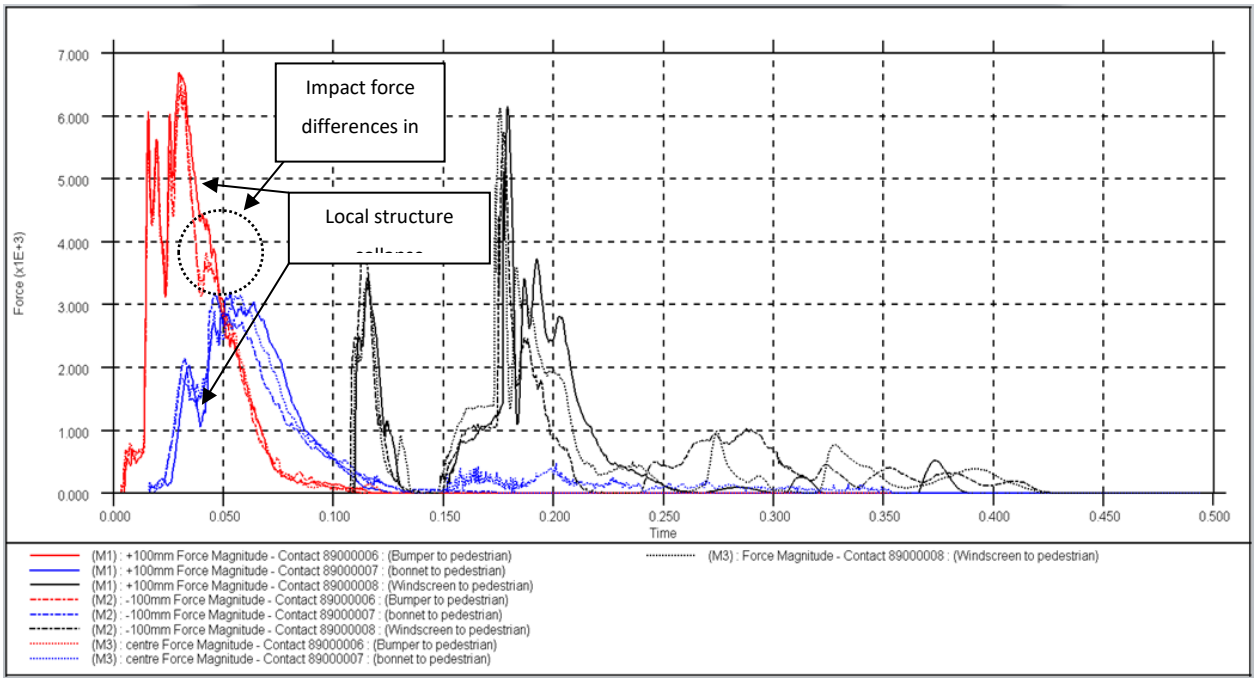

Fig.7: Contact forces against time curve of all 3 simulations

Considering Fig.6: it can be noted at the moment of head impact (time 0.19s) the head position relative to the windcsreen is different. For the case of -100mm, where the head impacts more at the back of the skull compared to the 2 other loadcases where the head in both cases impact the windscreen at the lobe. Based on these three runs and pending more detailed studies, it appears that the head final angle position to the windscreen is affected by the bumper local force magnitude and pattern.

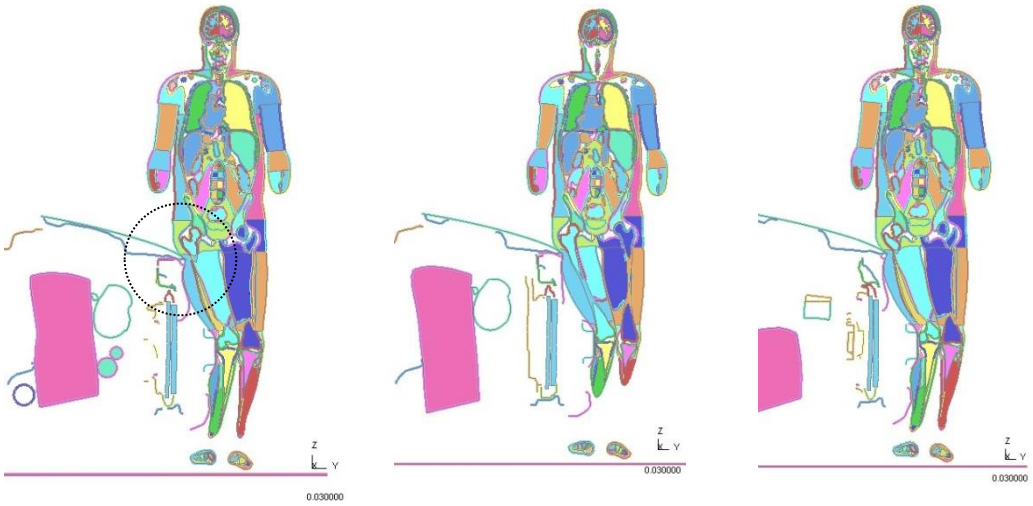

Fig.8: Focus on bumper collapse. Cross section through strcuture and pedestrian (-100mm Left, centre and +100mm Right)

As a summary, from the initial study undertaken in this paper, it is observed that the THUMS model is sensitive to the impact location (±100mm in centreline) as well as the local vehicle collapse. It is suggested that pedestrian body rotations are generated early in the first 0.05s. It is observed that the head linear motion is marginally affected and does not excurse across the vehicle when a static pedestrian impacts the vehicle centreline side on. Until this sensitivity is studied performing cadaver tests in a similar setup, it is not possible to affirm whether this sensitivity is numerical or physical.

3 Trauma Comparison against a Real-Life accident

This section investigates the capabilities of the THUMS human model to relate its trauma output to a pedestrian autopsy. From the UK Police Force (UKPF) accident database (Collision reference CV/1267/14J), a real world accident was selected, involving a sedan vehicle in a UK city environment. The pedestrian involved a 183cm tall elderly Caucasian male, weighing 61kg, who was impacted by a Seat Leon about the vehicle centerline (Fig.9:). The vehicle is a right hand drive.

The left side of vehicle windscreen was totally chattered and the front grid was partly broken.

Fig.9: Vehicle damage at the accident scene

The first contact point was the leading edge of the bumper and the marks on the bonnet revealed the position of impact. These marks are about 104mm offset from centreline of vehicle. These evidences can be observed from Fig.9:, as the bonnet is damaged in the said recorded areas.

From the witness statements, the pedestrian was in motion when he was hit. The pedestrian was elderly, hence its walking speed crossing the road has been assumed in the report to be 0.9m/s [8]. Observing the windscreen impact in Fig.9:, it can be seen that the location of the dent on the bonnet and the impact on the windscreen do not have the same distance from the bonnet centreline, proving that the pedestrian was in motion.

There is no shoe scuff mark to the road surface, consequently it was not possible to exactly establish an exact location of impact between the pedestrian and the collision vehicle on the carriageway. Therefore, throwaway distance was measured using the first shard of glass from the main debris field and the casualty's centre of mass (best practice dictates that a person's centre of mass is measured from around the navel area, which is 55% of the over-all height). Before first police investigator arrived, emergency services were present. In order to negate false measurement, main glass debris field clustered around the end of the bus stop was used to take throw away measurement as opposed to individual fragments of glass which could have adhered to footwear (Fig.10:).

Consequently, the throw-away distance was estimated to 28m approximately (*s*), as depicted in Fig.10:.

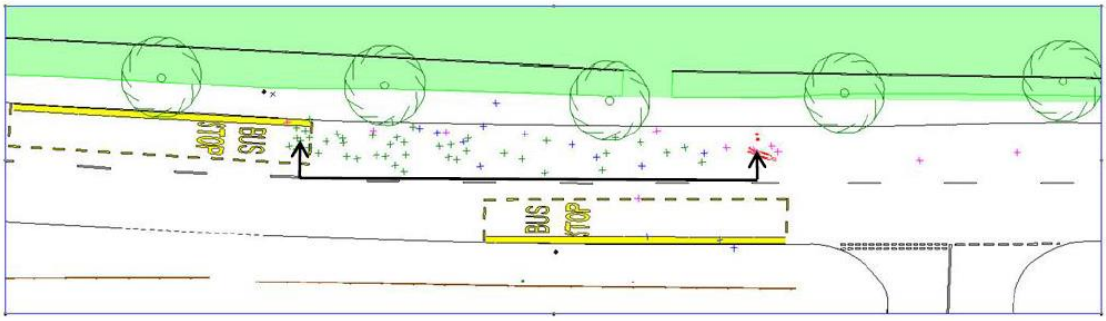

Fig.10: Measurement of pedestrian throw-away distance

During the site visit, the coefficient of friction (μ) has been measured to 0.7; consequently, it is possible to evaluate the vehicle impact speed [7] the based on μ, the throw distance *s* and g (9.81m/s^2), as per Table 1:

$Vmin = \sqrt{\frac{2\mu gs}{1+\mu^2}}$	$Vmax = \sqrt{\mu^2 + 2\mu gs}$
16.07 m/s (57.9km/h)	19.61 m/s (70.6km/h)

Table 1: Minimum and maximum vehicle impact speeds calculated from the throw distance and road surface condition

Consequently, it can be noted that, unless video evidence of the impact is obtained, it is very difficult to ascertain the exact throwaway distance and vehicle impact speed.

If the throw away distance is 28m and the vehicle travelling at 19.61m/s , then the approximate timing for the body to come at rest would be around 1.4s, which is currently out-of the reach of most computers, because of the runtime duration (computing 0.2s takes on Coventry University's hardware (160 cores per run) 24h). Consequently, should the throw distance be correlated, the current THUMS model should be able to do it, but to date it is not practical.

In the autopsy results, it was stated that the impacted leg was the right one, which is not logical, as the vehicle was on the left-hand side of the pedestrian vehicle before impact. Consequently, the left leg had to be hit first. As the pedestrian was in motion, it is suggested that his left leg was not touching the floor and was momentarily not load bearing. Consequently, the left leg must have been impacted first, but as no bearing load was present at the time, no damage was observed. As the weight was on the right leg, the impact force was therefore transmitted, causing injuries to this limbs (as recorded in the autopsy).

As the final stance was not exactly know, as a pre-study, the THUMS model was set with the legs side by side.

4 Analysis

The THUMS pedestrian model was impacted according to the accident report. It has been noticed that at European city Centre speeds (30km/h), the THUMS model was very stable.

At higher speeds, it was observed that the lower leg was numerically sensitive, and caused some instability in the computation.

The area of concern was located in the knee tendons. During a high speed impact, the tendons are stretching excessively and are suggesting that the femur would separate from the tibia and meniscus (Fig.11:).

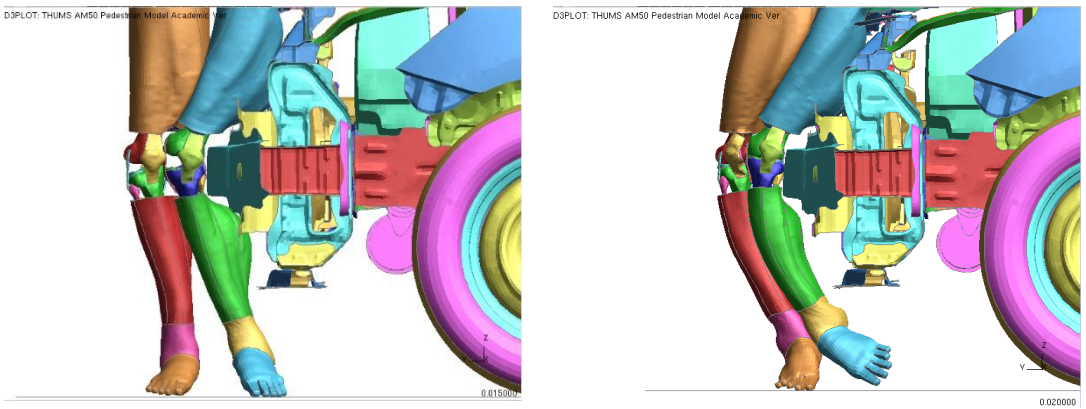

Fig.11: Femur separation from tibia and meniscus - original (Left) - after tendon material modifications (Right)

From the base THUMS model, means of stabilizing the knee area (negative volumes) included:

- Changing element formulation of the tendons from ‘1’ to ‘2’ and ‘10’
- Changing the hourglass control to stiffen the tendons
- Adding Eroding values to the tendon the material card to 10%
- Adding a CONTROL_SOLID switch to remove solids with negative volumes
- Changing the knee flesh element formulation from ‘13’ to ‘10’.

None of these changes gave the necessary stability in the knee area for such impact speeds. It has been observed that the THUMS 4.01 model does not contain any failure criterion in this knee area and maybe some improvements would be required to provide more stability to over-stretched solid elements.

As the autopsy only referred to a tibia and fibula fracture and not tibia separation from the femur, it has been assumed that the knee was intact. Consequently, the tendon material properties were altered from a ***SIMPLIFIED_MAT_RUBBER** to a simple ***MAT_ELASTIC** material card including a stiff Young’s Modulus to keep the leg together, hence ensuring a stable computation (Fig.11:).

The following results have included the modified tendon material properties described above and the contact forces are recorded (Fig.12:).

Comparing the bumper force levels from 30km/h to 57.9km/h and 70.6km/h, it can be noted that the contact force has risen from 6kN to 27kN and 32kN. This is therefore understandable that such impact forces could cause instabilities, as the impact speeds and therefore impact energy (squared on the velocity) is considerably higher, i.e. a minimum of 4 times from 30km/h.

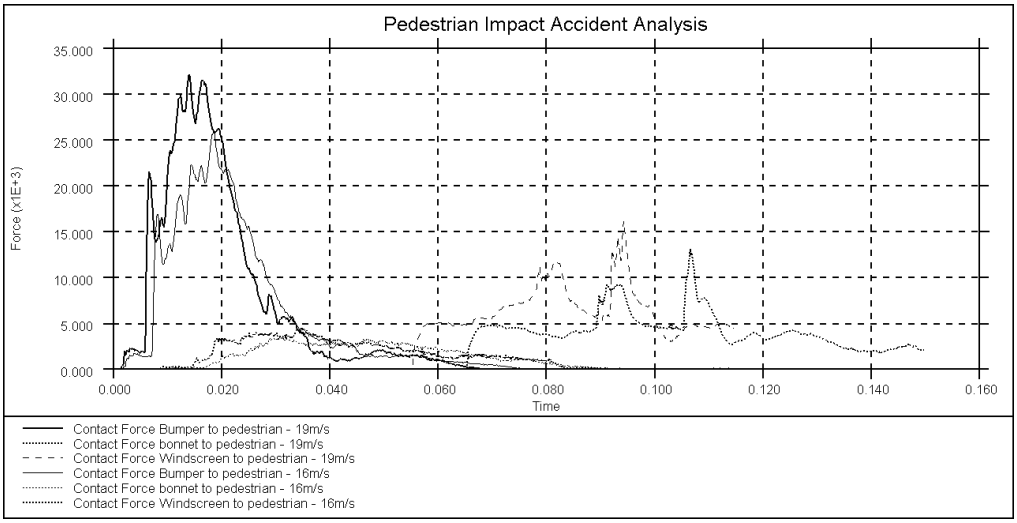

Fig.12: Pedestrian Impact Accident Analysis

The same conclusion can be drawn in the head contact force, which is doubled for both extreme accident speeds compared to a 30km European city impact.

5 Results

5.1 Pedestrian Kinematics.

The final pedestrian kinematics and vehicle damage are depicted in Fig.13:. Comparing the computer simulation vehicle damage to the vehicle bonnet dent on impact scene (Fig.9:), it can be noticed that the bonnet deformed shape is more representative of a 16m/s pedestrian impact, as the bonnet centre and edge's deformation look similar to the photo evidence.

Also, in the photo (Fig.9:), the bumper cover is still connected to the fender, hence also relates more to a 16m/s than a 19m/s impact.

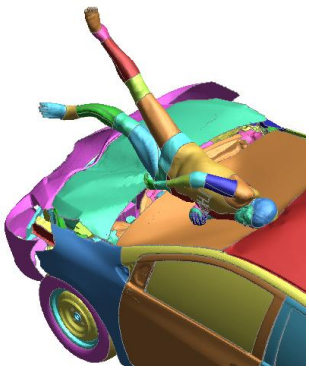

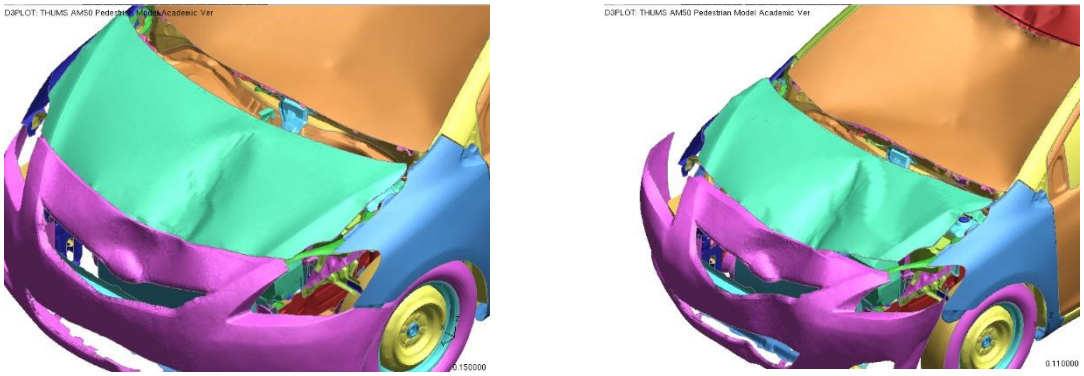

Fig.13: Pedestrian kinematics: 16m/s (Top Left), 19m/s (Top Right) and Vehicle Damage: 19m/s (Bottom Left), 19m/s (Bottom Right)

It can be observed that, in both velocity cases, the pedestrian head impacts the higher section of the windscreen. Considering the photo evidence in Fig.14:, it can be noticed that the impact is more outboard than in both simulations, suggesting that the pedestrian walking speed may have been higher than in the report.

Fig.14: Focus on the windscreen area (impact area more outboard than CAE model)

In the CAE models, the windscreen is damaged in 2 areas: lower third (elbow and shoulder) and upper (head), as depicted in Fig.13:. The Material definition of the windscreen in the Toyota Yaris model used [6], is based on a **`MAT_123: MODIFIED_PIECEWISE_LINEAR_PLASTICITY`** with no failure stress threshold set. Considering that the initial winsdcreen impact force ranges from 5kN to 10kN (Fig.12:), it is likely that the windscreen would have shattered and would have altered the final head impact locations.

The pedestrian trauma injuries relating to the lowest and highest impact velocities are now going to be extracted following different body region and will be assessed against the THUMS trauma criteria threshold [1]:

- Head and Neck
- Skeletal
- Internal Organ

5.2 Head and neck areas

5.2.1 Superficial head area

- Speed 16m/s

It can be observed that there are high strain areas in the left neck area. Lesions at the level of the lobes in temporal, frontal and occipital areas with lower strains on the right-hand side of the neck.

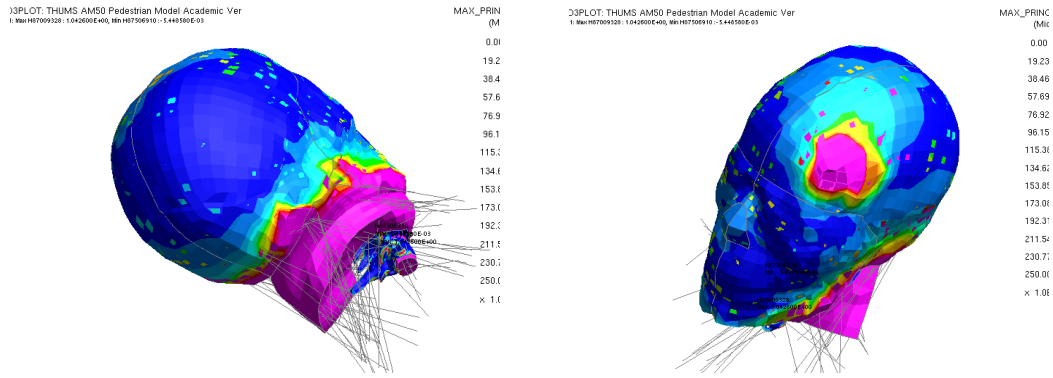

Fig.15: Posterior (Left) and Lateral view (Right) of head and neck at 16m/s

It can be observed an important risk of lesions around the neck, of the forehead left area. The locartion of these injuries relate to the autopsy report. i.e “abrasion the frontal forehead to the left of the midline and measuring 9x8cm“.

- Speed 19m/s

It can be observed that there is a high risk of lesions around the front left side of the neck with a higher area strain value higher than at 16m/s at the frontal lobe.

The abrasion area seems to relate more to the autopsy than at 16m/s.

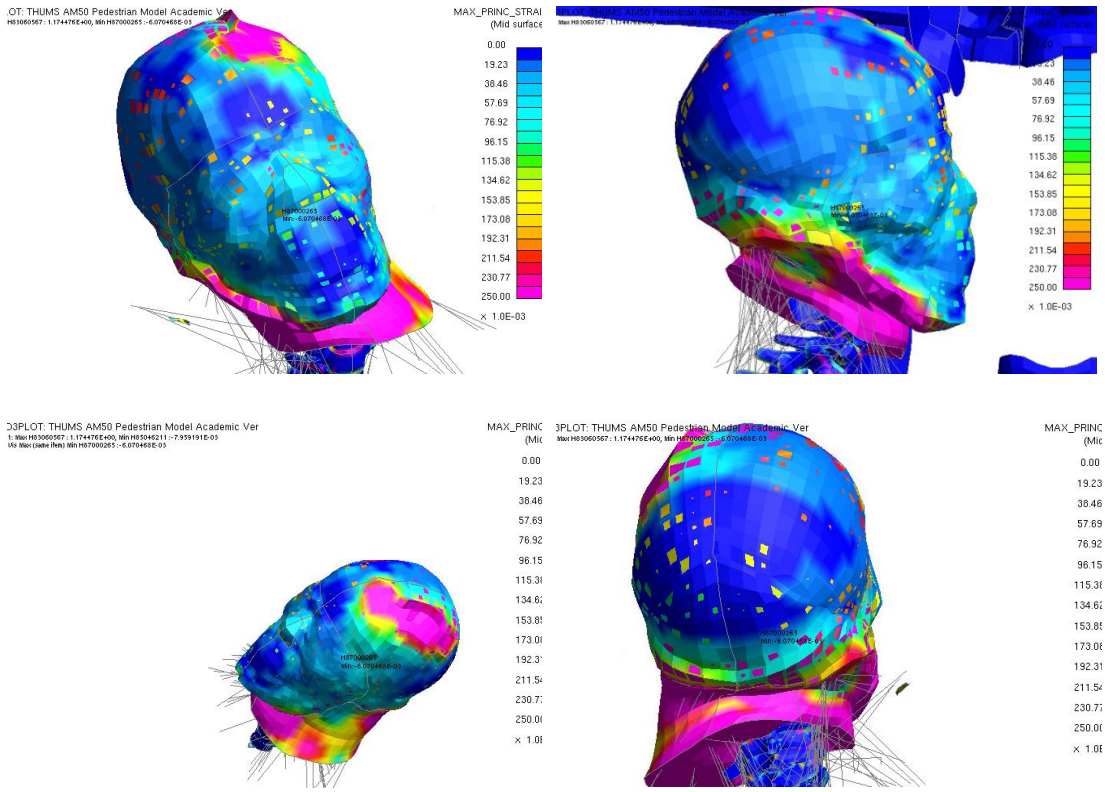

Fig.16: Frontal (Top left), lateral right (Top right), lateral left (bottom right) and posterior of head at 19m/s

The autopsy has concluded that there were massive right side abrasions with lacerations on supra-orbital ridge, nose bridge, forehead and scalp, however these have not shown in the computation. As the primary impact is on the left hand side of the pedestrian, it is proposed that these injuries have been sustained during the second phase of the impact, i.e. the contact against the road

The high strain area at the posterior region of the head is caused by the luxation of the shoulder, which is contacting the skull (Fig.17:), just below the ear at the level of the right temporal lobe. This computed event could have caused skull fracture, however it has not been mentioned in the autopsy.

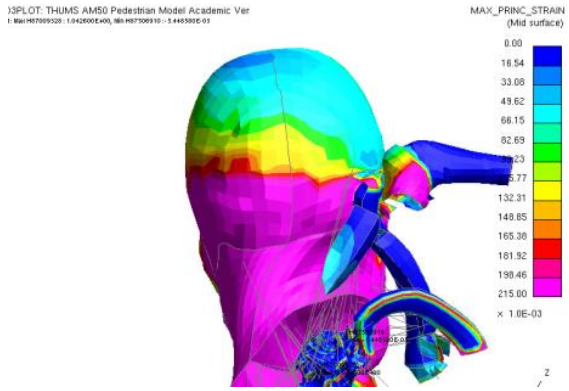

Fig.17: Shoulder luxation contacting the right temporal lobe

5.2.2 Intra Cranial Injuries (not referenced in the autopsy)

This area has not been referenced in the autopsy report, however some evidence computed by the THUMS model are referring to Diffuse Axon Injuries (DAI). At 16m/s the risks of DAI would have been high. The risk of DAI at 19m/s would have been certain considering the brain strain values, as depicted in Fig.18:.

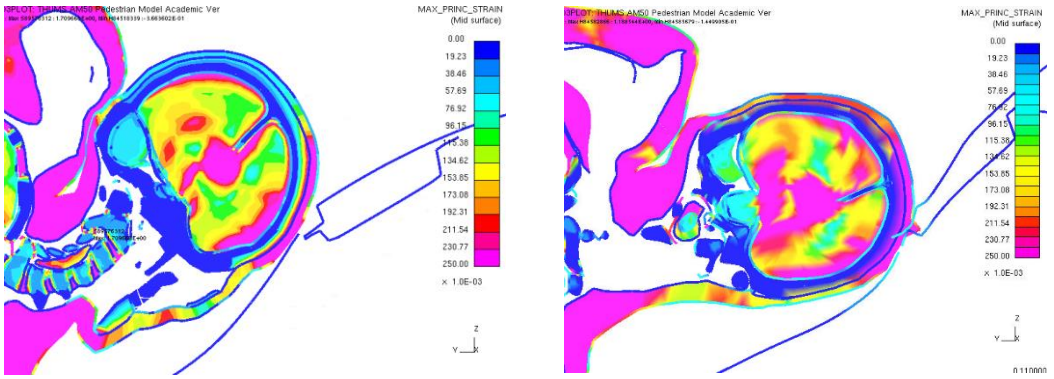

Fig.18: THUMS head cross section. DAI recorded by THUMS – 16m/s (Left), 19m/s (Right)

It can also be observed that the strain the grey matter of the brain is higher in the left hand side of the occupant's head as it is the orientation of it simpact against the windscreen, as depicted in (Fig.19:). This is more pronounced at 19m/s, where the strain is greater than 21.5% (Fig.19:).

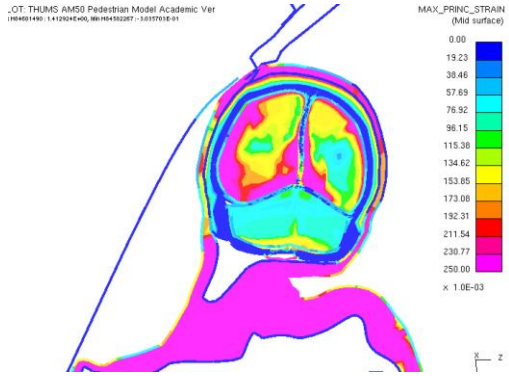

Fig.19: Head Posterior view. Strain maximum in head impacted area (19m/s)

5.2.3 Neck area: (not referenced in the autopsy)

The neck area has not been referenced in the autopsy report, however some evidence computed by the THUMS model are referring to a misalignment of the cervical vertebrae due to the impact of the head against the windscreen, which leads to all the following vertabrae to crush against each other. The reason that it may not have been captured in the autopsy may be because the windscreen chattered, hence reducing the load on the head compare to the current computer model which is less forgiving, as discussed previously.

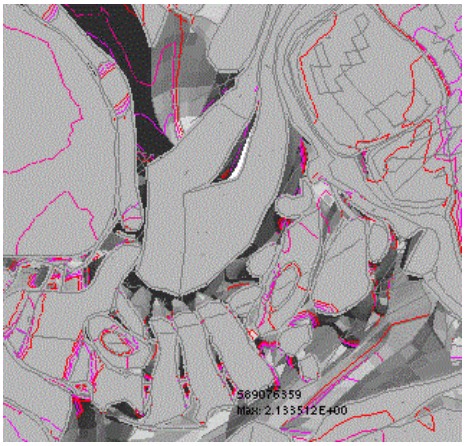

Fig.20: Cross section of the head and neck area showing vertebrae mode of compression

5.3 Skeletal

The autopsy report referred to the following trauma:

- Compound fracture through the distal aspect of the right tibia and fibia
- Transverse fracture which appeared unstable through 9th thoracic vertebrae

- Fractures to posterior and anterior aspects of the left 1st to 12th ribs
- Fractures to the anterior aspect of the right 1st and 9th ribs
- Fracture of the left clavicle
- Multiple fracture of the pelvis

Considering the pelvis area, it can be noticed that there is a high level of strains in the hip and pelvis areas. At 16m/s, strains are observed in the pelvis area, however these are less at 19m/s, where fractures are suggested, as per the autopsy (Fig.21:).

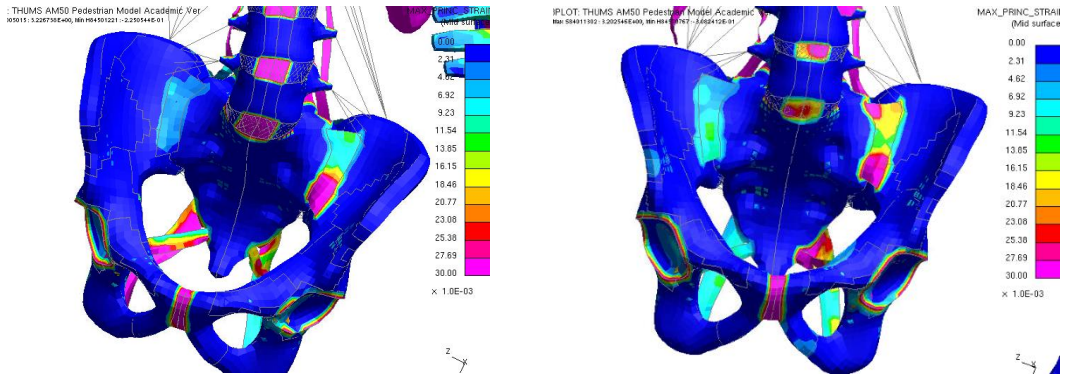

Fig.21: Comparison of pelvis strains. 16m/s (Left) and 19m/s (Right)

Focussing on the knee area, it can also be noted that the right knee at 16m/s contains high level of strains but not enough to suggest fracture. Conveniently, at 19m/s, there is a clear fracture of the tibia and fibia, as the autopsy suggests (Fig.22:).

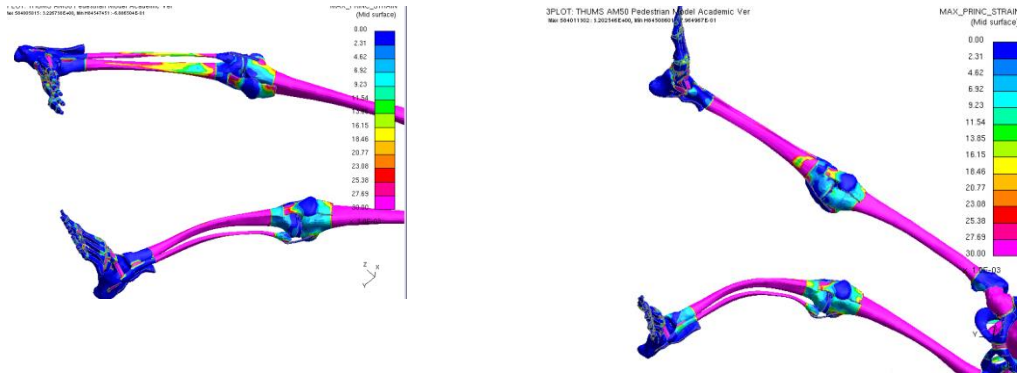

Fig.22: Comparison of tibia and fibia strains. 16m/s (Left) and 19m/s (Right)

It can be noted in Fig.22: that the left knee has been damaged on the THUMS model. In the autopsy results, it was stated that the impacted leg was the right one. As the

pedestrian was in motion, it is suggested that his left leg was not touching the floor and did not bear any load. The left knee fractures seen in Fig.22: are a consequence of the initial model posture assumption and consequntly should be ignored. It can be noted that in both speed cases, the THUMS predicts a femur fracture, which has not been observed in the autopsy.

For the case of the clavicles, in both speeds, the left clavicle is fractured, as depicted in Fig.23: from the autopsy report, however it is not clear where the clavicle is broken. For 16m/s, it is suggested from the strain plots that both ends are damaged, as per the autopsy.

At 19m/s the strain values are less than for the lower speed, which maybe be caused by the fact that the pedestrian landed differently on the bonnet giving a different loading in the clavicle area. These values do not suggest fracture.

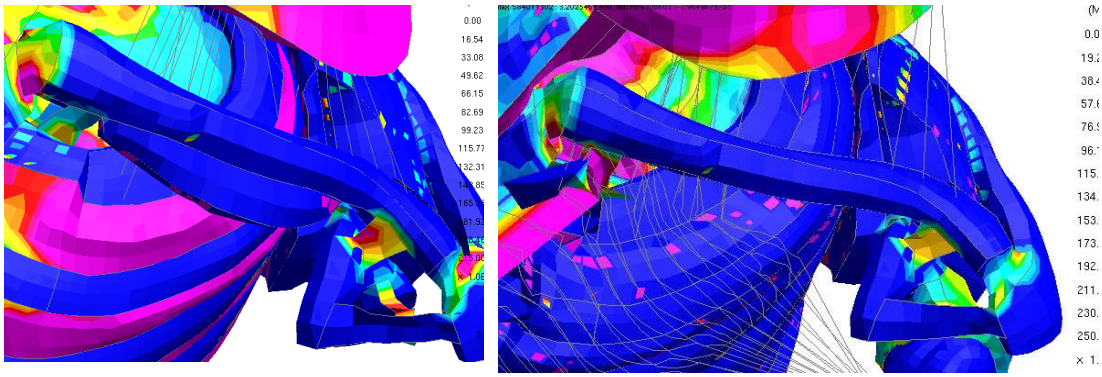

Fig.23: Clavicle fracture. 16m/s (Left), 19m/s (Right)

Considering the ribs, it can be observed that for both speeds, there is a risk of fracture of ribs 1 to 12 in the anterior area, with more important strains for 19m/s. In the posterior area, it can be seen that the 3rd to the 8th rib are likely to fracture at 19m/s (similar to the autopsy), while for 16m/s the damage would be focused mainly on the 8th rib (Fig.24:).

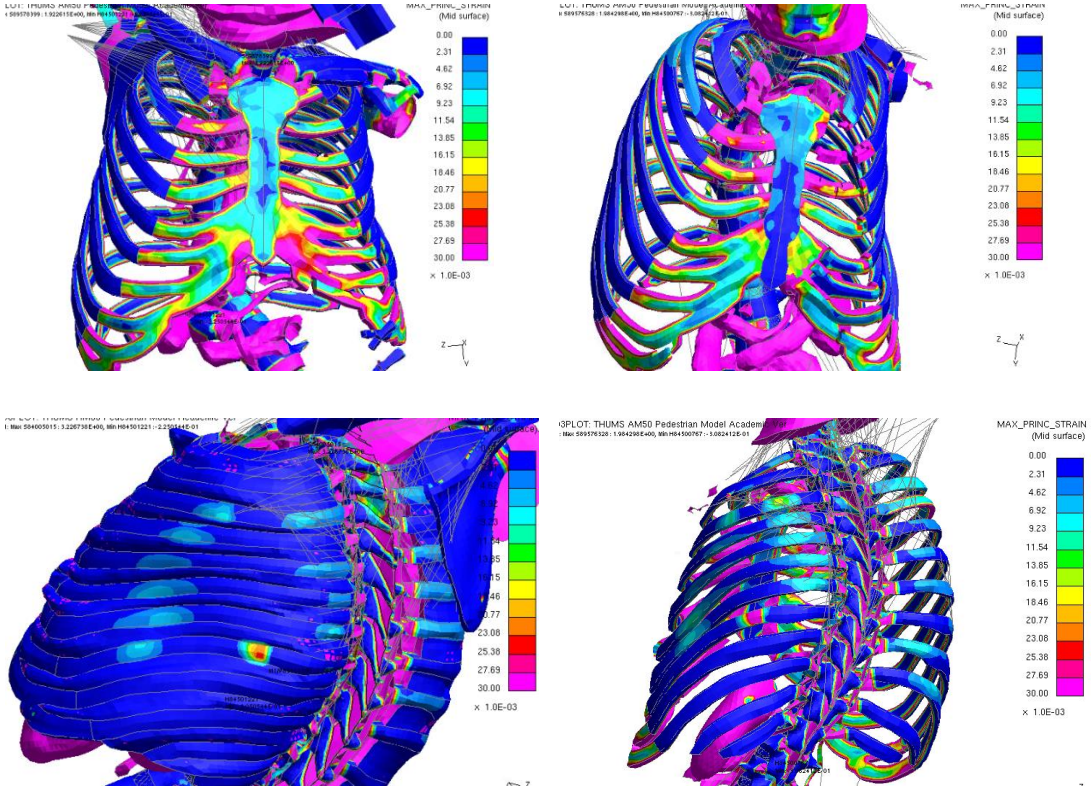

Fig.24: Comparison of rib risk fracture. 16m/s anterior (top left), lateral (bottom left) and 19m/s anterior (top right), lateral (bottom right)

5.4 Internal Organs

The THUMS model is able to output trauma values, which can be compared to the autopsy results [1].

Considering the heart, both speeds refer to local strains, however do not manage to capture the fact that the pericardial cavity is ruptured in the autopsy (Fig.25:).

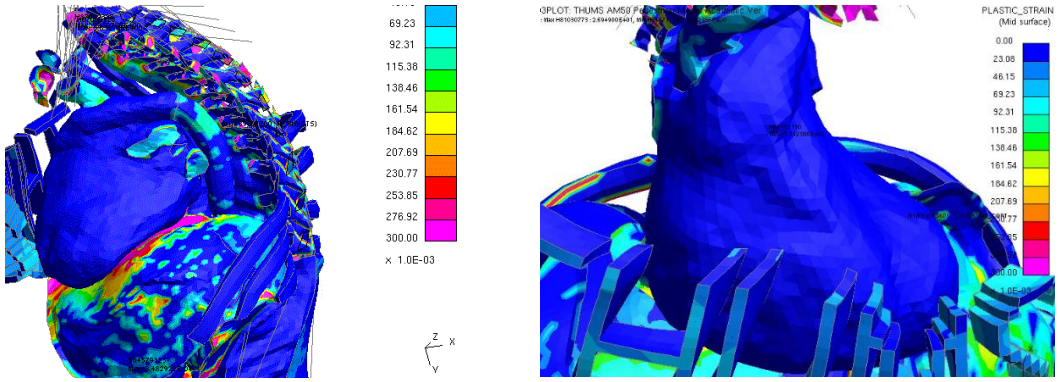

Fig.25: Strains in heart area. 16m/s (Left) and 19m/s (Right).

Concerning the gastro-intestinal system, the autopsy stated that “the liver showed obvious rupture over the anterior surface. There was rupture of the spleen“. The Uro-Genital system section of the autopsy related to “perinephric haemorrhage around both kidneys“

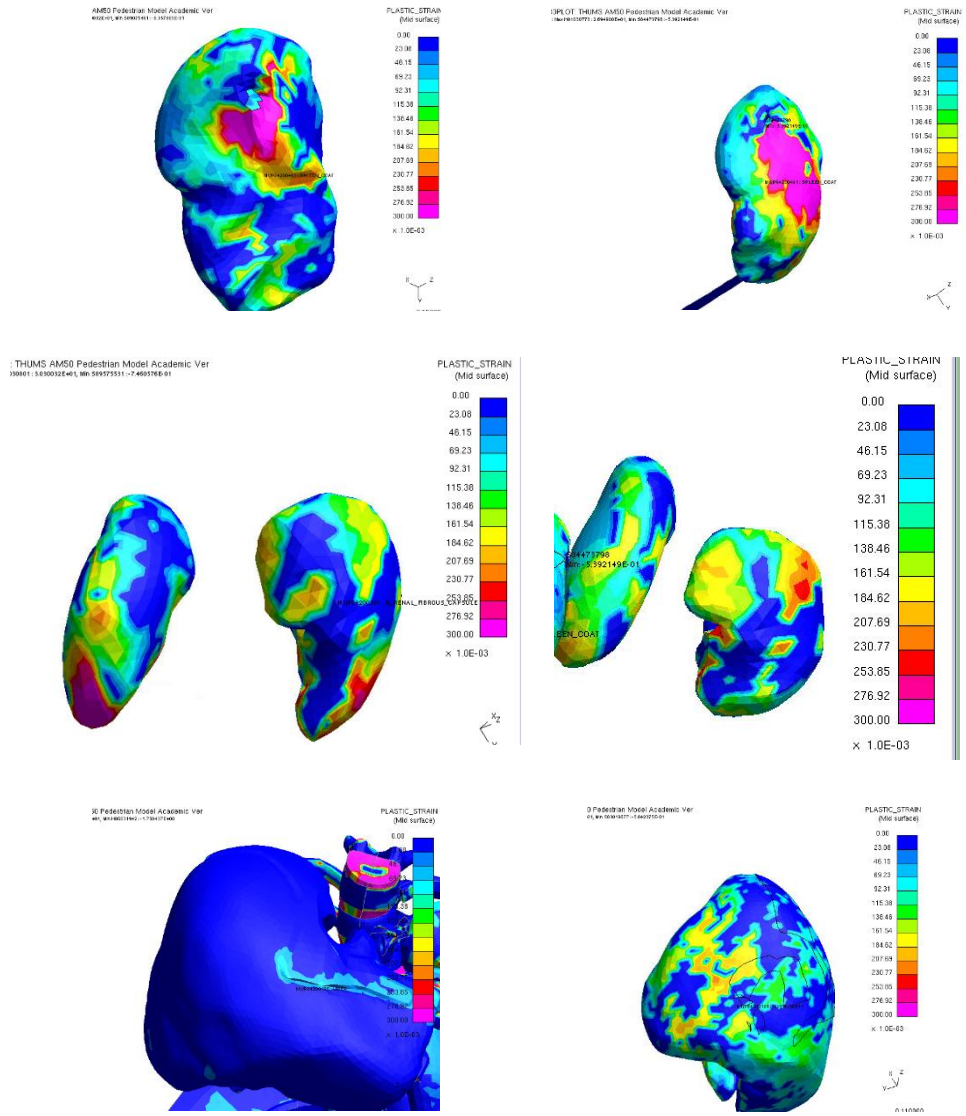

Fig.26: Strain in spleen (Top),kidneys (Middle) and liver (Bottom). 16m/s (Left) and 19m/s (Right).

Considering Fig.26:, it can be noted that at both speeds the strain values in the kidney exceed 30%. The area affected at 19m/s is larger and relates more to the autopsy results. For the spleen, there are strain levels for both speeds (again matching with the autopsy), however higher strain levels are observed at 19m/s. It can be noted that

no damage to the liver can be observed at 16m/s, while at 19m/s, the plastic strain value reached 18%, which is close to the 21% to confirm trauma.

6 Discussion

The study has shown that the computed pedestrian head end positions look different, because no failure criteria in the windscreen have been set in the standard Toyota Yaris computer model [6]. Consequently, in order to replicate the final head impact location, this windscreen feature would need to be implemented in future studies. Two areas have been highlighted by the THUMS model, referring to the neck area and the connection between the grey matter and the skull (DAI), but not in the autopsy. It is believed that this is caused by the fact that the computer model's windscreen does not numerically fail on impact, hence causing artificial forces in the head which is then compressing the vertebrae (Fig.20:). Consequently, the THUMS trauma outcome and the autopsy results diverge in the neck area. Overall, the THUMS model was able to compute trauma values to internal organs (liver, kidney and spleen) successfully matching the area referenced in the autopsy, especially at 19m/s. Heart damage was not correctly captured for either speed. The THUMS predictions were also promising in the ribs area, where comparable damage was observed at 19m/s in a comparable area. The clavicle damage was observed in the autopsy, but only well captured by the 16m/s impact, while marginal fracture was predicted for a 19m/s pedestrian impact.

There was a level of interpretation in the leg positions and the likelihood of which leg would have bared the initial body weight just before the impact. Nevertheless the trauma of the right leg accident outcome matched the autopsy results for 19m/s. Knowing, from the initial sensitivity study discussed in this paper that the primary leg impact to bumper has significant effect on the pedestrian body rotation, it is suggested that more left leg position variations need to be investigated to capture a wider range of kinematics and trauma outcomes to ascertain the initial pedestrian stance prior to impact.

It was also suggested that the pedestrian walking speed may have been faster than in the report. This can be observed by the impact offset from the bonnet contact area which is less pronounced in the CAE model which is using and

***INITIAL_VELOCITY_GENERATION** command setting the pedestrian walking pace at 0.9m/s. It has to be considered, however, that the victim was 8cm taller and 14kg lighter than the THUMS model used. Future studies would require personalizing the human computer model to represent the victim with more accuracy to ensure that mass distributions are representative; hence provide a more accurate kinematics and walking speed estimation.

The study has shown in detail the difficulties to evaluate the throw distance at the accident site and that, without video evidence, it is very difficult to be certain of the final distance. The throwaway distance has not been computed in this analysis because of the excessive runtime needed. This step in the future would be necessary, as other trauma injuries were recorded on the right hand side of the pedestrian and could only have been generated by a secondary impact, i.e. falling on the road (scalp bruising in head right area as well as to the right wrist and thumb). There does not seem to be an obvious solution to this computational challenge, as traumatology requires detailed meshes injury predictions, consequently long computation times.

The CAE computations have suggested that the impact speed was more likely to be 16m/s than at 19m/s. The bonnet damage looks comparable between the analysis and the photo evidence. It has to be noted that the vehicle model used was of the same type (Sedan), but not the same (Toyota Yaris vs. Seat Leon), consequently some uncertainties in the structural deformation may be present, but to date not quantifiable. It has to be noted that no exact scans of the damaged bonnet deformation were available to the authors to assess whether the depth of the dent, i.e. related to the impact energy, was comparable with the computer model. In this paper, the damage assessment is only visual. Deformation data would have been an adequate mean to assess whether the bonnets stiffness were comparable between the Toyota Yaris and the Seat Leon and perform any necessary structural adjustments. Scanning the damaged vehicle at the accident scene would certainly help towards answering this important information, which would be needed to fine-tune the accident reconstruction case.

Considering the trauma output from THUMS, it is suggested that the vehicle impact speed to be nearer 19m/s than 16m/s, which is in contradiction with the finding based on the vehicle bonnet damage. Consequently, considering the limitations of this study, it can be suggested that there is no apparent link between pedestrian trauma, vehicle speed and vehicle visual damage. More detail data input will be needed to refine the study and confirm this statement, like the potential bonnet structural differences. It has to be observed however that based on the findings of this paper; the range of vehicle impact speed calculated in the UK Police Force (UKPF) report is realistic.

7 Conclusions

The THUMS model has been tested against a 30km/h pedestrian impact scenario against a typical sedan vehicle, including different postures. The THUMS model proved to be stable at this speed. It has been observed that the kinematics of a pedestrian human model is sensitive at the early impact stage in the bumper area, as localized impact pattern responses dictate the body rotation during the accident.

The paper has shown that the knee area is numerically sensitive and would require some improvements to allow the model to compute with much higher impact speeds (16m/s to 19m/s). After local modification of the knee ligament material definition, the THUMS model has shown to be very stable and provide some useful trauma information, which in some area related to the autopsy report provided by UK Police Force (UKPF). The THUMS organ trauma (liver, spleen and kidney) results gave a good correlation with the autopsy, as well with the right leg fracture, ribs fracture and head lesions. These trauma injuries were commonly observed at 19m/s (all at 19m/s). It has been observed that the modelling of windscreen shattering is necessary as artificial neck load, computed by THUMS, were not present in the autopsy report in both speed impact scenarios. Overall, the THUMS traumas output against the autopsy were adequate and sometimes differed from the postmortem report because of uncertainties in pedestrian walking speed, bonnet stiffness and windscreen material modelling properties. More research would be needed to reduce these uncertainties, as well as studying other pedestrian accidents, to provide a complete and objective status on the validation the THUMS pedestrian model.

8 Acknowledgments

The authors would like to thank the UK Police Force for their support and for providing the accident data presented in this publication.

The authors are also grateful for the support provided by Yacine Diagne (Université de Reims) for her expertise in biomechanics, as well as Liliana Cowlan (ARUP) and Amit Prem (Coventry University) for their advice on model stability.

References

[1] THUMS, Total Human Model for Safety, AM50 Pedestrian Model. Academic Version 4.0_20111003, October 2011, Toyota Motor Corporation

[2] Charles K. Kroell, D. C. S. A. M. N., 1974. Impact Tolerance and Response of the Human Thorax II.

[3] Joshua M. Shaw, R. G. H. J. D. M. B. R. D. J. H. B., 2006. Oblique and Lateral Impact Response of the PMHS Thorax. *Stapp Car Crash Journal,* pp. 147-167.

[4] AsPeCSS, EU funded project. http://www.aspecss-project.eu/

[5] APROSYS, EU funded project. http://cordis.europa.eu/result/rcn/47920_en.html

[6] NCAC vehicle database, http://www.ncac.gwu.edu/vml/models.html

[7] Searle J: The Trajectories of Pedestrians, Motorcycles, Motorcyclists etc. Following a Road Accident SAE 831 622 (2007)

[8] Asher et al: Most older pedestrians are unable to cross the road in time; a cross-sectional study (2012)

Appendix II A Deterministic Method to Calculate the AIS Trauma Score from a Finite Element Organ Trauma Model (OTM)

C. Bastien*, C. Neal-Sturgess**, J. Christensen*, L. Wen*

*Institute for Transport and Cities, Coventry University, Priory Street, Coventry, CV1 5FB, UK
** University of Birmingham, School of Mechanical Engineering, Edgbaston, Birmingham, B15 2TT, UK

Abstract: Traumatic injuries are measured using the Abbreviated Injury Scale (AIS), which is a risk to life scale. New human computer models use stresses and strains to evaluate whether serious or fatal injuries are reached, unfortunately these tensors bear no direct relation to AIS. This paper proposes to overcome this deficiency and suggests a unique Organ Trauma Model (OTM) able to calculate the risk to life based on the severity on any organ injury, focussing on real-life pedestrian accidents. The OTM uses a power method, named Peak Virtual Power (PVP), and calculates the risk to life of brain white and grey matters as a function of impact direction and impact speed. The OTM firstly calibrates PVP against the medical critical AIS threshold observed in each part of the head as a function of speed. This base PVP critical trauma function is then scaled and banded across all AIS levels using the confirmed property that AIS and the probability of death is statistically and numerically a cubic one. The OTM model has been tested against four real-life pedestrian accidents and proven to be able to predict pedestrian head trauma severity. In some cases, the method did however under-estimate the head trauma by 1 AIS level, because of post-impact haemorrhage which cannot be captured with the employed Lagrangian Finite Element (FE) solver. It is also shown that the location of the injury predictions using PVP coincide with the post mortem reports and are different to the predictions made using maximum principal strain.

Keywords: Pedestrian trauma, head trauma, Peak Virtual Power (PVP), Abbreviated Injury Scale (AIS), Organ Trauma Model, OTM

1.0 Introduction

1.1 State of the Art injury indicators

Automotive Manufacturers design vehicles against legislative and consumer test protocols using crash test dummies with the purpose of creating safer vehicles for occupants and pedestrians. In spite of all their efforts, the number of fatalities keeps on increasing worldwide year by year [1], reaching 1.35 million in 2018. There are many parameters which can be attributed to this increase of death toll such as age, gender, speeding, etc., however, the steady rise in numbers begs the question whether the design tools currently used in the design process namely crash test dummies, are adequate to reverse this trend. Crash test dummies are anthropometric mechanical systems which can capture displacements, accelerations and forces, but do not contain internal organs. During the vehicle design process, dummies output information during the crash event which is cross-correlated to a probability of threat to life, based on injury severity. This trauma injury severity has been defined by medical professionals who have suggested a trauma injury scale or the Abbreviated Injury Scale (AIS). The AIS is an anatomically based, consensus derived, global severity scoring system that classifies each injury by body region according to its relative importance (threat to life) on a 6-point ordinal scale [2]. The latest revision of the AIS scale, which dates to 2015 [3], provides a standardised terminology to describe injuries and ranks injuries by severity. AIS is

internationally accepted and is the primary tool to conclude injury severity [2]. From an engineering perspective, injury can be estimated using engineering indicators based on injury criteria. Currently, injury indicators can be classified into two major categories: kinematics-based indicators, used in crash test dummies; and strain-based indicators, when using a human computer model.

The first category relates to kinematics-based criteria which describe the kinematic behavior of a structure. However, such criteria, for example the Head Injury Criterion (HIC), cannot be used to describe the material response during impact [4]. The second category relates to human computer models, like THUMS [6] [11][12], which contain internal organs. In this case, plastic strains are used as the criterion in bone fracture and principal strain is often used in organ injury studies. In the case of the THUMS human model [6][11][12] plastic strain criteria is used to evaluate the maximum AIS, with the following threshold listed in Table 38.

Tissue/Organ	Currently-used injury measurement	Injury description	AIS
Brain grey matter	Maximum 30% principal strain	Brain contusion	3-4
Brain white matter	21% maximum principal strain	Diffuse Axonal Injury (DAI)	4
Heart	30% maximum principal strain	Rupture	4
Liver	30% maximum principal strain	Rupture	4
Spleen	30% maximum principal strain	Rupture	4
Kidneys	30% maximum principal strain	Rupture	4
Skull	Maximum 3% plastic strain	Fracture	2-3

Table 38 Currently used injury criterion on brain and organs and corresponding AIS level [12]

However, in human body injury, elastic strain decreases when the load is decreasing, whereas plastic strain remains; and on a human body, injury remains although the impact pulse is removed. Therefore, in concept, elastic strain-based indicators are different to human body injury. Also, time effects, or strain rates, are not considered when using strain as an injury indicator. Considering the Eiband injury graphs [7], injuries are linked with impulse duration, hence considering a time dependency factor when computing trauma. Currently (2019), the trauma location cannot be predicted using the strain-based method. As a consequence, it can be concluded that kinematic and strain-based indicators are not realistic metrics to assess trauma injury. Also, when Table 38 is used in trauma assessment, it is not possible to conclude which plastic strain level represents AIS 1, 2, 3, 4 and 5.

Such limitations can be overcome using the Peak Virtual Power method (PVP) which was shown to statistically correlate with trauma observed in real-life accidents [8][9][10]. PVP is an energy-based engineering indicator which was proposed as an injury criteria, and is derived from the rate dependent form of the 2nd law of thermodynamics using the Clausius-Duhem

inequality, considering that irreversible work in a human body is equivalent to injury [8][9][10]. PVP takes the peak value of virtual power which indicates that it is monotonically increasing throughout the time history of an impact (Figure 169), and has been statistically proven to correlate with injury severity, with correlation coefficients (R^2) better than 0.98 [8][9][10], yet it has never been applied in a Finite Element formulation

On organ/tissue level, PVP can be extracted using the formula from Equation 14[8][9][10]:

$$PVP \propto AIS \propto max(\sigma \cdot \dot{\varepsilon})$$

Equation 14: Peak Virtual Power (PVP) formulation

Following Equation 14, PVP is extracted by multiplying the stress σ and the strain rate $\dot{\varepsilon}$ and memorizing the maximum value as the impact event is taking place, as illustrated in Figure 169. Trauma, the maximum value of the PVP, remains present during the duration of the impact and does not reduce when the load is removed.

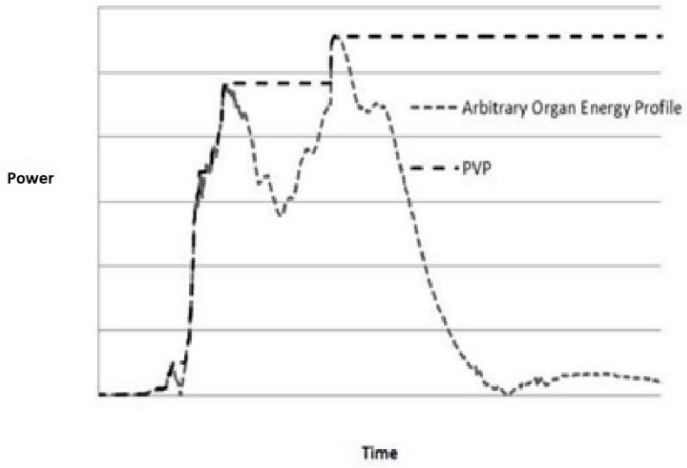

Figure 169: Illustartion of the PVP Concept

In order to extract PVP, several tensor candidates are available and need evaluation:

1. Plastic (stress/strain) component indicates that the stress/strain occurring in the plastic stage of the material when the yield stress is exceeded. This indicator is not adequate, because internal organs/tissues are made of water and collagen which are modelled as incompressible viscoelastic materials [8][9][10]. Under high strain-rate deformation, viscoelastic materials can essentially behave as elastic, which means that when using these material models there is no plastic components available from which to calculate PVP.
2. Principal (stress/strain) is the component acting on the main or principal plane where the shear is zero. Biomechanical injuries are the result of the separation (fracture, shearing, tearing or rupture) of biological tissues, hence ignoring shear components is also not representative.

3. The Von Mises criterion is the vector resultant from maximum shear stress, although it is usually quoted in terms of principal stresses. It is usually used as yield criterion for plastic deformation, taking shear into account.

Consequently, PVP, and therefore the AIS trauma level, can be extracted using the Von Mises vector resultant. The research proposed will answer the question whether trauma injury, extracted using PVP and then coded into an AIS, can be directly and deterministically extracted from a finite element model. The next section will discuss which parameters within the PVP equation affect trauma.

1.2 Physical parameters influencing PVP

When the PVP theory was derived from first principles using the Clausius-Duhem inequality, it was proven to accurately predict trauma against statistical real-life accident scenarios [8][9][10]. The base PVP theory fully correlated with belted and unbelted occupants accident data, and suggested that their respective trauma injury was a function of a cubic for belted and a square of the impact velocity for unbelted occupants, as per Equation 15 and Equation 16 [8][9][10].

$$PVP \propto AIS \propto V^2 \text{ [unbelted occupants]}$$

Equation 15: Relationship between PVP and velocity for unbelted occupants and belted occupants

$$PVP \propto AIS \propto V^3 \text{ [belted occupants]}$$

Equation 16: Relationship between PVP and velocity for belted occupants

In the case of pedestrian accidents (Figure 170), the real-life pedestrian accident data demonstrated that statistically the pedestrian trauma to impact velocity was proportional to the square of the impact speed for slight injuries and to the cubic of the impact speed for serious/ fatal injuries; but for the pedestrian cases no PVP theoretical derivations were successfully achieved to correlate with the real-life accident data.

Figure 170: A typical pedestrian accident – Pedestrian kinematics

This section of the paper will answer two main points:

1. The first point is to understand the parameters which influence PVP, i.e.

trauma injury. As the first derivation of PVP was using Continuum Damage Mechanics thermodynamic principles, another derivation will be here performed to highlight the key variable affecting trauma. This will be relevant later on in the paper.

2. The final point is to derive a theoretical PVP equation to confirm the trauma cubic relationship in the case of pedestrian impact.

During an impact, the kinetic energy of the organ is converted into strain energy, which is highlighted in Equation 17.

Organ kinetic energy = Organ strain energy

Equation 17: Conversion of Energy from Kinetic into strain during the impact

This energy transfer can be written mathematically as Equation 18, where m is the mass of the organ, v the impact speed, E the organ Young's modulus, and σ the von Mises stress.

$$\frac{1}{2}mv^2 = \frac{\sigma^2}{2E}vol$$

Equation 18 Transfer of Energy from Kinetic into strain during the impact (re-formulation)

Using the fact that m=$\rho \cdot vol$ (ρ is the density, 'vol' is the volume of tissue/organ), this leads to Equation 19, which represents the link between stress and velocity.

$$\sigma = \sqrt{\rho E}v$$

Equation 19: Relationship between stress and velocity

Utilising Equation 14 and Equation 19 as well as considering the strain rate $\dot{\varepsilon}$, PVP can be re-written as algebraic transformations illustrated in Equation 20.

$$\dot{\varepsilon} = \frac{v}{L}$$
$$PVP = \frac{1}{L}\sqrt{\rho E}v^2$$

Equation 20: Final Derivation of PVP as a function of geometry and material properties

It can be observed from Equation 20 that PVP depends on the organ material property (E and ρ) and its size/ shape (L). Consequently, it can be concluded that PVP is direction dependant, i.e. that the trauma injury sustained will depend on the impact direction. These statements answer the first point of this paper, which was to capture the parameters influencing trauma injury.

In the case of pedestrian trauma relationship with impact speed, in the case of serious injuries, following the statistical fits for occupants, it can be hypothesised that the impact energy needs to include the pedestrian ride down on the bonnet. Indeed, if the body is in contact with the vehicle for a longer duration, the ride-down needs also to be considered. For the shorter contact times, ride-down can be ignored, because pedestrian and vehicle separate very quickly, so the ride-down does not have any effect. As PVP is power based, it can be assumed that it is proportional to the rate of impact energy, as illustrated in Equation 21.

$$Impact\ Kinetic\ Energy \propto v^2 \rightarrow PVP \propto \frac{v^2}{\Delta t}$$

Equation 21: Effect of ride-down in pedestrian scenarios

Assuming that the pedestrian impact velocity reduces linearly during the impact, its ride-down (S) can be expressed as Equation 22 (Newton second law)

$$S = \frac{v}{2}\Delta t \text{ or } \Delta t = \frac{2S}{v}$$

Equation 22 Vehicle and pedestrian ride down – coupled system (crush distance)

By combining Equation 22 back into Equation 21, it can be shown that in the case of pedestrians, for serious injuries, the relationship between PVP and impact velocity is a cubic (Equation 23), as observed statistically in the real-life accident scenarios. This fact will be used later on in the paper.

$$PVP \propto Kv^3$$

Equation 23 Relationship between PVP and impact velocity in an uncoupled (pedestrian) impact

1.3 Purpose of the research

The proposed research aims at answering the question whether it is possible to extract the injury severity for soft tissue AIS organ injuries directly from the finite element model. The introduction section has highlighted that the trauma level, which can be calculated via PVP, was material, geometry, velocity and impact direction dependent. Using these four characteristics, it is proposed to create corridors of survivability (as a function of impact speed) and to test them against real-life scenarios in order to validate whether the PVP method is suitable to predict the trauma location as well as the trauma severity in a finite element environment. This study will be conducted using pedestrian accidents for which Police accident reports and Post-Mortems (PM) have been made available from the UK Police Force (UKPF). As most pedestrians die of head injuries [5], this paper will focus on defining a mechanical indicator to calculate the risk to life on brain tissues. The proposed research will be conducted in accordance with the Coventry University [17] and the NHS ethics protocols, ensuring respect of the deceased and full anonymity of data. An Information Sharing Agreement (ISA) has been signed between the UKPF and Coventry University setting the ethical and procedural requirements which have been met [18].

2.0 Methodology

The methodology used in this study is based on two phases. The first phase is the definition of the organ traumatology model (OTM) and the second one the traumatology model validation, based on real-world accident reconstruction; the phase I OTM method is pictured in Figure 171.

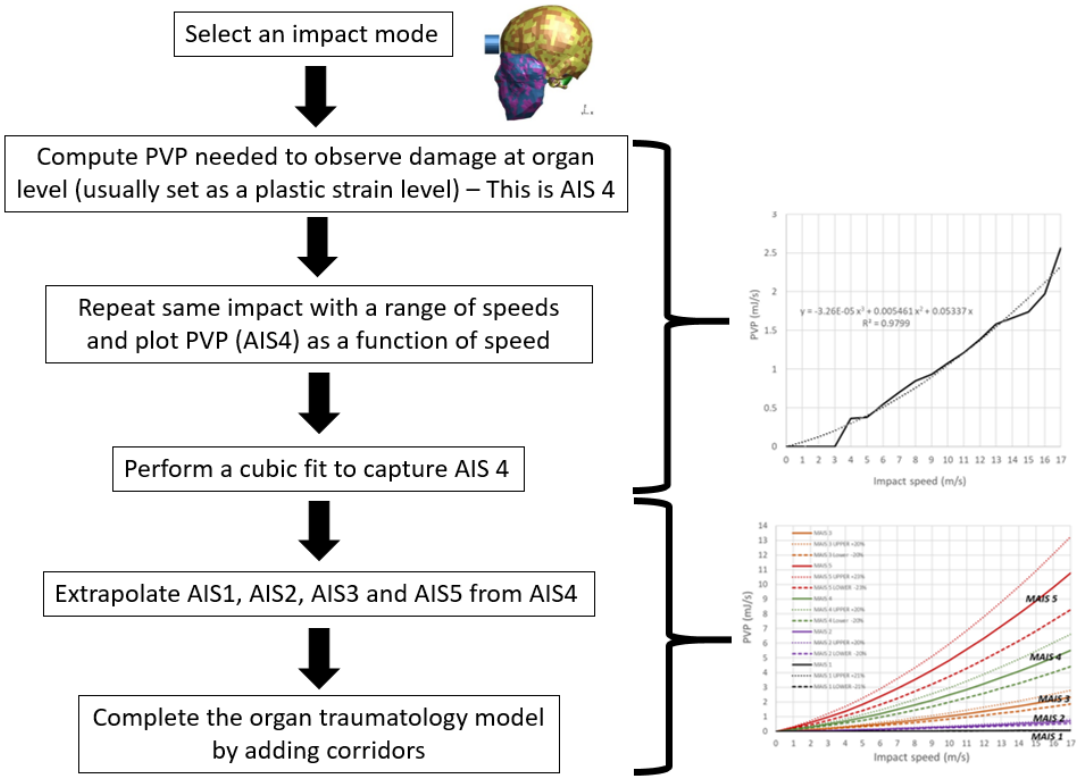

Figure 171: PHASE I: Organ Traumatology Model (OTM)

The research will consider the traumatology of the head in pedestrian impact scenarios and focus on the white and grey matter. The process starts by impacting the head in the three strategic locations (frontal, lateral and occipital), as documented by previous research [14] of pedestrian impacts, at velocity increments ranging from 2m/s to 17m/s. The upper value of 17m/s is the maximum velocity observed in the accidents provided by the UKPF. Also, this velocity relates to the maximum 64km/h frontal impact. Consequently, it is proposed that the range of speeds proposed would allow the use of this OTM in other modes of impact scenarios.

For each impact velocity in a defined scenario (frontal, lateral and occipital), the PVP of the first element in an organ reaching the critical level listed in Table 38, known as the threshold critical calibrated AIS value; the PVP value extracted at the time the damage is observed and plotted as a function of speed. This plot represents AIS 4 of this organ. The next stage is to capture the intermediate and ultimate AIS levels (AIS1, AIS2, AIS3 and AIS5), as well as their level of uncertainty.

Various studies collecting previous clinical research [8] have recorded the relationship between AIS and the risk to life. This data is plotted in Figure 172, and contains data from Baker, CCIS, NASS and Walder [13]. In order to remove the bias from each of the studies, the results from all the studies were averaged and extrapolated with a cubic relationship as well

as including a 95% confidence level corridor, as illustrated in Figure 175. It was previously observed that the risk to life and the probability of death were related to a cubic ($R^2 > 0.95$) [8][9][10]. At this point it is important to note that the cubic fit does not aim at interpolating between the AIS values, which are ordinal values; the interpolation function is only interrogated at integer AIS levels. The cubic relationship confirms that at the ordinal AIS values, the relationship between trauma levels is a cubic in the "frequency of death".

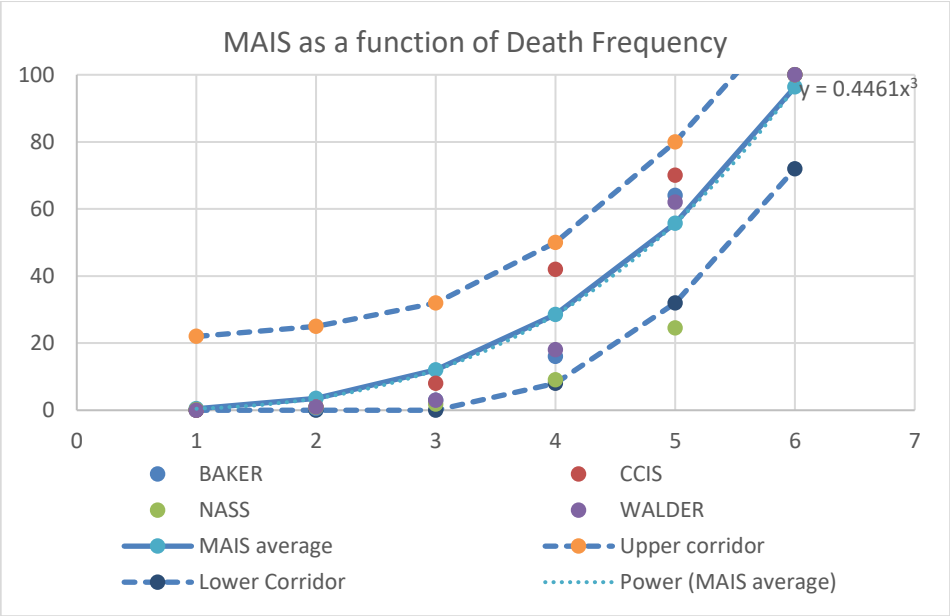

Figure 172 Curve fitting of MAIS and Probability of Fatality

Consequently, the probability of fatality of MAIS 5 can be expressed as Equation 24.

$$\frac{Probablity\ of\ fatality\ of\ MAIS5}{Probablity\ of\ fatality\ of\ MAIS4} = \frac{MAIS5^3}{MAIS4^3} = \frac{125}{64}$$

Equation 24: Probability of fatality of MAIS 5

Hence the ratio of AIS3, AIS2 and AIS1 taking AIS4 as reference are 27/64, 8/64 and 1/64 respectively.

The AIS tolerance corridors, based on the clinical studies used, can be extracted from Figure 172 and are listed in Table 39 and concludes the OTM trauma model generation (PHASE I).

MAIS level	Tolerance bound
1	+/- 21%
2	+/- 20%
3	+/- 20%

4	+/- 20%
5	+/- 23%

Table 39 Tolerance bounds of each MAIS level

Phase II will aim at validating the OTM model (Figure 173).

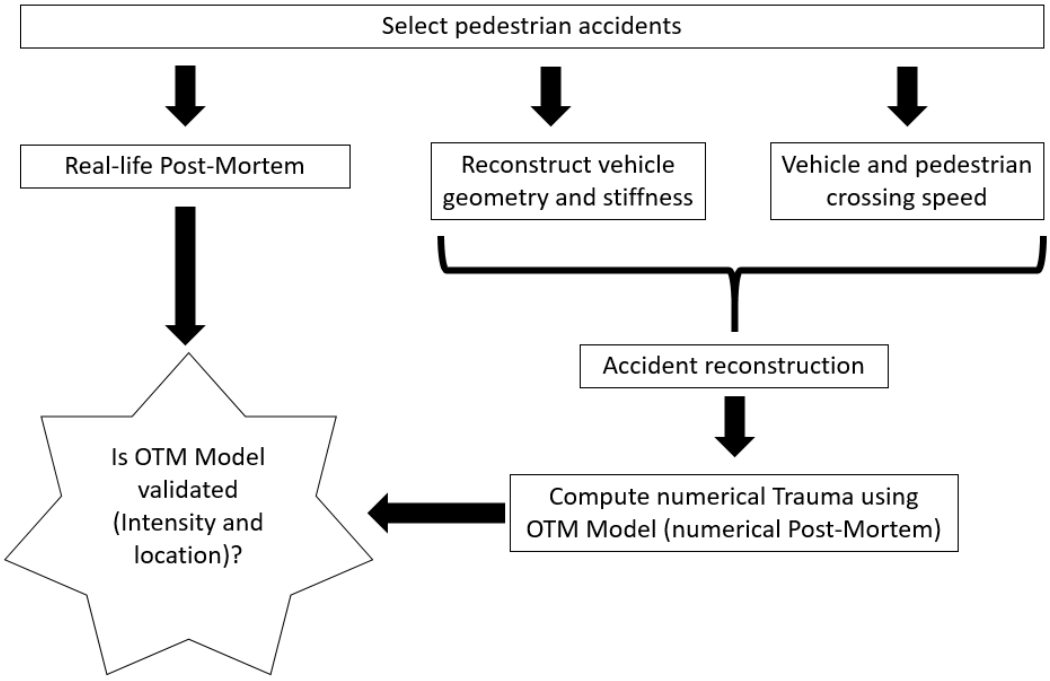

Figure 173: PHASE II. Validation of OTM trauma model

To do so, four accidents have been provided by the UKPF. For each accident, the real-life trauma is extracted from the Post-Mortem provided by the Coroner. The accident is numerically reconstructed, and the numerical trauma computed using the OTM model from Phase I.

In order to validate the OTM method, the trauma intensity (AIS level) and trauma location will be compared to the real-life trauma extracted from the post-mortem (PM).

3.0 Phase I: Calibration of OTM Trauma Model

A cylindrical impactor of 200g was created and positioned around the THUMS human head computer model in the forehead (Figure 174), lateral (Appendix A) and occipital (Appendix B) areas,. This approach was selected because the impact severity depends on the impact location [14]. The frontal impact computer model is illustrated in Figure 174. The temporal

and occipital impact models and interpolations can be found in Appendix A and Appendix B respectively.

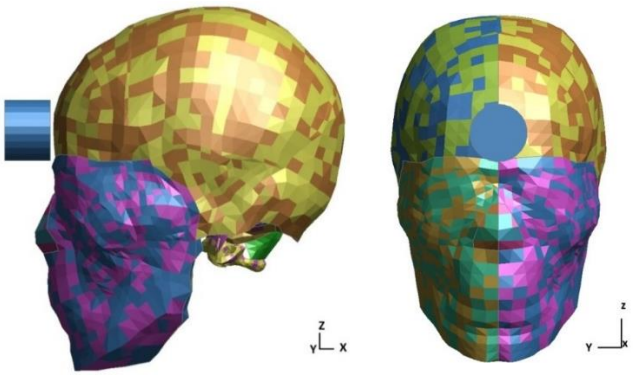

Figure 174 Scenario of frontal impact on THUMS' head

As described in the methodology, the impacts were conducted from 2.0m/s to 17.0m/s in 1m/s increments. Once the threshold plastic strain injury criterion is reached in one of the elements of the head, its PVP value at that specific time is extracted and plotted against impact speed. Brain contusion (grey matter) and Diffuse Axon Injury (DAI) (white matter) are classified as AIS 3 and AIS 4 level injuries respectively. Consequently, the PVP obtained for the critical plastic strain threshold obtained on grey matter relates to an AIS 3 brain contusion. The PVP threshold obtained on the brain white matter is equivalent to an AIS 4 Diffuse Axonal Injury (DAI). In the frontal impact scenario, the PVP threshold of AIS 3 brain contusion and AIS 4 DAI are shown in Figure 175 and Figure 176 respectively, including the corridors in Table 39.

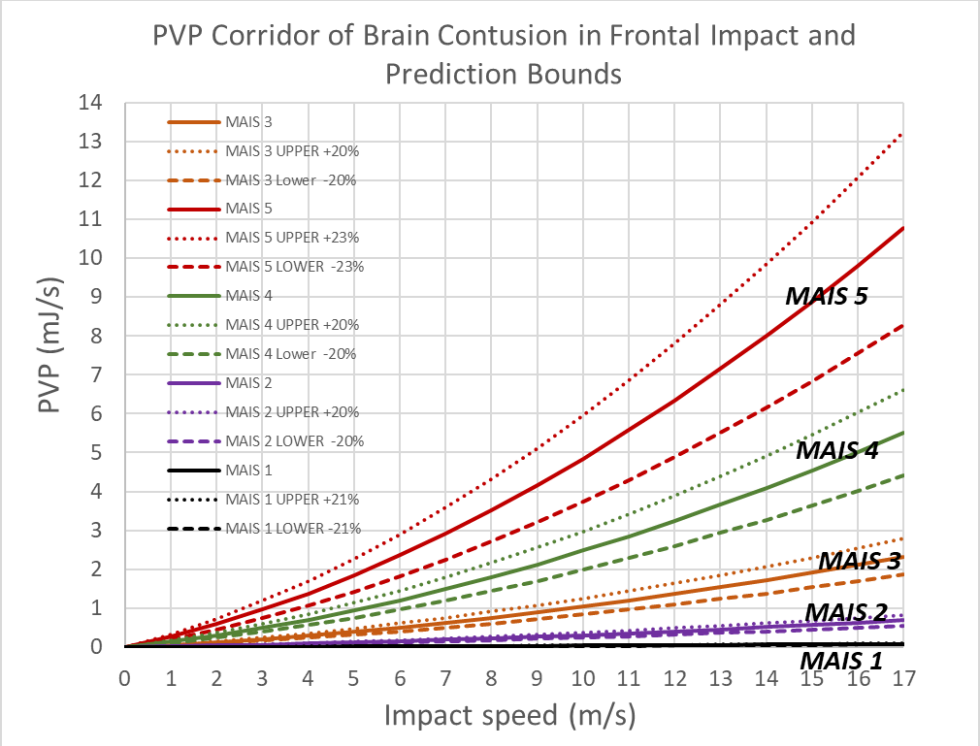

Figure 175: PVP corridor of brain contusion in frontal impact (grey matter)

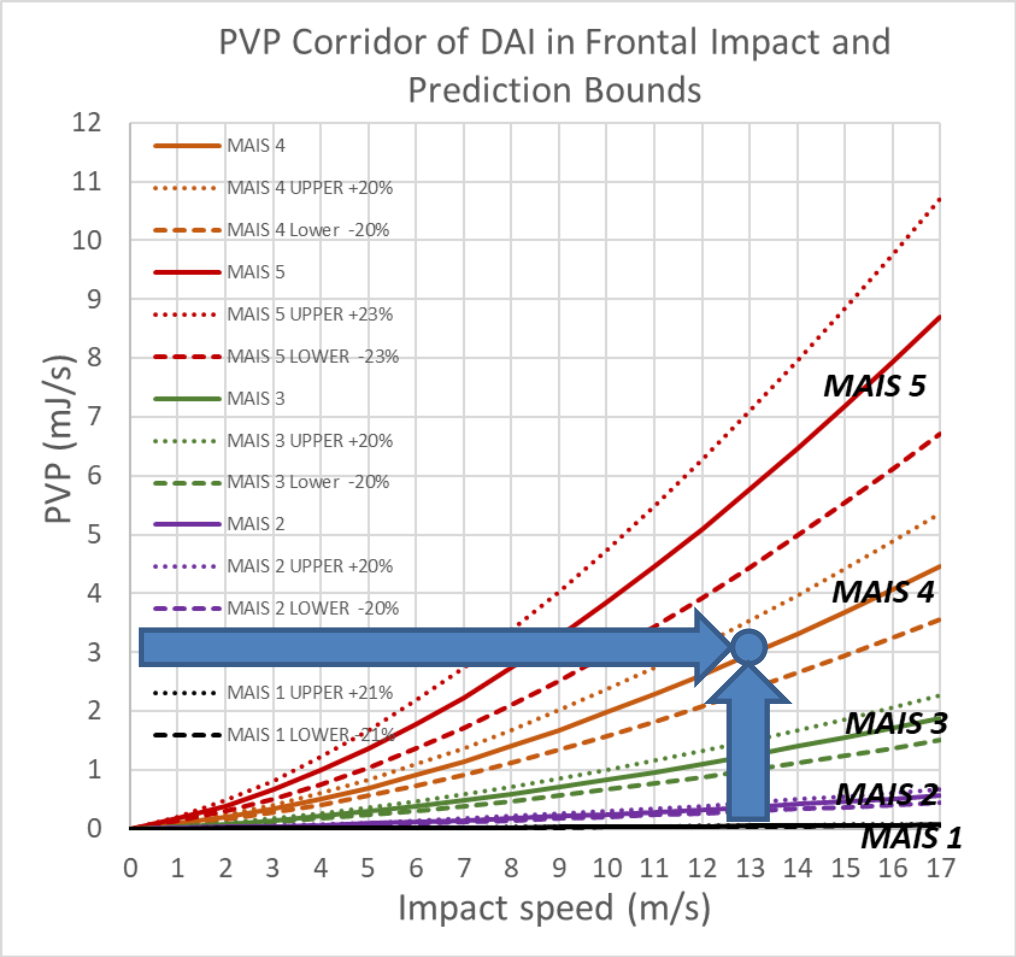

Figure 176: PVP corridor of DAI in frontal impact (white matter)

The graphs plotted, Figure 175 and Figure 176, represent an Organ Trauma Model (OTM), which maps the whole trauma response of an organ in a specific impact direction, against an impact speed. For a selected impact speed (abscise), the PVP can be read from the finite element model (ordinate). The AIS level can be extracted from these two values. As an example, in Figure 176, for an impact speed of 13m/s, should the PVP read 3mJ/s, then the expected AIS is 4.

4. PHASE II: Accident reconstruction and AIS validation

4.1 Accident reconstruction

The accident data in this section were provided by the UKPF and the Senior Coroner and consisted of detailed Police accident as well as PM reports. The accident reconstruction focused on re-creating the vehicle and the accident circumstances. In order to capture the pedestrian kinematics, the THUMS human model was scaled to match the height and weight of the deceased, and placed in the most likely gait [15][16], based on of accident report, to replicate an accurate head landing position on the windscreen.

The cases studies are listed in Table 40.

Case Id:	UK Police Force Reference	Vehicle	Mass (kg)	Height (cm)	Impact direction	Vehicle Impact Speed (m/s)
1	229-4818	Seat Leon	61.0	183	Left side impact (right leg forward)	16.0
2	213-2205	Toyota Corolla	58.6	165	Right side impact (right leg forward)	11.2
3	001-3484	Renault Clio	79.2	173	Side (left leg forward)	12.5
4	207-9077	Benz B180	56.4	165	from driver's near to far side	12.5

Table 40 Accident cases summary

Each vehicle stiffness was related to the EuroNCAP pedestrian scoring system [20][21][22][23] and the stiffness value characteristic inspired by the APROSYS project [25]. The method proposed varied in the way the contact characteristic was provided. In APROSYS Madymo was utilised, which favoured a contact force method which is well suited to multibody software.

In the case of a full Finite Element model containing soft tissues, i.e. for which the stiffness values were very low compared to bones, similar contact method could not be achieved, as it gave model instability. Consequently, a penalty method was preferred by tuning the thickness of a bonnet area by simply changing the thickness whilst still meeting the EuroNCAP test results. The thickness of these panels is listed in Appendix D. The accident kinematics can be seen in Appendix E. It can be noted that the impact locations computed are similar to the real-life scenario (Figure 200). The accident kinematics are illustrated in Appendix E, in Figure 201, Figure 202, Figure 203 and Figure 204.

4.2 Traumatology results (numerical and real-life)

Results are plotted in Figure 177 to Figure 190. Black dots represent the CAE prediction results, while the red ones show the injury result based on the autopsy reports.

4.2.1 Case 1: 229-4818

In case 1, the PM listed that trauma was present on the right side of the brain. The pathologist did not give any information about brain contusion and corresponding side symptoms on the grey matter. In the CAE simulation, an AIS 2 brain contusion is observed (Figure 177). AIS 2 injury is a moderate injury which has 1%-2% probability of fatality [1]. Comparing with no injury suggested in the autopsy report, it can be noted that the CAE prediction is acceptable. It can be noted that in Figure 180, the trauma is more pronounced on the right-hand side, albeit small (AIS2). It can be observed that principal plastic strain response in Figure 180 is very scattered across the brain and does not show any clear trauma location, if compared to the PM. As a matter of fact, both the left and right side of the grey matter are injured, which is not what is expected.

On the white matter (Figure 178), due to a subdural hemorrhage identified in the PM report, an AIS 4 injury can be concluded. From CAE simulation, an AIS 2-3 DAI was confirmed (PVP values landing between AIS 2 and AIS 3 corridors). Trauma on the right-hand side of the brain is also observed on Figure 165 if PVP is used. It can be noted that there is a higher trauma in the center of the white matter, but such is not listed in the PM report. Looking at the principal plastic strains, the values are again scattered and do not suggest a clear trauma location. The difference in trauma results is due to the fact that the THUMS human computer cannot predict blood loss post-accident but only mechanical injury at the time of the accident, as such hemorrhage and swelling cannot be predicted using FEA. However, one of the side effects of

DAI is hemorrhage, therefore corresponding hemorrhage can be assumed according to the AIS 3 prediction result.

Looking at the PVP values in the median area are higher than the right side of the brain. This has been missed in the PM. Nevertheless, the right impact location and trauma were predicted by the proposed method (right side of the brain). The PVP of the left-hand side of the brain is lower than the right-hand side of the brain, hence the trauma could have been missed in the PM. Looking at the principal plastic strains, the values are in excess of 100% which would suggest AIS 4 if not AIS 5, considering Table 38, which is contradictory to the PM outcome. In this case, maximum principal strain does not capture the location nor the trauma level.

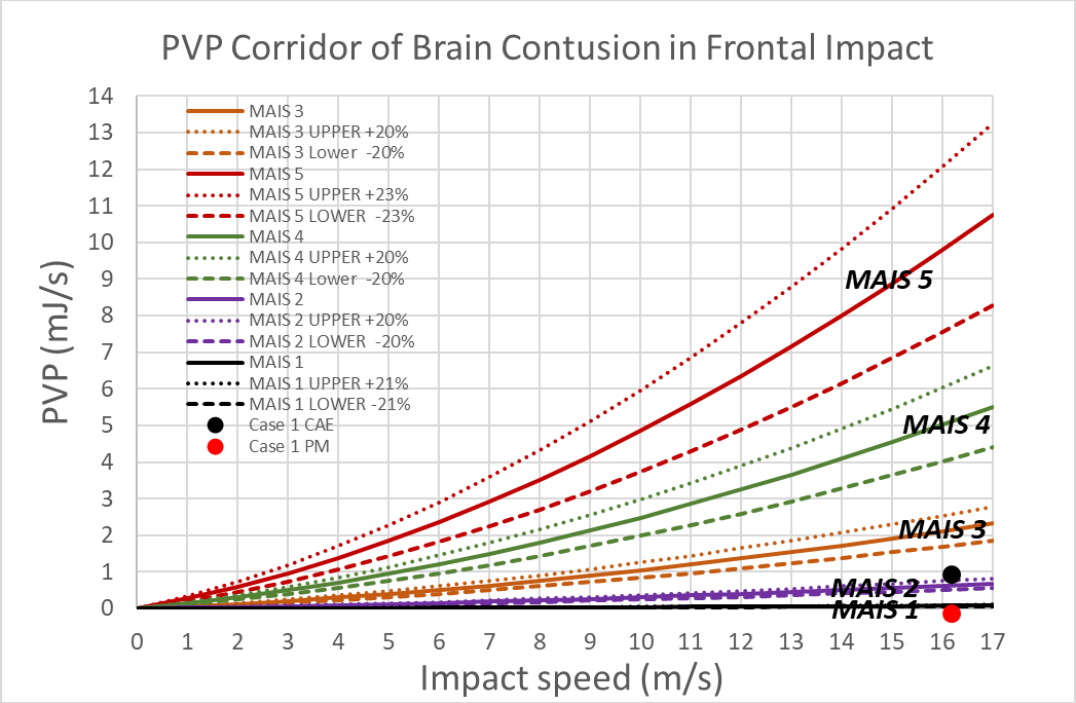

Figure 177: Case 1: Brain contusion result of case 1 from CAE and autopsy report (grey matter)

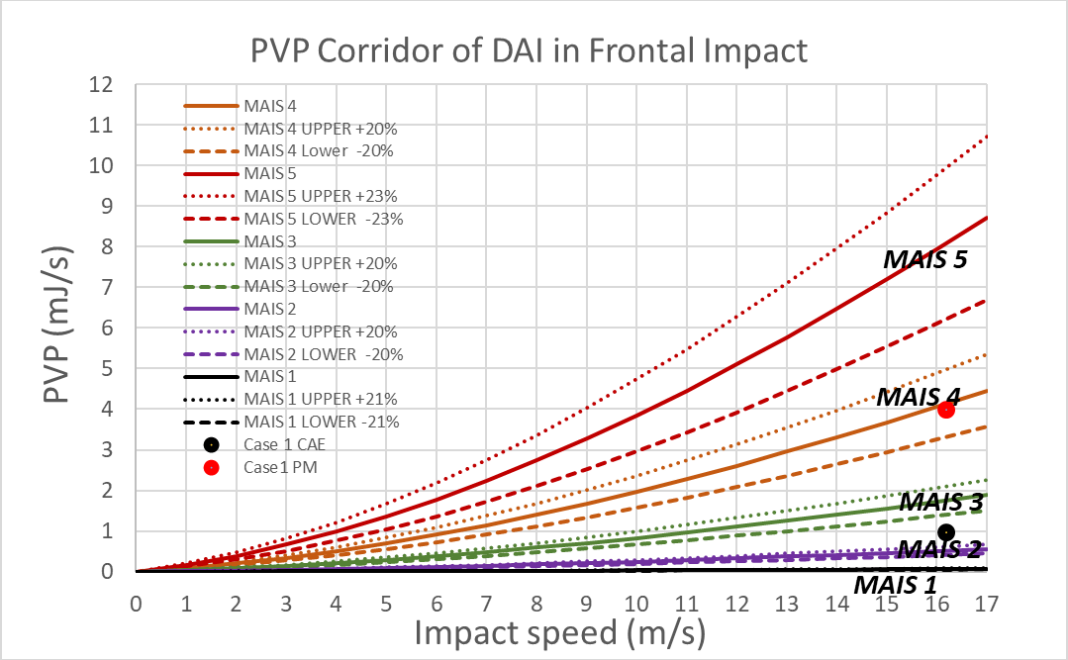

Figure 178: Case 1: DAI result of case 1 from CAE and autopsy report (white matter)

Comparing the location of the impact, PVP can be compared with the current method widely used which is the maximum principal strain (Figure 165). It can be noted that PVP computes a trauma location median with a slight bias to the right, while the plot with the maximum principal strain is not conclusive in location as well as in AIS outcome.

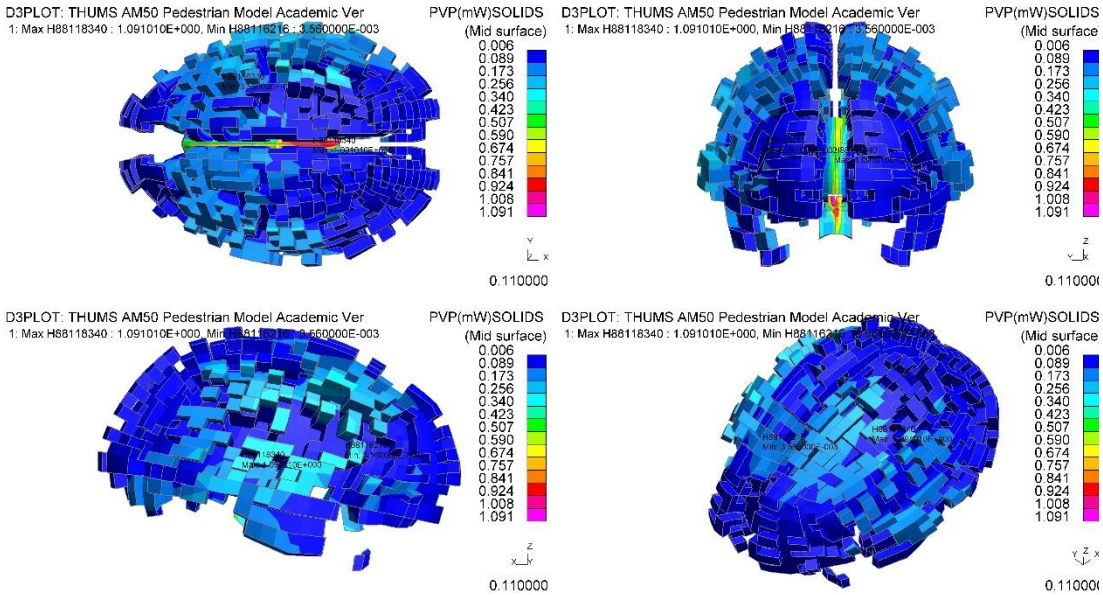

White Matter PVP results

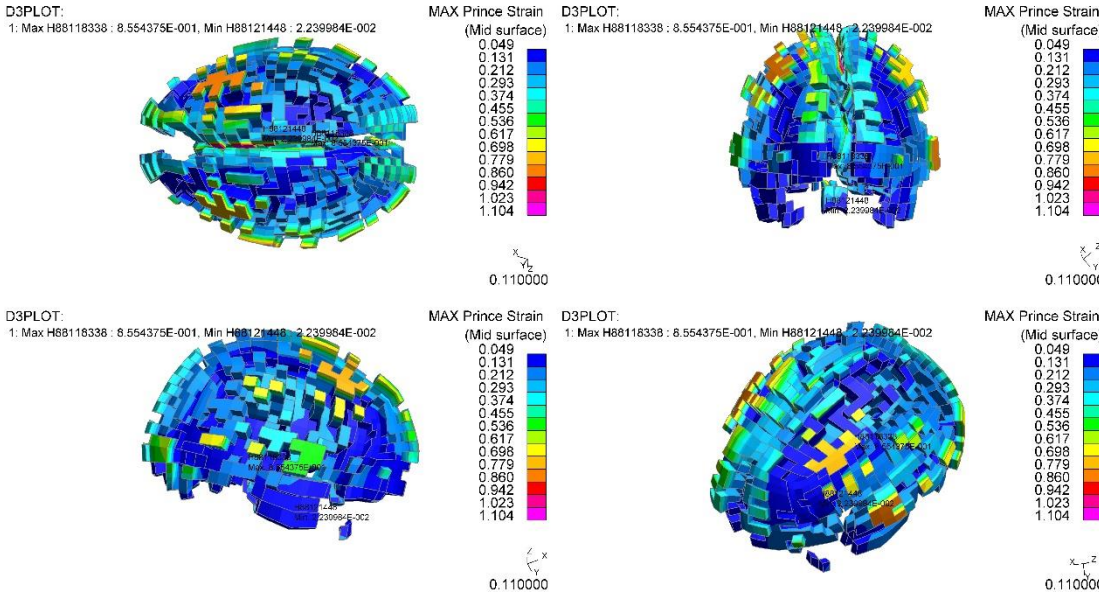

White Matter Principal Strain Results

Figure 179: Case1 - White Matter injury comparison between PVP and maximum principal strain

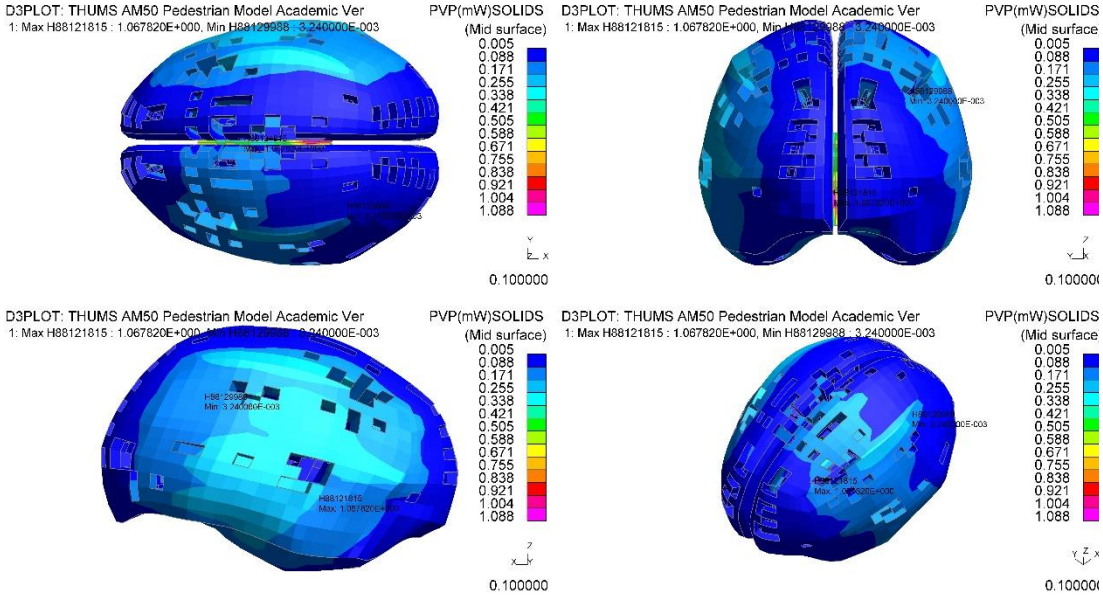

Grey Matter PVP results

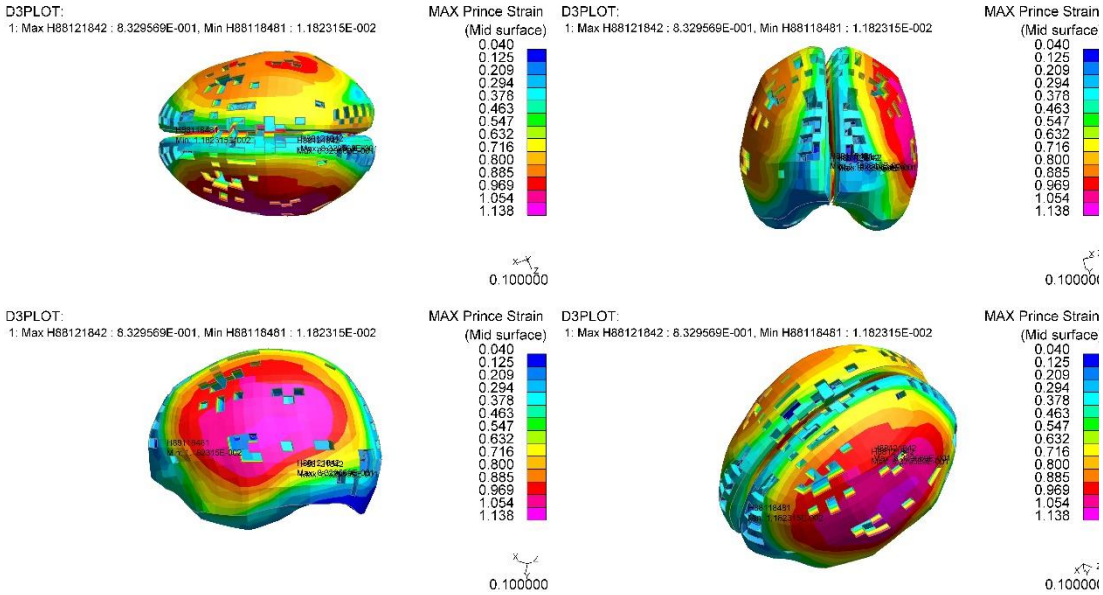

Grey Matter Principal Strain Results

Figure 180: Case 1 - Grey Matter injury comparison between PVP and maximum principal strain

4.2.2 Case 2: 213-2205

In case 2, the PM listed that trauma was present on the right temporal lobe. Considering the brain grey matter (Figure 181), the PVP prediction and autopsy report are comparable. On the white matter (Figure 182), an AIS DAI injury can be concluded from both the PVP prediction and the autopsy report.

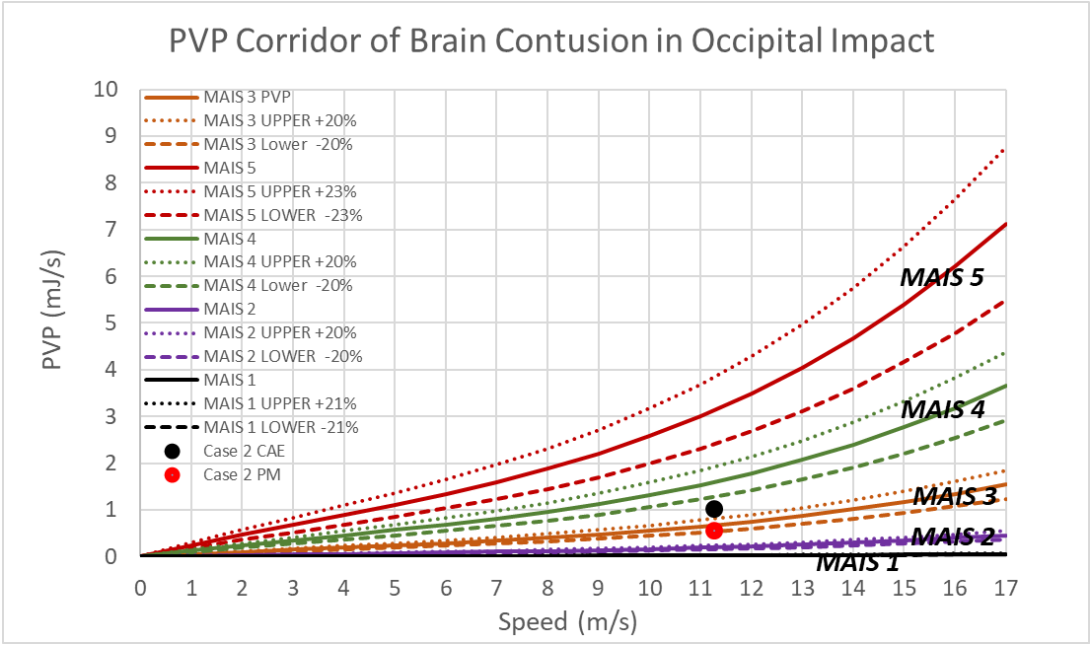

Figure 181: Case 2: Brain contusion result of case 2 from CAE and autopsy report (grey matter)

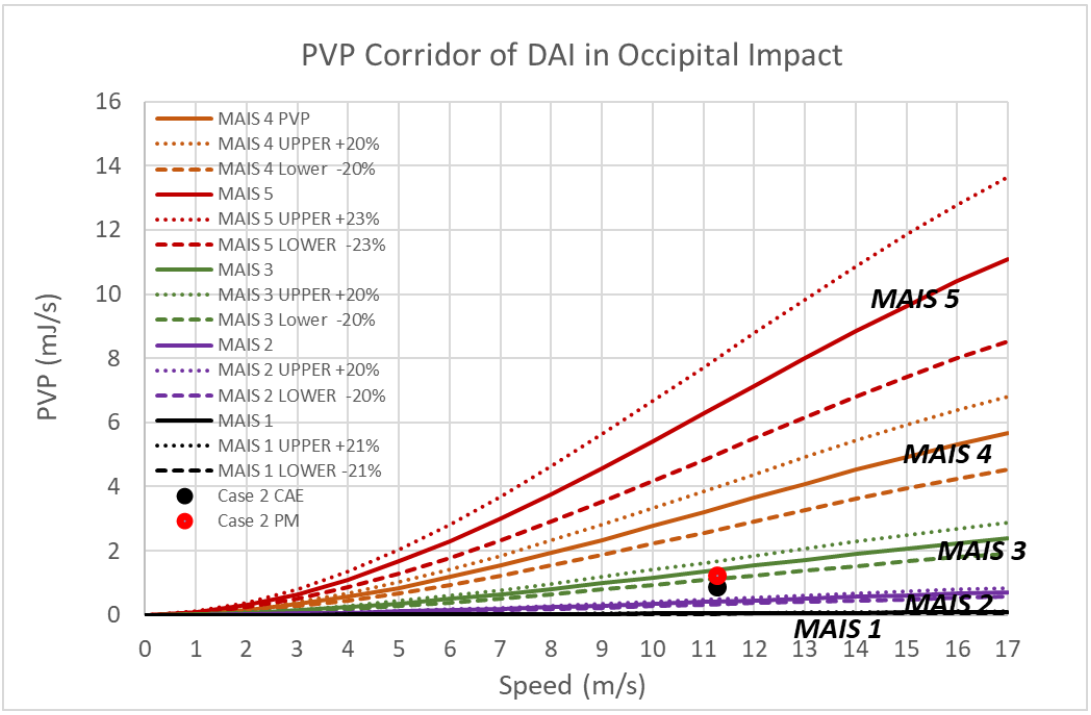

Figure 182: Case 2: DAI result of case 2 from CAE and autopsy report (white matter)

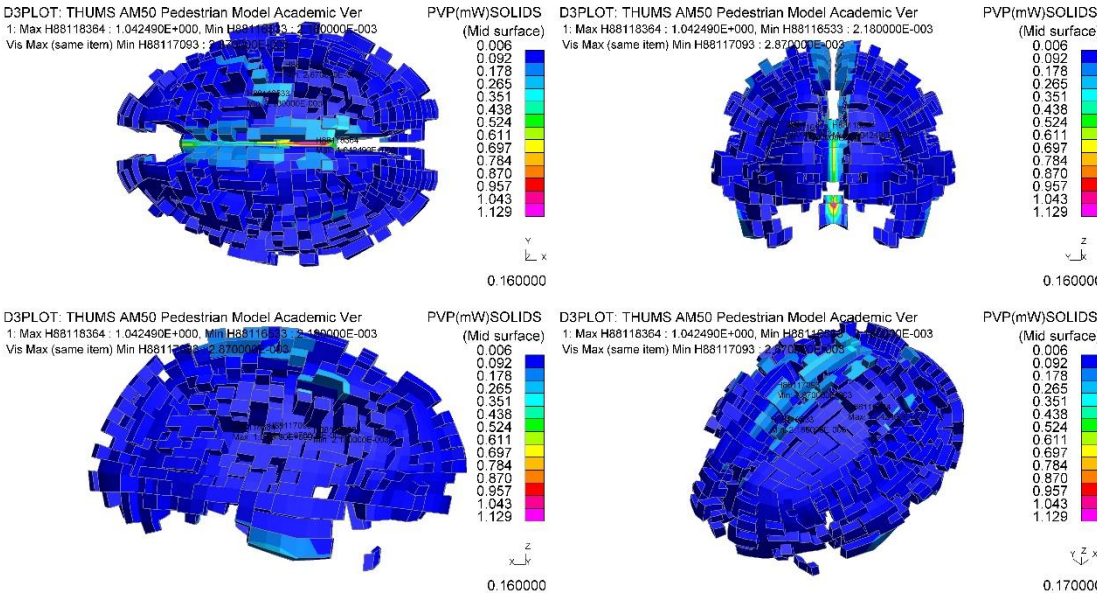

White Matter PVP results

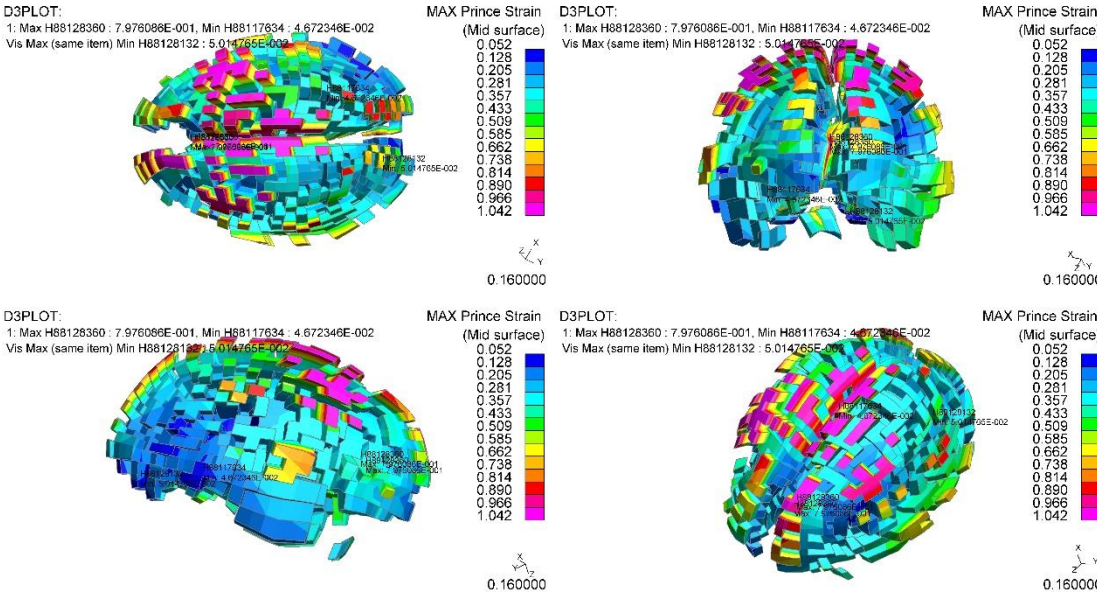

White Matter Principal Strain Results

Figure 183: Case 2 - White Matter injury comparison between PVP and maximum principal strain

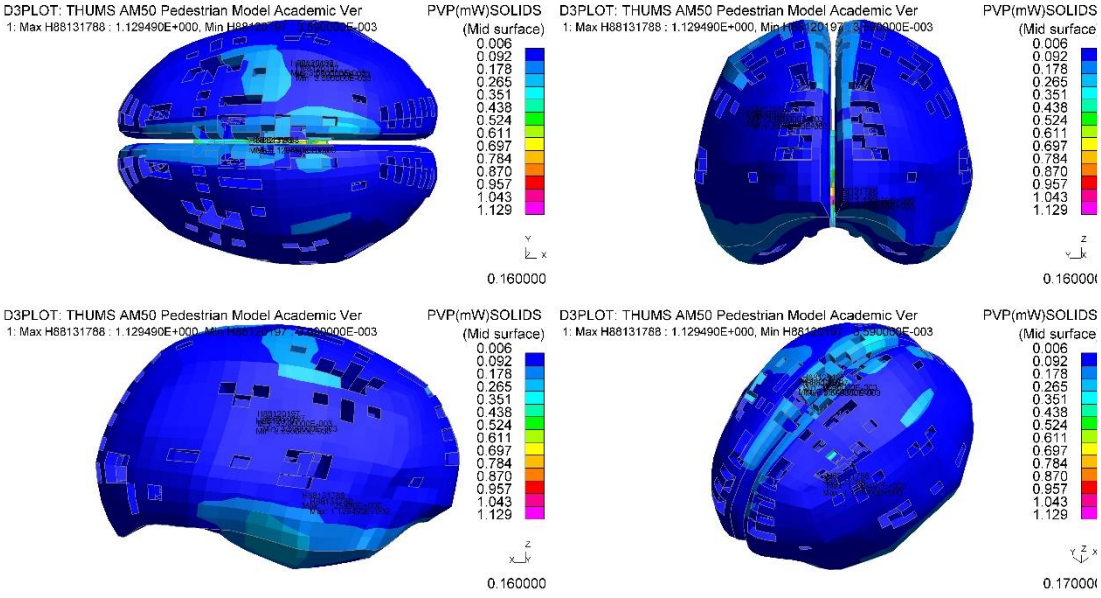

Grey Matter PVP results

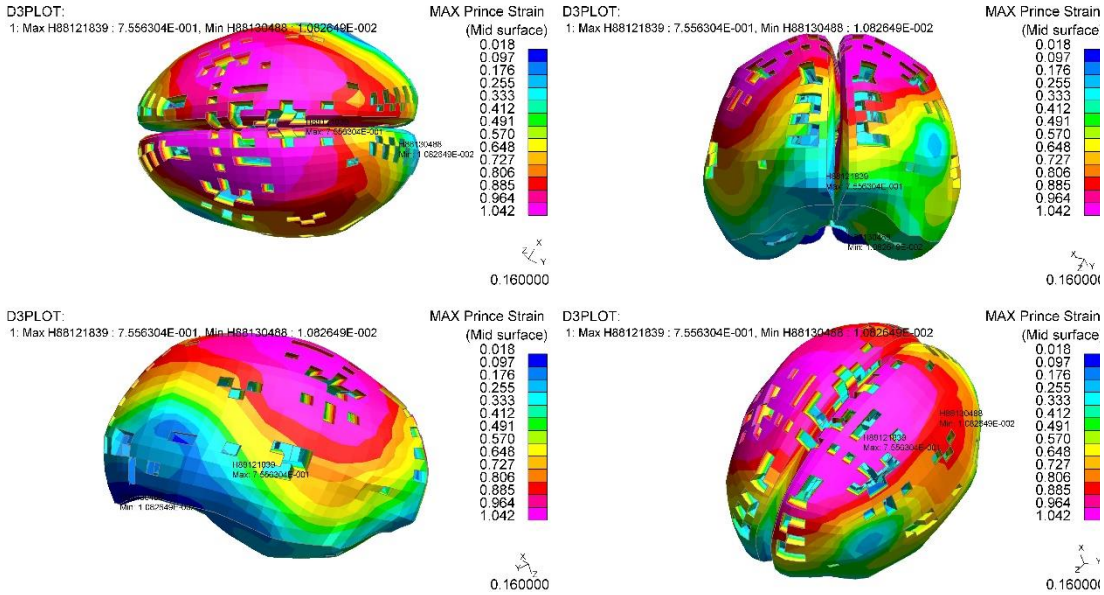

Grey Matter Principal Strain Results

Figure 184: Case 2 - Grey Matter injury comparison between PVP and maximum principal strain

It can be observed from Figure 184 that the right temporal area has been injured, just by looking at the PVP plot. It is suggested that the parietal lobe would be also damaged with an AIS2, but was missed in the PM. When the principal strain plots are observed, they suggest that the values are high around the parietal area, which is in the wrong location and not in the temporal area; these strain values also tend to scatter as in Case 1. Looking at the principal plastic strains, the values are in excess of 100% which would suggest AIS 4 if not AIS 5, considering Table 38, which is contradictory to the PM outcome. In this case, maximum principal strain does not capture the location nor the trauma level.

4.2.3 Case 3: 001-3484

In case 3, the pathologist did not observe any injury on the brain tissue, while using PVP, AIS 3 brain injury can be concluded on the grey matter (Figure 185) and AIS2 on the white matter (Figure 186). No injury description was given in the autopsy report; however, the pedestrian death was recorded as death from multiple injuries. Therefore, based on the autopsy report, MAIS of the pedestrian should be 0 which does not correlate with real-life accident. The fact that no injuries were recorded in the PM does not mean that the injury was not present but was probably too small to be observed by the pathologist. It can be suggested that PVP could suggest some trauma zones to the pathologist, like the upper lobes in this instance, which can be observed using the PVP output from Figure 187 and Figure 188.

Looking at Figure 187 and Figure 188, it can be noted that the PVP trauma plots are less scattered than using the standard maximum principal strain method. Also, in both cases, the maximum principal strain values are lower than the critical values from Table 38, but no AIS can be concluded from their values.

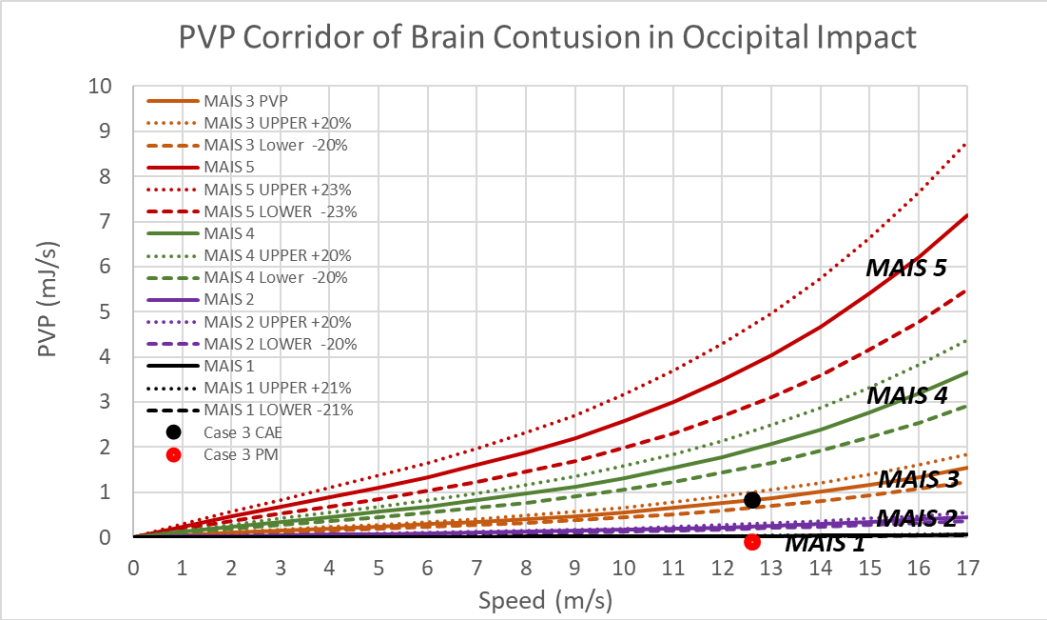

Figure 185: Case 3: Brain contusion result of case 3 from CAE and autopsy report

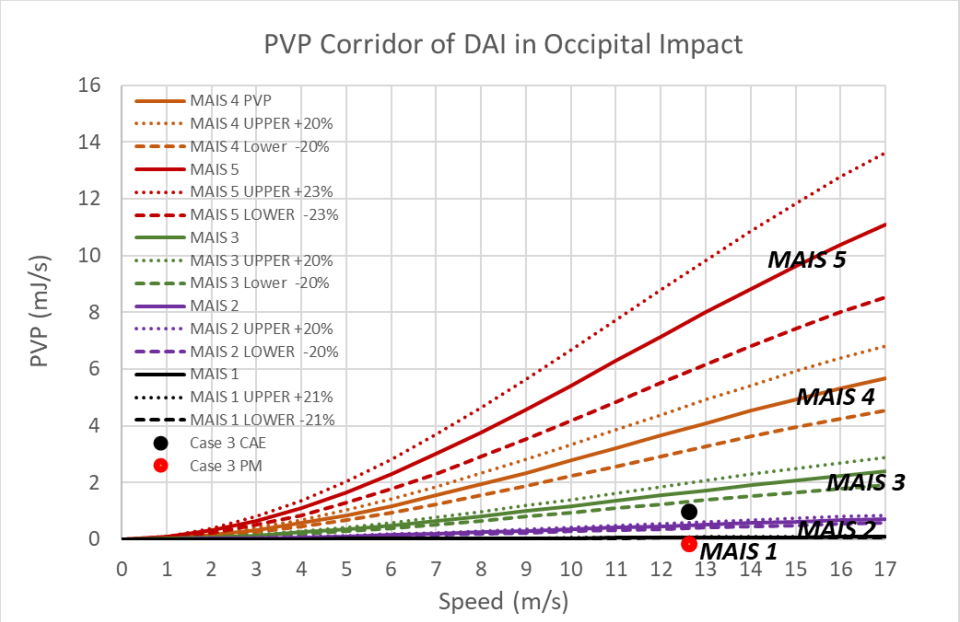

Figure 186: Case 3: DAI result of case 3 from CAE and autopsy report

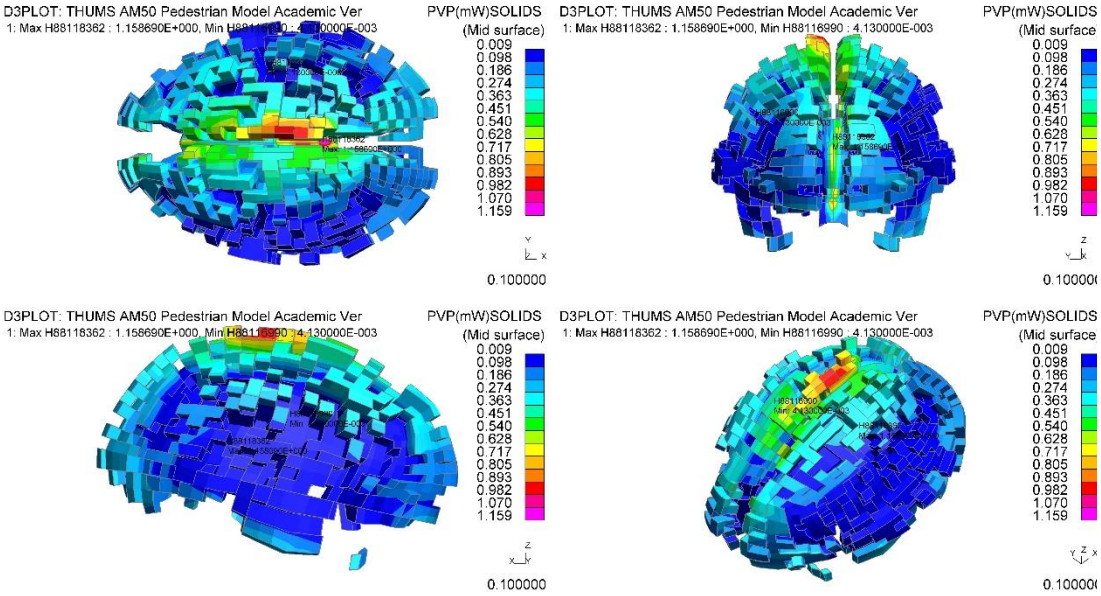

White Matter PVP results

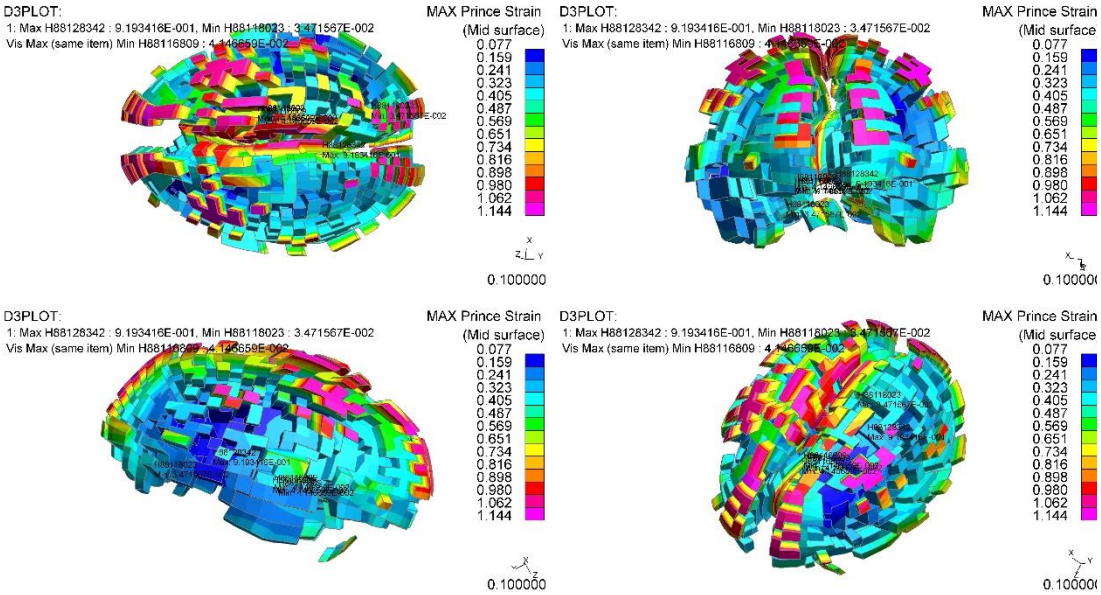

White Matter Principal Strain Results

Figure 187: Case 3 - White Matter injury comparison between PVP and maximum principal strain

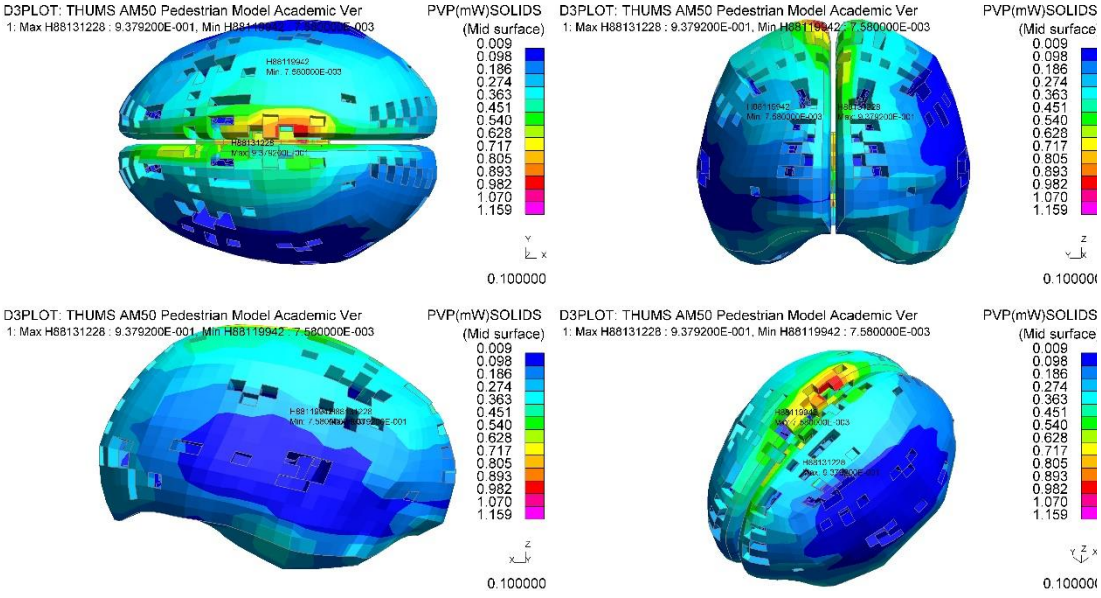

Grey Matter PVP results

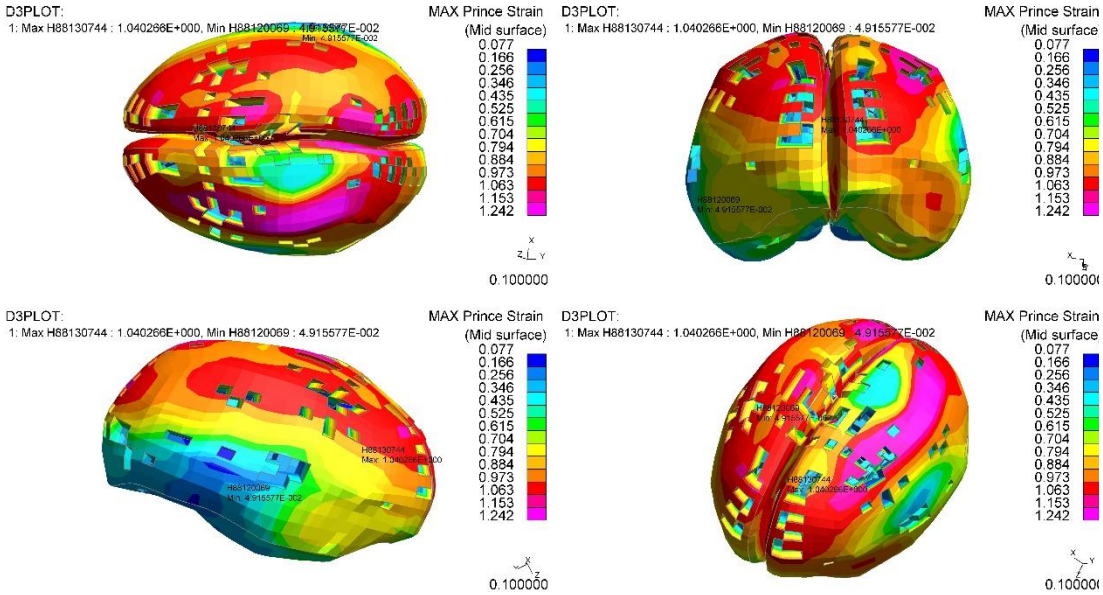

Grey Matter Principal Strain Results

Figure 188: Case 3 - Grey Matter injury comparison between PVP and maximum principal strain

4.2.4 Case 4: 207-9077

In case 4, the PM suggested extensive trauma on both lobes, which can be observed in the PVP plots from Figure 191 and Figure 192. No brain contusion was observed by the pathologist, and PVP suggests an AIS2 outcome (Figure 189), which is a reasonable match as AIS 2 may be too small to be observed during a PM. An AIS 4 caused by DAI was concluded in the autopsy report due to the subdural hemorrhage. On the white matter PVP predicted an AIS 3 (Figure 190). Again, due to the limitations, PVP/FEA cannot predict post-accident injury and so hemorrhaging is out of the capabilities of the PVP/FEA prediction. It can be noted that in the PVP plots of the white and grey matter, the maximum PVP appears in the median area of the brain. This was not captured in the PM. Regarding the maximum plastic strain, the same comment can be made, i.e. the location and the AIS predictions are not representative to what happened during the accident.

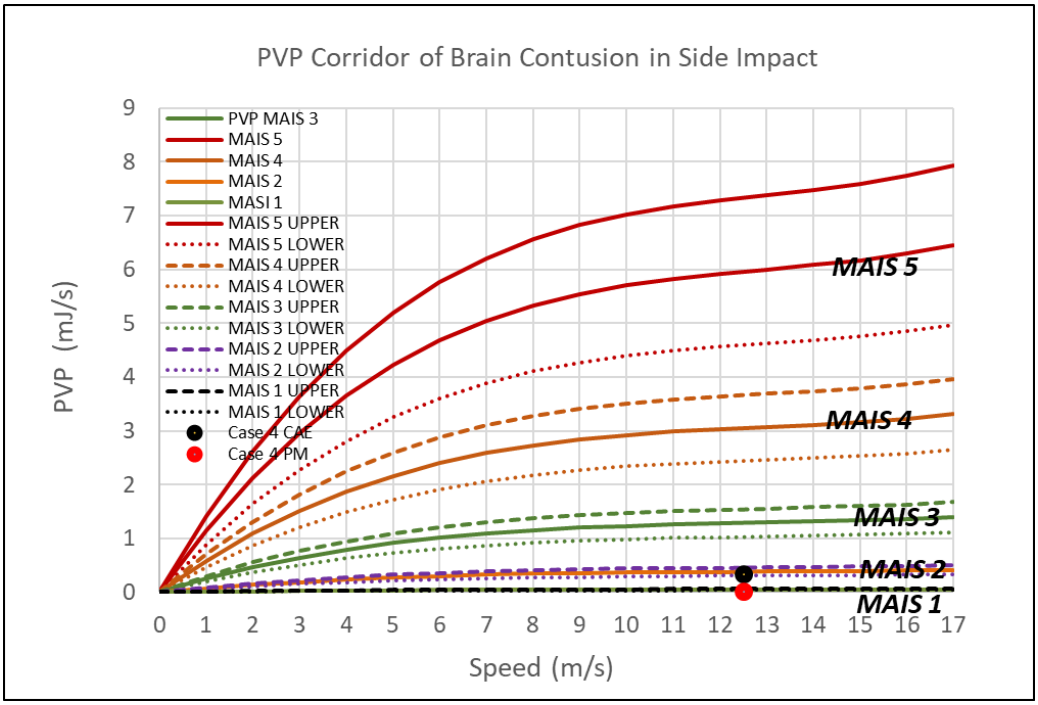

Figure 189: Case 4: Brain contusion result of case 4 from CAE and autopsy report Figure 186

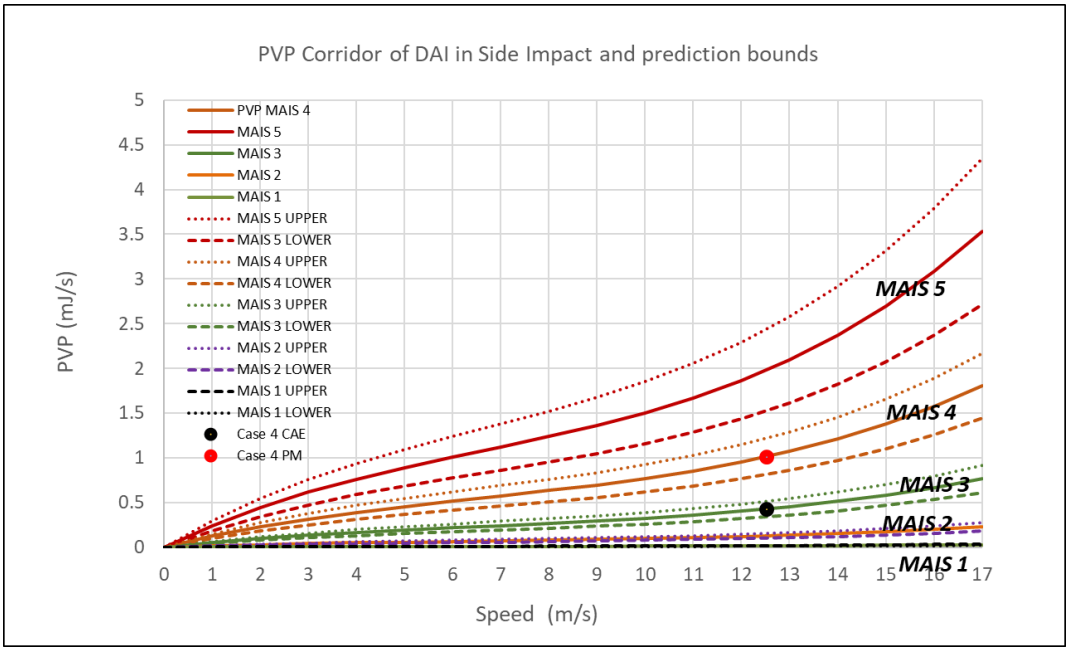

Figure 190: Case 4: DAI result of case 4 from CAE and autopsy report Figure 186

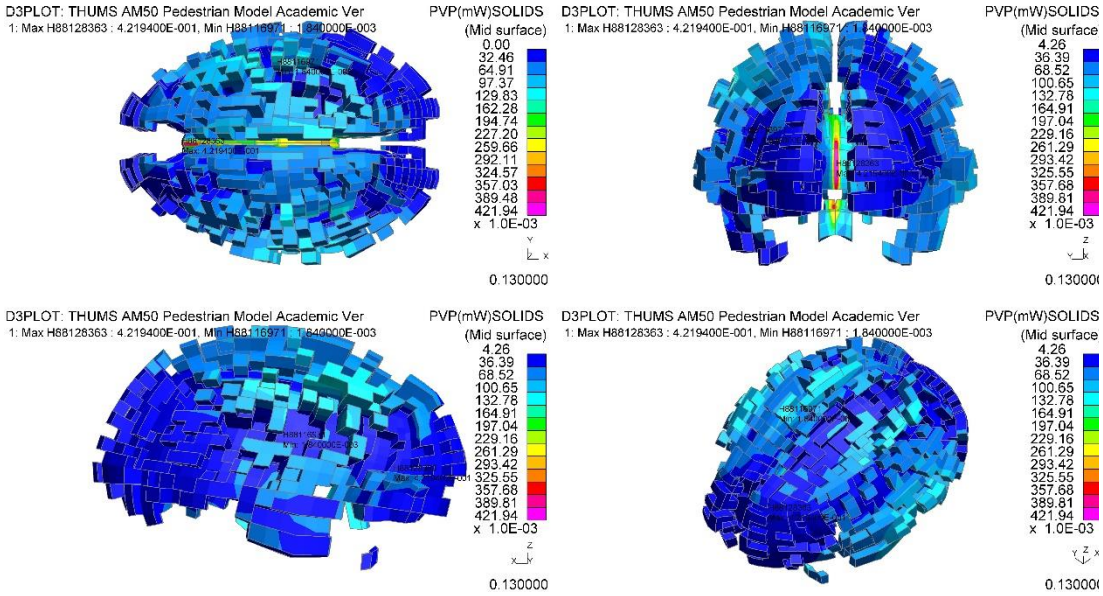

White Matter PVP results

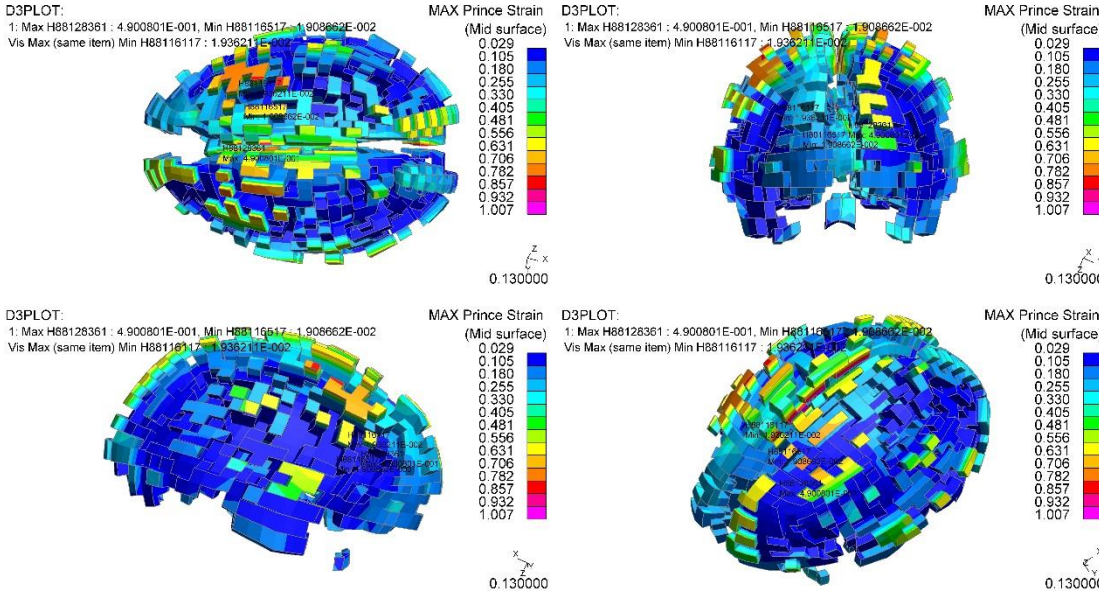

White Matter Principal Strain Results

Figure 191: Case 4 - White Matter injury comparison between PVP and maximum principal strain

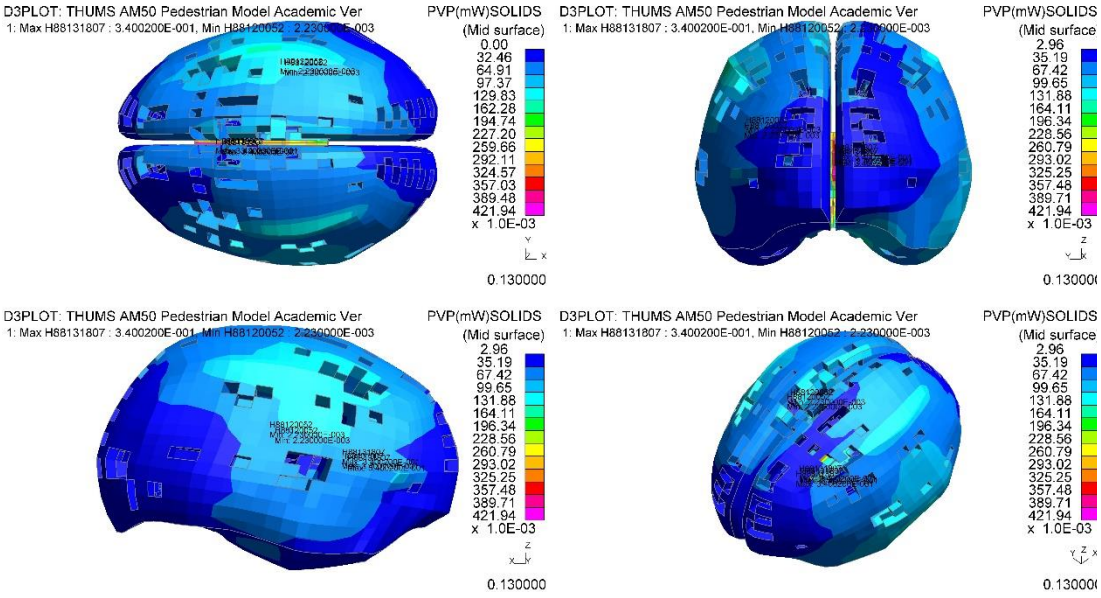

Grey Matter PVP results

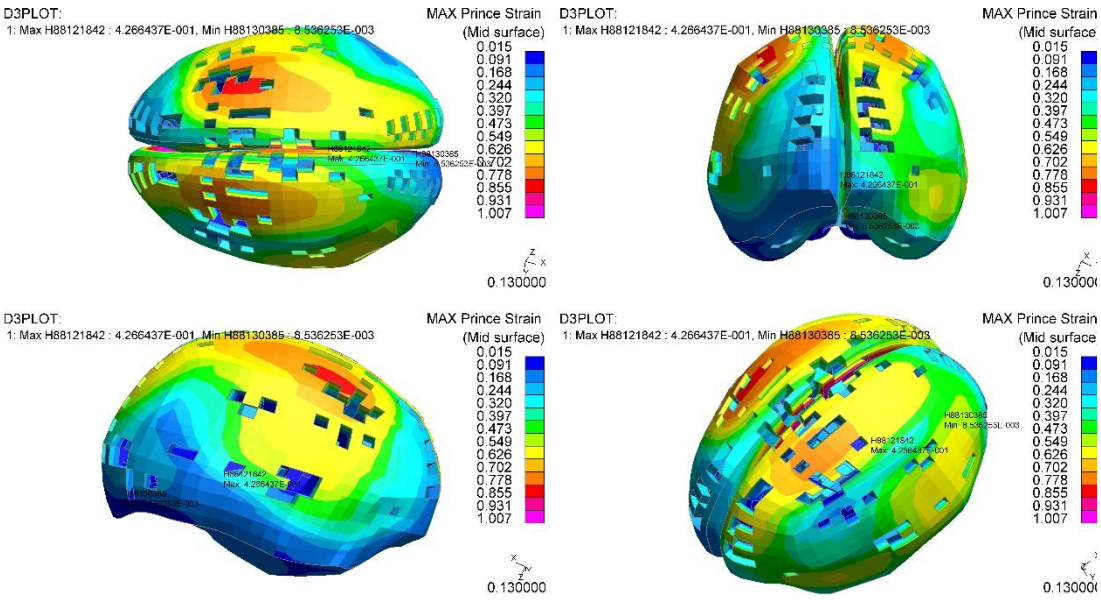

Grey Matter Principal Strain Results

Figure 192: Case 4 - Grey Matter injury comparison between PVP and maximum principal strain

5 Discussion

The results of the four accidents can be summarized in Table 41.

Case Id:	Vehicle	PM description	CAE location	Comments	Match (Y/N)
1	Seat Leon	Right parietal lobe (Haemorrhage)	88118340 (Centre of parietal lobe, not surface)	Haemorrhage is not of the prediction scope of THUMS.	Yes
2	Toyota Corolla	The inferior aspect of the right temporal lobe (Swollen)	88131788 (Left grey matter, but in midline of whole grey matter)	The maximum PVP is not located on the description of PM, but PVP distribution and trauma level can be clearly observed on right temporal lobe.	Yes
3	Renault Clio	No evidence of skull fracture and brain showed no evidence of contusion	88118362 (Centre of right white matter parietal lobe) 88121842 (Centre of right grey matter parietal)	Trauma is too small to be captured by a PM	No, but prediction plausible
4	Benz B180	Extensive haemorrhage within the left cerebral hemisphere with peripheral haemorrhage within both cerebral lobes.	88128363 (Left white matter frontal lobe)	The maximum PVP is not located on the description of PM, but PVP distribution and trauma level can be clearly observed on both lobes	Yes

In the first instance, it can be observed that the CAE predictions are of the same order of magnitude as the PM's. In Table 41: Summary of the accident study the instance of Case 1, the CAE prediction was AIS 3 while the PM predicted AIS 4. In the PM report, it was observed that the skull and the cranial cavity were

normal. The brain showed an area of subdural haemorrhage over the right parietal lobe, and also over the cerebellum in the midline and over right cerebella hemisphere. The cut surface of brain showed some small petechial haemorrhage present in right cerebella peduncle. No other brain injury was identified. In Case 1 it can be observed from Table 43 (Appendix F) that the PVP is located in the exact area of the PM, albeit right from the brain centreline. The pedestrian died, however, of a brain haemorrhage. The OTM model is based on a CAE model which can only predict mechanical damage, and not the blood loss, which is a fluid problem. Nevertheless, as a mechanical indicator it predicted the correct damage area.

In Case 2, CAE and PM both predicted an AIS of 3 on the brain, which is a serious injury. The PM listed that there was some subarachnoid haemorrhage. The brain appeared diffusely swollen to a mild degree and there were contusions on the inferior aspect of the right temporal lobe. These contusions were captured, however it was not possible to predict the haemorrhage and the swellings which are occurring post impact.

Case 3's PM was unremarkable, as no trauma was observed in the deceased ("No evidence of skull fracture and brain showed no evidence of contusion"). The CAE model predicted an AIS of 2 which is a moderate trauma. Maybe such trauma level is quite complicated to observe, as being low risk, hence it may be suggested that the CAE prediction is plausible.

Case 4 had some similarity with Case 2, except that there was some "significant" skull fracture, which had not been activated during the computations. This fracture is extending from the right temporal area coronally to the left temporal region. There was also a fracture of the base of skull on the left-hand side. A subarachnoid haemorrhage was identified and, on serial slicing through the brain, there was extensive haemorrhage within the left cerebral hemisphere with peripheral haemorrhage within both cerebral lobes. A 1cm haematoma was also noted in the right cerebellum. The computer model predicted an AIS 3 while the PM suggested an AIS 4. Again, it was not possible to predict the haemorrhage which is a post trauma effect which requires an Eulerian solving method to extract.

It can be noted that the UKPF is using the pedestrian kinematic effects to evaluate the vehicle impact speed, but not the Post-Mortem (PM), which contains vital information on the impact energy that was exerted to kill the pedestrian. It is not usually used since evidence from the PM would need to be presented by an expert (Home Office Forensic Pathologist). Overall the quality of autopsy reports (PM) is always questioned: just over half of PM reports (52%) (873/1,691) were considered satisfactory by experts, 19% (315/1,691) were good and 4%

(67/1,691) were excellent. Over a quarter were marked as poor or unacceptable. Proportionately, there were more reports rated 'unacceptable' for those cases that were performed in a local authority mortuary (21/214 for local authority mortuary cases versus 42/1,477 for hospital mortuary cases)" [19]. To date, experts tend to consider the research around PM currently to be limited regarding its use to predict speed, therefore would not use it in court during criminal proceedings. The PM is only used to state which organs failed, hence causing death, but not as evidence to add to the forensic case.

Overall, it can be observed that the comparison between PVP prediction result of pedestrian injury and autopsy report shows a promising correlation to risk to life applied to the head, in the trauma magnitude and location. This observation would suggest that it is possible to supplement the standard pedestrian head impactor numerical process with a human computer head model to assess the real trauma level of a pedestrian. With the current safety assessment processes which are using a head impactor, in ECE 127 [26] and EuroNCAP [27], which just evaluate HIC, it is only possible to evaluate the likelihood of linear skull fracture damage. This new method can go beyond the current limitations and predict the trauma outcome in the head's white and grey matter. In the case of EuroNCAP, as the bonnets are validated using calibration tests and then scaling of CAE prediction results, it would be possible to add this PVP method to simulate alongside the EuroNCAP protocol in order to supplement engineering assessment of brain injuries. Obviously, this suggestion would require a detailed test configuration setup, as the human head's trauma response is direction dependent; the current test assessment is made of half a sphere of rubber coated, aluminum consequently the proposed CAE assessment would require testing the 3 head directions studied in this report.

6 Conclusions

An Organ Trauma Model (OTM), based on Peak Virtual Power (PVP), was used to successfully extract the AIS risk to life, using the Finite Element method, to pedestrian white and grey matters in vehicle collisions. The OTM predicted trauma location as well as intensity, unlike current computer methods utilized. The OTM firstly calibrates PVP against the medical critical AIS threshold observed in each part of the head as a function of speed. This base PVP critical trauma function is then scaled and banded across all AIS levels using the property that AIS and the probability of death is statistically and numerically a cubic. The OTM was tested against four real-life accident scenarios for which PM data was available. The study concluded that PVP was a good candidate to predict AIS in a Finite Element head model, and that head trauma

under-predictions were due to haemorrhage, which is post-impact. This method, however, brings some benefits, as it allows the assessment of head white and grey matter injuries, which are currently not measured, and may live alongside the current EuroNCAP test protocol to enhance the protection of pedestrian head injuries.

7 Limitations and Further Work

- THUMS is a dynamic Lagrangian CAE model which cannot be used to predict post-accident effects like swelling and bleeding, but the material damage: in this case trauma. Consequently, a means to extract the post-impact trauma will require a fundamental rebuild of the computer model and include maybe SPH or ALE formulations to evaluate bleeding and swelling.
- In the future, this study will continue and focus on other internal organs, like the liver, heart and kidneys, and investigate whether the same level of correlation can be achieved, leading eventually to the CAE calculation of the Injury Severity Score (ISS).
- As PVP is material property dependent, it would be theoretically possible to calibrate the OTM model with material properties for older people (Young's Modulus and failure strain level), making the OTM method a universal trauma modeling method.
- It could be hypothesized that pre-existing medical conditions could be pre-stored as a PVP value which could be added to the PVP generated by the collision.
- In the future, the OTM should be able to model and consider also failure, so that, for example, a broken rib could pierce a lung. Maybe PVP could be also part of a fracture model.

Acknowledgements

The authors would like to thank the UK Police Force and the Coroners who made this research possible, as well as Dr Michal Orlowski and Mr Rohit Kshirsagar who have supported the authors with some of the CAE simulations and the post-processing of some trauma injuries.

References

[1] WHO (2018) "Road Traffic Injuries". www.who.int/news-room/fact-sheets/detail/road-traffic-injuries

[2] Hayes, W., M. Erickson, and E. D Power, Forensic Injury Biomechanics. Vol. 9. 2007. 55-86.

[3] Association for the Advancement of Automotive. Association for the Advancement of Automotive Medicine - ABBREVIATED INJURY SCALE (AIS). 2015 2015 [cited 2018; Available from: https://www.aaam.org/abbreviated-injury-scale-ais/.

[4] Michael Kleinberger, Emily Sun, and Rolf Eppi (1998) "Development of Improved Injury Criteria for the Assessment of Advanced Automotive Restraint Systems". Technical Report from National Highway Traffic Safety Administration (NHTSA). Download: criteria.pdf

[5] Chakravarthy, B., Lotfipour, S. & Vaca, F. E. 2007. Pedestrian injuries: emergency care

considerations. Western Journal of Emergency Medicine, 8.

[6] Livermore Software Technology Corporation. 2011. Total Human Model for Safety - THUMS [Online]. Livermore Software Technology Corporation. Available: http://www.lstc.com/thums [Accessed].

[7] Dennis F. Shanahan, M.D., M.P.H "Human Tolerance and Crash Survivability". Report from NATO. Download: citeseerx.ist.psu.edu/viewdoc/download?doi=10.1.1.212.5449&rep=rep1&type=pdf

[8] PVP: "The Entropy of Morbidity Trauma and Mortality ". https://arxiv.org/ftp/arxiv/papers/1008/1008.3695.pdf

[9] Sturgess, C.E.N., (2002) 'A Thermomechanical Theory of Impact Trauma'. Proc. IMechE, Part D:J. of Automobile Div., 2002. 216: p. 883-895.

[10] Sturgess, C.E.N. (2001) 'Peak Virtual Power - A Global Injury Criterion'. Passive Safety Network Workshop on Human Body Modelling 2001 [cited March 29 and 30, 2001; Available from: www.passivesafety.com/.

[11] Tomoyuki, M. & Junji , H. 2011. Development of A Finite Element Model Of The Total Human Model For Safety (Thums) And Application To Car-Pedestrian Impacts.

[12] Toyota Motor Corporation 2011. Documentation of Total Human Model for Safety (THUMS_AM50_V4AC_Document).

[13] Ulman, M. & Stalnaker, R. Evaluation of the AIS as a measure of probability of death. 1986 International IRCOBI Conference on Biomechanics of Impacts, 1986. 2-4.

[14] Bastien C., Wellings R., Burnett B., (2018) "An Evidence Based Method to Calculate Pedestrian Crossing Speeds in Vehicle Collisions". Accident Analysis & Prevention. 118, p. 66-76 11

[15] Wen, L., Bastien, C., Sturgess, C., (2015) "Stability of THUMS Pedestrian Model and its Initial Trauma Response Against a Real-Life Accident", LS-Dyna European, Conference 2015, Salzburg, Germany

[16] Bastien C., Orlowski, M., (2017) "Validation of a Finite Element Human Model Throw Distance in Pedestrian Accident Scenarios", LS-Dyna European Conference 2017, Würzburg, Austria

[17] Coventry University Ethics Protocol. [1] https://ethics.coventry.ac.uk/about/cu-ethics.aspx

[18] College of Policing (2018) "Information Sharing". www.app.college.police.uk/app-content/information-management/sharing-police-information/

[19] Warwickshire County Council (2018)" Policy for the Provision of Pedestrian Crossings and Pedestrian Facility at Traffic Signals Junctions Report: https://apps.warwickshire.gov.uk/api/documents/WCCC-770-190. Document accessed on 21/02/2018.

[20] Seat Leon EuroNCAP scoring. www.euroncap.com/en/results/seat/leon/10946?tab=3

[21] Toyota Corolla EuroNCAP scoring. www.euroncap.com/en/results/toyota/corolla/15742

[22] Renault Clio EuroNCAP scoring. www.euroncap.com/en/results/renault/clio/10944?tab=3

[23] Benz B180 EuroNCAP scoring. www.euroncap.com/en/results/mercedes-

benz/b-class/10982?tab=3

[24] Bastien, C., Wellings, R., Burnett, B. (2018) “An Evidence Based Method to Calculate Pedestrian Crossing Speeds in Vehicle Collisions”. Accident Analysis & Prevention Journal.

[25] APROSYS (Advanced Protection Systems) “APROSYS Report Summary”. Web link: https://cordis.europa.eu/result/rcn/47920_en.html

[26] European Parliament, UNECE 127 “Pedestrian Protection”. Legislative document. Link: www.unece.org/%20/fileadmin/DAM/trans/conventn/agn.pdf

[27] EuroNCAP (2018) “Pedestrian Protocol”. Technical report. Download: www.euroncap.com/en/for-engineers/protocols/pedestrian-protection/

Appendix A: AIS in Lateral Head Impact

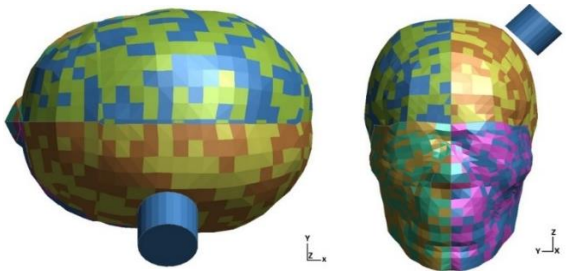

Figure 193 Scenario of parietal impact on THUMS' head

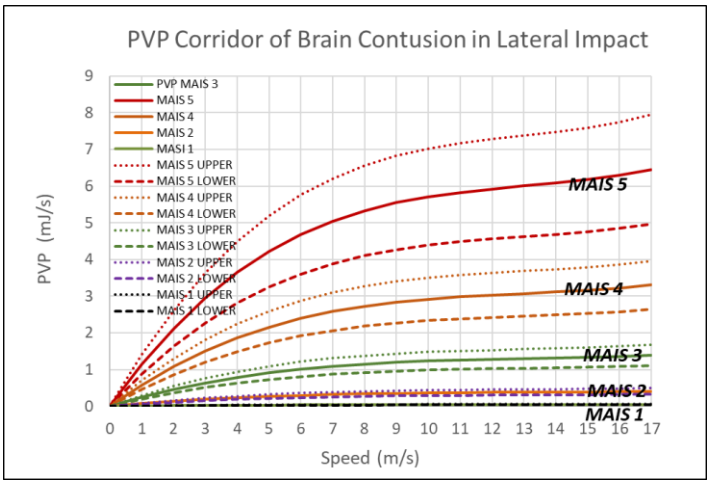

Figure 194 PVP corridor of brain contusion in lateral head impact

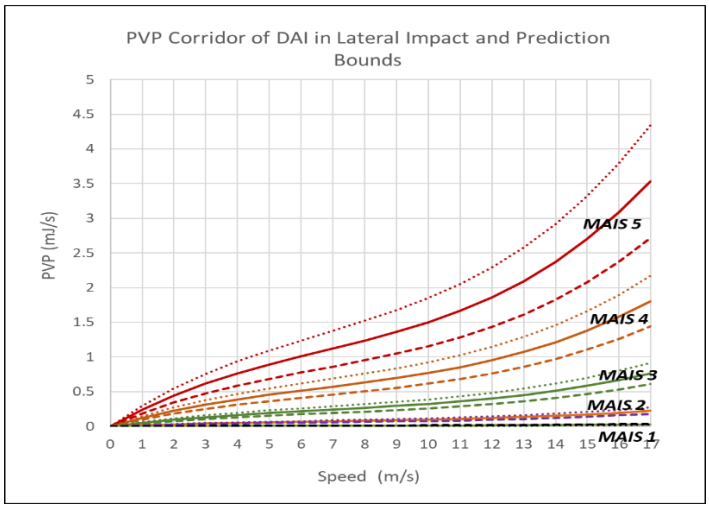

Figure 195 PVP corridor of DAI in head lateral impact

Appendix B: AIS in Occipital Head Impact

Figure 196 Scenario of Occipital impact on THUMS' head

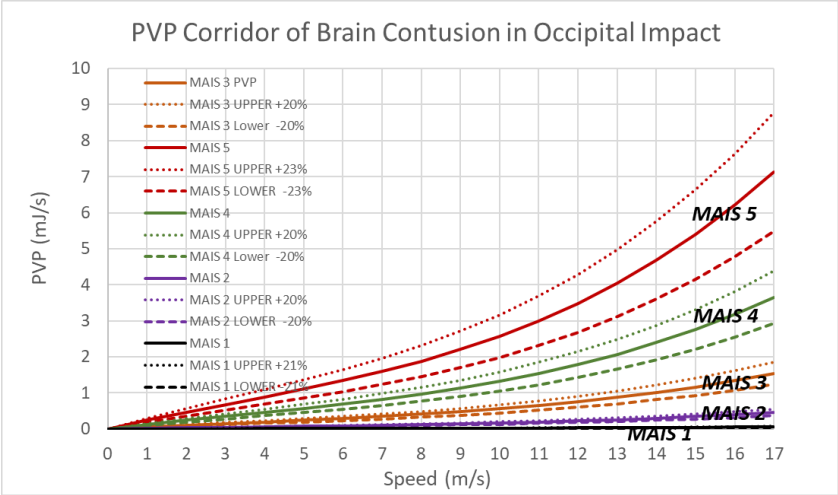

Figure 197 PVP corridor of brain contusion in occipital impact

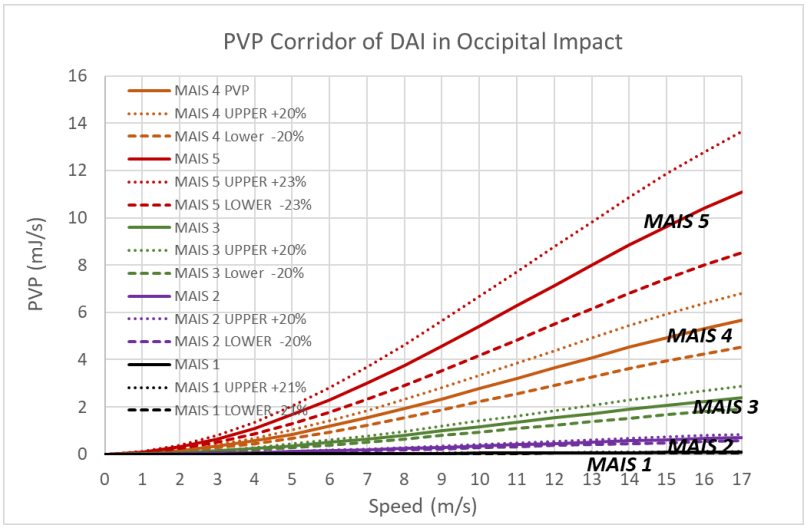

Figure 198 PVP corridor of DAI in occipital impact

Appendix C: Stiffness map of each vehicle

Case Id	EuroNCAP scoring	CAE model colour code
1 [20]		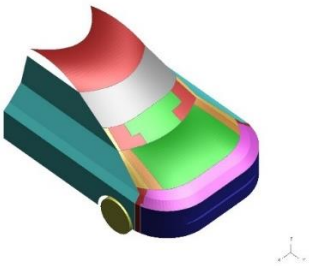
2 [21]		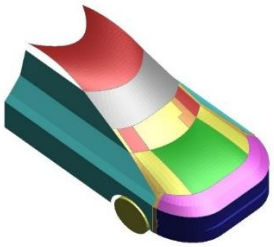
3 [22]		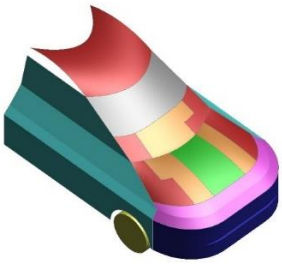
4 [23]		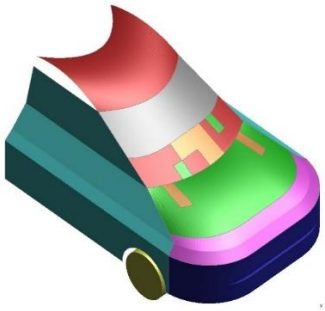

Appendix D: Stiffness characteristic vs EuroNCAP map

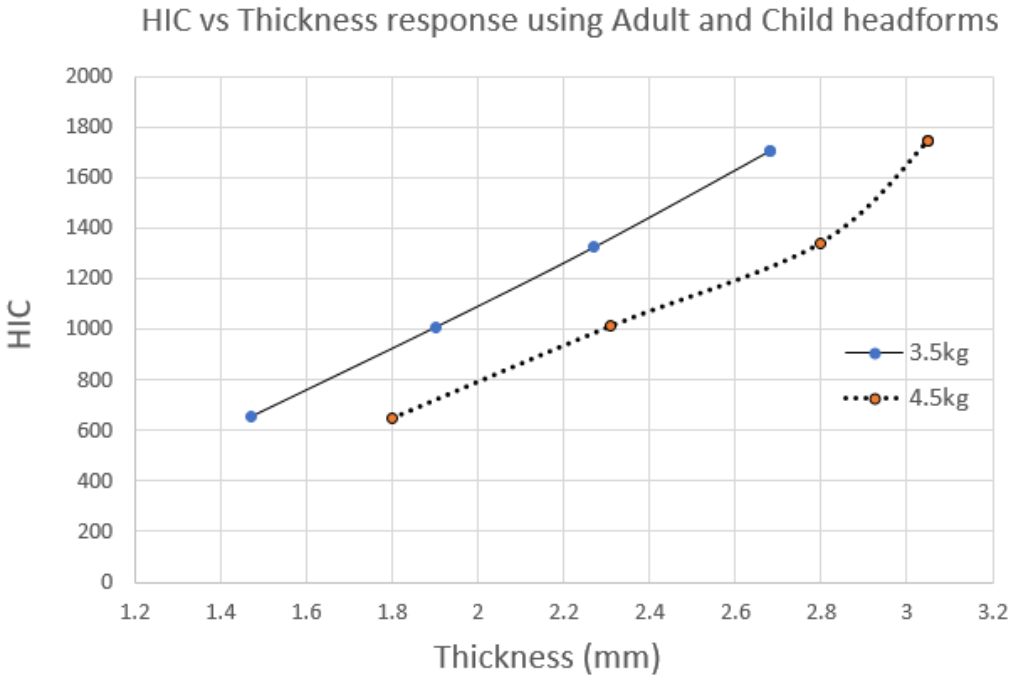

Figure 199 HIC vs thickness of 3.5kg and 4.5kg headforms

Average HIC value as per EuroNCAP scheme	Impactor Mass	
	3.5kg	4.5kg
	Panel thickness (mm)	Panel thickness (mm)
Green (<650)	1.47	1.80
Yellow (650 – 1000)	1.69	2.05
Orange (1000 – 1350)	2.09	2.56
Brown (1350 – 1700)	2.50	2.93
Red (>1700)	2.68	3.05

Table 42 Average HIC value using 3.5kg and 4.5kg headforms

Appendix E: Accident Kinematics (1/3)

Some materials have been removed from this thesis due to Third Party Copyright. Pages where material has been removed are clearly marked in the electronic version. The unabridged version of the thesis can be viewed at the Lanchester Library, Coventry University

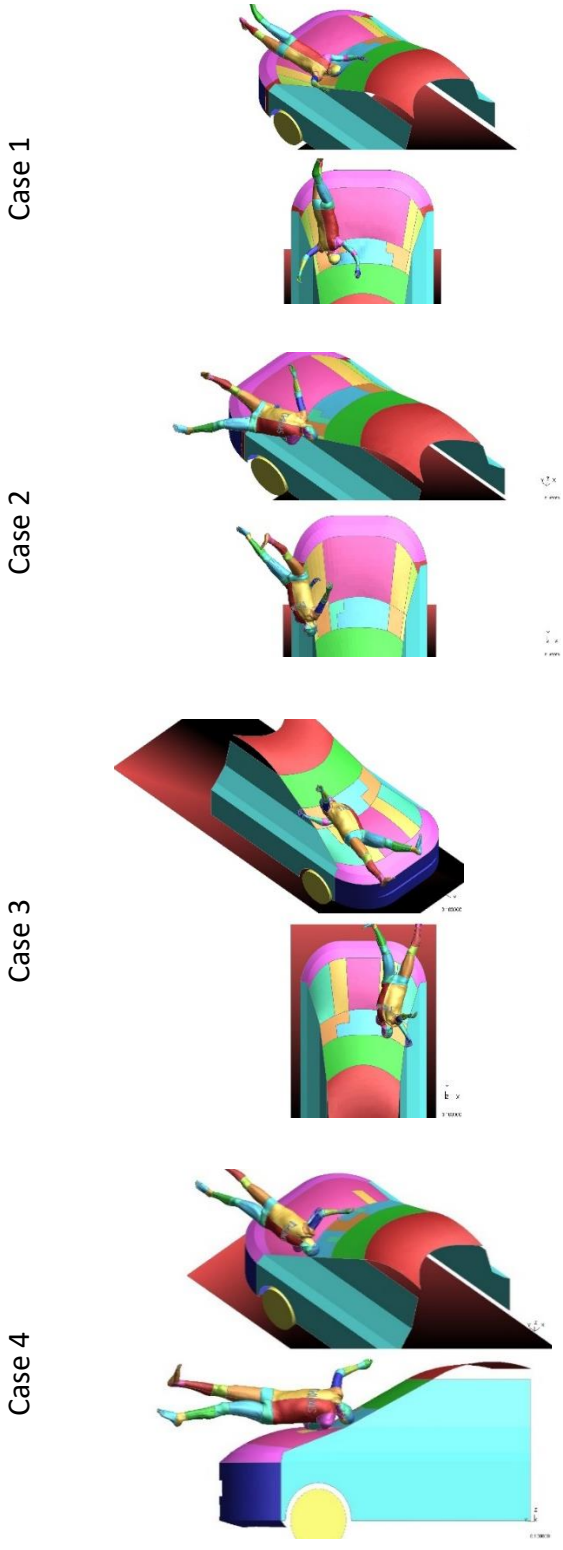

Figure 200: Validation of head impact location for each four accidents

Appendix E: Accident Kinematics (2/3)

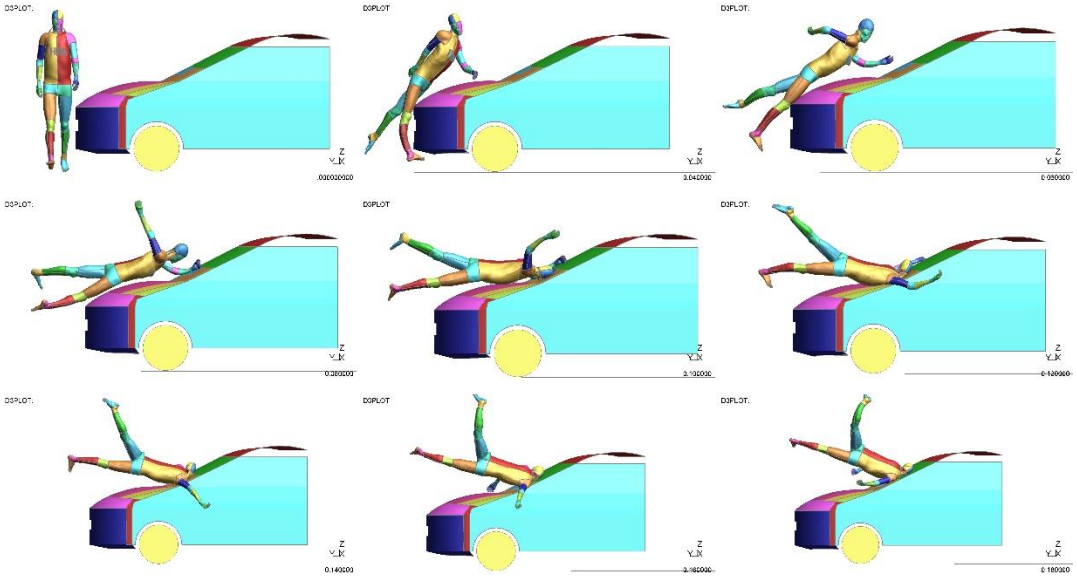

Figure 201: Seat Accident

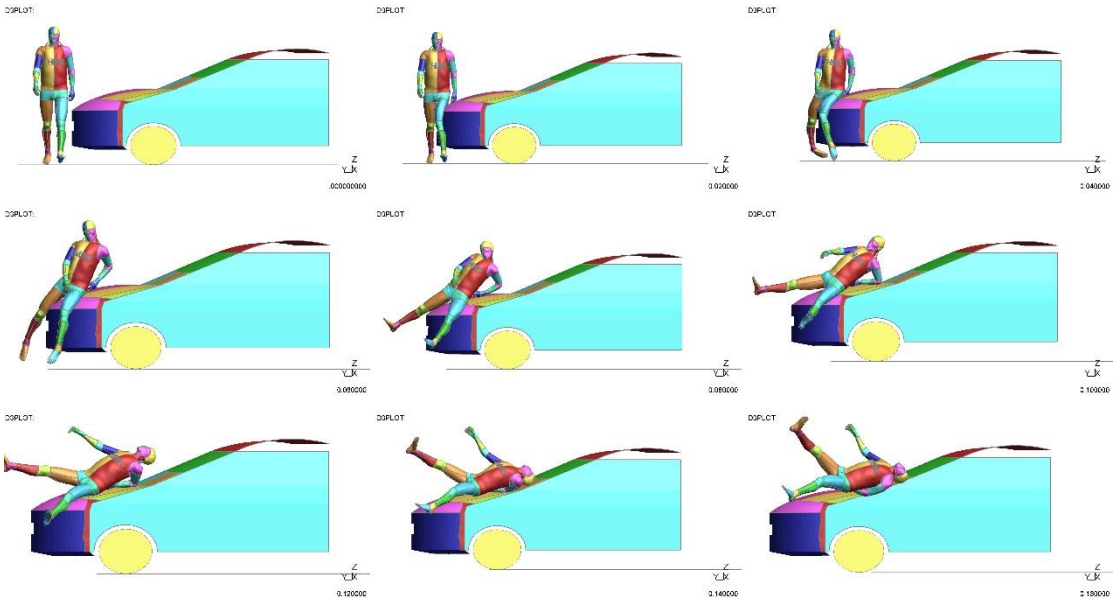

Figure 202: Toyota Accident

Appendix E: Accident Kinematics (3/3)

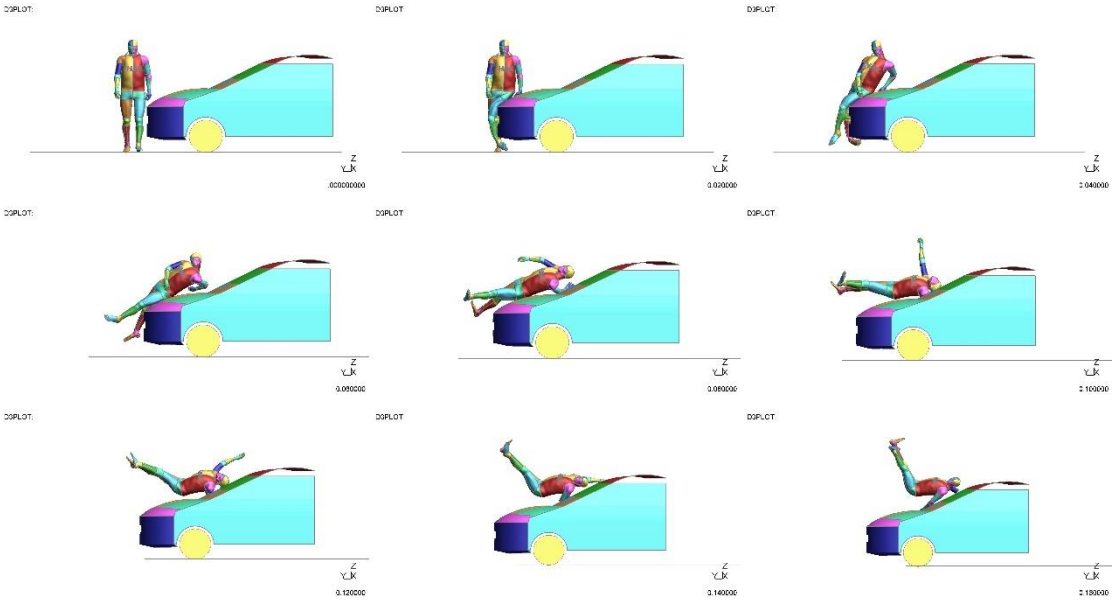

Figure 203: Renault Clio accident

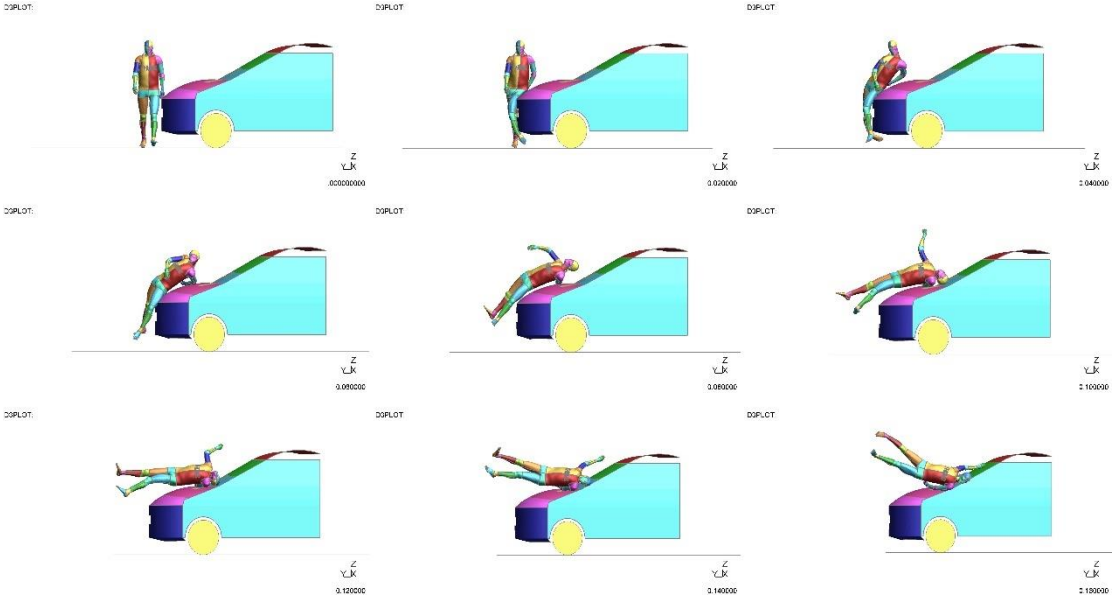

Figure 204: Benz B180 Accident

Appendix F: Head Trauma location and PVP value (1/2)

CASE Id and organ (white/ grey matter)	PVP value from CAE (mJ/s)	PVP calibration value (mJ/s)	Impact mode (frontal, lateral, occipital)	Left / Right	Location within the brain
Case 1 (grey matter)	1.07	0.00	Frontal	Right	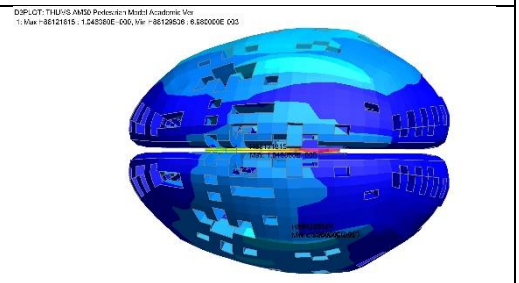
Case 1 (white matter)	1.09	4.10	Frontal	Right	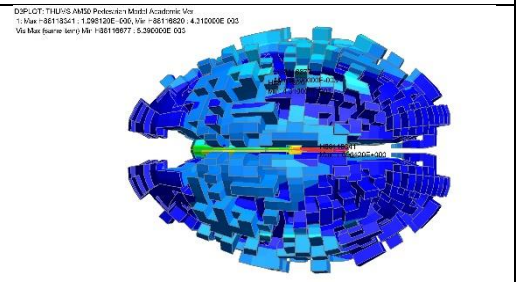
Case 2 (grey matter)	1.13	0.67	Occipital	Right	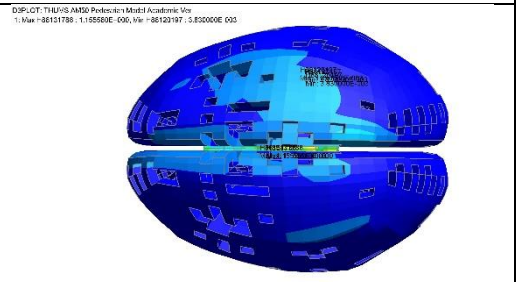
Case 2 (white matter)	1.04	1.39	Occipital	Right	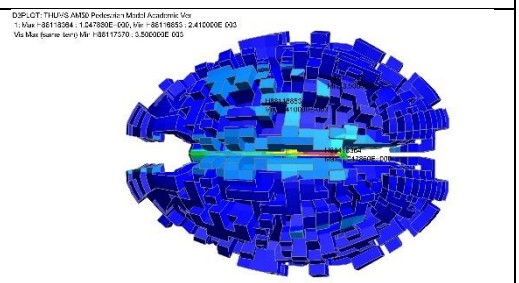

Appendix F: Head Trauma location and PVP value (2/2)

Case 3 (grey matter)	0.94	0.00	Occipital	Right	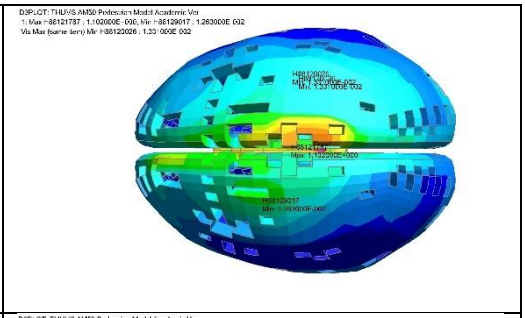
Case 3 (white matter)	1.16	0.00	Occipital	Right	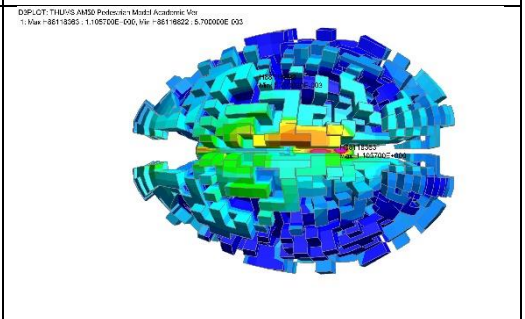
Case 4 (grey matter)	0.34	0.00	Lateral	Both	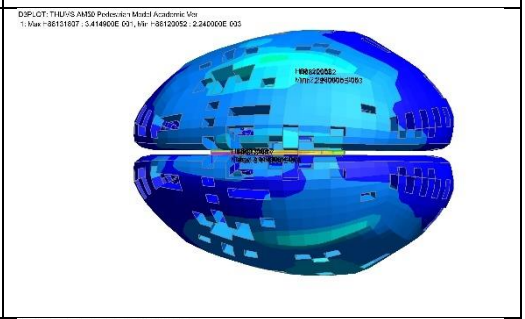
Accident 4 white matter	0.42	1.01	Lateral	Both	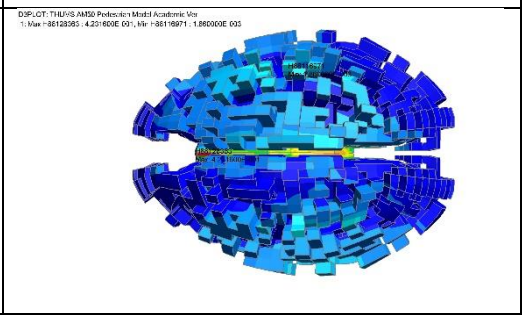

Table 43 PVP value and location of CAE result

Appendix III Additional Information

Part ID	88000001	88000004	88000011
Part Name	Frontal diploe	Parietal diploe	Occipital diploe
Material ID	MAT_105	MAT_105	MAT_012
Density (t/mm^3)	1.0e-9	1.0e-9	8.62e-10
Young's modulus (E) (MPa)	100.4	1090	
Poisson Ratio	0.22	0.22	
Yield stress (SIGY, MPa)	0.3514	4.794	1000000.0
Tangent modulus (ETAN)	80.75	759.3	40.0

Table A 1 Solid parts material properties used on THUMS skull

Part ID	88000002	88000003	88000006
Part Name	External table	Frontal internal table	Parietal internal table
Material ID	MAT_081	MAT_081	MAT_081
Density (t/mm^3)	2.12e-9	2.12e-9	2.12e-9
Young's modulus (E) (MPa)	14900	10900	10900
Poisson Ratio	0.22	0.22	0.22
Yield stress (SIGY, MPa)	95.88	47.94	47.94

Tangent modulus (ETAN	7593.0	7593.0	7593.0
Plastic strain at failure (EPPF)	1.0E21	0.1	6.0e-3

Table A 2 Shell parts material properties used on THUMS skull

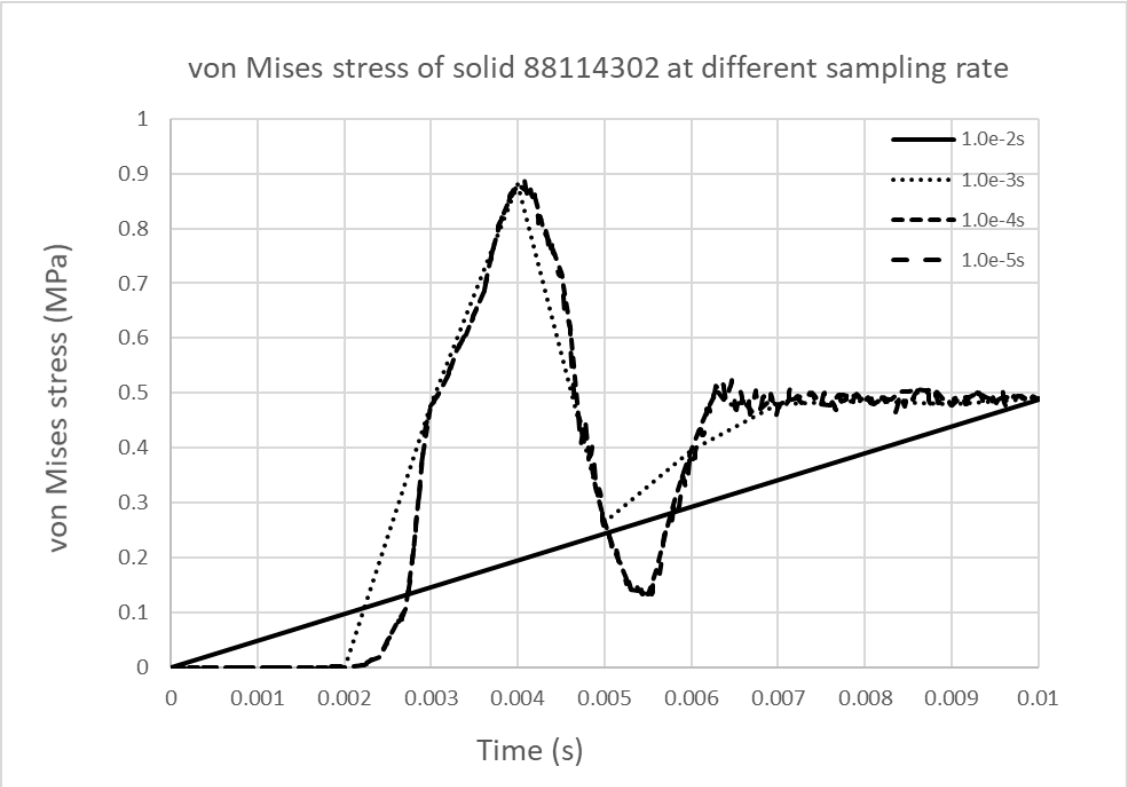

Figure A 1 von Mises stress of solid 88114302 at different sampling rate (1.0e-2s to1.0e-4s)

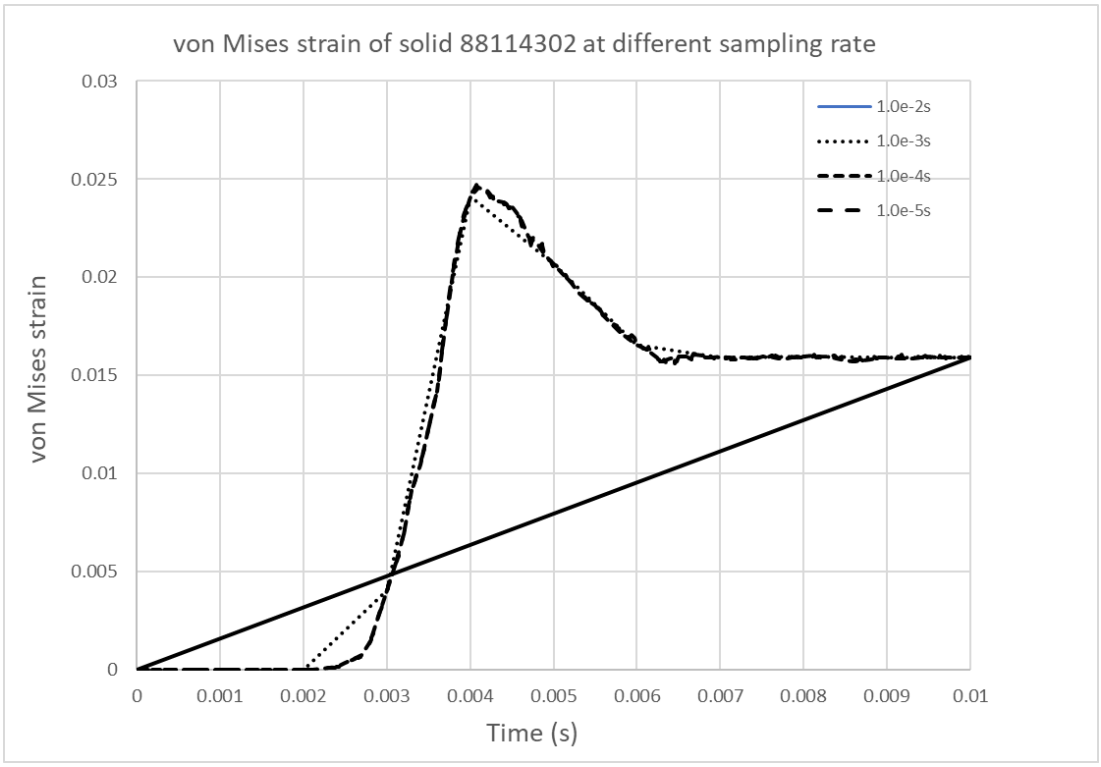

Figure A 2 von Mises strain of solid 88114302 at different sampling rate (1.0e-2s to1.0e-4s)

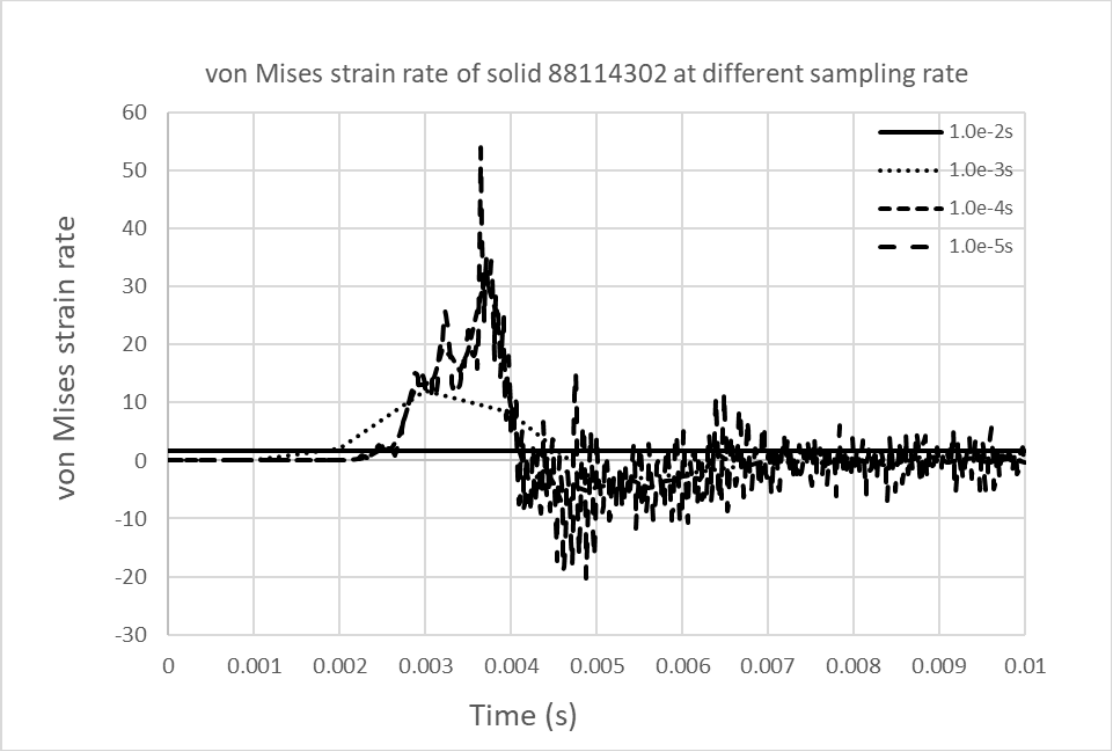

Figure A 3 von Mises strain rate of solid 88114302 at different sampling rate (1.0e-2s to1.0e-4s)

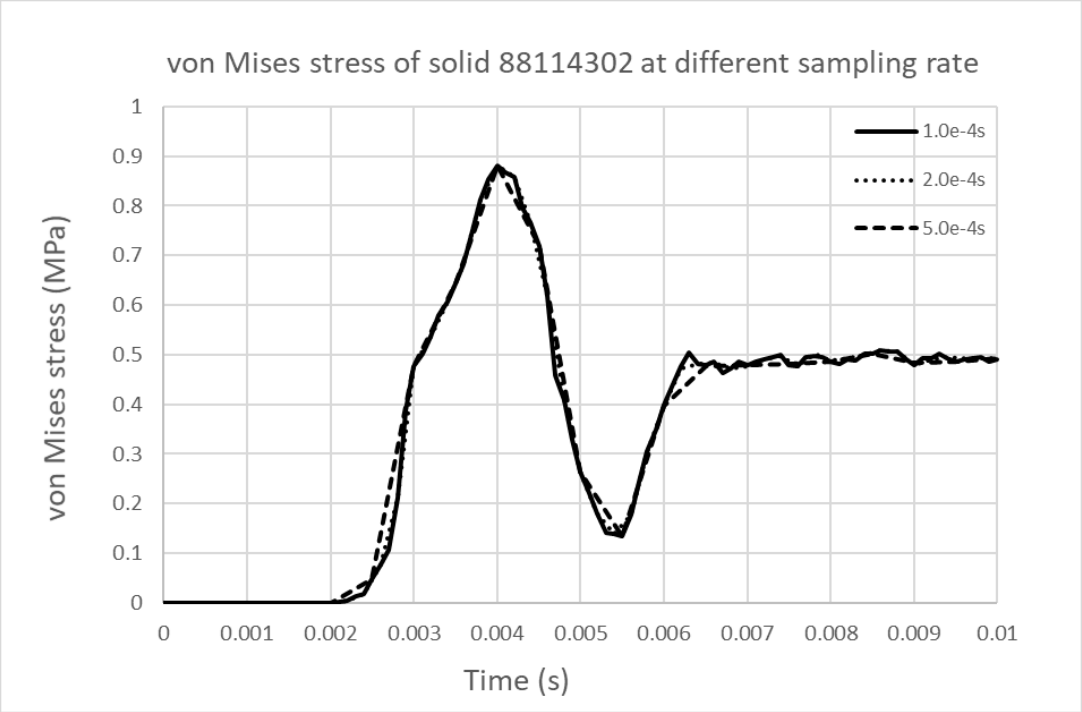

Figure A 4 von Mises stress of solid 88114302 at different sampling rate (1.0e-4s, 2.0e-4s and 5.0e-4s)

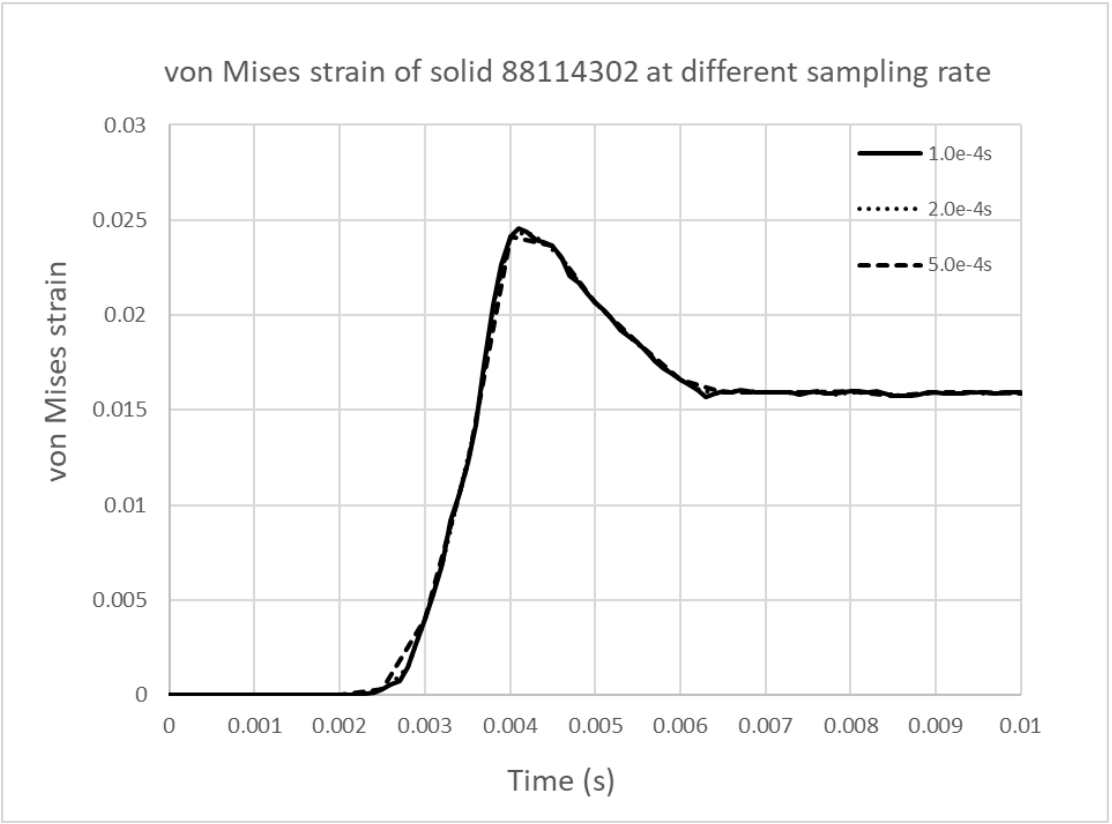

Figure A 5 von Mises strain of solid 88114302 at different sampling rate (1.0e-4s, 2.0e-4s and 5.0e-4s)

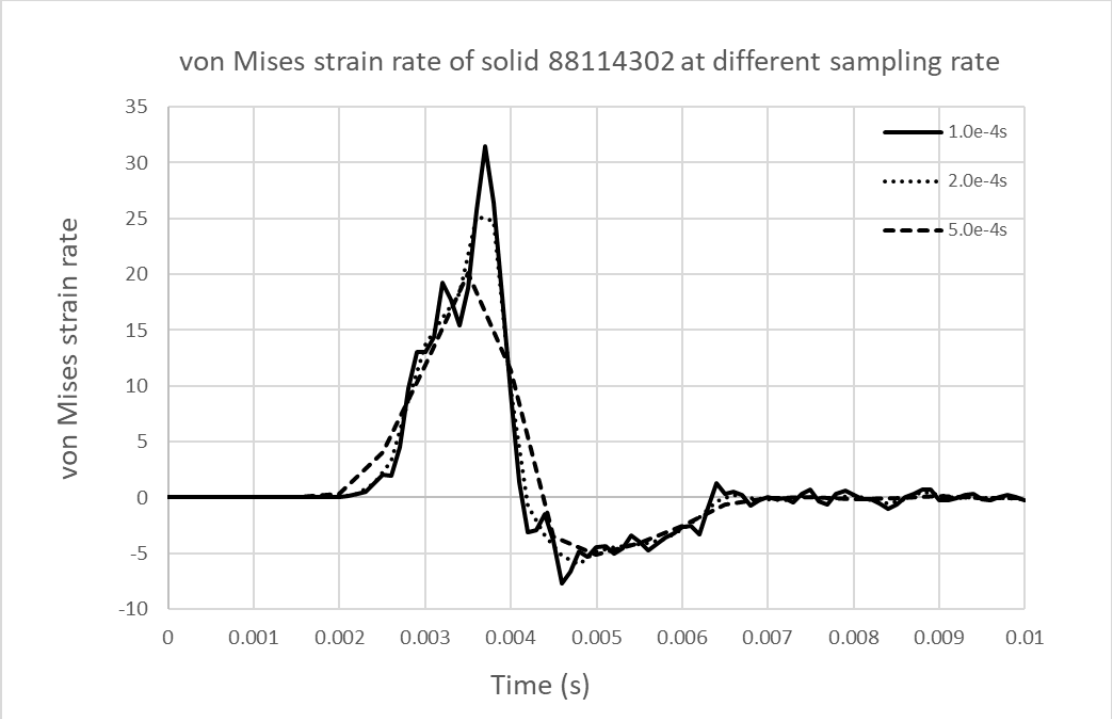

Figure A 6 von Mises strain rate of solid 88114302 at different sampling rate (1.0e-4s, 2.0e-4s and 5.0e-4s)

Appendix IV AIS Rating on Head and Neck

AIS level	Description of representative injury
1	• Pain and dizzy after head trauma; • Cervical spinal strain without bone fracture; • Minor rupture on jugulars (blood loss≤20%) and bruise;
2	• Retroactive amnesia; • Drowsiness and bluntness; loss of consciousness < 1 hour; • Thyroid rupture; • Simple skull fracture; • Incomplete brachial plexus injury; • Minor compression of vertical vertebrae (≤20%); • Spinous or intervertebral injury without nerve damage; • Contusion on nerve root; contusion and laceration of cranial nerve; • Carotid intimal tear and rupture (blood loss ≤20%); • Jugular rupture with thrombus (blood loss ≤20%); • Single lateral laceration on throat and vocal cords;
3	• Coma up to 6 hours; • Coma ≤1 hour with nerve disorder; • Skull basal fracture; • Crushing/open/depress (≤2cm) skull fracture; • Cerebral infarction and contusion; • Cerebella contusion (≤15ml and diameter≤3cm); • Minor cerebral swelling or oedema (pressure on ventricle, no pressure on brainstem); • Skull penetration (depth≤2cm); • Subarachnoid haemorrhage; • Pituitary damage; • Severe compression of cervical vertebrae (>20%); • Internal carotid tear and rupture (blood loss>20%); • Jugular rupture with thrombus (blood loss >20%); • Complete brachial plexus injury;

4	• Coma up to 6 hours with nerve disorder; • Response to pain stimulation only; • Skull depression>2cm; • Complex crushing fracture on basal; • Dural rupture or exposure and damage to brain tissue; • Brain contusion 30-50ml (diameter>4cm, central offset>5cm); • Mild brain swelling with pressure on ventricle and brainstem; • Large cerebella contusion (15-30ml, diameter>3cm); • Hematoma on epidural and subdural (adult≤30ml); • Oesophagus or trachea rupture without transection;
5	• Coma up to 24 hours; • Brainstem damage; • Extensive brain contusion (adult >50ml); • Extensive contusion on cerebella (total volume>30ml); • Extensive or bilateral hematoma on epidural (adult>30ml); • Brain swelling with no observation of ventricle and brainstem; • Perforation on brain or cerebella; • Transection on throat; • Oesophagus or trachea transection or abscission; • Complete spinal cord injury; fracture or dislocation on C4 and below

Table 44 AIS rating on head and neck (Deng, 2014)

Appendix V Rating on Thorax

AIS level	Description of representative injury
1	• Single rib fracture: thoracic spine strain; • Sternum abrasion; sternum contusion; • Main bronchus contusion with hematoma;
2	• Fracture on 2-3 ribs or several fractures on single rib (AIS 3 is concluded if hematopneumothorax is observed); • Sternum fracture; dislocation on thoracic spine; • Minor compression on thoracic spine (≤20%); • Oesophagus contusion or laceration of thoracic duct; • Diaphragm contusion with hematoma;

	• Phleborrhexis on oesophagus or bronchus (blood loss≤20%, AIS 3 is concluded if blood loss >20%); • Pleural laceration (AIS 3 is concluded if hematopneumothorax is observed);
3	• Exposure or crushing fracture on more than 1 rib (AIS 4 is concluded if hematopneumothorax is observed); • Fracture on more than 3 ribs on single side; • Lung contusion or laceration (AIS 3 is concluded if contusion and laceration are observed on both lungs or mediastinal hematoma is observed or blood loss>20%); • Unilateral pneumothorax or hemothorax; • Mediastinal emphysema; oesophagus laceration without perforation; Contusion on main bronchus or trachea without transection;
4	• Fracture on more than 3 ribs on both sides (AIS 5 is concluded if hematopneumothorax is observed); • Bilateral lung contusion (AIS 5 is concluded if blood loss >20%); • Mediastinal hematoma; bilateral pneumothorax (AIS 5 is concluded if blood loss >20%); • Pressure pneumothorax; • Rupture and perforation on oesophagus or bronchus without complete transection; • Tear on Thoracic aortic intimal (blood loss≤20%); incomplete spinal cord injury syndrome; • Diaphragm laceration with diaphragmatocele;
5	• Severe laceration of thoracic aorta; • Pericardium rupture with cardiac herniation; • Cardiac rupture; • Complex rupture or transection on oesophagus or main bronchus; • Throat and trachea separation; • Complete spinal cord damage or laceration; • Bilateral flail chest (mechanical ventilation required);

Table 45 AIS rating on thorax (Deng, 2014)

Appendix VI AIS Rating on Abdominal Location and Pelvic Cavity

AIS level	Description of representative injury
1	• Scratch, contusion and superficial laceration on vagina, labia, perineum, scrotum, testis or penis; • Lumbar strain; • Haematuria;
2	• Contusion, hematoma or superficial laceration without perforation on stomach, duodenum, small intestine, large intestine, rectum, bladder, ureter, urethra, mesenteric, liver, spleen, kidney, pancreas; laceration, contusion on gallbladder cysts no damage on gallbladder choledoch, iliac vein incomplete transaction (blood loss ≤20%); • Unilateral facet dislocation, vertebral compression fractures (≤20%), intervertebral disc injury no nerve root damage
3	• Laceration or perforation on stomach or duodenum (diameter ≤50-70%); rupture or perforation on small intestine, large intestine, rectum without transection, laceration on bladder without perforation, extensive laceration on ureter, urethra, uterus, anus, perineal, vulva, vagina and penis; • Tear on total, internal and external endometrial of celiac artery or iliac artery (blood loss ≤20%), rupture on postcava (blood loss ≤20%), iliac artery rupture (blood loss >20%); • Severe damage on mesenterium or retina (blood loss >20%), crush damage on ovary, sever damage on renicapsule; • Extensive laceration, avulsion on liver, spleen, bile cyst, kidney, pancreas; Dislocation on lumbar spine, vertebral compression fracture; • More than 1 nerve root damage; • Slippage on intervertebral disk with nerve root damage.
4	• Complex rupture, stomach avulsion, descendant duodenum rupture (diameter >75%), transaction or avulsion on small and large intestine, extending perforation from rectum to perineal or bladder, posterior urethral tissue destruction, uterine laceration, extensive tear on mesenterium; Rupture on bile cyst with choledoch or hepatic duct laceration or transection; abdominal aortic intimal tear (blood loss ≤20%), postcava rupture (blood loss>20%); • Incomplete paraplegia;

5	• Severe rupture with tissue loss, severe infection, total or extensive damage on duodenum, total or extensive damage on rectum with obvious fecal pollution in pelvic cavity; • Complete spinal cord damage, abdominal aorta and celiac artery rupture (blood loss >20%); • Spinal cord laceration with transaction and crushing damage;

Table 46 AIS rating on abdominal location and pelvis cavity (Deng, 2014)